Mechanisms of Cell Growth

Sinead Anne Roberts

Thesis submitted for the degree of Doctor of Philosophy

Medical Research Council, Laboratory for Molecular Cell Biology

University College London

Declaration

I, Sinead Anne Roberts confirm that the work presented in this thesis is my own. Where information has been derived from other sources, I confirm that this has been indicated in the thesis.

Signed……..Date……

Abstract

Cell growth, the addition of mass and volume, is required for the development and homeostasis of all organisms. In mammalian cells, cell growth and size homeostasis usually requires an instructive signal in the form of a growth factor with loss of this signal resulting in cell atrophy.

The primary Schwann cell has proven a powerful system to study cell growth *in vitro* – underlining the requirement of growth factors for mammalian cells biogenesis. Using this system, IGF-1 was identified as a Schwann cell growth factor that drives cell volume addition. In contrast, NRG-1 has no effect on Schwann cell volume, but does drive mitochondrial biogenesis - highlighting that cell growth can be non-uniform, diverging from the simple coordinate addition of volume and organelles.

In this thesis, I demonstrate that the addition of mass and volume can be uncoupled during cell growth. IGF-1 drives coordinate addition of cell mass and volume, whereas sustained Raf/MEK/ERK activation drives addition of protein mass and specific organelles in the absence of an increase in cell volume. Furthermore, the addition of volume can be uncoupled from mass accumulation, downstream of IGF-1. This demonstrates that factors other than protein mass limit volume addition.

To investigate the regulation of cell volume I took two approaches: Firstly, a cellular approach - comparing plasma membrane dynamics in growing and growth factor-starved cells. I show that membrane turnover is extremely fast with the whole membrane internalised ~ three times an hour. Moreover, this rapid and ATP-dependent rate is maintained in starved, autophagic cells - indicating that it is an essential cellular process. The speed of membrane turnover however, precluded using this approach to identify how cells deliver membrane to the cell surface to drive plasma membrane expansion. Secondly, a biochemical approach - to identify important signalling pathways. I identify a critical role for de novo lipogenesis for both the addition and maintenance of cell volume and SREBP-2 as an essential transcription factor mediating this process.

Acknowledgements

I would like to thank Alison Lloyd, for all I have learnt from her and for critically reading this thesis. I would also like to thank my thesis committee of Julie Pitcher, Mark Marsh and Robin Ketteler, all the Lloyd laboratory members (past and present) Marc Kirschner and Ran Kafri for their guidance and discussions. Thank you to Nikki Stevenson, Catherine Hogan, Luca Crepaldi, Victor Quereda and Anne-Laure Cattin for helpful reading of parts of this thesis. A tremendous thanks also to my year group- Liz Durkin, Kasia Anton, Justyna Nitarska, Catia Caetano and Jennifer Jermy- for their friendship, scientific discussions and help over the years. Finally, I wish to thank my parents for their boundless support and encouragement.

Contents

Abstract……..……...……3

Acknowledgements……..……..…4

Contents……..……....5

List of Figures……..……..10

List of Tables……..……..……14

Abbreviations……..……..……15

Chapter 1: Introduction……..……..20

1.1 Introduction to Cell Growth……..……..20

1.2 Schwann Cell Model System……..……..21

1.3 Cell Growth vs. Proliferation……..……..22

1.4 Cell Growth: How is Cell Size Determined?……..……..…24

1.4.1 Proliferating cell populations……..……...……25

1.4.2 Non-Dividing cell populations……..……..……38

1.4.3 Cell size, growth rates and the underlying rates of synthesis and degradation……...……45

1.5 Cell Size: Organelle Biogenesis, Macromolecule Addition and Water Uptake……..……..48

1.5.1 Macromolecule Addition: Protein……..48

1.5.2 Macromolecule Addition: Lipid……..……...53

1.5.3 Water Uptake……..……....64

1.5.4 Organelle Biogenesis and Uniform and Non-Uniform Cell Growth……..66

1.6 Growth Factor Regulation of Cell Growth……..……...68

1.7 Signalling Pathways Regulating Cell Growth……..……70

1.7.1 PI3K/ Akt Dependent Cell Growth……70

1.7.2 mTORC1 Signalling……73

1.7.3 ERK Dependent Cell Growth……76

1.7.4 Myc Dependent Cell Growth……77

1.7.5 Other Signalling Pathways……79

1.7.6 Crosstalk Between Signalling Pathways……80

1.8 Nutrient Regulation of Cell Growth and Cell Size……80

1.9 Growth Factor and/ or Nutrient Withdrawal; the Effects……83
on Cell Growth and Metabolism

1.10 Cell Growth and Disease……85

1.11 Summary……88

1.12 Thesis Aims……89

Chapter 2: Materials and Methods……90

2.1 Cell Culture……90

2.2 Cell Size Measurements……94

2.3 Molecular Biology……97

2.4 Western Blotting……103

2.5 Immunofluorescence and Fluorescent Labelling of……110
Subcellular Components

2.6 Fluorescence Microscopy……115

2.7 Image Quantification After Fluorescence Microscopy……117

2.8 Transmission Electron Microscopy (TEM) ……119

2.9 Measuring De Novo Lipid Synthesis……121

2.10 Endocytosis and Recycling of Cell Surface Protein……121
(Cell Surface Biotinylation)

2.11 Endocytosis and Recycling of Cell Surface Lipid……123

2.12 Endocytosis and Recycling of Fluid-Phase (Fluorophore-……124
Conjugated Dextran)

2.13 Statistical Analysis……125

Chapter 3: Biogenesis Downstream of the PI3K/Akt……126
and Raf/MEK/ERK Signalling Pathways

3.1 The Addition of Mass and Volume can be Uncoupled……128
During Cell Growth

3.2 IGF-1 Dependent Cell Volume Addition is PI3K and……138
mTORC1 Dependent, but MEK Independent

3.3 Addition of Mass is PI3K, mTORC1 and MEK……145
Dependent

3.4 IGF-1 Stimulation and Raf Kinase Activation Drive the……152
Addition of Mitochondrial Volume and an Increase in
Endoplasmic Reticulum (ER) Labelling

3.5 The Nucleus and Trans Golgi Network do not show……160
Gross Morphological Changes after IGF-1 or Raf Kinase Activation

3.6 The cis-Golgi and Organelles Associated with Lipid……164
Metabolism Increase Downstream of IGF-1

3.7 Chapter 3: Summary……174

3.8 Chapter 3: Discussion……175

3.8.1 The Addition of Mass, Volume and Organelle Content……175
can be Uncoupled During Cell Growth

3.8.2 The Biological Implications of Uncoupling the Addition……180
of Cell Mass, Volume and Organelle Content

3.8.3 Regulating Cell Mass, Volume and Organelle Content……182

3.8.4 Organelles Driving the Addition of Cell Mass and……185
Volume

3.8.5 Signalling Pathways Driving Cell Growth……186

3.8.6 Conclusion……188

Chapter 4: Plasma Membrane Growth and the……..……..…190

Dynamics of Plasma Membrane Turnover

4.1 Serum Drives Cell Growth: Cells in the Presence of…….……191

Serum Add Mass, Volume and Plasma Membrane

4.2 Starved Cells Upregulate the Catabolic Process of Autophagy……..199

4.3 Endocytosis and Recycling Rates of Membrane Lipids……..……..203

are Equivalent and Rapid in Starved and Growing Cells

4.4 Fluid-Phase Endocytosis and Recycling Rates are Similar……..……213

in Starved and Growing Cells

4.5 Membrane Protein Endocytosis and Recycling Rates are Similar……..…216

in Starved and Growing Cells

4.6 Chapter 4: Summary.……..……..…….……221

4.7 Chapter 4: Discussion.……..……..……...……222

4.7.1 Plasma Membrane Growth…….……222

4.7.2 The Rapid Rate of Plasma Membrane Turnover …….....…226

4.7.3 The Rate of Plasma Membrane Trafficking is…….……229

Equivalent in Starved and Growing Cells

4.7.4 Conclusion…….……230

Chapter 5: The Role of Lipogenesis in Cell…….……232

Volume Addition

5.1 IGF-1, but not Raf Kinase Activation, Induces Expression of……..……233

Genes that Drive Fatty Acid and Sterol Synthesis

5.2 IGF-1 Dependent Cell Volume Addition Requires SREBP-2 and……...239

is Inhibited by Inhibitors of De Novo Lipogenesis

5.3 Expression of Constitutively Active SREBP-2 or SREBP-1a is not…….251

Sufficient to Drive Addition of Cell Volume

5.4 Addition of Fatty Acids and Cholesterol to the Cell Culture Medium……..265

(in a Chemically Defined Supplement) does not Drive Cell Volume

Addition

5.5 Addition of Fatty Acids and Cholesterol to the Cell Culture Medium……..269
Does not Rescue Cell Volume Addition after SREBP-2 siRNA
Knockdown or Chemical Inhibition of Sterol Synthesis
5.6 Chapter 5: Summary……..……..……..……272
5.7 Chapter 5: Discussion……..……..……..……..…273
5.7.1 SREBP-2 and De Novo Lipogenesis are Required for……..……273
the Addition and Maintenance of Schwann Cell
Volume
5.7.2 Inducing SREBP Activity is not Sufficient to Drive……..……277
Cell Volume Addition
5.7.3 Other Factors can Limit Cell Volume……...…280
5.7.4 Conclusion……..……282

Chapter 6: Final Discussion……..……..…….283

Reference List……..……..……285

List of Figures

Chapter 1:

Figure 1.1: Cell growth vs. cell division……...26
Figure 1.2: Initially large and small cells converge to a common……30
mean size if growth rates are size independent
Figure 1.3: Nutrient regulated ribosome biogenesis determines……..32
the critical size threshold to pass Start
Figure 1.4: A spatial gradient of Pom1 extends from the distal tips…….33
of the cell to the cell centre and inhibits mitotic entry
Figure 1.5: The effect of a 'switch-up' to an increased growth and……..37
division rate on subsequent cell cycle length in the presence
and absence of a Cell Size Checkpoint
Figure 1.6: The level of NRG1 Type III growth factor signalling……...40
determines myelinating Schwann cell size through positive
and negative regulation of the biogenic Akt pathway
Figure 1.7: Cell growth rates are determined by the underlying rates…….47
of synthesis and degradation
Figure 1.8: De novo fatty acid and sterol synthesis……..……..55
Figure 1.9: The domain structure of the SREBP proteins……....57
Figure 1.10: Sterol-dependent processing of the inactive ER-bound……..60
precursor SREBP proteins to generate the mature active
transcription factor
Figure 1.11: Signalling through the IGF-1 Receptor……..……..……..70
Figure 1.12: Activation of PI3K, Akt and mTORC1……..……..……72

Chapter 3:

Figure 3.1: IGF-1 drives an increase in cell volume……..……....130
Figure 3.2: Image processing of raw Quantitative Phase Microscopy…..……131
(QPM) images
Figure 3.3: Cell mass and volume can be uncoupled during cell……...132
growth
Figure 3.4: IGF-1 and Raf kinase activation drive an increase in cell……...134
protein mass
Figure 3.5: There is a strong correlation between cell dry mass,……..136
quantified by QPM, and protein mass, quantified by
succinimidyl ester labelling
Figure 3.6: IGF-1 and Raf kinase activation drive an increase in cell……...137
protein mass
Figure 3.7: IGF-1 drives sustained signalling through the……..……141
PI3K/Akt/mTORC1 pathway and Raf kinase activity drives
sustained pERK activation
Figure 3.8: IGF-1 dependent cell volume addition is PI3K dependent……..142
Figure 3.9: IGF-1 dependent cell volume addition is mTORC1……..…143
dependent
Figure 3.10: IGF-1 dependent cell volume addition is MEK……..……144
independent
Figure 3.11: Addition of mass is PI3K and mTORC1 dependent……..…147
Figure 3.12: In contrast to cell volume, addition of mass is MEK……....148
dependent
Figure 3.13: Inhibitors used are specific, with respect to the analysed…….150

pathways
Figure 3.14: IGF-1 stimulation and Raf kinase activation drive the..……154
addition of mitochondrial volume
Figure 3.15: IGF-1 stimulation and Raf kinase activation drive the……...155
addition of mitochondrial volume
Figure 3.16: Raf kinase dependent increase in mitochondrial volume…….157
is not an artefact of tamoxifen treatment
Figure 3.17: IGF-1 stimulation and Raf kinase activation drive an……159
increase in the KDEL receptor, suggesting an increase in the
size of the endoplasmic reticulum
Figure 3.18: There is no significant change in nuclear volume after……161
IGF-1 stimulation or Raf kinase activation
Figure 3.19: IGF-1 stimulation and Raf kinase activation do not drive……..163
a significant change in trans-Golgi network (TGN) volume
Figure 3.20: IGF-1 stimulation drives an increase in cis-Golgi volume…….165
Figure 3.21: IGF-1 drives an increase in the number of lipid droplets……..168
per cell
Figure 3.22: IGF-1 drives an increase in the number and total volume……169
of lipid droplets per cell
Figure 3.23: IGF-1 drives an increase in peroxisome number per cell…….171
Figure 3.24: IGF-1 drives an mTORC1 dependent increase in……..……172
peroxisome number per cell
Figure 3.25: IGF-1 drives a MEK independent increase in peroxisome……173
number per cell

Chapter 4:

Figure 4.1: Serum drives the linear addition of cell volume……..……..192
Figure 4.2: Serum drives addition of cell volume……..……..……..193
Figure 4.3: Serum drives addition of cell protein mass……..……..……194
Figure 4.4: Serum drives addition of plasma membrane……..……..196
Figure 4.5: Serum drives addition of plasma membrane……..……..198
Figure 4.6: Serum suppresses autophagy……..……..……201
Figure 4.7: Serum suppresses autophagy……..……..……202
Figure 4.8: Regulation of plasma membrane size……..……..……205
Figure 4.9: Accumulation of fluorescence intensity over time……..……..207
represents membrane endocytosis and recycling
Figure 4.10: Endocytosis and recycling rates of membrane lipids are……..209
similar in starved and growing cells (serum-starved and
serum-treated cells)
Figure 4.11: The whole plasma membrane turns over faster in starved……...210
cells compared to growing cells (serum-starved vs
serum-treated cells)
Figure 4.12: Intracellular accumulation of FM1-43 is ATP-dependent……..212
Figure 4.13: Fluid-phase endocytosis and recycling rates are similar……..214
in starved and growing cells (serum-starved and
serum-treated cells)
Figure 4.14: Fluid-phase endocytosis and recycling rates are similar……..215
in starved and growing cells (serum-starved and
serum-treated cells)
Figure 4.15: The rate of total membrane protein endocytosis is similar……...218
in starved and growing cells (serum-starved and
serum-treated cells)

Figure 4.16: The rate of membrane protein recycling is similar in……220
starved and growing cells (serum-starved and serum-treated cells)

Chapter 5:

Figure 5.1: IGF-1 increases the amount of cytoplasmic precursor and……...235
nuclear mature SREBP proteins
Figure 5.2: IGF-1 increases the mRNA expression of key SREBP……..…236
target genes that drive de novo fatty and sterol synthesis
Figure 5.3: IGF-1 increases de novo lipogenesis from extracellular……238
pyruvate
Figure 5.4: siRNA knockdown of SREBP-2 blocks IGF-1 dependent…...……241
cell volume addition and reduces the volume of control (no factor) and Raf kinase activated cells
Figure 5.5: mRNA levels of the SREBP targets FASN & HMGCoR……..….242
after siRNA knockdown of SREBP-2
Figure 5.6: siRNA knockdown of SREBP-1 does not inhibit cell……244
volume
Figure 5.7: mRNA levels of the SREBP targets FASN & HMGCoR……..245
after siRNA knockdown of SREBP-1
Figure 5.8: Addition of volume is blocked by inhibitors that block fatty…..……247
acid and/ or sterol synthesis
Figure 5.9: Cells look unhealthy in the presence of fatty acid……248
synthesis inhibitors
Figure 5.10: Addition of protein mass is blocked by inhibitors that……..….250
block fatty acid synthesis
Figure 5.11: Schematic of the ER.mSREBP-1a and -2 fusion……...252
constructs
Figure 5.12: Expression of ER.mSREBP-1a and ER.mSREBP-2 in……..…254
Normal Schwann (NS) and NSΔRafER (NR) cells
Figure 5.13: Anti-ERα immunofluorescence demonstrates the……..…256
proportion of cells expressing the ER.mSREBP-1a or -2 construct
Figure 5.14: Anti-SREBP immunofluorescence demonstrates the……257
proportion of cells expressing the ER.mSREBP-1a or -2 construct
Figure 5.15: Activation of ER.mSREBP-1a or -2 induces the mRNA……...259
expression of FASN, a key SREBP target gene
Figure 5.16: Activation of ER.mSREBP-1a or -2 can induce the……..…260
mRNA expression of HMGCoR, a key SREBP target gene
Figure 5.17: Tmx does not induce the mRNA expression of FASN……..261
a key SREBP target gene
Figure 5.18: Activation of SREBP-1a or -2 has no effect on……..……263
Schwann cell volume
Figure 5.19: Activation of Raf kinase and SREBP-1a or -2 has no……264
effect on Schwann cell volume
Figure 5.20: IGF-1 drives an increase in cell volume independent of……..…267
residual fatty acids on the bovine serum albumin (BSA) used in the cell culture medium
Figure 5.21: Supplementing the cell culture medium with a……..……268
chemically defined mixture of fatty acids and cholesterol does not drive cell volume addition, although IGF-1 induced FASN

and HMGCoR mRNA expression is inhibited
Figure 5.22: Supplementing the cell culture medium with a chemically……270
defined mixture of fatty acids and cholesterol does not rescue
the cell volume inhibition downstream of SREBP-2 knockdown
(siRNA)
Figure 5.23: Supplementing the cell culture medium with a chemically……271
defined mixture of fatty acids and cholesterol does not rescue
the cell volume inhibition downstream of simvastatin

List of Tables

Chapter 2:

Table 2.1.1: Inhibitors……100
Table 2.3.1: Gene specific primers……107
Table 2.3.2: Basic cycling conditions used for qPCR……108
Table 2.3.3: DNA constructs used in the thesis……110
Table 2.4.1: PBS + protease inhibitors……112
Table 2.4.2: Buffer A……112
Table 2.4.3: Buffer C……113
Table 2.4.4: SDS-PAGE gel recipes, showing final concentrations (to 2s.f.)……114
Table 2.4.5: Solutions used for protein extraction and Western blotting……115
Table 2.4.6: Antibodies used for Western blotting……116
Table 2.5.1: Antibodies used for immunofluorescence……119
Table 2.6.1: Wavelengths used to excite/ emission spectra wavelengths collected for fluorescence microscopy……123
Table 2.8.1: EPON recipe……127
Table 2.9.1: Cleavage buffer recipe……130

Abbreviations

4EBP	eukaryotic initiation factor 4E binding protein
ACC	acetyl-CoA carboxylase
ACLY	ATP-citrate lyase
ADP	adenosine diphosphate
AMP	adenosine monophosphate
AMPK	AMP-activated protein kinase
APS	ammonium persulfate
AQP2	Aquaporin-2
AQP7	Aquaporin-7
ATP	adenosine triphosphate
B2M	beta-2 microglobulin
BACE1	beta-secretase 1
BCA	bicinchoninic acid assay
BSA	bovine serum albumin
CBP	CREB-binding protein
CDK	cyclin-dependent kinase
cDNA	complementary deoxyribonucleic acid
CHO	Chinese Hamster Ovary
CME	clathrin mediated endocytosis
CNS	central nervous system
COPII	coat protein complex II
DDSA	dodecenyl succinic anhydride
DIC	differential interference contrast
Dlg1	disks large homolog 1
DMEM	Dulbecco’s Modified Eagle Medium
DMP-30	2,4,6-tris(dimethylaminomethyl) phenol
DMSO	dimethyl sulfoxide
DNA	deoxyribonucleic acid
PLL	Poly-L-lysine
dNTP	deoxyribonucleotide triphosphate

DTT	dithiotheitol
PMSF	phenylmethanesulfonylfluoride
EDTA	ethylenediaminetetraacetic acid
EGFR	epidermal growth factor receptor
eIF2α	eukaryotic initiation factor 2 α
EM	electron microscopy
ER	endoplasmic reticulum
ER	oestrogen receptor
ERK	extracellular signal-regulated kinase
EtOH	ethanol
FASN	fatty acid synthase
FCS	foetal calf serum
FOXO	forkhead box O
GAPDH	glyceraldehyde 3-phosphate dehydrogenase
GCN2	general control nonrepressed 2
GH	growth hormone
GPCR	G-protein coupled receptor
Grb2	growth factor receptor bound protein-2
GSK3β	glycogen synthase kinase 3 β
HDAC3	histone deacetylase 3
HMGCoA	3-hydrocy-3-methylglutaryl-CoA
HMGCoR	HMG-CoA reductase
HMGCS1	HMG-CoA synthase 1
hr	hour
HRP	horseradish-peroxidase
IGF-1	insulin like growth factor-1
IL-2	interleukin-2
IL-3	interleukin-3
IL-4	interleukin-4
IL3R	interleukin-3 receptor
INSIG	Insulin-induced gene
IRES	internal ribosome entry site
IRS-1	insulin receptor substrate-1
KDEL	lysine- aspartic acid- glutamic acid- leucine
LB	lysogeny broth

LC3b	microtubule-associated protein 1 light chain-3B
LDL	low density lipoprotein
LDLR	low density lipoprotein receptor
MAPK	mitogen activated protein kinase
MEK	mitogen activated protein kinase kinase
MNA	methyl nadic anhydride
mRNA	messenger ribonucleic acid
mTORC1	mammalian target of rapamycin complex 1
mTORC2	mammalian target of rapamycin complex 2
N:C	nuclear: cytoplasmic
NA	numerical aperture
Na_3VO_4	sodium orthovanodate
NaCl	sodium chloride
NADPH	nicotinamide adenine dinucleotide phosphate
NaF	sodium fluoride
NaN_3	sodium azide
NaOH	sodium hydroxide
NFAT	nuclear factor of activated T-cells
NGF	nerve growth factor
NR	NSΔRafER cells
NRG1	neuregulin-1
NS	normal Schwann cell
PAGE	polyacrylamide gel electrophoresis
PBS	phosphate buffered saline
PC	phosphatidylcholine
PDK1	3-phosphoinositide dependent protein kinase-1
PEX	peroxin
PFA	paraformaldehyde
PGC1α	peroxisome proliferator-activated receptor γ co-activator 1α
PI3K	phosphoinositide 3-kinases
PIP_2	phosphatidylinositol (4,5)-diphosphate
PIP_3	phosphatidylinositol (3,4,5)-triphosphate
PKA	protein kinase A
PLA2	phospholipase A2
PLC	phospholipase C

PPARα	peroxisome-proliferator activated receptor
PTEN	Phosphatase and tensin homolog
QPM	quantitative phase microcopy
Rb	retinoblastoma protein
RER	rough endoplasmic reticulum
RIPA	radio-immunoprecipitation assay
RNA	ribonucleic acid
ROI	region of interest
RPM	revolutions per minute
rRNA	ribosomal ribonucleic acid
RSK	ribosomal s6 kinase
RT-qPCR	real time quantitative polymerase chain reaction
RTK	receptor tyrosine kinase
S1P	site-1 protease
S2P	site-2 protease
S6K	S6 kinase
SA:V	surface area: volume
SCAP	sterol regulatory element-binding protein cleavage-activating protein
SDS	sodium dodecyl sulphate
ser	serine
SER	smooth endoplasmic reticulum
Shc	Src homology 2 containing transforming protein
SOS	Sons of sevenless
TGN	trans-Golgi network
siRNA	silencing ribonucleic acid
SNARE	soluble NSF attachment protein
SRE	sterol response element
SREBP	sterol response element binding protein
SRF	serum response factor
TACE	tumour necrosis factor-α-converting enzyme
TAG	triacylglycerol
TAZ	transcriptional co-activator with PDZ-binding motif
TBS	tris buffered saline
TBS-T	tris buffered saline-tween 20

TCA	tricarboxylic acid
TEM	transmission electron microscopy
thr	threonine
TM	melting temperature
Tmx	tamoxifen
TOP	terminal oligopyrimidine tract
TRIM-NHL	tripartite motif-NHL
Tris	tris(hydroxymethyl)aminomethane
TSC	tuberous sclerosis complex
UVR	ultraviolet radiation
vLDL	very low density lipoprotein
YAP	Yes-associated protein
Yki	Yorkie
ΔΔCT	delta delta cycle threshold

Chapter 1: Introduction

1.1 Introduction to Cell Growth

The development and homeostasis of multicellular organisms depends on the proper control of cell size and number, which is orchestrated through the coordination and regulation of cell growth, cell division and cell survival (Conlon and Raff, 1999). Deregulation of any one of these processes can prevent the development of a proportionally sized and functional adult as well as cause disease, including cancers.

Mammalian cells usually require instructive signals to grow, divide and survive; growth factors are required to drive cell growth, mitogens drive cell division and survival factors promote cell survival (Conlon and Raff, 1999). Although a single factor may promote more than one of these processes, cell growth, division and survival are distinct and can be- and often are- independently regulated (Conlon and Raff, 1999, Zetterberg et al., 1984). In multicellular organisms such independent control helps provide the flexibility necessary to produce the multiple specialised cell types with different sizes, numbers and lifetimes the organism needs. In addition, given that cells in multicellular organisms are bathed in a nutrient rich environment permissive for cell growth, division and survival, the requirement for instructive signals prevents uncoordinated cellular and organ growth. In contrast to multicellular organisms, unicellular yeast do not require intercellular coordination of growth, division and survival. So it is perhaps unsurprising that the regulation of these processes in yeast appears to be simpler; the presence of appropriate nutrient conditions is sufficient to promote cell growth and division (Grewal and Edgar, 2003). Whereas the mechanisms and regulation of mammalian cell division and survival have been and continue to be heavily researched, the field of cell growth remains relatively understudied.

Cell growth is the addition of mass and/or volume and occurs through the addition of cytosol and organelles. Growth must occur in a specific and tightly regulated manner to ensure each cell and each cell type in a multicellular organism develops and maintains the machinery it requires to function. Growth factors drive the addition of mass and volume by activating pathways that promote nutrient uptake and stimulate macromolecular synthesis, whilst

inhibiting the bulk degradation of cell components by autophagy (Conlon and Raff, 1999, Lum et al., 2005a, Rathmell et al., 2000, Wullschleger et al., 2006).

1.2 Schwann Cell Model System

The rat primary Schwann cell system used in these studies has several properties that make it a powerful system in which to study cell growth (Conlon and Raff, 2003, Conlon et al., 2001, Echave et al., 2007, Echave et al., 2009). Schwann cells can be cultured indefinitely as primary cells, maintaining genetic stability and primary checkpoints- including normal growth control (Mathon et al., 2001). This is in contrast to many mammalian cell culture systems, which tend to use transformed, immortalised or cancer cell lines that exhibit deregulated cell growth, survival and cell-cycle progression.

Linked to this, as mammalian cells Schwann cells are dependent on instructive signals in the form of growth factors, mitogens and survival factors to grow, divide and survive, respectively. Schwann cells produce an autocrine survival factor that has no effect on division or cell growth (Cheng et al., 1998). This, in combination with the fact that defined serum-free Schwann cell culture conditions have been developed, means it is possible to maintain Schwann cells in conditions free from added growth factors, mitogens and survival factors. Such conditions provide a clean background against which to study the effects of adding specific extracellular factors or genetic changes on, for example, cell growth.

If cells are dividing it is difficult to dissect the specific effects a factor has on cell growth. First, because the growth promoting effects of a factor will be spread over an increasing number of cells and, second, because cell populations dividing *in vitro* are asynchronous and differences in cell metabolism and biogenesis can be affected by cell cycle stage (Bryan et al., 2010, Son et al., 2012, Tzur et al., 2009). The second point is particularly problematic if the cell cycle distribution between the two populations being compared is different. As certain extracellular factors/ genetic changes can be both mitogenic and growth promoting, a simple strategy can be used so that the effects on cell growth can be studied independently of any effect on cell

division; the Schwann cells are cell cycle arrested using the reversible DNA polymerase α inhibitor aphidicolin. This induces a G1/S cell cycle arrest, but cell growth continues (Collins et al., 2012, Conlon et al., 2001, Conlon and Raff, 2003, Costa et al., 1992, Echave et al., 2009, Ikegami et al., 1978).

1.3 Cell Growth vs Proliferation

As already touched upon, cell growth and proliferation are distinct and separable processes. Cell growth is the addition of mass and volume, whereas proliferation is the progression through the cell cycle and division to create two daughter cells. There are similarities between the regulation of growth and proliferation. In mammalian cells, both usually require an instructive signal in the form of an extracellular growth factor or mitogen, respectively, and certain extracellular factors can act both as a mitogen and a growth factor (Zetterberg et al., 1984). Moreover growth and proliferation are often coupled, such as cells dividing exponentially *in vitro*, or in transit amplifying populations *in vivo* where the aim is to produce large numbers of approximately identical cells. However the two processes can be separated and are frequently differentially regulated; a cell can divide in the absence of growth, as occurs in early zygotic divisions, and grow (add mass and volume) in the absence of cell division, as occurs during the post-mitotic growth of neurons and muscle (Conlon and Raff, 1999).

Furthermore, whereas proliferation is an all or nothing event- a cell is either in or out of the cell cycle- the processes that drive cell growth are continually active in all cells. Any cell, whether it is adding mass or volume or maintaining cell size, undergoes continuous biosynthesis to replace damaged macromolecules and organelles and in order to adapt to changing intra- and extra- cellular environments and carry out cell-type specific functions. Biogenesis is therefore a necessary function in all living cells. In contrast cells can- and often will- survive in the absence of proliferation, as evidenced by the numerous post-mitotic or quiescent cells in adult mammals *in vivo*.

The separation of cell growth and proliferation has been highlighted using the Schwann cell experimental system described in Section 1.2. First, studies by Conlon *et al* demonstrated that distinct extracellular factors drive

Schwann cell growth (addition of cell volume) and proliferation (Conlon et al., 2001). They showed that Insulin Like Growth Factor-1 (IGF-1) is a Schwann cell growth factor that, alone, has no effect on cell cycle progression. In contrast neuregulin (NRG1) is a mitogen, but cannot drive cell volume addition. This means that, in the absence of a growth factor such as IGF-1, cells treated with NRG1 become progressively smaller as they divide without having added volume during the cell cycle (Conlon et al., 2001).

Subsequent studies showed that the separation of Schwann cell growth and proliferation is achieved, at least in part, through differential use of distinct signalling pathways. Proliferation depends on signalling through the ERK pathway and growth depends on signalling through the PI3K/ Akt pathway (Echave et al., 2009). These effects correlate with sustained signalling through the two pathways; whereas both IGF-1 and NRG1 transiently activate ERK and PI3K/Akt/mTOR signalling to similar and robust levels, proliferation is associated with sustained signalling through the ERK pathway and cell volume addition with sustained signalling through the PI3K/Akt/mTOR pathway (Echave et al., 2009). The importance of these pathways in cell growth will be highlighted throughout this Introduction and described specifically in Section 1.7. However it is worthwhile to note at this point that the PI3K/ Akt/ mTORC1 pathway has been shown to be important for cell growth in most, if not all, systems in which it has been studied (Bohni et al., 1999, Echave et al., 2009, Gao and Pan, 2001, Kwon et al., 2001, Leevers et al., 1996, Montagne et al., 1999, Porstmann et al., 2008, Ruvinsky et al., 2005, Shima et al., 1998, Wullschleger et al., 2006).

A further example that cell growth and proliferation are independently regulated can be highlighted using the Schwann cell; although loss of the retinoblastoma protein (Rb) drives both Schwann cell growth and proliferation, the two processes can be uncoupled. Whereas blocking E2F-dependent transcription, which is the best-characterised Rb effector, is sufficient to prevent cell cycle progression, it is not sufficient to block cell growth- thus demonstrating they are independently regulated (Collins et al., 2012).

Although cell growth and division are independent processes it is clear that proliferation cannot be indefinitely separated from cell growth. At some point a cell dividing in the absence of additive growth will become too small and/

or contain insufficient functioning organelles to continue to divide. In this way, division may become dependent on growth. In line with this, haematopoietic cells that have been growth factor and mitogen starved for a number of weeks *in vitro* will take several days to re-enter the cell cycle after re-stimulation with their growth factor and mitogen, interleukin-3 (IL-3), perhaps suggesting they need to reach a minimum size/ biogenic capacity for cell cycle progression (Lum et al., 2005a).

To summarise: growth (addition of mass and volume) and proliferation (progression through the cell cycle) are distinct and separable processes, although they may often be coupled. In the Schwann cell at least, the separation of growth and proliferation is achieved in part through differential use of distinct signalling pathways; ERK drives proliferation and PI3K/ Akt drives addition of cell volume. Finally, one of the most striking differences between growth and proliferation is that whereas a cell is either in or out of the cell cycle and can survive in either context, the biogenic processes that drive cell growth must be continuously active in all cells.

1.4 Cell Growth: How is Cell Size Determined?

Organism size is determined by the balance between the rates of cell growth, division and survival (Conlon and Raff, 1999). These are separable processes that can be independently regulated, as already discussed. However, during the development of multicellular organisms they must be co-ordinately regulated in order to produce a correctly proportioned adult and this appears to be achieved, in part, through the autonomous control of tissue and organ size (Conlon and Raff, 1999, Wolpert, 2010). This can include both organ intrinsic and extrinsic (systemic) size controls. Murine thymus glands and salamander eyes and limbs are examples of organ intrinsic control; if additional of these organs are transplanted into donor animals, each will grow to its normal adult size (Metcalf, 1963, Potter and Xu, 2001). In contrast, the spleen appears to be an example of extrinsic control of organ size; when the equivalent experiment is performed with foetal spleens, the total spleen mass will equal that of one normal size adult spleen (Metcalf, 1964). The mechanism that exert organ size control are poorly understood, however recently the extracellular

ligand regulated Salvador Warts Hippo pathway has emerged as an important regulator of tissue and organ size in both *Drosophila* and mammals (Heallen et al., 2011, Lee et al., 2010, Pan, 2010, Song et al., 2010). The canonical target negatively regulated by this kinase cascade is the transcriptional co-activator Yorkie (Yki), in *Drosophila*, and Yes-associated protein (YAP) or transcriptional co-activator with PDZ-binding motif (TAZ), in mammals; phosphorylation by the upstream kinase Warts (*Drosophila*), or Lats1/2 (Mammals) excludes Yki/ YAP/ TAZ from the nucleus and can result in their ubiquitination and degradation (Pan, 2010). These co-activators promote the expression of genes regulating proliferation, e.g. cyclin E, apoptosis, e.g. DIAP1, and growth, e.g. the miRNA *bantam*, to control tissue and organ size (Pan, 2010). This thesis focuses on the mechanisms directly regulating cell growth and cell size, however it is important to remember that *in vivo* growth control, including growth factor availability, can be determined by the surrounding tissue as well as systemic delivery of extracellular factors and nutrients.

1.4.1 Proliferating cell populations

Cell size is determined by growth vs. division

The mean cell size of proliferating cell populations is determined by the balance between the rates of cell growth and cell division (Figure 1.1). If one of either of these rates is altered the mean cell size of the population will shift to a new steady state size that represents the new balance between growth rate and cell cycle time. This provides a simple mechanism to vary cell size, which is able to produce the multiple cell types of different sizes observed *in vivo*.

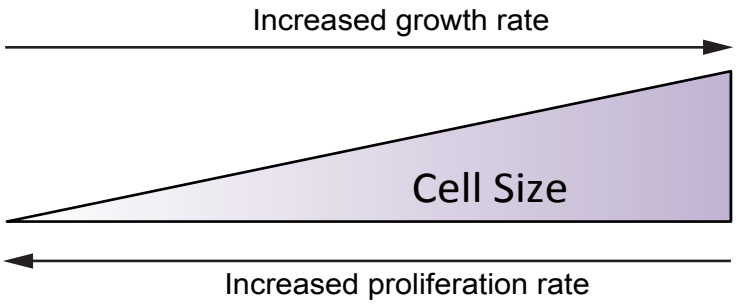

Figure 1.1 Cell growth vs. cell division

The independent regulation of cell growth and cell division provides a simple mechanism to vary cell size in vivo. A high rate of cell growth increases cell size, whereas a higher rate of cell division reduces cell size.

The ability to vary cell size by changing the balance between cell cycle time and growth rate has been demonstrated *in vitro* using the Schwann cell. In this system, increasing the concentration of the mitogen NRG1 whilst maintaining a constant concentration of the growth factor IGF-1 (and thus a constant growth rate) drives increasing rates of cell cycle progression and, as a result, a decrease in the mean cell size in the population (Conlon et al., 2001). *In vivo*, the developing *Drosophila* epidermis provides a similar example, demonstrating the physiological relevance of this mechanism. In this tissue, temporally regulated signalling from mitogens (ecdysone and, later, the Epidermal Growth Factor Receptor) and growth factors (insulin) means this tissue undergoes an initial period of cell growth in the absence of cell division, followed by a reciprocal period of division in the absence of growth before, finally, the two processes become coupled (Ninov et al., 2009). As a result cell size changes as the epidermis develops.

Moreover, multiple genetic studies have demonstrated that cell growth does not usually depend on cell-cycle progression. Movement through the cell cycle in eukaryotic cells is driven by cyclin-dependent kinases (CDKs), which are regulated by a number of positive (e.g. cyclins) and negative (e.g. CDK inhibitory kinases) signals. This controls the ordered transition from one cell cycle phase to the next (G1 to S to G2 to M phase). Numerous studies have provided examples where the cell cycle is arrested- as a result of disruption to cell cycle machinery- but cell growth continues (Johnston et al., 1977, Jorgensen and Tyers, 2004, Neufeld et al., 1998). In the budding yeast *Saccharomyces cerevisiae*, for example, the Cln cyclins (Cln1, 2 and 3) are

major regulators of the G1-S phase transition and loss of these genes blocks cell cycle progression (Cross, 1990, Nash et al., 1988, Richardson et al., 1989). However, cell growth continues. Similarly, in the *Drosophila* wing, loss of dE2F- a transcription factor that drives entry into S phase from G1- or overexpression of the dE2F inhibitor dRBP (drosophila retinoblastoma protein) blocks cell cycle progression but not cell growth (Neufeld et al., 1998). In both examples, because cell growth continued in the absence of cell division, cell size increased. Similarly, accelerating rates of cell division by disrupting negative regulators of the cell cycle does not necessarily accelerate growth rate. Dominant mutations in the Cln cyclins in *S. cerevisiae*, or overexpression of dE2F in the *Drosophila* wing decrease cell size by enhancing rates of cell cycle progression without significantly affecting cell growth rates (Hadwiger et al., 1989, Neufeld et al., 1998, Sudbery et al., 1980).

Nonetheless, parts of the cell cycle machinery can regulate both cell cycle progression and growth, which may be a way to couple the two processes during the proliferative expansion of certain tissues *in vivo,* when large numbers of homogenous cells need to be produced (Fero et al., 1996, Kiyokawa et al., 1996, Nakayama et al., 1996). Mice that have lost the cell-cycle inhibitor P27 (a CDK inhibitor), for example, are significantly larger than their wild type counterparts as a result of excessive proliferation, coupled with enhanced cell growth. The effect is dose dependent as heterozygous mice are sized midway between the wild type and knockout mice and, similarly, the organs most affected by the loss are those that express P27 most highly. It is not clear whether cell autonomous growth and division rates are elevated in the absence of P27, or whether cell growth and division simply persists for longer. The above example notwithstanding, like cell cycle rates, cell growth can be accelerated without a corresponding acceleration in proliferation. In the *Drosophila* wing disc, for example, overexpression of the critical regulators of cell growth dAkt or dMyc increases cell and organ size without affecting cell cycle progression (Edgar, 1999, Johnston et al., 1999, Verdu et al., 1999).

Interestingly, although cell growth does not usually require cell cycle progression, growth rates can be affected by cell cycle position. Studies in fission yeast (*Schizosaccharomyces Pombe*), budding yeast (*S. cerevisiae*) and mammalian cells have demonstrated that growth rate varies with cell cycle

phase (Bryan et al., 2010, Goranov and Amon, 2010, Son et al., 2012, Tzur et al., 2009). In mammalian transformed lymphoblasts and IL3-dependent B cells (FL5.12 cell line), G1 growth rates are initially slow and then accelerate rapidly, before slowing during S phase and again at the G2-M transition (Son et al., 2012, Tzur et al., 2009).

So, although the rates of cell growth and division can be independently regulated, in some situations the two processes are interdependent. Linked to this, a highly controversial area of research in the cell growth and proliferation field has been whether there is control of cell size at division in any one dividing cell population. This is the so-called 'Cell Size Checkpoint' debate.

The 'Cell Size Checkpoint' debate

If there is a 'Cell Size Checkpoint', it is adaptable and therefore does not appear to be intrinsically determined. This is because, as described above, changing mitogen and/ or growth factor concentration in mammalian cells can change cell size. Similarly, increasing nutrient availability- the primary determinant of yeast growth and division rates- increases yeast cell size (Jorgensen and Tyers, 2004).

The requirement for a 'Cell Size Checkpoint' centres around whether the independent regulation of cell growth and cell division is sufficient to maintain the control of cell size in proliferating populations, or whether a mechanism must be invoked to ensure a cell only divides when it has reached a certain threshold size. Essentially, whether cell growth (growth rate and/ or cell size) must regulate cell-cycle progression to control cell size at division. To explain this further: consider a steady state proliferating population. It has a constant mean cell size. To maintain this stationary state each cell must approximately double its mass and volume before dividing. However, there is inevitably variability in cell size about the mean across the population. This means there are some smaller cells and some larger cells. The theoretical requirement, or not, for a Cell Size Checkpoint rests on whether cell growth rates are size dependent (so-called 'exponential' growth). Specifically, whether larger cells grow faster than smaller cells. If they do and there is no control over cell size at division then, because there is variation in cell size within a population, the largest cells would become ever larger than the smallest cells because they

would grow at increasingly faster rates. This would cause cell sizes in the population to become increasingly divergent. Therefore, if cell growth rates are cell size dependent then maintenance of a constant mean cell size and size distribution in the population requires a cell intrinsic ‘Cell Size Checkpoint’ that ensures a cell divides when, and only when, it reaches a specified size. In this way cells that are smaller at the start of G1 will more than double their mass before dividing, whereas cells that are larger would less than double their mass.

In contrast, if cell growth rates are cell size independent (so-called ‘linear’ growth rates) then the mean and variance in cell size of the population can be maintained without the need for a size checkpoint. This is because, on average, every cell will add the same amount of mass and volume per unit time. So across each cell cycle, smaller cells will usually more than double in size and larger cells will usually less than double in size. Over time, the size of any larger or smaller cell will converge to the population mean, thus maintaining the constant mean and distribution of cell sizes in the population- without the need for an intrinsic cell size checkpoint (Figure 1.2).

Figure 1.2 Initially large and small cells converge to a common mean size if growth rates are size independent

In dividing populations, if growth rates are independent of cell size then- regardless of its starting size- each cell will add the same amount of mass and volume across each cell cycle. This means any cells that are initially larger or smaller than the mean size of the population will return to the mean size after a number of cell divisions.
The graph above shows two cells with starting sizes of 2 and 10 units (a.u.). Across each cell cycle each cell adds 5 units, before dividing to produce two daughter cells. This means, initially, the smaller cell more than doubles in size across each cell cycle and the larger cell less than doubles in size. Therefore over a number of cell divisions the size of the cells converges to a common mean (Figure adapted from Conlon and Raff, 2003).

The reasoning for larger cells having higher growth rates than smaller cells is that larger cells are likely to contain more biosynthetic machinery (e.g. ribosomes) and, as a result, carry out higher rates of synthesis and subsequent accumulation of mass. Indeed, there is evidence from a number of systems that ribosome number and the rate of protein synthesis correlates with cell size (Conlon and Raff, 2003, Dolznig et al., 2004, Elliott and McLaughlin, 1978, Moore, 1988, Popolo et al., 1982, Zetterberg and Killander, 1965b). However, larger cells may also contain more degradative machinery and therefore higher rates of degradation might balance the increased rate of synthesis (Conlon and Raff, 2003, Dolznig et al., 2004). The mechanistic relationship between synthesis, degradation and cell growth rate will be discussed in more detail in Section 1.4.3. This Section focuses on the evidence for and against size dependent cell growth rates and the existence of a Cell Size Checkpoint.

There is evidence of size dependent growth rates and a Cell Size Checkpoint in yeast (Di Talia et al., 2007, Godin et al., 2010, Johnston et al., 1977, Jorgensen et al., 2002, Jorgensen et al., 2004, Jorgensen and Tyers,

2004, Moore, 1988, Nurse, 1991, Popolo et al., 1982). Studies that have quantified cell growth rates at the single cell level- measuring the increase in buoyant mass or accumulation of a fluorescent marker of cell protein content- have demonstrated that growth rates increase as cell size increases in *S. cerevisiae* (Di Talia et al., 2007, Godin et al., 2010).

A Cell Size Checkpoint has two key features: a critical size threshold and a mechanism to sense when the critical size is reached. In *S. cerivisiae*, the size threshold exists at the end of G1, prior to the onset of S phase (at the 'Start', or 'Restriction point', where the cell commits to cell cycle entry) (Johnston et al., 1977). The threshold appears to be set- at least in part- by nutrient driven ribosome biogenesis, which negatively regulates progression through Start (Figure 1.3) (Jorgensen et al., 2002, Jorgensen et al., 2004, Jorgensen and Tyers, 2004). In rich nutrient conditions, where rates of ribosome biogenesis are high, there is a strong repression of Start and cells must reach a larger cell size before this repression is overcome and they pass through Start (Jorgensen and Tyers, 2004). Disrupting signalling between nutrients and ribosome biogenesis renders cell size insensitive to changes in carbon (nutrient) availability, demonstrating this mechanism is essential to determine the correct nutrient regulated size threshold (Jorgensen et al., 2004, Jorgensen and Tyers, 2004). It remains to be elucidated how ribosome biogenesis negatively regulates Start.

What proxy of cell size do yeast measure to know when the critical size threshold has been reached? If cells are treated with sublethal doses of the protein synthesis inhibitor cycloheximide they grow to a bigger size and accumulate more ribosomes before they pass the threshold ('Start'). This may suggest they 'monitor' the rate of protein translation (or a consequence of protein translation, e.g. accumulation of a cell cycle regulator) to control entry through Start (Figure 1.3) (Jorgensen and Tyers, 2004, Moore, 1988, Popolo et al., 1982).

Figure 1.3 Nutrient regulated ribosome biogenesis determines the critical size threshold to pass Start
Schematic demonstrating how ribosome biogenesis sets the critical size threshold and the cell senses protein synthesis as a proxy of cell size: Nutrients promote ribosome biogenesis, in part via activation of the putative transcription factor Sfp1 and the kinase Sch9. This represses entry into S-phase (progression through Start) by an unknown mechanism and sets the critical size threshold; because the more nutrients available, the greater repression of Start. Downstream of ribosome biogenesis, protein synthesis rate increases. This promotes progression through Start, possibly as a result of accumulation of activator(s) of cell cycle progression. At a certain point this becomes sufficient to overcome the repression of Start, Cln3 will be activated and Cln3 drives progression through Start. Modified from Jorgensen & Tyers, 2004.

Recently, a distinct Cell Size Checkpoint Mechanism based on a geometric measure (cell length) has been described in the fission yeast, *Schizosaccharomyces Pombe.* These rod-shaped cells grow by distal extension and, in wild type nutrient rich conditions, divide when they have grown to a length of 14μm. This cell size threshold is controlled by a spatial gradient of the mitotic inhibitor Pom1 kinase that extends from the cell tips, where Pom1 is localised, to the middle of the cell, where the mitotic targets of Pom1 are found (Figure 1.4) (Martin, 2009, Martin and Berthelot-Grosjean, 2009, Moseley et al., 2009, Pan and Chang, 2009). When the cell has elongated such that Pom1 concentration at the centre reaches a critical low, Pom1's target, the kinase Cdr2, is no longer inhibited. Active Cdr2 inhibits Wee1 and thus releases the cyclin-dependent kinase Cdk1 from inhibition by Wee1. Cdk1 then drives mitotic

entry (Figure 1.4 B). It is not yet understood how Pom1 inhibits Cdr2- whether Pom1 phosphorylation inhibits Cdr2 activity, or whether Pom1 regulates Cdr2 localisation and interaction with Wee1 (Martin, 2009, Martin and Berthelot-Grosjean, 2009, Moseley et al., 2009, Pan and Chang, 2009). This cell length checkpoint mechanism does not exclude the possibility that there is also a link to ribosome/ protein synthesis rates in *S. pombe*.

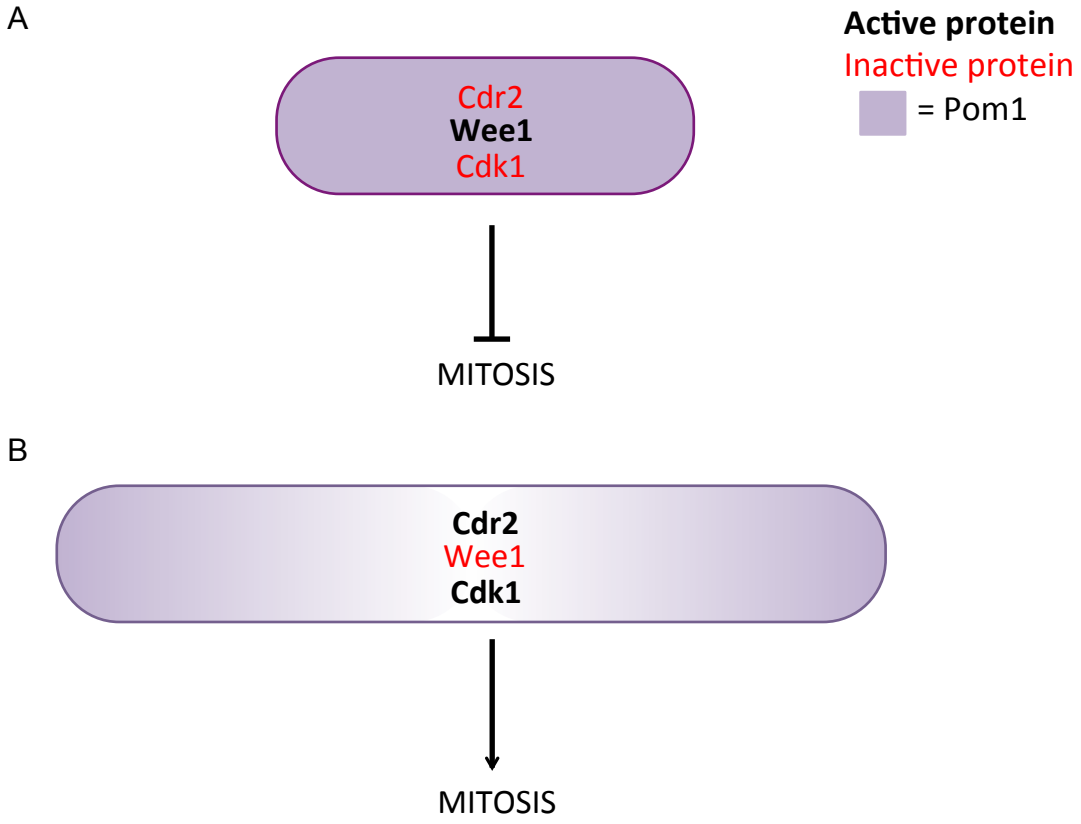

Figure 1.4 A spatial gradient of Pom1 extends from the distal tips of the cell to the cell centre and inhibits mitotic entry

A) In short cells, a gradient of Pom1 located at the distal tips extends to the centre of the cell and is sufficiently strong to inhibit Cdr2. Therefore Wee1 is active and inhibits mitotic entry by phosphorylating and inhibiting the cyclin-dependent kinase Cdk1.
B) When cell length increases, the concentration of Pom1 at the centre of the cell is no longer sufficient to inhibit Cdr2. Active Cdr2 inhibits Wee1, Cdk1 is active and mitosis proceeds.

Whilst there is clear evidence for cell size dependent growth rates and a Cell Size Checkpoint in yeast, in mammalian cells the issue remains controversial (Conlon et al., 2001, Dolznig et al., 2004, Echave et al., 2007, Fantes and Nurse, 1977, Godin et al., 2010, Tzur et al., 2009). Early work suggested that the rate of cell growth increased across G1 (Anderson et al.,

1969, Elliott and McLaughlin, 1978, Killande.D and Zetterbe.A, 1965a, Killande.D and Zetterbe.A, 1965b, Zetterberg and Killander, 1965a). Although this might reflect size dependent growth rates, it is also possible that growth rates are simply regulated by cell cycle stage, independent of cell size. Recent studies from the Manalis and Kirschner groups have demonstrated, using independent methods, that the growth rate of mouse haematopoietic cells appears to be size dependent (Godin et al., 2010, Son et al., 2012, Tzur et al., 2009). The Manalis group quantified the buoyant mass of single cells of different sizes over time and found cell growth rate increased with cell size, i.e. growth was exponential (Godin et al., 2010, Son et al., 2012). The Kirschner group derived lymphoblast growth rate as a function of cell size from cell populations using a mathematical model proposed by Collins and Richmond in 1962 (Tzur et al., 2009). So, whereas the Manalis group quantified the growth rate of single cells, the Kirschner group used the size behaviour of cell populations to determine the relationship between cell size and growth rate. Both groups reached the same conclusion: cell growth rate increased with cell size.

If mammalian growth rates are size dependent, as suggested by these studies, this implies there must be a Cell Size Checkpoint. Interestingly, several studies have shown that the variation in cell size (volume or mass) in cell populations decreases just prior to the onset of S phase, suggesting that the size of the cells entering S phase is regulated- consistent with a Cell Size Checkpoint (Killande.D and Zetterbe.A, 1965a, Killande.D and Zetterbe.A, 1965b, Son et al., 2012). Most interestingly, the recent findings of Son et al suggest a possible mechanism by which cells sense when the critical size threshold is reached. They find that the variation in growth rate (increase in mass per unit time) in both mouse lymphoblasts and IL-2 dependent B cells (FL5.12 cell line) constricts to an even greater degree than cell size before cells enter S phase (Son et al., 2012). This suggests the cells might monitor growth rate (or a consequence of growth rate) as a proxy of cell size to regulate entry into S phase, implying that the mechanism may be similar to that in *S. cerevisiae*, which appears to monitor protein synthesis rate (Jorgensen and Tyers, 2004, Moore, 1988, Popolo et al., 1982).

However, in contrast to haematopoietic cells, evidence suggests Schwann cell growth rates are independent of cell size (Conlon and Raff, 2003). Conlon and Raff used Schwann cells that were cell cycle arrested in early S phase using the DNA polymerase α inhibitor aphidicolin to study rates of cell growth independent of cell division and in the absence of confounding effects of cell cycle stage on growth rates. They found that the increase in cell volume and protein mass of cells growing in the presence of serum was independent of cell size: cell volume and protein mass increased linearly over a five-fold increase in cell volume measured across 5 days in continuous culture. As shown in Figure 1.2, if growth rates are size independent- as suggested by this study- there is no need for a Cell Size Checkpoint to maintain constant mean cell size in proliferating populations.

It is possible that in some cell types cell growth rate is size dependent, e.g. lymphoblasts, and in other cell types it is not, e.g. Schwann cells. It may be relevant that the lymphoblasts and B cells in which size dependent growth rates were quantified were transformed or immortalised, whereas the Schwann cells are primary cells. It is also possible that the findings of the Schwann cell study reflect the cell cycle stage at which the cells were arrested. Given that the cells are arrested at the onset of S phase and that Son et al propose that growth rates of cells of different sizes converge at the G1-S transition (i.e. growth rates become somewhat uncoupled from cell size), it is interesting to speculate whether the lack of correlation between Schwann cell size and the rate of mass and volume addition was because the cells were arrested at a point where rates of cell growth are largely uncoupled from cell size. Further work is required to clarify the relationship between cell size and growth rates in mammalian cells.

The existence of a mammalian Cell Size Checkpoint has also been investigated using an alternative approach that is not based on quantifying the relationship between growth rate and cell size. Such studies used so-called ‘Switch’ experiments, where cells are switched between a condition where growth and division rates were slower and cells were smaller and a condition where growth and division rates were faster and cells were larger (the increase in growth rate was greater than the increase in division rate and hence cell size increased) (Conlon and Raff, 2003, Dolznig et al., 2004, Echave et al., 2007). If a Cell Size Checkpoint exists, the constraints of such a checkpoint mean the

new size should be achieved in one cell cycle. This means that when cells are switched up from the ‘slow’ to the ‘fast’ condition, the first cell cycle in the ‘fast’ condition should be elongated as the cells have to more than double their size to reach the new larger size threshold. Conversely, when cells are switched down from the ‘fast’ to the ‘slow’ condition, the first cell cycle in the ‘slow’ condition should be shortened as cells reach the size threshold before they have doubled in size. In contrast, if there is no Cell Size Checkpoint, in both cases, the cell growth and division rates should rapidly switch to those of the new condition and cell size will gradually adjust to the new mean size over a number of cell cycles. Figure 1.5 shows the difference between cell behaviour in a switch down if there is (Figure 1.5 A) and is not (Figure 1.5 B) a Cell Size Checkpoint.

Figure 1.5 The effect of a ‘switch-up’ to an increased growth and division rate on subsequent cell cycle length in the presence and absence of a Cell Size Checkpoint

A) In the presence of a Cell Size Checkpoint, switching cells up to a higher growth and division rate with a larger mean cell size will increase the length of the first cell cycle to adjust the cell to the new size within one cell cycle.
B) If there is no Cell Size Checkpoint, cells will rapidly switch up to the new higher growth and division rates and cell size will adjust slowly to the new larger mean cell size over a number of cell cycles. Modified from Echave et al. 2007.

However, these studies have also yielded conflicting findings. In the Schwann cell, consistent with the Schwann cell growth rate study, there is no evidence to support a Cell Size Checkpoint (Conlon and Raff, 2003, Echave et al., 2007). When cells are switched up or down their growth and proliferation rates rapidly change in response to changes in the strength of the growth factor and mitogenic signals, whereas cell size takes several cell divisions to adjust to the new mean size (Echave et al., 2007). In contrast, Dolznig et al found that, when erythroblasts are switched down, the duration of the first cell cycle in the new condition is shortened and so cell size is rapidly reduced within one cell cycle- suggesting the existence of a Cell Size Checkpoint (Dolznig et al., 2004). It must be noted that the difference in cell size between the 'slow' and 'fast' growth conditions were smaller in this study than in the Schwann cell studies and could be adjusted across one cell cycle with or without the existence of a Cell Size Checkpoint. In addition, Dolznig et al used inhibitors to slow rate of cell cycle progression and transformed cells to increase the rate of cell cycle progression. These factors may have influenced the findings of this paper. Based on these growth rate and switch studies, it remains unclear whether mammalian cell growth rates are size dependent and whether, or not, there is a mammalian Cell Size Checkpoint.

To summarise: Mean cell size in proliferating cell populations is determined by the balance between rates of cell growth and division, which can be independently controlled. It is not clear whether steady state proliferating mammalian cell populations also require an intrinsic 'Cell Size Checkpoint' that regulates cell size at division in order to maintain a constant mean cell size and size variance in the population. There is evidence to suggest a checkpoint exists in proliferating yeast populations.

1.4.2 Non-Dividing cell populations

Determining cell size

Although many cell types undergo extensive post mitotic growth (the most notable examples being skeletal muscle, neurons and myelinating Schwann cells) sooner or later non-dividing mammalian cells attain a final cell size. This size is often maintained for long periods of time, sometimes even for

the remainder of the organism's lifetime. The question is, how does a cell 'know' when to stop growing- in other words, how is final cell size determined?

The mechanisms regulating this are largely poorly understood, however in some cell types, it has been shown that the amount of growth factor signal a cell receives determines final cell size. This is nicely demonstrated during the development of the peripheral nervous system. Myelinating Schwann cells associate with axons in a 1:1 ratio and ensheath the axon in multiple layers of myelin membrane, forming the myelin sheath. The thickness of the sheath, and therefore the radial growth, of the Schwann cell is determined by the amount of growth factor (NRG1 Type III) expressed on the cell surface of the ensheathed axon (Michailov et al., 2004, Taveggia et al., 2005). Larger calibre axons produce more NRG1 Type III and, as a result, are surrounded by a thicker myelin sheath and therefore a larger Schwann cell (Figure 1.6). This is an adaptive response because larger axons require a thicker myelin sheath for efficient axonal signal transduction. Proving that it is the amount of growth factor that determines final Schwann cell size, experimentally manipulating NRG1 Type III signalling during myelination is sufficient to change the final size of the myelin sheath and the Schwann cell *in vitro* and *in vivo* (Garratt et al., 2000a, Garratt et al., 2000b, La Marca et al., 2011, Michailov et al., 2004, Taveggia et al., 2005). It seems to be the amount of axonal NRG1 Type III and not the availability of the receptor on the Schwann cell that is limiting *in vivo*, because mice heterozygous for neuronal NRG1 display hypomyelination, whereas mice heterozygous for the ErbB2 subunit of the NRG1 receptor, the heterodimeric ErbB2/ErbB3 receptor, in the Schwann cell have normal myelination (Michailov et al., 2004). NRG1 signalling and therefore Schwann cell size is further modified by the activity of BACE1 and TACE, two proteases that activate and inactivate, respectively, NRG1 by cleaving distinct sites in the extracellular domain of the growth factor (Hu et al., 2008, Hu et al., 2006, La Marca et al., 2011).

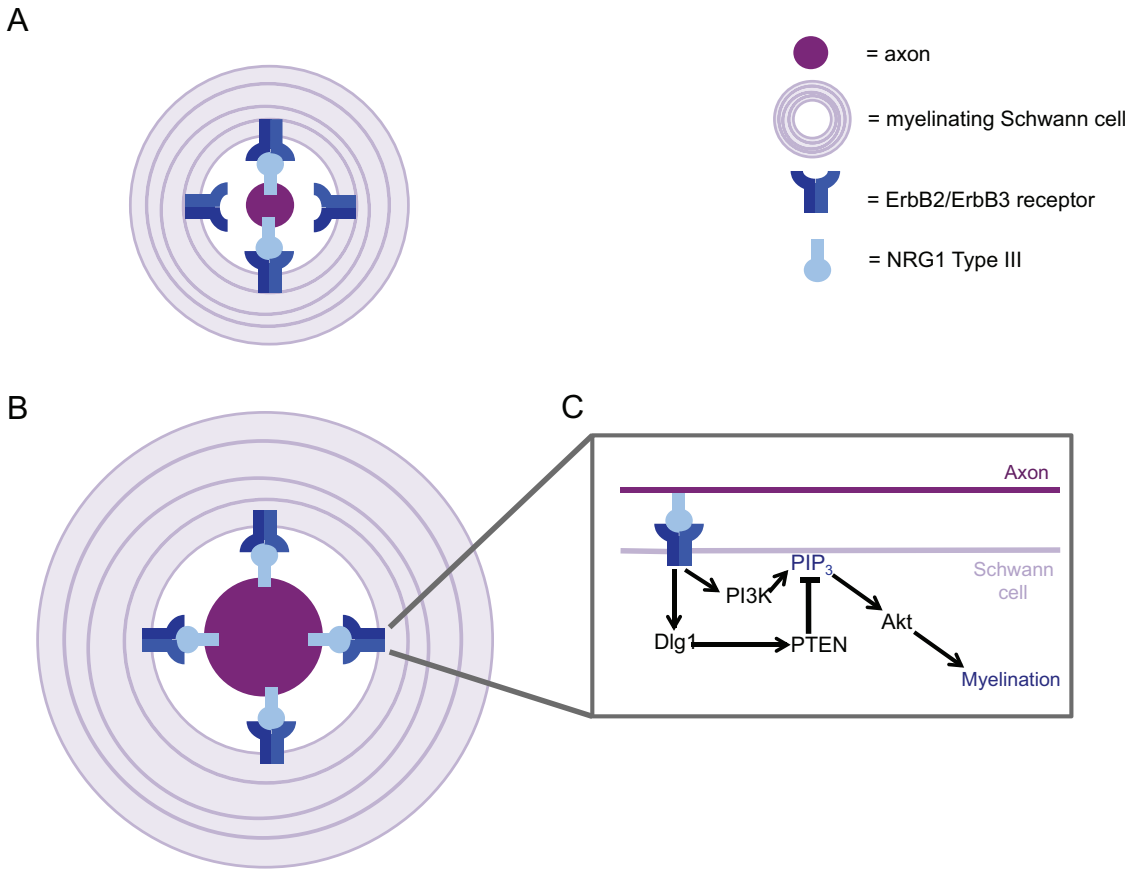

Figure 1.6 The level of NRG1 Type III growth factor signalling determines myelinating Schwann cell size through positive and negative regulation of the biogenic Akt pathway

NRG1 Type III expressed by axons determines the thickness of the myelin sheath and, consequently, final Schwann cell size. This is achieved, at least in part, because the NRG1 regulates both activation and attenuation of Akt signalling, which is necesary for myelination. The schematic shows how the level of axonally expressed NRG1 Type III regulates the thickness of the myelin sheath:
A) Small calibre axons express low levels of NRG1 Type III resulting in relatively low level myelination and, consequently, a smaller Schwann cell.
B) Large calibre axons express high levels of NRG1 Type III resulting in more extensive myelination and a larger Schwann cell. Signalling pathways involved in the control of myelination downstream of NRG1 Type III are depicted.

The mechanism by which NRG1 Type III controls Schwann cell size is not fully understood, however evidence suggests it is achieved in part by the dual regulation of both positive and negative regulators of the biogenic PI3K/ Akt/ mTORC1 pathway. So, NRG1 Type III not only activates this pathway, but also stabilises the lipid phosphatase PTEN (phosphatase and tensin homolog deleted on chromosome 10), a negative regulator of Akt activation, by stabilising the PTEN scaffold Dlg1 (discs like homolog 1) (Figure 1.6) (Cotter et al., 2010, Macklin, 2010, Maurel and Salzer, 2000). Both the positive (Akt/ mTORC1) and negative (Dlg1/PTEN) signals are critical for attaining the correct final Schwann cell size (Goebbels et al., 2010, Sherman et al., 2012).

Presumably growth is attenuated and final cell size attained when the activity of PTEN becomes strong enough to suppress Akt activation (Macklin, 2010). Interestingly, Akt/ mTORC1 may not be the only effector downstream of PTEN that drives cell growth as expression of constitutively active Akt in Schwann cells does not drive hypermyelination, whereas loss of PTEN does (Flores et al., 2008, Goebbels et al., 2010). How a stronger NRG1 signal drives greater and/ or more sustained growth before the inhibitory effect of PTEN blocks further growth is not clear.

This is not the only reported example of a growth factor determining final cell size. Nerve Growth Factor (NGF) controls sympathetic neuron size. These neurons extend, often very long, axons to innervate their target tissue. Although it is target innervation that inhibits further axonal extension, it is the level of target derived nerve growth factor (NGF) that determines the extent of axon and dendrite branching and therefore final neuron size (Glebova and Ginty, 2004, Purves et al., 1988, Snider, 1988, Voyvodic, 1989). This can be demonstrated *in vivo*, as manipulating NGF levels results in a corresponding change in neuronal size (Purves et al., 1988).

It remains to be seen whether growth factor determination of cell size is a widespread phenomenon- certainly other signals could also determine final cell size. For example, analogous to the limiting growth factor hypothesis described above, competition for limiting nutrients may also determine cell size. Nutrient dependent regulation of cell growth will be discussed further in Sections 1.8. In addition, extrinsic mechanical forces exerted on a cell can also determine cell size. This may occur in the form of compressive and extensive forces from surrounding tissue; these forces inhibit and promote chondrocyte growth, respectively (Villemure and Stokes, 2009). In addition, shear forces from fluid flow can also negatively regulate cell growth, as is the case in kidney epithelium (Boehlke et al., 2010). In kidney epithelial cells shear stress, sensed by the primary cilia (ubiquitous mechanosensory organelles). This activates AMP-Activated Protein Kinase (AMPK), which inhibits mTORC1 and, as a result, inhibits further cell growth and therefore determines final cell size. In the kidney fluid flow rate is determined by tubule geometry and is important for maintaining efficient filtration of the blood. Therefore, the authors speculate that having cell

growth (and therefore tubule geometry) determined by shear stress, i.e. fluid flow rate, helps ensure optimal blood filtration.

Growth factors, nutrient levels and extracellular mechanical forces are all examples of how cell extrinsic factors can determine final cell size. However final cell size can also be determined by cell intrinsic mechanisms. For example, cell ploidy is directly correlated with cell size in all organisms where it has been studied (Fankhauser, 1945, Henery et al., 1992, Flemming et al., 2000, Nurse, 1985). In some cases this relationship is causal; manipulating ploidy in murine embryonic cells, salamander larval cells and the hyopdermis of the nematode *Caenorhabditis elegans* induces a corresponding change in cell size, for example. Increasing ploidy is not universally sufficient to increase cell size, however. In the naturally polyploid cells of the *Drosophila* muscle wall and nematode hypodermis for example, endoreplication is necessary but not sufficient to drive cell growth (Demontis and Perrimon, 2009).

Maintaining cell size

It is clear that several factors can determine and influence final cell size in non-dividing cells. Ultimately final cell size is attained and maintained when the rates at which the cell is accumulating/ synthesising material equals the rate at which material is degraded/ lost. This means the signal(s) that determine cell size must, directly or indirectly, regulate the rates of these processes so that they become equal. Irrespective of whether growth factors determine final cell size, both cell growth and maintaining mammalian cell size usually require the presence of a growth factor signal. One of the primary reasons for this is that growth factor activated pathways are required to maintain sufficient nutrient uptake to sustain cell metabolism. In the absence of a growth factor signal, cells undergo autophagy to provide the energy and substrates to prolong survival and, as a result, atrophy (Conlon and Raff, 1999, Echave et al., 2007, Edinger and Thompson, 2002, Franklin and Johnson, 1998, Kirkland and Franklin, 2007, Lum et al., 2005a, Vander Heiden et al., 2001).

It is not clear if the growth factor signal to maintain cell size must be as strong as it was during the preceding period of additive growth- given that maintaining hyperactive growth factor signalling can cause cell hypertrophy in a number of systems (Adams and McCue, 1998, Barton-Davis et al., 1998, Flores

et al., 2008, Goebbels et al., 2010, Lupu et al., 2001, Musaro et al., 2001, Musaro et al., 1999, Porstmann et al., 2008, Purves et al., 1988, Walenkamp and Wit, 2007). Furthermore, in some cases the signal to maintain cell size seems to be distinct from the signal that drives the preceding cell growth. In myelinating Schwann cells, for example, disrupting NRG1/ ErbB signalling (the signal that determines cell size) in the adult after myelination is complete and Schwann cells have attained their final size has no effect on myelin sheath thickness and Schwann cell size (Atanasoski et al., 2006, Fricker and Bennett, 2011, Fricker et al., 2011, Garratt et al., 2000a, Garratt et al., 2000b, Michailov et al., 2004). Moreover, inhibition of PI3K in myelinated cultures *in vitro* does not induce demyelination, suggesting the intracellular signalling pathways that regulate myelin sheath growth and size homeostasis may also be distinct (Maurel and Salzer, 2000). What signal maintains cell size homeostasis in the adult Schwann cell is not clear.

In a subset of *Drosophila* neurons (class IV dendritic arborisation neurons), signals important for maintenance of dendrite size have been elucidated (Emoto et al., 2006, Parrish et al., 2007). In these cells the kinase Hippo (Hpo) regulates both cell growth and subsequent cell size homeostasis, but through distinct downstream effectors (inhibition of the transcriptional co-activator Yorkie and activation of the Polycomb repressor complex, respectively) (Emoto et al., 2006, Parrish et al., 2007). Hippo signalling negatively regulates growth and, consistent with this, loss of Hippo during development is associated with increased branching and crossing of dendrites in these cells (Emoto et al., 2006, Pan, 2007). However, in the mature neuron dendrites are not maintained if Hippo signalling is lost (Emoto et al., 2006, Parrish et al., 2007). Interestingly, loss of Hippo signalling has no effect on axon maintenance in these same neurons, indicating it cannot be the only pathway that regulates size maintenance (Emoto et al., 2006). Further studies in other cell types are required to determine, first, whether distinct signalling pathways are commonly used for cell growth vs size maintenance and, second, whether Hippo/Warts signalling (and it's homologues in other systems) is a common regulatory mechanism for cell size maintenance and what other signalling pathways also regulate size homeostasis in different contexts.

Changing cell size

Although many non-dividing adult cells can maintain cell size homeostasis for long periods of time, this does not mean they are no longer receptive to physiological growth stimuli. Skeletal and cardiac muscle cells remain incredibly plastic throughout life and grow/ atrophy in response to stimuli such as mechanical load and innervation. In skeletal muscle there is some understanding of how these signals regulate protein synthesis and degradation to regulate cell growth/ atrophy. Reduced mechanical load, i.e. inactivity, or denervation leads to skeletal muscle atrophy, primarily through an increase in proteasome dependent protein degradation (Bodine et al., 2001a, Jagoe and Goldberg, 2001, Medina et al., 1995). Although mechanical load (resistance exercise) drives muscle hypertrophy, interestingly, during exercise protein synthesis is depressed and there is net loss of mass (Dreyer et al., 2006, Williamson et al., 2006). After exercise both protein synthesis and protein degradation rates increase, but the increase in synthesis is greater and more prolonged than the increase in degradation and therefore muscle mass increases (Biolo et al., 1995). Muscle hypertrophy and atrophy (and protein synthesis and degradation) are correlated with activation of IGF-1/ PI3K/ Akt and mTORC1 signalling in the muscle (Baar and Esser, 1999, Dreyer et al., 2006, Williamson et al., 2006, Sacheck et al., 2004, Sandri et al., 2004, Stitt et al., 2004, Gulve and Dice, 1989, Zdanowicz et al., 1995). Forced activation of this pathway drives hypertrophy and prevents atrophy (Barton-Davis et al., 1998, Bodine et al., 2001b, Glass, 2003, Lai et al., 2004, Musaro et al., 2001, Rommel et al., 2001). Akt inhibits protein degradation through inhibition of the ubiquitin ligase (Atrogin-1) that labels proteins for proteasome mediated degradation (Sacheck et al., 2004, Sandri et al., 2004, Stitt et al., 2004).

The regenerative capacity of the peripheral nervous system (PNS) after injury is another very good example of cells that retain the capacity to grow throughout life. Following nerve injury and separation of the axon from its target, cell growth is reactivated to drive axon extension to re-innervate the target and achieve functional recovery. This regenerative growth depends on the activity of the kinase mTORC1 (Section 1.7). Axonal outgrowth is enhanced when mTORC1 activity is increased and, reciprocally, is partially blocked if mTORC1 is inhibited (Abe et al., 2010). Most interestingly, the lack of regenerative

capacity in the central nervous system (CNS) seems to be, in part, due to the inability to reactivate mTORC1 in neurons after injury; in fact, forced activation of mTORC1 in CNS neurons after injury promoted regenerative growth (Liu et al., 2010, Park et al., 2008). Interestingly, the findings of Abe *et al* also highlight the importance of appropriate inactivation of regenerative growth- as continued mTORC1 hyperactivity drives axonal hypertrophy and incorrect target innervation *in vivo* (Abe et al., 2010). These examples highlight that although adult cells may have reached and maintain cell size homeostasis, sometimes for long periods of time, many remain receptive and responsive to growth stimuli.

1.4.3 Cell size, growth rates and the underlying rates of synthesis and degradation

How do growth factors drive growth and set cell size? Cell growth occurs when rates of synthesis exceed rates of degradation of cell material. As described in Section 1.4.1, cell growth rates may be cell size dependent or independent. These two modes of cell growth will require different regulation of synthetic and degradative rates- although it is not understood how this is achieved, it is possible to model possible mechanisms (Figure 1.7).

If cell growth rates are cell size independent the simplest situation would be for a growth stimulus, e.g. a growth factor, to 'set' a rate of synthesis and a rate of degradation that do not change with cell size (Figure 1.7 A i). However, experimental evidence suggests that, at least for cell protein, this model is unlikely. Conlon & Raff found that although the rate of cell volume addition during Schwann cell growth is cell size (volume) independent, rates of both protein synthesis and protein degradation increase as cell size increases (Conlon and Raff, 2003). For this to give a size independent growth rate, the rate of synthesis and degradation must increase by the same absolute amount per unit increase in cell size.

If cell growth rates are positively size dependent, so larger cells grow faster than smaller cells, the rate of synthesis must increase faster than the rate of degradation as cell size increases. Demonstrated in Figure 1.7 are growth rates that increase linearly with cell size, which was the relationship Godin et al observed for *E. coli, S. cerevsiae* and mammalian lymphoblasts (Godin et al.,

2010). However other relationships are possible- growth rates may increase exponentially with increases in cell size, for example. Several mechanisms are possible to achieve the linear, size dependent growth rate shown in Figure 1.7. Rates of degradation may remain unchanged, whilst rates of synthesis increase with cell size (Figure 1.7 B i). Alternatively, both may increase but the increase in synthetic rate is greater than the increase in degradation rate (Figure 1.7 B ii). An interesting third possible mechanism is that the fold-change in each rate per unit increase in cell size is equivalent (Figure 1.7 B iii). In this case, because the rate of synthesis exceeds the rate of degradation at any size, an equivalent fold-change in both rates means the rate of synthesis increases by a greater absolute amount than the rate of degradation. This means that as cell size increases, the difference between the rate of synthesis and degradation, i.e. the growth rate, increases.

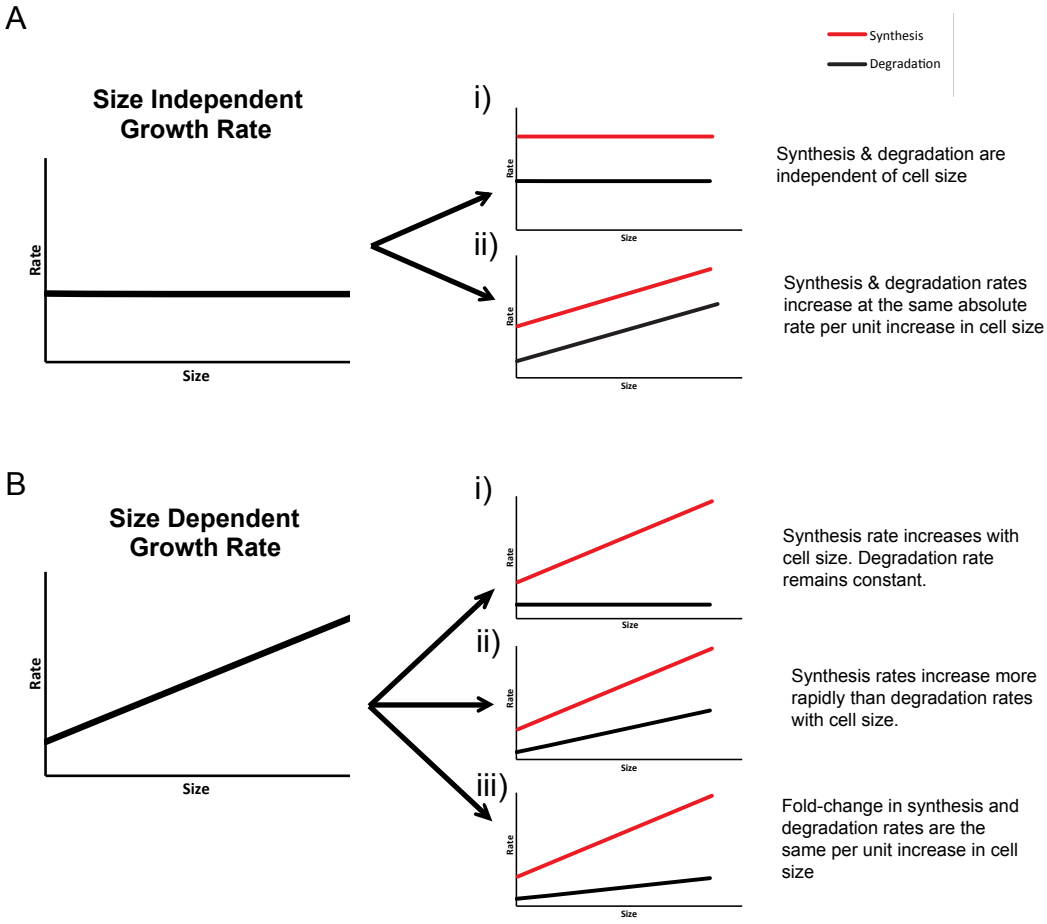

Figure 1.7 Cell growth rates are determined by the underlying rates of synthesis and degradation

Cell growth rates are determined by the underlying rates of synthesis vs degradation. Shown are possible mechanisms to ensure a:
A) Size independent growth rate.
B) Linear and positively size dependent growth rate.

Interestingly, there is evidence to suggest that protein synthesis and degradation are coupled downstream of growth factor (NGF) signals in sympathetic neurons (Franklin and Johnson, 1998, Kirkland and Franklin, 2007). In the presence of NGF, suppressing protein synthesis using mild doses of the protein synthesis inhibitor cycloheximide led to a corresponding decrease in the rate of protein degradation (Kirkland and Franklin, 2007). As a result, neurite outgrowth continued and did not slow. The authors proposed that this coupling mechanism helps ensure cell growth can be maintained at a constant rate in spite of natural stochastic fluctuations that are likely to occur in the absolute rate of both these processes.

1.5 Cell Size: Macromolecule Addition, Water Uptake & Organelle Biogenesis

The size of the cell, in other words its mass and volume, is determined by the amount of organelles and cytosol contained within the plasma membrane. Breaking this down further, cell size is largely the sum of the water and macromolecules that constitute the cytosol, organelles and plasma membrane. Therefore, to understand the control of cell growth and cell size, it is necessary to understand how biogenic stimuli regulate macromolecular and water accumulation and organelle biogenesis.

1.5.1 Macromolecule Addition: Protein

Cellular Protein

Proteins are fundamental cell macromolecules. They comprise more than 50% of the dry mass of the cell and are essential as structural elements within the cell (e.g. cytoskeletal actin), as well as being major signalling molecules and effectors for most cell functions (as enzymes- kinases, phosphatases, hydrolases and so on) (Alberts, 2002). The cell can acquire the amino acid monomers for protein synthesis by uptake of exogenous amino acids via amino acid transporters in the plasma membrane (Palacin et al., 1998). Of the 20 amino acids, 9 are essential in human cells and therefore can only be obtained in this way. The remaining 11 amino acids can be obtained by uptake or synthesised de novo from Tricarboxylic Acid (TCA) cycle intermediates in the mitochondria. In addition, amino acids released when intracellular proteins are degraded can be recycled in de novo protein synthesis. Amino acids can also be oxidised to generate cellular energy- the mechanism/ pathway by which this catabolism occurs varies depending on the amino acid (Alberts, 2002).

Protein Synthesis and Degradation

Ribosomes translate mRNA into protein by catalysing the successive addition of amino acids, via the formation of high-energy peptide bonds, to form a polypeptide chain. The translation of most mRNAs requires at least 9 eukaryotic initiation factors and involves the formation of an initiation complex at the 5'-cap of the mRNA (Jackson et al., 2010). This complex 'scans' the 5'-UTR of the mRNA until it reaches an initiation codon, at which point the remaining

ribosomal subunit joins the complex and translation begins. The translation of a fraction of mRNAs, at least in some conditions, is mediated not via this 'scanning' mechanism (Jackson et al., 2010). Instead, Internal Ribosome Entry Sites (IRES), sequences within the mRNA, directly recruit the ribosome, bypassing the 5'-cap. Translation elongation requires two elongation factors (eEF1 and eEF2) that mediate the codon-by-codon movement of the ribosome along the mRNA (Jackson et al., 2010).

Protein degradation occurs by one of two mechanisms: ubiquitin-dependent proteasomal degradation, or lysosomal degradation. A large proportion of nascent proteins are rapidly degraded by the proteasome because they have not been properly synthesised, including truncated polypeptide chains and misfolded proteins (Buchberger et al., 2010). The double-membrane bound lysosomes contain a variety of hydrolytic enzymes to catalyse the breakdown of cell components- including proteases, which hydrolyse proteins into their constituent amino acids. Lysosomes catalyse the degradation of bulk cellular components downstream of the autophagy pathway (Mizushima, 2007). In addition, certain proteins are selectively taken up and degraded by the lysosome (Dice, 1990).

Regulation of Protein Biogenesis & Cell Growth

Given that proteins are major structural, signalling and enzymatic components of the cell they are, unsurprisingly, essential for cell growth. As described in Section 1.4.2 'Changing cell size', dynamic control of protein synthesis and degradation rates downstream of growth and atrophy signals (e.g. IGF-1 and denervation, respectively) appear to underly the remarkable plasticity in skeletal muscle size (Medina et al., 1995, Sandri et al., 2004, Stitt et al., 2004, Lecker et al., 1999, Davis and Fiorotto, 2009, Kimball, 2002, Williamson et al., 2006). Moreover, cells and organisms with mutations in genes involved in protein synthesis display reduced cell growth (Grewal et al., 2005, Jorgensen et al., 2002, Jorgensen et al., 2004, Oliver et al., 2004). Simply blocking protein synthesis is somewhat of a sledgehammer approach to demonstrate the importance of protein biogenesis in cell growth, however it is effective. Protein synthesis requires a large investment of cellular energy and biosynthetic resources, which is due in large part to ribosome biogenesis. This in itself requires the coordination of all three RNA polymerases, the synthesis of

79 ribosomal proteins and the sum action of more than 200 proteins (Rudra and Warner, 2004). Rapidly proliferating HeLa cells produce ~7500 ribosomes a minute, which is estimated to require the synthesis of ~300,000 proteins, and yeast rDNA transcription is thought to constitute 60% of the total transcription in the cell (Warner, 1999, Mayer and Grummt, 2006).

With the above points in mind, it is perhaps unsurprising that global protein synthesis is tightly regulated by the factors that regulate cell growth and biogenesis. This is partly achieved by regulating the rate of ribosome biogenesis, which is closely coupled to the rate of protein synthesis in order to prevent waste of cell energy and substrates (amino acids, nucleotides e.t.c) (van Riggelen et al., 2010, Wullschleger et al., 2006, Hardie, 2011). It is also achieved through the regulation of protein translation rates, which occurs primarily at the level of translation initiation (Jackson et al., 2010). It must be noted that, in addition to the mechanisms described here that concern how global protein turnover is regulated, individual proteins are also subject to specific control of their transcription, translation and degradation rates.

Growth factors promote protein synthesis both by increasing nutrient uptake, and therefore amino acid availability, and by positively regulating ribosome biogenesis and translation initiation. One of the major effectors of growth factor activated protein synthesis is mTORC1. As already described, mTORC1 is a central regulator of cell growth and, as such, regulates many aspects of biogenesis and bioenergetics (Porstmann et al., 2009, Wullschleger et al., 2006). Protein synthesis is regulated at multiple levels by mTORC1, or its homologues in other organisms. Quantifying the rate of ^{35}S-Methionine incorporation into nascent protein in the presence and absence of mTORC1 inhibition demonstrated that loss of signalling through this pathway reduces protein synthesis, although the kinetics of this can vary in different cell types (Herbert et al., 2000, Wang et al., 2000, Hsieh et al., 2012, Thoreen et al., 2012, Thoreen et al., 2009). At the transcriptional level mTORC1 activates all three RNA polymerases, which are required for ribosome biogenesis (Mayer and Grummt, 2006, Claypool et al., 2004, Grewal et al., 2007, Guertin et al., 2006, Hannan et al., 2003, Mayer et al., 2004). At the translational level; inhibiting mTORC1 appears to supress the translation of almost all mRNAs. A subset of mRNAs are especially sensitive to mTORC1 inhibition- namely those

containing pyrimidine rich 5'-TOP, or TOP-like sequences (Hsieh et al., 2012, Thoreen et al., 2012). These genes mainly encode proteins involved in protein synthesis, including ribosomal genes, and their enhanced downregulation is likely to amplify the suppression of protein synthesis upon mTORC1 inhibition. It was thought that mTORC1 dependent control of translation was mediated by the p70 S6 Kinases (S6K), however subsequent studies did not support this and, recently it was shown that mTORC1 controls translation initiation via negative regulation of 4EBP1, an inhibitor of cap-dependent translation (Hsieh et al., 2012, Jefferies et al., 1997, Pende et al., 2004, Thoreen et al., 2012)

A number of other metabolic/ biogenic stimuli in addition to growth factors regulate mTORC1 activity, including amino acid availability; amino acid deprivation inhibits mTORC1 activation (Kim et al., 2002, Nicklin et al., 2009). This is dominant to growth factor regulation, which presumably ensures that translation does not begin when it cannot be completed due to lack of substrates and conserves a large amount of cellular resources through the particular suppression of ribosome biogenesis. In addition, amino acid deprivation also inhibits protein synthesis independent of mTORC1, by activating GCN2, an inhibitory kinase of the translation initiation factor eIF2α. Both these mechanisms are described in more detail in Sections 1.8 & 1.9, where nutrient regulation of cell growth is discussed.

In addition to mTORC1, other growth factor activated signalling pathways also regulate protein synthesis to promote cell growth (James and Zomerdijk, 2004, Roux et al., 2007, van Riggelen et al., 2010). Of particular importance, Myc dependent cell growth is characterised by an increase in protein synthesis associated with an increase in rRNA, ribosome and nucleolar density (Grewal et al., 2005, Iritani and Eisenman, 1999, Johnston et al., 1999, Kim et al., 2000, Pierce et al., 2004, Schreiber-Agus et al., 1997, Schuhmacher et al., 1999, Wu and Johnston, 2010).

As well as increasing protein synthesis, growth factors can also promote protein accumulation by suppressing protein degradation. IGF-1 drives muscle growth in part by suppressing Atrogin-1 mediated proteasome dependent degradation, downstream of PI3K/ Akt, as described in Section 1.4.2 'Changing Cell Size' (Sacheck et al., 2004, Sandri et al., 2004, Stitt et al., 2004). Although many of the biogenic effects of PI3K/ Akt are mediated by mTORC1, this

function is mTORC1 independent. Enhanced proteasomal degradation underlies muscle atrophy and Atrogin-1 knockout mice exhibit decreased atrophy after denervation, therefore suppression of this degradative pathway is likely to be an important mechanism for IGF-1/ Akt mediated muscle growth (Sandri et al., 2004, Stitt et al., 2004, Bodine et al., 2001a).

Although growth factors may suppress protein degradation rates, this does not preclude that (limited) protein degradation is necessary during cell growth- for example to clear effete proteins and organelles, preventing them accumulating and potentially inhibiting functional growth. Indeed, in skeletal muscle, inhibiting autophagy and therefore bulk degradation leads to muscle atrophy (Masiero and Sandri, 2010). The role of protein degradation in cell growth has been best studied in neuronal cells and remains controversial. Some studies found that proteasomal degradation was required for neurite outgrowth and/ or axonal extension, whereas other studies found that inhibiting proteasome dependent degradation enhanced these processes (Inoue et al., 2004, Kavakebi et al., 2005, Laser et al., 2003, Song et al., 2009, Verma et al., 2005). The conflicting findings of these studies may be explained by differences in type of neuron and/ or growth conditions, as well as the differentiation state of the cell during the study. This may indicate that cells have different requirements for degradative machinery during different stages and types of cell growth.

In summary: proteins are a major cellular macromolecule, playing essential structural and functional roles within the cell. As such, protein function is inevitably necessary for cell growth. Protein turnover is dynamically controlled downstream of positive and negative growth stimuli, two of the most notable being growth factors and amino acid deprivation, respectively. The kinase mTORC1 regulates protein biogenesis downstream of both these stimuli, although mTORC1 independent pathways are also significant. The importance of protein turnover in cell growth is particularly apparent in skeletal muscle, where the control of protein turnover is a significant determinant in the growth/ atrophy of this tissue in response to positive/ negative extracellular stimuli.

1.5.2 Macromolecule Addition: Lipid

Cellular Lipids

Lipids are a critical cell component and have numerous functions; they are the primary constituents of all biological membranes, they are the cell's major energy storage molecule, they are the basis of certain post-translational protein modifications and, finally, a number of lipids are signalling molecules. Numerous classes of lipids are found in the cell and each performs specific functions. Phospholipids form the basis of cell membranes and cholesterol, glycolipids, sphingolipids and ether lipids are all also important membrane lipids. Triacylgycerols (TAGs) and sterol esters are the main lipid storage molecules and other lipids, as well as derivatives of the aforementioned lipids, act as signalling molecules. Across these classes more than 1000 lipid species are found within the cell (Sleight, 1987). The basic building blocks of all higher order lipids are fatty acids and/ or sterols.

Lipid metabolism is very dynamic- the acyl groups of triacylglycerols and phospholipids are highly labile and undergo continual turnover and remodelling. There is also constant so-called 'futile cycling' of TAGs into free fatty acids and glycerol and back again (Watt and Steinberg, 2008). Compared to protein, where there is distinct degradative machinery, lipid breakdown is less defined- lipases facilitate remodelling, as well as complete breakdown, of lipid species. There is some evidence that the rates of phosphatidylcholine (PC) synthesis and degradation are coupled to maintain correct cellular levels of PC (Walkey et al., 1994, Baburina and Jackowski, 1999). There is also evidence that the turnover of different lipids can be coupled- namely PC and cholesterol, the two major components of the plasma membrane (Kellner-Weibel et al., 1998, Shiratori et al., 1994). This may facilitate the maintenance of correct membrane lipid composition, which is vital for proper membrane function. Changes in composition alter the physical properties of the membrane, e.g. fluidity, and this can, amongst other things, affect the organisation and function of membrane proteins (Spector and Yorek, 1985).

Several organelles play a direct role in cell lipid metabolism. Fatty acid and sterol synthesis occurs in the cytoplasm via substrates from the mitochondria and the peroxisomes. Then, the smooth endoplasmic reticulum,

lipid droplets and cis-Golgi are all sites of synthesis and modification of one or more higher order lipids. Breakdown and remodelling of phospholipids can occur in the cell membranes they are part of and triacylglycerols are broken down on lipid droplets and in the lysosome. The fatty acid precursors of higher order lipids are oxidised in the mitochondria and/ or peroxisomes, depending on the fatty acid.

Uptake of exogenous lipids

In vivo, most mammalian cells acquire most of their lipids from uptake of exogenous lipids from the circulation. In the absence of sufficient exogenous lipid, cells carry out de novo fatty acid and sterol synthesis to provide the precursors for higher order lipogenesis however, in most adult cell types the rate of de novo lipogenesis is low. Notable exceptions are adipocytes and hepatocytes, which convert excess carbohydrate from the diet into storage lipids via de novo fatty acid and sterol synthesis, and steroid-hormone producing cells, such as the testis.

Lipoproteins and free fatty acids bound to albumin are the primary circulating lipids (Shen et al., 1977, Spector et al., 1980). Circulating free fatty acids are taken up both by passive diffusion across the membrane and facilitated protein-mediated transport. Once inside the cell free fatty acids are converted with the addition of a CoA molecule and can enter metabolic and signalling pathways. Lipoproteins have a neutral lipid core, containing varying amounts of TAGs and cholesteryl esters (depending on the type of lipoprotein) and this is surrounded by a monolayer of phospholipid and cholesterol studded with apolipoproteins (Shen et al., 1977). TAGs are primarily found in Very Low-Density Lipoproteins (vLDL); cell surface lipoprotein lipases hydrolyse the TAGs at the extracellular side of the plasma membrane and a small proportion of the released fatty acids are taken up by the cell directly- the remainder become bound to albumin and continue to circulate (Goldberg et al., 2009). Cholesterol is mainly found circulating as Low-Density Lipoproteins (LDL) that are recognised by cell-surface LDL receptors (LDLR), internalised by endocytosis and delivered to the lysosome where they are hydrolysed by lysosomal lipases to release free cholesterol and fatty acids that can be used by the cell (Jeon and Blacklow, 2005).

De novo fatty acid and sterol synthesis

The carbon backbone for de novo fatty acid and sterol synthesis comes from cytoplasmic acetyl-CoA, which is derived primarily from mitochondrial citrate, a tricarboxylic acid cycle intermediate (Lynen, 1966). Fatty acid and sterol synthesis also requires reducing power, in the form of nicotinamide adenine dinucleotide phosphate (NADPH), and ATP. Citrate transporters export citrate from the mitochondria to the cytosol where it is hydrolysed to acetyl-CoA and oxaloacetate by the enzyme ATP-Citrate Lyase (ACLY). The cytosolic acetyl-CoA can then be used for fatty acid or sterol synthesis.

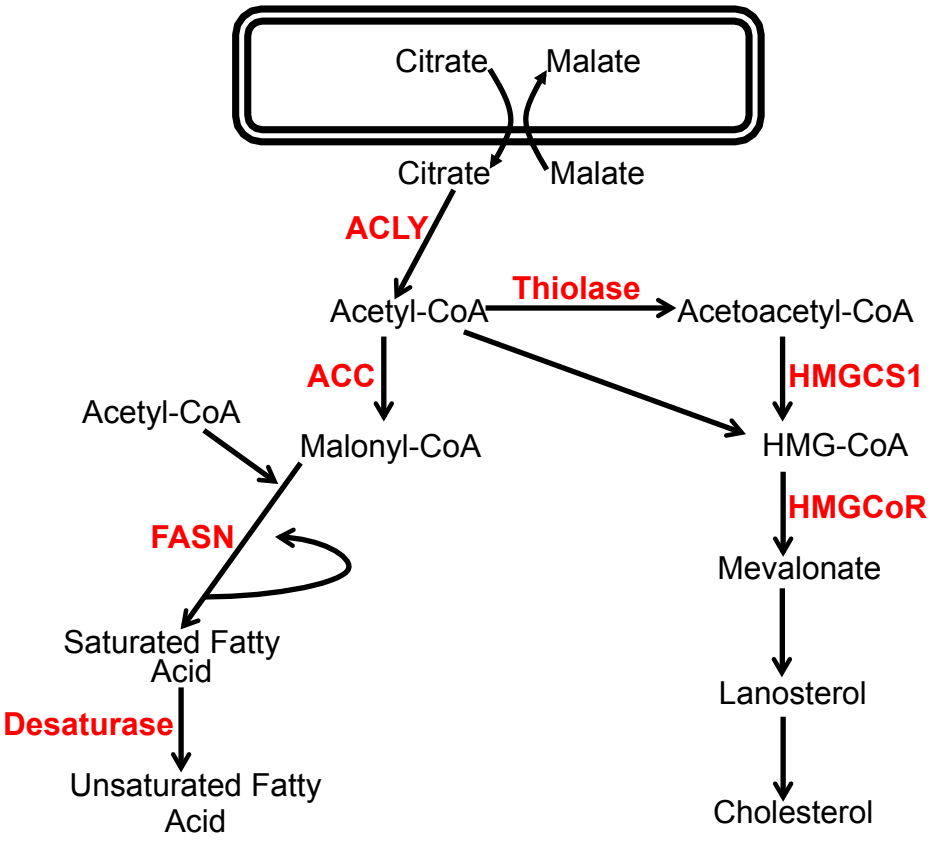

Figure 1.8 De novo fatty acid and sterol synthesis

Schematic of the de novo fatty acid and sterol synthesis pathways. Mitochondrial citrate is exported to the cytoplasm where it is converted to Acetyl-CoA, which serves as the precursor for both de novo fatty acid and sterol synthesis.

During the synthesis of fatty acids, acetyl-CoA is carboxylated to malonyl-CoA by the enzyme acetyl-CoA carboxylase (ACC); this is the committed step of fatty acid synthesis. One molecule of malonyl-CoA and one

molecule of acetyl-CoA then react in a condensation reaction catalysed by the enzyme Fatty Acid Synthase (FASN), yielding a four-carbon product. This then undergoes successive rounds of addition of the 2-carbon malonyl-CoA molecules via FASN mediated condensation reactions to yield the 16-carbon straight chain saturated (i.e. no double bonds in the carbon backbone) fatty acid palmitate (Figure 1.8) (Wakil et al., 1983). Desaturation of fatty acids occurs by desaturase enzymes.

In cholesterol synthesis one molecule of acetyl-CoA reacts in a condensation reaction with one molecule of acetoacetyl-CoA (synthesised from acetyl-CoA by the action of the enzyme thiolase) in a condensation reaction catalysed by the enzyme HMG-CoA synthase 1 (HMGCS1). This produces 3-hydroxy-3-methylglutaryl-CoA (HMGCoA), which is then reduced to mevalonate by the action of HMGCoA reductase (HMGCoR). In a series of three reactions, 6 molecules of mevalonate react to produce one molecule of lanosterol and this is then converted to cholesterol in a series of 19 reactions (Figure 1.8) (Rudney and Sexton, 1986). HMGCoR is the rate-limiting enzyme for cholesterol biosynthesis.

Regulation of de novo fatty acid and sterol synthesis

The SREBPs are basic helix-loop-helix-leucine zipper (bHLH-Zip) transcription factors (Bengoechea-Alonso and Ericsson, 2007). Two genes encode three isoforms of the protein; the SREBF1 gene encodes SREBP-1a and -1c (also known in rat as adipocyte determination and differentiation factor 1, or ADD1) that differ in their first exon as a result of alternative transcriptional start sites and the SREBF2 gene encodes SREBP-2 (Bengoechea-Alonso and Ericsson, 2007, Hua et al., 1996, Eberle et al., 2004, Yokoyama et al., 1993). The three proteins share a high degree of homology and a common domain structure- an N-terminal transactivation domain followed by a DNA binding domain, two transmembrane domains and a C-terminal regulatory region- and all bind as homodimers to sterol regulatory elements (SRE) and certain E-boxes in the promoters of target genes (Figure 1.9) (Amemiya-Kudo et al., 2002, Shimano, 2001, Sato et al., 1994).

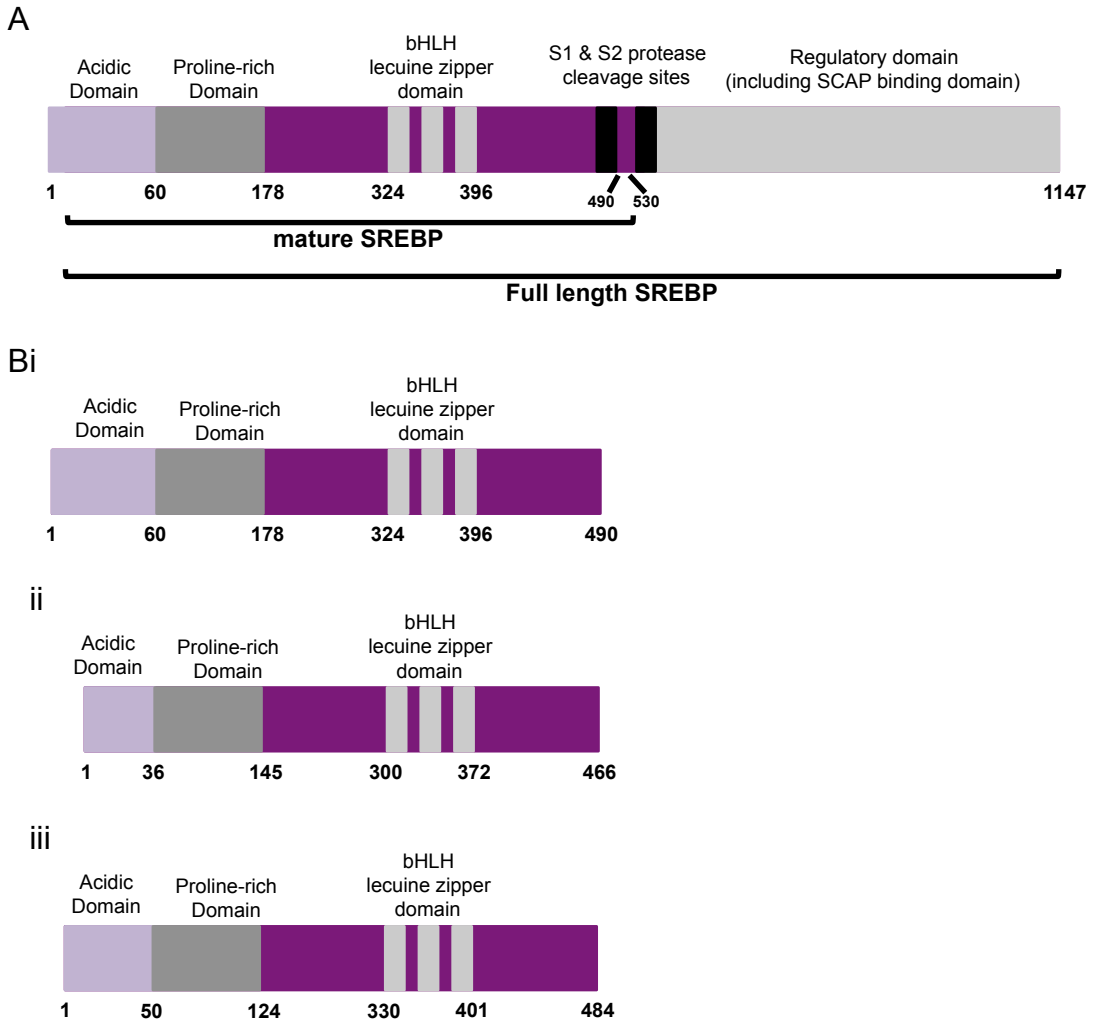

Figure 1.9 The domain structure of the SREBP proteins

Domain structures of:
A) The full-length SREBP proteins. Numbers refer to the amino acid positions in human SREBP-1a.
B) The mature SREBP proteins (mSREBPs), i) SREBP-1a and ii) SREBP-1c are transcribed from different transcriptional start sites of the same gene (Srebp1), resulting in a longer and shorter N-terminal acidic transactivation domain, respectively and iii) SREBP-2, encoded by the Srebp2 gene.

The SREBPs regulate the genes involved in de novo fatty acid and cholesterol synthesis. In many cell types, SREBP-1c primarily regulates the genes involved in fatty acid synthesis (e.g. FASN & ACC), SREBP-2 primarily regulates the genes involved in cholesterol synthesis (e.g. HMGCoR) and SREBP-1a regulates both subsets (Amemiya-Kudo et al., 2002, Horton et al., 2002, Horton et al., 2003b, Shimano et al., 1997a, Horton et al., 2003a). SREBP-1c and -2 are also SREBP targets as they contain SREs in their promoters (Horton et al., 2003a). There appears to be differences in SREBP-1

isoform expression *in vivo* and in vitro. *In vivo* most tissues seem to express higher levels of SREBP-1c compared to SREBP-1a (Shimomura et al., 1997b, de Preux et al., 2007). In contrast, *in vitro* SREBP-1a appears to be the major expressed isoform- in cells derived from a variety of tissues including those assayed *in vivo* (Shimomura et al., 1997b). The reason for this is not clear.

In addition to their well-characterised role driving de novo fatty acid and sterol synthesis, the SREBPs also regulate wider cell metabolism, seemingly to facilitate lipogenesis. The SREBPs promote the expression of glucose-6-phosphate dehydrogenase (G6PD), the rate-limiting enzyme in the oxidative branch of the pentose phosphate pathway, for example, which produces NADPH to provide the reducing power for processes including de novo lipogenesis (Duvel et al., 2010, Liang et al., 2002, Shimano et al., 1999). Furthermore, the SREBPs promote the synthesis of the major cell membrane phospholipid, phosphatidylcholine (PC), by activating gene expression of both pathways the cell uses to synthesise PC (as well as by providing the substrates for PC synthesis via de novo fatty acid synthesis) (Ridgway and Lagace, 2003, Walker et al., 2011, Kast et al., 2001). Interestingly, the SREBPs also drive expression of the LDL receptor, which, by facilitating uptake of exogenous lipid (namely cholesterol), reduces the need for the cell to carry out the metabolically expensive SREBP driven process of de novo lipogenesis (Horton et al., 2002). Aside from metabolic targets, the cell cycle inhibitor p21 is also a direct SREBP transcriptional target; moreover overexpression of SREBP-1 can drive cell cycle arrest and senescence in different cell types (Inoue et al., 2005, Kim et al., 2010, Nakakuki et al., 2007).

Although the SREBPs are sensitive to distinct, although sometimes overlapping, upstream regulation, they are processed via essentially identical pathways to give the mature active protein. All three SREBP isoforms are synthesised as inactive precursors that localise to the endoplasmic reticulum (ER) membrane where they are found in complex with SREBP cleavage activating protein (SCAP) via an interaction between the C-termini of both proteins (Sakai et al., 1997). Forming a complex with SCAP is necessary for the ER-to-Golgi translocation of SREBP in COPII coated vesicles (DeBose-Boyd et al., 1999, Matsuda et al., 2001, Sakai et al., 1998, Sun et al., 2005). In the Golgi SREBP undergoes two successive proteolytic cleavages catalysed by the site-1

and site-2 proteases (S1P and S2P), two resident Golgi membrane proteins (DeBose-Boyd et al., 1999, Duncan et al., 1997, Duncan et al., 1998). This releases the mature active N-terminal region of the SREBP protein (mSREBP, ~490 amino acids), which then translocates to the nucleus, binds to the promoter of target genes and activates transcription (Figure 1.10). It is thought that having a precursor pool translated and held in the ER allows the cell to respond rapidly to a requirement for fatty acid and sterol synthesis through rapid activation of the SREBPs.

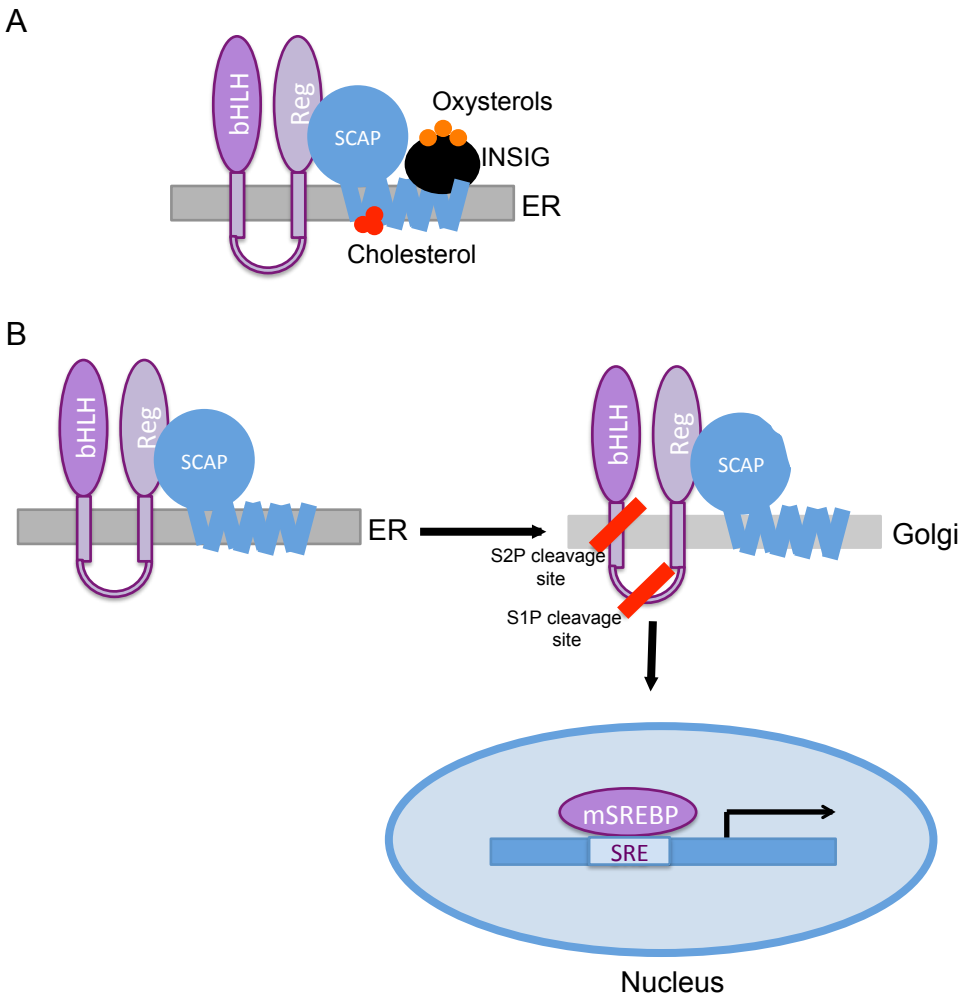

Figure 1.10 Sterol-dependent processing of the inactive ER-bound precursor SREBP proteins to generate the mature active transcription factor

Schematic of the sterol-dependent regulation of the SREBP proteins.
A) In high sterol conditions cholesterol binds to SCAP, which changes the conformation of the protein and facilitates the binding of oxysterol-bound INSIG to the SREBP-SCAP complex. As a result, the SREBP-SCAP is retained in the ER.
B) In low sterol conditions, where cholesterol is not associated to SCAP and oxysterols are not bound to INSIG, INSIG cannot bind to SCAP. This allows the SREBP-SCAP complex to interact and become incorporated in COPII vesicles that carry the complex to the Golgi. In the Golgi S1P and S2P proteases cleave the full-length precursor SREBP protein to release the mature N-terminal SREBP protein (mSREBP) that can then translocate to the nucleus and regulate the transcription of target genes.

There is careful feedback control on SREBP processing (and therefore activation) by the products of de novo fatty acid and sterol synthesis, which likely helps conserve cellular resources as de novo lipogenesis is metabolically costly (Hannah et al., 2001, Takeuchi et al., 2010, Walker et al., 2011, Shimomura et al., 1997a). The feedback inhibition mechanism is best understood for sterol dependent regulation of SREBP processing. When sterol levels in the cell rise, the level of sterols in the ER membrane increases. Cholesterol binds to the sterol-sensing domain of SCAP, which induces a conformational change in the protein and allows oxysterol bound Insulin-Induced Gene 1 or 2 (INSIG1 or 2) to bind to the SREBP-SCAP complex (Motamed et al., 2011, Radhakrishnan et al., 2007, Radhakrishnan et al., 2004, Yabe et al., 2002, Yang et al., 2002). This prevents the export of SCAP/ SREBP to the Golgi, the proteolytic steps that generate the mature, active nuclear SREBP protein and therefore activation of de novo lipogenesis (including sterol synthesis) (Espenshade et al., 2002, Goldstein et al., 2006, Sun et al., 2005, Sun et al., 2007, Yabe et al., 2002, Yang et al., 2002).

Conversely, when sterol levels are low INSIGs cannot bind to SCAP and subsequent translocation and processing of SREBP is facilitated (Gong et al., 2006, Yabe et al., 2002, Yang et al., 2002). Moreover, the stability of the INSIGs is decreased when they are not bound to SCAP and so INSIG levels in the ER fall, which further helps to sustain the ER-to-Golgi transport of the SREBP-SCAP complex. Interestingly, whereas SREBP-2 seems to be sterol regulated in all cell types where it has been studied, both *in vitro* and *in vivo*, there are cell type and/ or *in vitro* to *in vivo* differences in the sterol sensitivity of SREBP-1. In HeLa cells, primary fibroblasts and primary endothelial cells *in vitro*, SREBP-1 processing increases upon sterol deprivation. However, in mouse and hamster liver *in vivo* sterol deprivation actually leads to a decline in SREBP-1 levels, concomitant with the increase in SREBP-2 (Du et al., 2006, Sheng et al., 1995, Shimomura et al., 1997b, Wang et al., 1994, Zhou et al., 2004). The reason for this is not clear- it may reflect coordination between levels of fatty acids and sterols so that sterol synthesis is preferentially activated over and above fatty acid synthesis when sterol levels fall.

Unsaturated fatty acids and phosphatidylcholine (PC) also regulate SREBP processing. Unsaturated fatty acids block nuclear SREBP accumulation

at least in part by increasing the stability of INSIG1 (Hannah et al., 2001, Lee et al., 2008, Yabe et al., 2002, Yellaturu et al., 2009a). Phosphatidylcholine (PC) depletion activates processing of SREBP-1, but not SREBP-2 (Walker et al., 2011). How this specificity is achieved is not known.

Once in the nucleus, DNA binding stimulates GSK3 dependent phosphorylation, FbW7 mediated ubiquitination and rapid proteasome dependent degradation of the SREBP- thus attenuating SREBP activity (Hirano et al., 2001, Punga et al., 2006, Sundqvist et al., 2005, Sundqvist and Ericsson, 2003). SREBP activity requires coactivators and recruitment of the coactivator p300/CBP helps stabilise SREBP by acetylation (Giandomenico et al., 2003). Therefore the balance between activity dependent phosphorylation, ubiquitination and p300/ CBP dependent acetylation will help determine SREBP stability and therefore net activity, i.e. expression of target genes.

Lipogenesis in cell growth

As cells grow and increase in volume and mass it is inevitable that they use lipids for membrane biogenesis. This is highlighted dramatically during Schwann cell myelination- in rodents, Schwann cell myelin membrane surface expands by up to ~10,000 fold in the first 10 weeks of postnatal life (Webster, 1971). Unsurprisingly, this requires SREBP dependent lipogenesis and expression of the SREBPs and their downstream lipogenic targets peaks in the myelinating Schwann cell during active myelination (Verheijen et al., 2009, Leblanc et al., 2005).

As would be expected, lipogenesis has been shown to be necessary for growth in a number of systems. Lipogenesis is necessary for the growth of several rapidly growing and proliferating tumour cell model systems (Bauer et al., 2005, Brusselmans et al., 2005, Hatzivassiliou et al., 2005, Kim et al., 2010, Kuhajda et al., 2000, Menendez and Lupu, 2007, Porstmann et al., 2005, Porstmann et al., 2008). In addition, organ and cell size is reduced in *Drosophila* lacking dSREBP and, as a result, de novo lipogenesis (Porstmann et al., 2008). In fact, driving constitutive SREBP activity is sufficient to drive the growth of certain cell types *in vivo*; transgenic mice overexpressing nuclear SREBP-1a or -1c in the liver, or -1a in adipocytes develop marked hypertrophy

of the respective tissues (Horton et al., 2003b, Kotzka et al., 2012, Shimano et al., 1997a).

Consistent with a role for lipogenesis in cell growth, growth factor and growth factor activated signalling pathways positively regulate both lipoprotein uptake and de novo lipogenesis (Duvel et al., 2010, Li et al., 2010, Peterson et al., 2011, Porstmann et al., 2005, Porstmann et al., 2008, Smith et al., 2008, Yellaturu et al., 2009a, Du et al., 2006, Luu et al., 2012, Demoulin et al., 2004, Hegarty et al., 2005, Zhou et al., 2004). This is most well described for the insulin/ IGF-1 and the downstream PI3K/ Akt/ mTORC1 pathway. In fact, constitutively active Akt is sufficient to drive addition of cell volume in human retinal epithelial cells, dependent on the SREBPs and de novo lipogenesis (Porstmann et al., 2005). The mechanism(s) by which these signals activate SREBP dependent transcription and de novo lipogenesis is not always completely understood, however it is clear they activate SREBP maturation from the precursor form, as well as alter the stability and transcriptional activity of the mature proteins (Duvel et al., 2010, Li et al., 2010, Peterson et al., 2011, Porstmann et al., 2005, Porstmann et al., 2008, Smith et al., 2008, Yellaturu et al., 2009a, Du et al., 2006, Luu et al., 2012, Yellaturu et al., 2009b, Hegarty et al., 2005).

The best understood example of extracellular factor driven SREBP maturation seems to be the action of insulin on SREBP-1c in hepatocytes. In these cells insulin drives two PI3K/ Akt dependent mechanisms: first, phosphorylation of the SREBP-1c precursor and, second, downregulation of the liver specific isoform of INSIG (INSIG2a). Both of these events enhance the interaction between the SREBP-1c/ SCAP complex and COPII and therefore increases the rate of ER-to-Golgi transport and subsequent cleavage and activation of SREBP-1c (Yellaturu et al., 2009a, Yellaturu et al., 2009b, Yecies et al., 2011). Although similar mechanisms may operate in other cell types, INSIG2A is a liver specific INSIG isoform. This highlights another key point- it seems the SREBPs exhibit cell type specific responses to growth factor/ Akt activation. For example, Akt appears to drive SREBP-2 processing in some cell types and not others (Chinese Hamster Ovary (CHO) cells and HepG2 hepatocytes vs. human retinal epithelial cells, respectively) (Du et al., 2006, Luu

et al., 2012, Porstmann et al., 2005, Porstmann et al., 2008). What underlies these differences is not clear.

In addition to the PI3K/Akt pathway, insulin and IGF-1 also activate MAPK ERK signalling and insulin can drive ERK dependent phosphorylation on SREBP-1a and -2, which increases SREBP transcriptional activity (Kotzka et al., 2004, Kotzka et al., 2000, Roth et al., 2000). This occurs, at least in part, because the phosphorylation inhibits SREBP sumoylation; sumoylation promotes recruitment of a HDAC3 co-repressor complex to the SREBP and subsequent repression of SREBP dependent transcription (Arito et al., 2008, Hirano et al., 2003).

Recently, a particularly novel mechanism of SREBP-1 regulation has been discovered downstream of mTORC1; mTORC1 regulates hepatic SREBP nuclear localisation and activity by phosphorylating and blocking the nuclear accumulation of the multifunctional protein, lipin1 (Peterson et al., 2011). Nuclear lipin1 excludes SREBP from the nucleus thus blocking its activity. It will be interesting to determine whether this mechanism is universal, or specific to hepatocytes, which have a particularly dynamic function in organism lipid metabolism and homeostasis.

1.5.3 Water Uptake

Approximately 70% of a cell's weight is water (Luby-Phelps, 2000); some of this exists as free water and the rest is in hydration complexes with intracellular ions and organic molecules. Water is not just the medium in which cytoplasmic contents are held and reactions carried out- it is also a participant in many cellular reactions. It is required for hydrolytic reactions, including the catabolic degradation of macromolecules, and is produced in condensation reactions, including the anabolic synthesis of protein, carbohydrates and lipids. Water is taken up and lost by mammalian cells, according to the osmotic pressure gradient across the plasma membrane, both as a result of passive diffusion across the plasma membrane and facilitated transport through water channels, otherwise known as aquaporins (King et al., 2004, Verkman, 2011). So far 13 aquaporins have been identified in humans (Verkman, 2011).

The regulation of cell volume is critical for cell function and survival. Water movement into and out of the cell has the capacity to dramatically

change cell volume in a short space of time and so it is unsurprising that it is tightly regulated. Cell shrinking and swelling caused by inappropriate water movement affects, among other things, membrane integrity (by disrupting cell:cell junctions and membrane structure) and cytosolic protein function (by affecting the concentration and proximity of proteins in the cytosol) (Lang, 2007).

The relationship between cell volume and cell water content has been studied primarily with respect to how water movement is regulated to maintain a constant cell volume. To avoid shrinking or swelling a cell must maintain osmotic equilibrium across the plasma membrane. This is an active process because extracellular and intracellular osmolarity both undergo constant fluctuations. For some cells these fluctuations are very large; in the kidney medulla, for example, extracellular osmolarity can fluctuate approximately 4-fold away from isotonicity (~300mmol/L to 1400mmol/L) in a matter of hours (Lang, 2007, Lang et al., 1998). Most cell types experience milder fluctuations in intra- and extra- cellular osmolarity. When intra- or extra- cellular osmolarity changes it creates an osmotic pressure gradient across the plasma membrane. This drives a net movement of water across the membrane to restore the osmotic equilibrium across the membrane, which causes the cell to shrink/ swell according to whether the cell had become hypo-/ hyper- tonic to the surrounding medium. ‘Sensors’ detect this change and trigger the cell to adjust its intracellular osmolarity to reverse the osmotic gradient and subsequent change in cell volume (so-called Regulatory Volume Increase/ Decrease) (Lang, 2007). The ‘sensors’ that detect the change in cell volume are not clear, although numerous, not necessarily mutually exclusive, models have been proposed and they all have a certain amount of supporting evidence. The proposed mechanisms include detection of changes in membrane tension, cytosolic pH (swelling acidifies the cytosol) and macromolecular crowding (changes in the properties and behaviour of molecules at high concentrations) (Burg, 2000, Lang, 2007, Lang et al., 1998). The cell adjusts its intracellular osmolarity through movement of ions into/ out of the cytoplasm, primarily through regulating plasma membrane ion channels, and the uptake and synthesis/ release and degradation of organic osmolytes, as appropriate (Burg and Ferraris, 2008, Lang, 2007). Whilst it is clear that water movement across the plasma membrane is carefully regulated to control cell volume, how water

uptake is controlled as cells add volume during cell growth- and how this relates to the biogenic aspects of cell growth- is not clear.

1.5.4 Organelle Biogenesis and Uniform and Non-Uniform Cell Growth

Cell mass and volume represents the sum of the cell organelles and cytosol. Unsurprisingly, given the energetic and biosynthetic investment required, organelle biogenesis is a carefully regulated process, according to the needs of the cell. It is also complex, requiring the coordinated synthesis and localisation of multiple component molecules.

There is a basal rate of organelle biogenesis in all cells to replace certain organelles or organelle sub-structures that have worn out and been degraded, usually by autophagy. Turnover can also be an integral part of a structure's function. This is perhaps best demonstrated by the plasma membrane. The plasma membrane forms the barrier between the intra- and extra- cellular environments, protecting the integrity of the cytosol. However, as the interface between these two environments, it is also necessarily the site of communication and substance exchange between them (Conner and Schmid, 2003). This means the plasma membrane has essential roles in cell signalling, nutrient uptake, cell surface homeostasis, migration, adhesion and, where appropriate, cell surface polarisation (Conner and Schmid, 2003). As a result, the plasma membrane is incredibly dynamic, constantly turning over in order to perform each of these functions. As with all cellular structures, the size of the plasma membrane will depend on the balance between the rates of accumulation and loss of material.

Cell organelle content can also rapidly change in response to specific stimuli. Given that growth factors drive cell growth, it is unsurprising to find that growth factor activated signalling pathways drive organelle biogenesis. In the Schwann cell, activation of both the PI3K and ERK signalling pathways is required for IGF-1 and NRG1 dependent mitochondrial biogenesis, mediated by the transcription factor, estrogen-related receptor alpha (ERRα) (Echave et al., 2009). Similarly, mTORC1 has been shown to drive mitochondrial gene expression by promoting the formation and activity of a transcription factor complex containing the transcription factor Yin-Yang 1 (YY1) and the

transcriptional co-activator peroxisome-proliferator-activated receptor co-activator alpha (PGC1-α) (Cunningham et al., 2007).

There are examples where there is coordinated addition of cell mass, volume and organelles during cell growth. In steady state proliferating cell populations described in Section 1.4.1, for example, each cell will roughly double its mass, volume and organelle content across each cell cycle before dividing to produce two daughter cells with an approximately equivalent composition to the starting mother cell. However, considering the diversity in cell size, morphology and organelle content across different cell types *in vivo*, as well as across the lifetime of individual cell types, it is clear that non-uniform cell growth is a frequent event- where one or more parts of the cell, be it molecule or organelle, grows at a different rate to the rest of the cell. Differential cell growth ensures cells are adapted to their specific function. Adipocytes, for example, develop large lipid droplets that occupy a large proportion of the cytosol, which means they are effective lipid storage sites. In contrast, skeletal muscle cells have few small lipid droplets but have extensive mitochondria, which enable the cells to produce large amounts of ATP to drive muscle function. Moreover, an increase or decrease in muscle use leads to a corresponding change in the amount of mitochondria per cell, demonstrating how morphological changes (growth) can allow a cell to adapt to environmental changes.

Non-uniform cell growth is particularly well demonstrated by examples of differential organelle biogenesis within a single cell type. B cells, for example, pass through two distinct phases of organelle biogenesis after they are activated in an immune response. Initially there is an increase in cell volume, accompanied by a large increase in cytosolic ribosome density and mitochondrial size, as well as partial expansion of the endoplasmic reticulum (ER) (Shohat et al., 1973). This is followed by a disproportionate expansion of the ER compared to cell volume such that the ER fills the majority of the cytosol (Kirk et al., 2010, Shohat et al., 1973). During this time, cytosolic ribosome numbers fall, ribosomes become associated with the expanding ER and there is no further increase in mitochondrial size (Kirk et al., 2010, Shohat et al., 1973). The expansion of the ER is required for the mature plasma cell to synthesise and secrete large amounts of immunoglobulins and is a clear example where

differential organelle biogenesis is critical for the cell to perform its function (Federovitch et al., 2005, Rush et al., 1991).

Distinct growth stimuli appear to be able to control differential organelle biogenesis, for example. In the Schwann cell, IGF-1 drives a proportional increase in cell and mitochondrial volume. In contrast, IGF-1 and NRG1 synergise to increase mitochondrial volume, whilst cell volume is equivalent to in the presence of IGF-1 alone- and therefore mitochondrial density increases (Echave et al., 2009). This example is especially noteworthy because NRG1, as described in Section 1.3, was not classically described as a Schwann cell growth factor because it does not induce cell volume addition. However the mitochondrial finding clearly demonstrates that NRG1 has biogenic capabilities and therefore could be described as a growth factor. This is particularly interesting because it highlights that cell growth needs to be considered in a more sophisticated manner than simply the addition of cell volume.

1.6 Growth Factor Regulation of Cell Growth

The emphasis on growth factors throughout this Introduction will have highlighted their key features. Namely; growth factors are required for mammalian cell growth (the addition of cell mass and volume), can determine final cell size and are also required to maintain cell size homeostasis. Cell growth control is the control of the rates of accumulation and loss of intracellular contents. Therefore, unsurprisingly, growth factors regulate cell growth by promoting accumulation (by driving expression of nutrient transporters and anabolic pathways, i.e. the uptake and synthesis of material) and suppressing bulk loss (by suppressing catabolic pathways such as autophagy) (Conlon et al., 2001, Edinger and Thompson, 2002, Vander Heiden et al., 2001, Luu et al., 2012, Sacheck et al., 2004, Stitt et al., 2004).

Many growth factors act through Receptor Tyrosine Kinases (RTKs), including IGF-1, NGF and the NRGs that have been used to describe growth factor functions in preceding sections. RTKs are integral plasma membrane proteins with an extracellular ligand binding domain, a transmembrane domain and a cytoplasmic domain (Lemmon and Schlessinger, 2010). Binding of the

extracellular growth factor to its cognate receptor drives a structural change in the receptor, inducing autophosphorylation on one or more tyrosine residues in the intracellular domain of the protein. This facilitates the recruitment of adapter proteins that bind to the activated intracellular domain of the receptor and lead to activation of the downstream signalling pathways.

IGF-1 and its homologues are perhaps the best-characterised growth factors- driving growth in diverse organisms, from *Drosophila* to mammals (Laron, 2004, Chen et al., 1996, Lupu et al., 2001). Indeed, Growth Hormone (GH), which regulates much of post-natal developmental growth in mammals, does so in large part through stimulating production of IGF-1 (Conlon and Raff, 1999). The IGF-1 Receptor (IGF1R) is a heterotetrameric protein consisting on two α and two β chains, that form the extracellular ligand (IGF-1) binding and transmembrane and intracellular kinase domains of the oligomer, respectively (Manning and Cantley, 2007, Tognon and Sorensen, 2012). Binding of IGF-1 to the receptor results in the transphosporylation of tyrosine residues in the activation loop of the receptor, followed by further phosphorylation of specific tyrosine residues in the intracellular domain of the protein. This phosphorylation allows the binding of adapter proteins and the activation of downstream signalling pathways (Figure 1.11). For example, PI3K is recruited to the IGF1R via the insulin receptor substrate adapter proteins (IRS1-4), as well as through direct binding to the C-terminal domain of the receptor. This recruits PI3K to the plasma membrane where it can phosphorylate phosphatidylinositol (4,5)-bisphosphate (PIP_2) to generate $PI(3,4,5)P_3$ (PIP_3), resulting in activation of Akt and downstream signalling (Manning and Cantley, 2007). ERK signalling is also activated downstream of IGF-1. In the canonical pathway, this is via recruitment of src homology 2 containing transforming protein (Shc), growth factor receptor bound protein-2 (Grb2) and the Ras guanine exchange factor, Sons of sevenless (SOS), which can then activate the membrane anchored small GTP-ase Ras and, downstream of this, the MAPK ERK cascade. Activated Ras can also activate PI3K that has been recruited to the IGF1R, via PI3Ks catalytic subunit.

Loss of IGF-1 signalling during development leads to impaired growth and dwarfism and, reciprocally, high levels of circulating IGF-1 contribute to excess growth and resulting gigantism (Laron, 2004, Lupu et al., 2001,

Walenkamp and Wit, 2007). The primary intracellular signalling pathway IGF-1 (as well as other growth factors) activates to drive cell growth is the PI3K/ Akt/ mTORC1 pathway (Demoulin et al., 2004, Hegarty et al., 2005, Zhou et al., 2004, Rommel et al., 2001, Sacheck et al., 2004, Macklin, 2010). The role of PI3K/Akt, mTORC1 and other growth factor activated signalling pathways is discussed in the following Section.

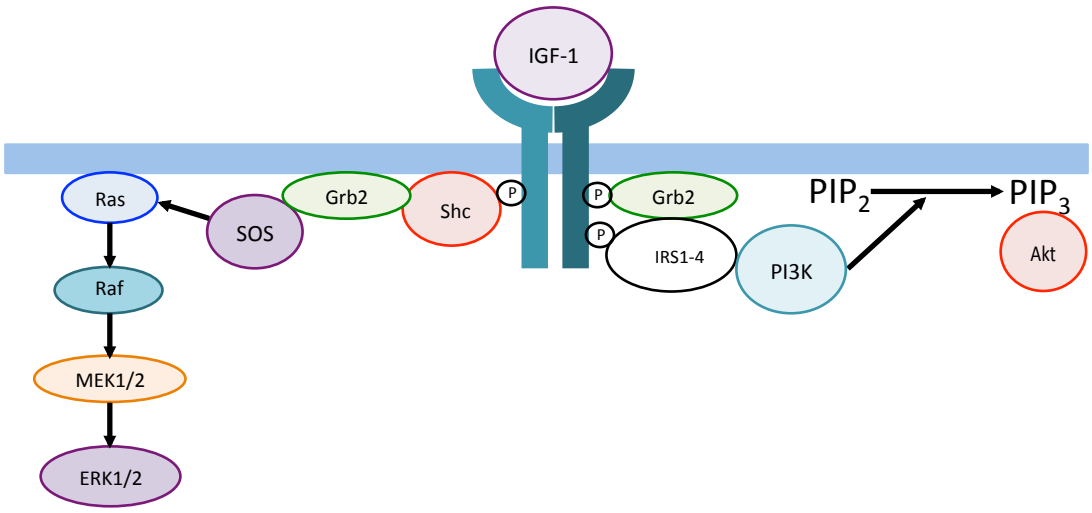

Figure 1.11 Signalling through the IGF-1 Receptor

Schematic of the activation of the IGF-1 receptor (IGF1R) by IGF-1:
IGF-1 binds and activates its cognate heterotetrameric Receptor Tyrosine Kinase (RTK), the IGF1R. This induces autophosphorylation of the intracellular domain of the receptor, which results in the recruitment and binding of a number of adapter proteins to the receptor. These include the insulin receptor substrate-1 (IRS-1), which leads to the activation of PI3K/ Akt signalling; PI3K binds to IRS-1 and the activated receptor and, thus, is recruited to the plasma membrane where it can phosphorylate PIP_2 to PIP_3. Akt binds PIP_3 and is subsequently activated. The Raf/ MEK/ ERK MAPK cascade is also activated downstream of the IGF-1 receptor: The Ras guanine exchange factor Sons of sevenless (SOS) is recruited to the plasma membrane where it can interact with and activate the Ras GTPase by the adapter proteins src homology 2 containing transforming protein-2 (Shc) and growth factor receptor bound protein-2. Activated Ras activates Raf to activate the MAPK cascade (Tognon and Sorensen 2012).

1.7 Signalling Pathways Regulating Cell Growth

1.7.1 PI3K/ Akt Dependent Cell Growth

In vitro and *in vivo* studies in every system studied show that signalling through this pathway drives cell growth and hyper-/ hypo- activation of Akt drives cell hyper-/ hypo- trophy in a number of different models (Chan et al., 2011, Collins et al., 2012, Echave et al., 2009, Flores et al., 2008, Lai et al., 2004, Leevers et al., 1996, Maurel and Salzer, 2000, Peng et al., 2003,

Porstmann et al., 2005, Porstmann et al., 2008). In addition to cell growth, the PI3K/ Akt pathway also promotes cell survival, proliferation and migration (Manning and Cantley, 2007, Kockel et al., 2010).

Akt (also known as protein kinase B, PKB) binds to the PIP_3 generated by PI3K activity via its pleckstrin homology (PH) domain (Figure 1.12) (Manning and Cantley, 2007). Once at the plasma membrane Akt is activated by phosphorylation at two sites, by distinct kinases; PDK1 (phosphatidylinositol-dependent kinase-1) on threonine 308 and mTORC2 on serine 473 (Alessi et al., 1997, Sarbassov et al., 2005b). PI3K signalling is antagonised by the lipid phosphatase PTEN that dephosphorylates PIP_3 to PIP_2 (Song et al., 2012). Akt is an AGC family serine-threonine kinase and there are 3 mammalian isoforms of the protein, encoded by different genes (Akt1, Akt2, Akt3). As already described, mTORC1 is the major downstream effector of Akt in promoting cell growth. Activated mTORC1 activates a negative feedback loop to attenuate IGF-1/ PI3K signalling by phosphorylating (directly and indirectly) insulin receptor substrate-1 (IRS-1), which promotes its degradation (Manning and Cantley, 2007). In addition, the mTORC1 effector S6 Kinase (S6K) can phosphorylate and inhibit the Rictor subunit of the mTORC2 complex (Dibble et al., 2009, Julien et al., 2010). It seems likely these negative feedback loops help prevent hyperactivation of the PI3K pathway in response to growth factor stimulation.

Akt promotes nutrient uptake by increasing the cell surface expression and/ or activity of glucose, amino acid, transferrin and lipoprotein receptors (Edinger and Thompson, 2002, Elstrom et al., 2004, Manning and Cantley, 2007, Plas et al., 2001, Wieman et al., 2007). Once inside the cell, these nutrients are used in Akt driven metabolism; for example for de novo biogenesis or proteins and lipids from nutrient-derived mitochondrial precursors (as described in Sections 1.5.1 & 1.5.2) (Elstrom et al., 2004, Hagiwara et al., 2012, Manning and Cantley, 2007, Porstmann et al., 2008, Wise et al., 2008).

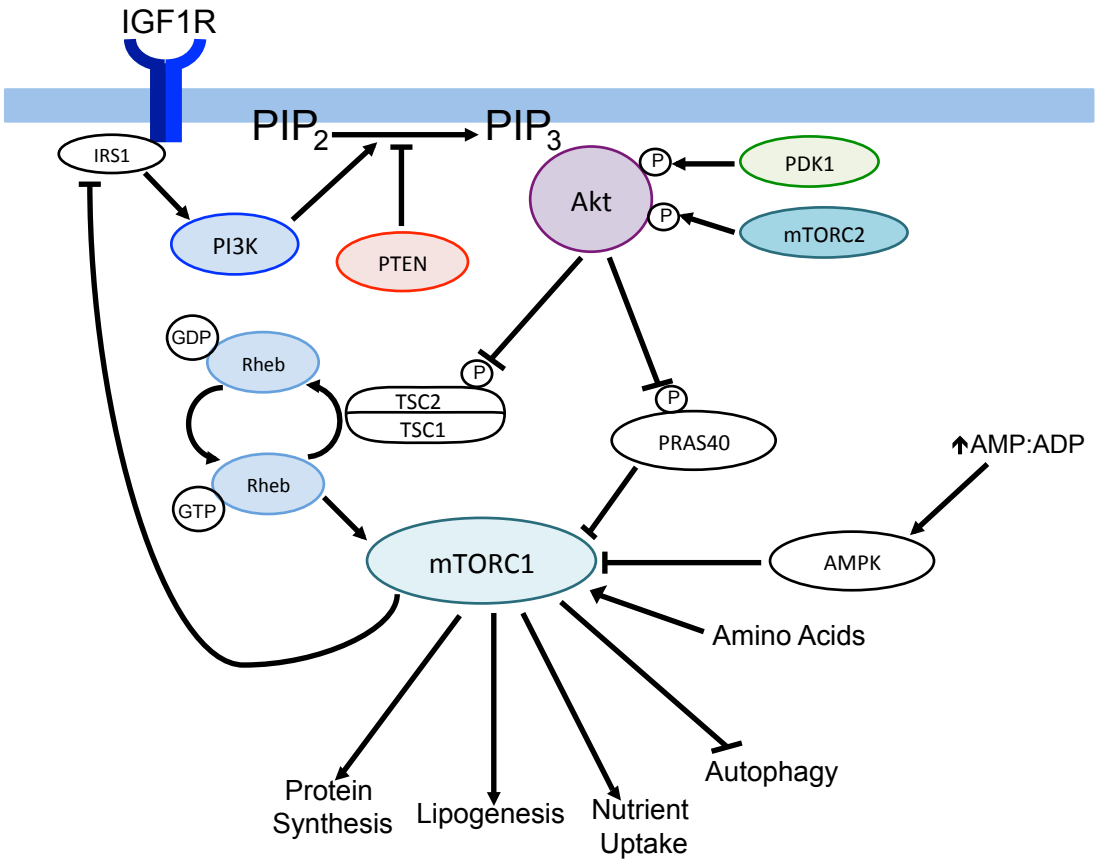

Figure 1.12 Activation of PI3K, Akt and mTORC1

Schematic of the activation of PI3K, Akt and mTORC1:
Activated Receptor Tyrosine Kinases, e.g. the IGF-1 Receptor (IGF1R) activate PI3K (in the case of the IGF1R, via activation of the Insulin Receptor Substrate 1 (IRS1), for example). PI3K generates PIP3 from PIP2, which is antagonised by the lipid phosphatase PTEN. Akt binds to PIP3 at the plasma membrane where it can be activated by phosphorylation by PDK1 and mTORC1. Akt activates mTORC1 by phosphorylating and inhibiting two negative regulators of mTORC1, TSC2 and PRAS40. mTORC1 is activated by Rheb on the lysosome (not shown) and mTORC1 localisation to the lysosome depends on the presence of amino acids. Cellular energy stress activates AMPK, which inhibits mTORC1 by direct phosphorylation as well as by an activating phosphorylation on TSC2 (not shown). Not shown in this schema, but also regulating mTORC1 activity, are hypoxia, which acts upstream of the TSC1/TSC2 complex and phosphatidic acid, which stabilises the mTORC1 complex.In addition, ERK can directly and indirectly phosphorylate and inhibit TSC2 and phosphorylate the Raptor subunit of mTORC1, which increases the activity of the complex. mTORC1 feedback inhibits PI3K/ Akt activity by promoting the phosphorylation and degradation of IRS1 (Memmot and Dennis 2009, Sancak et al., 2010, Laplante and Sabatini 2012).

The mTORC1 pathway is a critical downstream effector of Akt induced cell growth and signalling through this pathway will be discussed in more detail in the following Section. However, Akt also regulates mTORC1-independent targets to drive cell growth (Berwick et al., 2002, Chan et al., 2011, Luu et al., 2012, Porstmann et al., 2008, Sandri et al., 2004, Stitt et al., 2004, Wieman et al., 2007, Yecies et al., 2011). These include the FOXO transcription factors and the kinase glycogen synthase kinase 3 (GSK3β), which are both inhibited

by Akt phosphorylation and both have roles in Akt dependent cell growth and metabolism (Manning and Cantley, 2007, Porstmann et al., 2008, Sandri et al., 2004, Stitt et al., 2004, Sundqvist et al., 2005). Inhibition of FOXO1, for example, is required for the Akt dependent inhibition of Atrogin-1 and, as a result, proteasomal degradation (Sandri et al., 2004, Stitt et al., 2004).

Both mTORC1 dependent and independent effects are apparent across all the metabolic pathways regulated by Akt- often converging on the regulation on the same protein. For example, in the haematopoietic FL5.12 cell line, Akt promotes mTORC1-independent expression of the Glut1 glucose transporter at the cell surface (Wieman et al., 2007). However, mTORC1 potentiates the activity of the transporter (Wieman et al., 2007). Similarly, as described in Section 1.5.2, Akt drives mTORC1-dependent processing and activation of the master regulators of lipogenesis, the SREBPs, but mTORC1-independent stabilisation of the active SREBPs (Luu et al., 2012, Porstmann et al., 2008). Moreover, mTORC1 is not sufficient to drive hepatic lipogenesis *in vivo* in the absence of Akt (Wan et al., 2011, Yecies et al., 2011). This appears to be, at least in part, because Akt is required to downregulate the negative regulator of SREBP processing and activation, INSIG2A (Yecies et al., 2011).

Interestingly, there are findings that suggest PI3K/ Akt is required for biogenesis even under conditions where the pathway is not activated i.e. signalling is at basal/ control levels. In the Schwann cell, for example, loss of Rb drives cell growth in the absence of PI3K/ Akt/ mTORC1 activation (Collins et al., 2012). However, inhibiting PI3K blocks Rb dependent cell volume addition (Collins et al., 2012). Similarly, expression of Myc in immortalised human fibroblasts does not activate Akt, however Akt is required for Myc to drive rRNA transcription (Chan et al., 2011). This suggests basal flux through the PI3K/ Akt pathway may be required for cell growth and biogenesis, even where the pathway itself is not the driving force.

1.7.2 mTORC1 Signalling

The mTOR kinase is found in two distinct multi-subunit complexes in the cell, mTORC1 and mTORC2 (Laplante and Sabatini, 2012, Zhou and Huang, 2010). Both complexes contain the mTOR kinase, but differ in other subunits- most notably Raptor and Rictor, present in mTORC1 and 2, respectively.

Studies using the inhibitor Rapamycin that directly inhibits mTORC1 but not mTORC2 (via interaction with Raptor), as well siRNA mediated silencing and knock-outs of complex specific subunits have demonstrated that the two complexes have distinct regulatory inputs and functions (Laplante and Sabatini, 2012, Zhou and Huang, 2010). In contrast to mTORC1, mTORC2 is not considered a major regulator of cell growth and biogenesis- although the complex is one of the kinases that phosphorylates and activates Akt at the plasma membrane (Sarbassov et al., 2005a, Wullschleger et al., 2006, Zhou and Huang, 2010). Confirming that mTORC1 is a critical mediator of PI3K/ Akt dependent cell growth, inhibiting mTORC1 blocks PI3K/ Akt mediated cell growth in numerous systems (Goebbels et al., 2010, Meikle et al., 2008, Narayanan et al., 2009, Porstmann et al., 2005, Zhou et al., 2009).

mTORC1 is activated by the GTP-bound form of the small GTPase Rheb. This is inhibited by the TSC1/TSC2 complex, which acts as a Rheb GTPase-activating protein (GAP) (Huang and Manning, 2008). Numerous upstream signals converge to regulate mTORC1, highlighting that it is a central node in cellular signalling (Sengupta et al., 2010), These include growth factors, amino acid availability and cellular energy and oxygen levels. Many of these act by regulating the activity of the TSC1/ TSC2 complex. Extracellular factors primarily regulate mTORC1 signalling via Akt, which phosphorylates and inactivates two negative regulators of mTORC1, PRAS40 and TSC2 (Inoki et al., 2002, Oshiro et al., 2007, Potter et al., 2002, Sancak et al., 2007, Vander Haar et al., 2007). ERK can also inhibit TSC2 as well as phosphorylate the Raptor subunit of mTORC1, potentiating the activity of the complex (Carriere et al., 2008, Carriere et al., 2011, Ma et al., 2005, Rolfe et al., 2005, Winter et al., 2011). Amino acid availability regulates mTORC1 activation by controlling the localisation of the complex and therefore the interaction with its activator, Rheb (Discussed in more detail in Sections 1.8 and 1.9) (Inoki et al., 2003a, Kim et al., 2008a, Sancak et al., 2010, Sancak et al., 2008, Kim et al., 2012, Zoncu et al., 2011). Amino acid availability is dominant to growth factor signalling, which likely ensures protein synthesis is not activated when substrates are limiting. Cellular energy deprivation (also discussed in more detail in Section 1.9) and hypoxia also inhibit mTORC1 (Sengupta et al., 2010). Within the mTORC1 complex; phosphatidic acid can stabilise the complex by binding to Raptor and there is mutual inhibition between the mTOR subunit and a recently discovered

subunit Deptor- although the physiological significance of this interaction is not yet fully understood (Foster, 2009, Peterson et al., 2009).

mTORC1 promotes cell growth and biogenesis via a number of mechanisms, as has been detailed through this Introduction. The roles of mTORC1 in protein synthesis and lipogenesis have been described in detail in Sections 1.5.1 and 1.5.2. mTORC1 also promotes the synthesis of ATP, NADPH and precursors for such macromolecular synthesis by promoting nutrient uptake, activating the pentose phosphate pathway, increasing glycolytic flux and promoting mitochondrial gene expression (Cunningham et al., 2007, Duvel et al., 2010, Edinger and Thompson, 2002, Grewal et al., 2007, Laplante and Sabatini, 2010, Mayer and Grummt, 2006, Peterson et al., 2011, Porstmann et al., 2008, Schieke et al., 2006, Thoreen et al., 2012, Wullschleger et al., 2006). For example, mTORC1 has been shown to promote glucose uptake and glycolysis study in mouse embryonic fibroblasts (MEFs) *in vitro* via activation of the transcription factor hypoxia inducible factor 1α (HIF1α) and the pentose phosphate pathway via activation of the SREBPs (Duvel et al., 2010). In addition to these biosynthetic and bioenergetics functions, mTORC1 further promotes an anabolic phenotype by suppressing bulk degradation by autophagy (Jung et al., 2010, Kim et al., 2011). This is mediated, at least in part, by direct phosphorylation of Ulk1, a kinase that drives autophagy initiation (Kim et al., 2011). The fact mTORC1 regulates multiple aspects of cell metabolism can provide a way to coordinate biogenesis downstream of positive and negative metabolic stimuli.

The S6 kinases (S6K1/2) and 4EBP proteins (4EBP1/2) are the best known mTORC1 substrates and are activated and inhibited, respectively, by mTORC1 phosphorylation (Fingar et al., 2002, Sengupta et al., 2010). These substrates mediate the effects of mTORC1 on protein synthesis. S6K promotes mRNA processing, translation elongation and ribosome biogenesis through regulation of the mRNA processing protein SKAR, eukaryotic elongations factors and the ribosomal protein S6, respectively (Laplante and Sabatini, 2012). Inhibition of 4EBP1 promotes cap-dependent translation initiation (Hsieh et al., 2012, Thoreen et al., 2012). Consistent with an important role for S6K and 4EBP downstream of mTORC1, disrupting signalling through each can inhibit and promotes cell growth, respectively (Miron et al., 2001, Sarbassov et

al., 2005a). Some functions of mTORC1 are known to be independent of these effectors; for example, mTORC1 phosphorylates and inhibits Ulk1, a component of the autophagy machinery, to inhibit autophagy and lipin1 to regulate SREBP activity and the de novo lipogenic pathway (Kim et al., 2011, Peterson et al., 2011).

1.7.3 ERK1/2 Dependent Cell Growth

The Raf/ MEK/ ERK MAP kinase (MAPK) cascade has been implicated in the regulation of diverse cellular processes including proliferation, differentiation, survival and migration. Raf kinase is activated by the small GTPase Ras downstream of extracellular factor receptors, including Receptor Tyrosine Kinases and G-Protein Coupled Receptors (Mendoza et al., 2011). Activated Raf phosphorylates and activates the MAPK kinases MEK1/2, which in turn phosphorylate and activate the MAPKs ERK1/2. Activated ERK phosphorylates and regulates a number of cytosolic (e.g. p90 ribosomal S6 kinase (RSK)) and nuclear (e.g. c-Fos) targets and there is evidence to suggest the two ERKs (ERK1 and ERK2) have distinct cellular functions (Lloyd, 2006, Yoon and Seger, 2006).

The cellular response to ERK in a number of systems seems to depend on the kinetics and strength of the ERK signal (Marshall, 1995). For example, in the neuronal PC12 cell line sustained and strong ERK activation drives differentiation, whereas transient ERK signalling is associated with proliferation (Marshall, 1995). In contrast, in differentiated myelinating Schwann cells *in vitro* and *in vivo*, sustained and strong ERK signalling drives dedifferentiation, whereas lower levels are required for differentiation (Harrisingh et al., 2004, Napoli et al., 2012, Newbern et al., 2011).

As mentioned above, ERK signalling can activate mTORC1 in some situations. ERK and its target RSK can both directly phosphorylate and inhibit TSC2 and phosphorylate the mTORC1 subunit Raptor, potentiating mTORC1 activity, including driving protein synthesis (Carriere et al., 2008, Carriere et al., 2011, Ma et al., 2005, Rolfe et al., 2005, Winter et al., 2011). In addition, ERK has been shown to directly regulate factors that drive rRNA transcription and cap-dependent translation initiation, suggesting it can promote protein synthesis independent of effects on mTORC1- although this effect may be modest

(James and Zomerdijk, 2004, Roux et al., 2007). Indeed, overexpression of MEK1 in cardiac myocytes *in vitro* and *in vivo* can drive hypertrophy, which has been associated with increased protein synthesis in vitro (Bueno et al., 2000, Ueyama et al., 2000). This data demonstrates that, in some systems, ERK does have a role driving cell growth.

Like Akt, ERK can also promote lipogenesis. ERK mediated phosphorylation enhances SREBP transcriptional activity and therefore lipogenic gene expression, as described in Section 1.5.2 (Arito et al., 2008, Kotzka et al., 2004, Kotzka et al., 2000, Roth et al., 2000). Moreover, liver hypertrophy driven by overexpression of mature SREBP-1a in this tissue is prevented by mutation of the MAPK phosphorylation sites in the protein, suggesting a physiological role for ERK in SREBP mediated lipogenesis in the liver (Kotzka et al., 2012).

Interestingly, Raf/ MEK/ ERK and Akt signalling have been shown to regulate distinct and independent aspects of sensory axon outgrowth *in vitro*- whereas hyperactivation of Raf1 drives axonal elongation, hyperactivated Akt increases axon calibre and branching (Markus et al., 2002). This suggests that, in this context, they regulate at least some distinct targets. One possible ERK regulated, Akt independent target is the transcription factor serum response factor (SRF). *In vitro*, overexpression of SRF is sufficient to drive axon outgrowth and this requires MEK, but not PI3K (Wickramasinghe et al., 2008). Although it is not clear which SRF targets are important for axon outgrowth, given that axon elongation is going to require cytoskeletal remodelling and extension, one attractive candidate is actin, which is induced by SRF in this system (Wickramasinghe et al., 2008). Finally, studies in the Schwann cell demonstrate that ERK is required for mitochondrial biogenesis downstream of synergistic IGF-1 and NRG-1 signalling- demonstrating that ERK can have a functional role in organelle biogenesis (Echave et al., 2009).

1.7.4 Myc Dependent Cell Growth

Aside from PI3K/ Akt and mTORC1, Myc can also play an important role in regulating cell growth in a number of systems. Myc dependent cell growth is associated with increased protein biogenesis; including increased rRNA levels, ribosome and nucleolar density, protein synthesis and cell protein content

(Chan et al., 2011, Grewal et al., 2005, Iritani and Eisenman, 1999, Johnston et al., 1999, Kim et al., 2000, Pierce et al., 2004, Saucedo and Edgar, 2002, Schreiber-Agus et al., 1997, Schuhmacher et al., 1999, Wu and Johnston, 2010). Myc also drives glycolysis, mitochondrial biogenesis and activity and glutamine metabolism- apparently switching mitochondrial metabolism to being increasingly dependent on glutamine-derived carbon, as opposed to glucose-derived carbon (Fan et al., 2010, Gao et al., 2009, Graves et al., 2012, Kim et al., 2008b, Li et al., 2005, Morrish et al., 2008, Osthus et al., 2000, Wise et al., 2008). These have been shown to be important for Myc dependent survival and proliferation- although their role in Myc dependent cell growth per se has not been investigated, given their function in cell bioenergetics and biosynthesis, it would not be surprising if they were required.

Like the PI3K/ Akt pathway, Myc can be activated downstream of extracellular factor receptor signalling. In *Drosophila*, two negative regulators of dMyc have been specifically linked to regulation of cell growth- the TRIM-NHL proteins, Brat and MeiP26 (Betschinger et al., 2006, Frank et al., 2002, Herranz et al., 2010, Neumuller et al., 2008). Loss of either of these proteins increases dMyc levels and cell size, associated with an increase in nucleolar size- analogous to dMyc overexpression (Betschinger et al., 2006, Herranz et al., 2010, Neumuller et al., 2008). Interestingly, miRNAs have been implicated in MeiP26 regulation of dMyc, the first studies associating this relatively new field with regulation of cell growth (Herranz et al., 2010).

Interestingly and importantly, dMyc and PI3K dependent cell growth appear to be driven, in part, by distinct mechanisms. In *Drosophila* fat cells, overexpression of PI3K and dMyc drive equivalent increases in cell volume (Grewal et al., 2005). However, only dMyc drives a significant increase in nucleolar size and rRNA levels, suggesting dMyc drives significantly higher rates of protein synthesis than PI3K (Grewal et al., 2005). It is important to note that this does not mean PI3K does not also upregulate protein synthesis in this system- as described in Section 1.7.1, enhanced protein biogenesis is a well characterised effect of PI3K/ Akt/ mTORC1 signalling. However it does suggest that in *Drosophila* fat cells, there may be a greater role for protein synthesis in dMyc dependent cell growth and other aspects of biogenesis, e.g. lipogenesis, have significant roles in PI3K dependent cell growth.

1.7.5 Other Signalling Pathways

As discussed in Section 1.7.3, the transcription factor SRF may mediate Raf driven axonal outgrowth. SRF has also been shown to be involved in cardiac muscle growth (Zhang et al., 2001a, Zhang et al., 2001b). During development, SRF is required for cardiac muscle growth and, in the adult, overexpression of SRF in cardiac muscle drives pathological hypertrophy (Zhang et al., 2001a, Zhang et al., 2001b). SRF also regulates skeletal muscle growth and maintenance during development and in the adult but, interestingly, SRF does not appear to directly regulate cell growth in this context- it regulates secretion of interleukin-4 (IL-4), which then acts to drive muscle growth (Charvet et al., 2006, Guerci et al., 2012).

Another signalling pathway that has been shown to regulate growth in a number of cell types is the calcineurin pathway. Calcineurin is a calcium activated serine/ threonine phosphatase. The primary substrates of calcineurin are the nuclear factor of activated T-cell proteins (NFATs) that, once dephosphorylated, translocate to the nucleus and act as transcriptional coactivators within a number of different transcriptional complexes (Hogan et al., 2003). Section 1.4.2 'Determining Cell Size' has already described that NRG1 driven Schwann cell myelination involves the PI3K/ Akt pathway. In addition, and also important for myelination, NRG1 signalling activates calcineurin-NFAT signalling via a phospholipase C (PLC) dependent increase in intracellular calcium, independent of PI3K (Kao et al., 2009). Loss of calcineurin in Schwann cells leads to hypomyelination (Kao et al., 2009). Calcineurin is also required for NGF-dependent axonal outgrowth, by both NFAT dependent and independent mechanisms (the latter by regulating NGF receptor endocytosis and therefore signalling dynamics), as well as pathological cardiac hypertrophy (Bourajjaj et al., 2008, Graef et al., 2003, Molkentin et al., 1998, Wilkins et al., 2004).

Finally, the retinoblastoma protein (Rb) is a well-known tumour suppressor and its role regulating the cell cycle in this context has been extensively studied (Giacinti and Giordano, 2006). However, more recently it has been shown that Rb also specifically regulates cell growth (Collins et al., 2012). Most interestingly, Rb dependent growth is independent of the classic

Rb targets important for cell-cycle regulation, the E2F transcription factors, as well as PI3K/ Akt/ mTORC1, MEK/ ERK and c-Myc activation.

These examples demonstrate that diverse signalling pathways can be involved in regulating cell growth in different contexts and show that they can act in parallel with, independent of or in a different context to the classic PI3K/ Akt pathway. However, many of these pathways remain poorly understood.

1.7.6 Crosstalk Between Signalling Pathways

As will have become clear throughout this introduction, particularly in the formative parts of this Section 1.7, numerous pathways can converge on common upstream regulators of biogenesis (e.g. mTORC1) or downstream cellular processes (e.g. lipogenesis). The effects of multiple signals can be additive- for example Akt and ERK can phosphorylate TSC2 on distinct sites to drive additive activation of mTORC1, as assayed by phosphorylation of the mTORC1 target, S6 kinase (S6K) (Winter et al., 2011). Distinct pathways can also synergise to drive a novel growth output- in Schwann cells loss of Rb, which drives strong short-term growth, can synergise with Ras, which drives weak sustained growth, to drive strong and sustained cell growth (Collins et al., 2012). In other cases a pathway may be required for the activation of another- such as the case in human fibroblasts where Akt is required for Myc to drive rRNA transcription, although Akt itself is not activated (Chan et al., 2011). There are also situations where signalling pathways can antagonise one another- PI3K and ERK signalling can negatively, as well as positively, regulate each other (Mendoza et al., 2011).

1.8 Nutrient Regulation of Cell Growth and Cell Size

In addition to growth factors, nutrients are critical for cell growth and maintenance. Not only as the substrates for biogenesis, but also as direct regulators of growth factor activated signalling pathways and biogenesis (Metallo and Vander Heiden, 2010, Wellen and Thompson, 2012, Wullschleger et al., 2006). This means there is strong interdependence on combined nutrient and growth factor availability to maintain cellular biogenesis: growth factors are necessary for nutrient uptake and metabolism and, reciprocally, nutrients are

required to promote growth factor signalling (Barata et al., 2004, Edinger and Thompson, 2002, Plas et al., 2001, Rathmell et al., 2000, Vander Heiden et al., 2001, Wieman et al., 2007). Coupling cell growth to nutrient availability likely ensures growth only occurs when the substrates are available to fuel this energetically demanding process (Edgar, 2006, Guthrie and Brown, 1968, Winick and Noble, 1966).

Nutrients regulate biogenesis both at the systemic and cellular level. In mammals, circulating nutrient levels are kept within narrow physiological limits; this is achieved through the regulation of tissue metabolism to store/ mobilise nutrients from/ into systemic circulation as required (Berg, 2002). The metabolism of the liver, skeletal muscle and adipose tissues are particularly dynamic in response to whole body feeding/ fasting and they play a critical role in the regulation of circulating nutrient levels. Feeding causes blood glucose levels to rise, which stimulates the release of insulin. Insulin promotes glucose and fatty acid uptake by tissues, through activation of PI3K/Akt signalling. A certain amount of excess glucose is taken up by the liver and skeletal muscle and stored as glycogen and any remainder is converted to triacylglycerols (TAGs) and stored primarily in adipose tissue. Initial starvation, e.g. overnight, causes blood glucose levels to fall, which inhibits insulin release and stimulates glucagon release. This drives the breakdown and release of previously stored glycogen as glucose to maintain circulating blood glucose levels. Under these conditions many tissues switch to using circulating fatty acids as an energy source, which preserves circulating glucose for tissues that cannot utilize fatty acids, such as the brain. The feedback control of systemic nutrient levels and the plasticity of the metabolism of certain tissues helps ensure a constant supply of nutrients to all tissues to maintain cell size and growth, as appropriate, in the face of fluctuating nutrient intake by the organism.

At the cellular level, nutrient regulation of growth factor signalling is perhaps best understood for the regulation of mTORC1 by amino acids (Kim et al., 2002, Nicklin et al., 2009). Removal of amino acids (in particular the essential branched chain amino acid leucine) rapidly inactivates mTORC1 (Kim et al., 2002). Amino acids regulate mTORC1 localisation and therefore access to its activator, the small GTPase Rheb (Inoki et al., 2003a, Kim et al., 2008a, Sancak et al., 2010, Sancak et al., 2008, Kim et al., 2012, Zoncu et al., 2011).

Specifically; amino acid signalling from inside the lysosome drives nucleotide loading of the Rag GTPases, which form part of the Ragulator/Rag complex, via a v-ATPase that physically interacts with this complex (Zoncu et al., 2011). When activated, the Rag GTPases recruit mTORC1, via its subunit Raptor, to the lysosome membrane. This allows mTORC1 to interact with Rheb, which is also localised on this membrane (Kim et al., 2008a, Sancak et al., 2010, Sancak et al., 2008). Targeting mTORC1 to the lysosomal membrane by addition of a lysosome localisation motif to the protein overcomes amino acid dependent regulation (Sancak et al., 2010). In the absence of amino acids, the binding protein SH3BP4 binds the inactive Rag GTPase complex and impairs conversion of the complex to the active form, which further ensures mTORC1 remains inactive (Kim et al., 2012). As they control mTORC1 localisation, amino acids are dominant to the numerous other factors that regulate mTORC1, including growth factors and cellular energy status (AMPK).

Amino acids further regulate protein synthesis downstream of mTORC1- highlighting the importance of preventing activity of biogenic pathways when the necessary substrates are unavailable. This regulation is via the eiF2α kinase, GCN2. In both yeast and mammalian cells, amino acid starvation activates GCN2, which phosphorylates the translation initiation factor eiF2α on serine 51. This phosphorylation reduces the activity of eiF2α and therefore inhibits translation initiation and protein synthesis (Sonenberg and Hinnebusch, 2009). In yeast GCN2 is activated by the binding of uncharged tRNAs, which would be present in the cell upon amino acid shortage (Dong et al., 2000). It is likely mammalian GCN2 is activated by a similar mechanism, as the tRNA binding domains of GCN2 are conserved and critical for mammalian GCN2 function (Sood et al., 2000). Importantly, although the translation of most mRNAs is suppressed upon GCN2 activation, the translation of the transcription factor ATF4 is increased; ATF4 promotes expression of genes involved in amino acid import and synthesis, as well as other stress responses to cope with the amino acid shortage, and, thus, aims to relieve the amino acid shortage in the cell (Harding et al., 2000, Harding et al., 2003, Chen et al., 2004).

Most interestingly, although this aspect of GCN2 activity specifically targets the protein synthesis machinery, long-term leucine deprivation suppresses lipogenesis in the liver, in a GCN2 dependent manner. Leucine

starvation inhibits lipid synthesis through downsregulation of SREBP-1c, a master regulator of lipid synthesis, in the livers of *Gcn+/+* mice, but not in the livers of *Gcn-/-* mice (Guo and Cavener, 2007). Again, this likely highlights the importance of appropriate coordination of multiple aspects of biogenesis.

Recent evidence has also shown that nutrients can control growth factor signalling by direct post-translational modifications of proteins. In B cells dependent on the growth factor IL-3, glucose is necessary to promote the cell surface expression of the IL-3 receptor (IL3R) (Wellen et al., 2010). In the absence of glucose, amino acid uptake is reduced and cells atrophy- even in the continued presence of IL-3. It transpires that glucose is required as the substrate of the hexosamine pathway that provides the moiety for the N-glycosylation and subsequent cell surface expression of IL3R. As most growth factor receptors are N-glycosylated and this is known to affect their surface expression, this could be a universal phenomenon (Metallo and Vander Heiden, 2010). Nutrient dependent post-translational modifications do not seem to be limited to glucose dependent glycosylation. Zhao *et al* found that nutrient dependent acetylation in the liver regulated the activity of enzymes involved in a range of metabolic pathways, including glycolysis and fatty acid synthesis (Zhao et al., 2010). Protein acetylation depends on the availability of acetyl-CoA, which depends on nutrient availability. Ultimately, nutrient availability is necessary even to provide the ATP for protein phosphorylation, which is necessary for a vast array of cellular functions including growth factor signalling and biogenesis (Wellen and Thompson, 2012).

1.9 Growth Factor and/ or Nutrient Withdrawal; the Effects on Cell Growth and Metabolism

As nutrient and growth factor signalling are interdependent, the effects of growth factor and nutrient withdrawal overlap. As a direct effect of losing growth factor signalling, growth factor activated anabolic pathways are repressed and this helps conserve cellular energy and metabolites. In addition, catabolic pathways- namely autophagy- that are suppressed by growth factor signalling are activated. This appears to provide substrates to fuel necessary biogenesis and prolong cell survival. In line with this, Yu *et al* showed that mTORC1 is

reactivated in rat kidney cells upon protracted serum (nutrient and growth factor) starvation, which the authors hypothesise is due to the result of the replenishment of intracellular amino acids by autophagy (Yu et al., 2010). Despite this, because starvation and catabolism causes cellular atrophy, it will ultimately lead to cell and organism death (Edinger and Thompson, 2002, Lum et al., 2005a, Rathmell et al., 2000, Vander Heiden et al., 2001).

The cell also activates a number of adaptive responses to cope with the effects of growth factor and nutrient withdrawal. Depletion of cellular energy, as can occur downstream of starvation, increases the AMP/ADP: ATP ratio in the cell. This activates the heterotrimeric kinase AMPK (AMP-activated protein kinase), a highly conserved eukaryotic sensor of cellular energy status (Hardie, 2011). AMPK suppresses most anabolic pathways- acting to acutely regulate metabolic enzymes via phosphorylation, as well as mediating longer-term transcriptional changes (Mihaylova and Shaw, 2011, Hardie, 2011). Using lipid metabolism as an example; AMPK phosphorylates and inhibits HMGCoR and ACC to repress de novo fatty acid and sterol synthesis, as well as phosphorylating and inactivating SREBP-1 to inhibit expression of these, and other, lipid synthesis genes (Carling et al., 1987, Li et al., 2011, Sato et al., 1993). AMPK also inhibits mTORC1 by phosphorylating and activating the mTORC1 inhibitor TSC2, as well as by direct phosphorylation of the Raptor subunit of the mTORC1 complex (Inoki et al., 2003b, Gwinn et al., 2008). This further suppresses anabolism and activates catabolism, as already described.

Although most anabolic processes are blocked, AMPK drives mitochondrial biogenesis, through the activation of the transcriptional co-activator peroxisome proliferator-activated receptor γ co-activator 1α (PGC1-α) (Zong et al., 2002). This increases the cells capacity for oxidative phosphorylation and helps restore the energy balance within the cell. Interestingly, AMPK also promotes the surface expression of nutrient transporters and nutrient uptake (Bonen et al., 2007, Chen et al., 2008, Kurth-Kraczek et al., 1999). However, if AMPK is activated under starvation conditions, this cannot be sufficient to maintain adequate nutrient uptake in growth factor deprived cells because cells atrophy (Edinger and Thompson, 2002, Lum et al., 2005a, Rathmell et al., 2000, Vander Heiden et al., 2001). Indeed, AMPK also activates catabolic pathways to provide cell metabolites-

activating autophagy by direct phosphorylation and activation of Ulk1, a component of the autophagic machinery, as well as indirectly via inhibition of mTORC1 (Egan et al., 2011, Kim et al., 2011).

During development, the growth of certain tissues is protected from the effects of nutrient deprivation. So called 'organ-sparing' preserves the growth and maintenance of the CNS at the expense of other organs. Starvation, unsurprisingly, attenuates net growth of developing *Drosophila* larvae. However, CNS growth is maintained. Whereas most tissues depend on nutrient dependent signals to drive cell growth, the growth of neural progenitor cells (the cell lineage that forms the brain tissue) is regulated by a nutrient independent extracellular factor, Jelly belly (Jeb) (Cheng et al., 2011). Jeb drives downstream activation of the critical growth-promoting PI3K pathway, thus liberating neural lineages from growth restriction upon nutrient deprivation (Cheng et al., 2011). Interestingly, this only occurs after *Drosophila* larvae have passed a nutrient-dependent 'critical weight gain' threshold and neuroblasts have begun to grow and divide (Sousa-Nunes et al., 2011). Presumably this ensures growth is restricted until the animal has acquired enough resources to complete development even if subsequent starvation occurs.

1.10 Cell Growth and Disease

Carefully regulated and coordinated cell growth is required for the development and maintenance of a functional organism; loss of proper growth control results in disease. At the most basic level this is seen when systemic growth factor signalling is misregulated during development; too much Growth Hormone (GH) drives acromegaly/ gigantism, whereas too little GH or the inability to respond to GH or IGF-1, the primary mediator of the effects of GH, leads to growth retardation and dwarfism (Walenkamp and Wit, 2007).

Improper cell growth disrupts normal cell and tissue function. Highlighting this, recent evidence suggests Autistic Spectrum Disorders (ASD) may result from hypertrophic neuronal growth that disrupts neuronal wiring and connectivity. A subset of ASD sufferers have inactivating mutations in negative regulators of mTORC1 and, at the age of onset, a considerable proportion of

autism sufferers have significantly larger brains than age-matched controls (Butler et al., 2005, Courchesne et al., 2007, Wiznitzer, 2004). Moreover, this enlargement is associated with areas of the brain involved in social and emotional processing- the functions affected in autistic individuals (Courchesne et al., 2007). Consistent with a causative role for impaired mTORC1 signalling in ASDs, mice lacking PTEN or TSC1 (two negative regulators of mTORC1 activity) in specific subsets of neurons develop neuronal hypertrophy and display impaired social interactions, reminiscent of the type found in ASD patients (Kwon et al., 2006, Meikle et al., 2008, Meikle et al., 2007, Tsai et al., 2012). Importantly, blocking mTORC1 activity with rapamycin reversed both the hypertrophy and a number of the behavioural phenotypes- demonstrating a causative role for mTORC1 and, potentially, hypertrophy in the ASD-related phenotypes (Meikle et al., 2008, Tsai et al., 2012, Zhou et al., 2009).

ASDs may represent a disorder caused by subtle changes in cell growth and subsequent organ disorganisation. However a more overt example of diseases associated with overgrowth are cancers. The formation of a tumour cell mass requires deregulated cell growth, in addition to deregulated proliferative and survival controls. As a result, tumour cell metabolism is geared towards macromolecular synthesis and biogenesis; most tumours display biogenic and bioenergetic characteristics of rapidly growing and proliferating cells (DeBerardinis et al., 2007, Vander Heiden et al., 2009). This includes high rates of aerobic glycolysis (Warburg effect), glutaminolysis and nutrient import, which all help drive high rates of de novo fatty acid, protein and nucleotide synthesis (Deberardinis et al., 2008b, Vander Heiden et al., 2009, Warburg, 1956, Menendez and Lupu, 2007).

Whereas normal cells usually require growth factor signalling to drive biogenesis, tumour cells are largely liberated from this regulatory control by mutations that result in activation of the key growth regulating pathways Akt, mTORC1 and/ or Myc (Lum et al., 2005a, Meyer and Penn, 2008, Shaw and Cantley, 2006, Wullschleger et al., 2006). Indeed, inherited mutations in negative regulators of growth such as PTEN and TSC1/2 predispose to tumour development (Bonneau and Longy, 2000, Inoki et al., 2005, Sampson, 2003). It must be noted that these pathways also regulate other processes that contribute to tumourigenesis, e.g. cell survival and cell cycle progression, which

means it is difficult to prove that the deregulated growth has a causative role in the cancer (Meyer and Penn, 2008, Vivanco and Sawyers, 2002). In support of this causation however is evidence that targeting tumour cell metabolism and biogenesis, such as by blocking fatty acid synthesis, can reduce the growth of numerous tumour cells (Bauer et al., 2005, Brusselmans et al., 2005, Hatzivassiliou et al., 2005, Menendez and Lupu, 2007, Kuhajda et al., 2000). Furthermore, as described earlier, recent findings from our lab showed that oncogenic Ras and loss of the tumour suppressor Rb, two pathways deregulated in most cancers, synergise to strong and sustained cell growth in both primary Schwann cells and fibroblasts *in vitro* (Collins et al., 2012, Hahn and Weinberg, 2002). Interestingly, Rb does not activate PI3K/ Akt signalling, which suggests other cooperating pathways may also be required to drive the prolific cell growth characteristic of many tumours.

One example of cell overgrowth that is particularly interesting with respect to disease is cardiac hypertrophy. This is because, depending on the hypertrophic stimulus, it can be physiological or pathological. Exercise and pregnancy drive physiological hypertrophy, characterised by increased myocyte size, which includes a proportional increase in the expression of myofibril proteins and mitochondrial biogenesis, and efficient vascularisation of the enlarged muscle tissue. In contrast, hypertension and myocardial infarction are examples of stimuli that cause pathological hypertrophy, where there is a lack of coordination between the biogenic processes described for physiological hypertrophy and disproportionate expansion of certain regions of cardiac muscle, leading to impaired cardiac function (Ojamaa, 2010, Schaub et al., 1997). These examples demonstrate that hypertrophy can be beneficial in adult organisms, but highlight that this must be properly coordinated- otherwise tissue function is compromised and disease results.

Most interestingly, distinct signalling pathways drive physiological and pathological hypertrophy. Activation of IGF-1 and PI3K/ Akt signalling in the heart can drive physiological hypertrophy and loss of signalling through this pathway prevents exercise induced physiological hypertrophy (DeBosch et al., 2006, DeBosch and Muslin, 2008, Dorn and Force, 2005, Kehat and Molkentin, 2010, Kim et al., 2008c, McMullen et al., 2003, Shioi et al., 2000). However, disruption of IGF-1/ PI3K/ Akt signalling does not prevent pathological

hypertrophy induced by pressure overload, suggesting that this might be mediated by distinct signalling pathways (DeBosch et al., 2006, McMullen et al., 2003). Indeed, the calcineurin-NFAT pathway appears to be important in this regard- transgenic mice that overexpress calcineurin or NFAT3 in the heart develop pathological hypertrophy and, reciprocally, loss of calcineurin-NFAT signalling blocks pathological hypertrophy (Bourajjaj et al., 2008, Bueno et al., 2002, Molkentin et al., 1998, Wilkins et al., 2004). Interestingly, although SRF is required for cardiac muscle growth during development, transgenic mice overexpressing SRF in cardiac myocytes develop pathological hypertrophy (Zhang et al., 2001a, Zhang et al., 2001b). Again, this highlights that activation of biogenic signalling pathways must be properly controlled in order to prevent disease.

From these examples it is clear that disrupted cell growth underlies a range of diverse diseases and can be caused by inappropriate changes in systemic signalling as well as cell intrinsic genetic changes. By understanding the mechanisms that underlie normal cell growth control it should be possible to determine how this control becomes deregulated during disease and, potentially, develop therapeutics to target this deregulation. Reciprocally, understanding the mechanisms underlying diseases resulting from deregulated growth can give an insight into normal cell growth control- particularly in high penetrance inherited genetic disorders.

1.11 Summary

Cell growth, the addition of mass and/ or volume, is critical for the development and homeostasis of all organisms. Loss of cell growth control, leading either to hyper- or hypo- trophy, causes disease. Mammalian cell growth and size maintenance usually requires an instructive growth factor signal, which drives nutrient uptake, promotes anabolism and suppresses bulk degradation. In the absence of such a signal cells atrophy, because they cannot utilise sufficient extracellular nutrients to maintain cell metabolism.

Cell growth is distinct and separable from cell proliferation, which is simply progression through the cell cycle. In dividing cell populations, cell size is

determined by the balance between growth and division. In non-dividing populations, where there is no cell division to limit cell size, another signal must determine final cell size- in some tissues this is the level of growth factor signal a cell receives. In addition to growth factors, signals such as extracellular nutrient availability and mechanical forces can also regulate cell growth and cell size. The PI3K/ Akt/ mTORC1 pathway appears to be a central and regulator of cell growth downstream of diverse biogenic stimuli.

Cell growth may be uniform (i.e. the coordinate addition of cell mass, volume and organelle content), however it can also be non-uniform, resulting in the disproportionate expansion of one part of the cell, e.g. an organelle, compared to the rest. In every case, growth is closely coupled to the needs of the cell; presumably to prevent waste of cellular resources.

Finally, the primary Schwann cell is a powerful model system in which to study cell growth. Schwann cells can be cultured indefinitely as primary cells that maintain intact checkpoints, including normal growth control. Moreover, Schwann cells produce their own survival factor that has no effect on cell growth or division, which means the cells survive in conditions free from added extracellular factors. This provides a clean background against which to study the effects of adding specific factors on cell growth.

1.12 Thesis Aims

Cell growth, the addition of cell mass and volume, is regulated by growth factor activated signalling pathways. Studies in the Schwann cell have identified that organelle (mitochondrial) biogenesis can be differentially regulated downstream of distinct extracellular factors (IGF-1 and NRG1) and uncoupled from cell volume addition, dependent on activation of the PI3K and ERK signalling pathways. The objectives of this thesis work were to use the *in vitro* Schwann cell system to investigate:

1. The regulation of cell growth and biogenesis downstream of the PI3K/Akt and ERK signalling pathways.
2. The cellular changes and signalling required for cell volume addition during cell growth.

Chapter 2: Materials and Methods

Plastic ware was purchased from Falcon, reagents from Sigma and tissue culture dishes from Nunc, unless otherwise specified. All kits were used according to manufacturers instructions, unless otherwise specified. Solutions were made up with MilliQ deionised water (ddH_2O).

2.1 Cell Culture

Primary Schwann Cells

Primary Schwann cells were purified from the sciatic and brachial nerves of postnatal day 7 Sprague Dawley rats, according to the method of Cheng et al (Cheng et al., 1995). This method yields cultures of >99.9% purity by immunfluorescence for cell markers. Cells were maintained in culture in low-glucose (1g/l), no glutamine DMEM plus phenol red (Lonza) supplemented with 3% charcoal stripped foetal calf serum (FCS) (Biosera), glutamine (4mM) (Gibco), Kanomycin (100μg/ml), gentamycin (2μg/ml) (Gibco), forskolin (1μM) (Ascent Scientific) and GGF on Poly-L-Lysine (PLL) (2.4μg/ml) coated dishes. Medium with these supplements is hereafter described as complete medium. Cells were cultured at 37°c in 10% CO_2 and 95% humidity. Cells were passaged on reaching ~80% confluency.

NSΔRafER Cells

NSΔRafER cells were generated by the co-culture of primary Schwann cells with a producer line expressing ΔRafER retrovirus, pre-treated with mitomycin C (Lloyd et al., 1997). After several days cultures were transferred to selective medium containing G418 (0.4mg/ml) (Gibco). Drug resistant colonies were pooled and expanded. Activation of the RafER construct was achieved by the addition of tamoxifen (Tmx) in ethanol (100nM) (VWR) (Harrisingh et al., 2004). Cells were cultured in low-glucose no glutamine DMEM minus phenol red (Gibco), with supplements and in conditions as described above.

Generation of ER.mSREBP1a and ER.mSREBP2 expressing Schwann cells by retroviral transduction

Phoenix amphotropic packaging cells were used to produce the retrovirus titre required to infect the NS cells. Phoenix cells were seeded onto 100mm dishes in 10% FCS containing high glucose (4500mg/l) DMEM at a density of $5x10^6$ cells per dish. The following morning the cells were medium changed in 4ml fresh medium and transfected as follows: 6.2µg DNA + 5.5µl attractene (QIAGEN) + plain DMEM to a total volume of 1860µl was mixed in a 2ml eppendorf and incubated at room temperature for 15 minutes before being added directly to the cells. After 4 hours the cells were medium changed into 10ml of fresh medium and left for 24 hours and then media changed into 6ml fresh medium (the smaller volume concentrates the virus). After a further 24 hours the 6ml of media, containing the virus, was collected into a falcon and the cells given 6ml fresh medium. After filtering the virus-containing medium through a 0.45µm filter (Millipore), polybrene was added to a final concentration of 4µg/ml. This virus was used immediately to infect normal or NSΔRafER Schwann cells (seeded the previous day onto 100mm dishes at a density of $5x10^5$ cells per dish) as follows: the Schwann cell medium was aspirated and replaced with the prepared virus solution and the cells incubated with the virus for 3 hours at 37°c. The Schwann cells were then media changed back into normal Schwann cell culture medium and left overnight. The virus collection/ infection was repeated over the next two days so that in total 3 infections were carried out. This was to ensure maximal retroviral transduction efficiency. After the final infection, successfully transduced cells were selected by antibiotic selection. All constructs used in this thesis contain the puromycin resistant gene therefore cells were incubated in normal medium containing the addition of 0.5-1µg/ml puromycin. Selection was continued until parallel plates of cells infected with a non-puromycin resistant construct and undergoing the same puromycin selection were dead, approximately 3 days. Cells were then cultured in normal Schwann cell medium, as described in section 2.1.

Protocol for Cell Cycle Arrest and Transfer to Defined Growth Factor-Free Conditions

Cells were seeded onto PLL, fibronectin (10μg/ml) and laminin (50ug/ml) coated dishes in complete medium for 24 hours prior to being treated with the DNA polymerase α inhibitor aphidicolin (1μg/ml) in complete medium for 24 hours. Cells were then switched into defined factor-free medium plus aphidicolin for a further 24 hours. Two types of defined factor-free medium were used, as described in the results chapter:

1. Minimal Medium: DMEM containing transferrin (100μg/ml), bovine serum albumin (BSA) (100μg/ml) (Gibco), putrescine (16.1μg/ml) and selenium (39ng/ml). In certain experiments delipidated BSA (Sigma) was used to make the Minimal Medium, as specified in the Results chapter.

2. SATO: DMEM containing transferrin (100μg/ml), BSA (100μg/ml), putrescine (16.1μg/ml), selenium (39ng/ml), thyroxine (50ng/ml), triiodothyrine (50ng/ml) and progesterone (60ng/ml).

After this treatment cells were switched to medium containing +/- extracellular factors, as specified in individual experiments. Extracellular factors used in this study were: complete medium, defined medium, IGF-1 (100ng/ml) (Autogen Bioclear) in defined medium, Tmx in defined medium (to activate the RafER construct; ethanol was added (v:v) to control cells). At the concentration used, IGF-1 is saturating for cell volume addition (Conlon et al., 2001).

Exogenous Fatty Acids and Cholesterol

A chemically defined mix of fatty acids and cholesterol (Chemically defined lipid concentrate, Gibco) was added, in dilutions as described in the results, in defined medium plus aphidicolin in a 30 minute pre-incubation prior to the addition of extracellular factors in the experimental protocol described above.

Inhibitors

Inhibitors were added in defined medium plus aphidicolin in a 30 minute pre-incubation prior to the addition of extracellular factors in the experimental protocol described above. The exception is chloroquine. Chloroquine was added 7 hours prior to the end-point assay being performed, which in all cases

is after any extracellular factors were added. See Table 2.1.1 for list of inhibitors.

Inhibitor	Function	Concentration	Company
Rapamycin	Inhibits mTORC1	0.15μg/ml	Sigma
ZSTK474	Inhibits class I PI3K's	500nM	Alexis Biochem
PD184532	Inhibits MEK	0.75μM	Axon
NaN_3	Inhibits aerobic respiration to deplete cellular ATP	20mM	Sigma
NaN_3/NaF	Inhibits aerobic respiration/ glycolysis to deplete cellular ATP	5μg/ml/126μg/ml	Sigma
Chloroquine	Inhibits lysosome acidification to inhibit lysosome function	25μM	Sigma
Cerulenin	Inhibits fatty acid synthase and HMGCoA Reductase to inhibit de novo fatty acid and sterol synthesis	7.5μg/ml	Cayman Chemicals
Simvastatin	Inhibits HMGCoA Reductase to inhibit de novo sterol synthesis	5μM	Sigma
C75	Inhibits fatty acid synthase to inhibit de novo fatty acid synthesis	3μg/ml	Sigma

Table 2.1.1 Inhibitors

Transient transfection of cells with siRNA

Cells were plated onto PLL and fibronectin coated 6-well dishes (150,000 cells per well) in complete medium. The following day cells were transfected with siRNA duplexes as follows: FlexiTube siRNA (Qiagen) stock solutions (20μM in ddH_2O) were diluted in plain DMEM to generate siRNA working solutions of 0.4μM (SREBP-2 siRNA oligo's) or 0.8μM (SREBP-1 siRNA oligo's). Then, siRNA/lipid complexes were prepared by sequentially adding 88μl plain DMEM + 12μl siRNA working solution + 6μl HiPerfect (Qiagen) (volumes shown are for a single well). Complexes were left to form at room temperature for 15 minutes. In this time, cells were medium changed with 2.3ml fresh complete medium and then the total volume (106μl) of siRNA/lipid complex was added dropwise to the cells and incubated overnight for 18 hours. After this time, cells were medium changed into Minimal Medium plus aphidicolin and left for 24 hours before being changed into Minimal Medium plus aphidicolin +/- extracellular factors, as specified in the results. After a further 24 hours, cell volume was assayed using the Coulter Counter. Knockdown was verified by RT-qPCR.

2.2 Cell Size Measurements

Coulter Counter: Cell Volume

Cells cultured in 6-well dishes were gently washed 1x with PBS (PAA) and removed from the dish in 500μl pre-warmed trypsin-EDTA. Trypsin activity was quenched with the addition of 1500μl medium containing 3% FCS and the total volume was transferred to 6ml Isoton II (Beckman Coulter) in an acuvette cup (Beckman Coulter) and the volume of >5000 cells was measured using a Multisizer 4 Coulter Counter (Beckman Coulter) and data analysed in the accompanying software. Each condition within an experiment was measured in duplicate or triplicate.

Quantitative Phase Microscopy (QPM): Cell Dry Mass and Cell Volume

Cells were cultured on PLL, fibronectin and laminin coated glass-bottomed dishes (Mattek, P35G-1.0-14-C). Imaging was performed on a Quantitative Phase Microscope (QPM) custom built from a Nikon Eclipse TE2000-E

microscope (Nikon). The imaging process is a Diffractive Phase Microscope Method. The microscope stage was contained within a 37℃ heated environmental chamber supplied with a humidified gas mixture (90% air/ 10% CO_2). Samples were imaged in conditioned medium filtered using a 0.2μm filter to remove interfering cellular debris. Samples were carried to the microscope in a heated chamber to avoid cooling of the cell culture medium and were placed on the microscope stage 20 minutes before imaging to allow motion within the culture medium created during the transfer to settle.

Images were taken in MetaMorph (Molecular Devices) and analysed within MatLab (MathWorks) using algorithms developed by Seungeun Oh (Kirschner Lab, Harvard Medical School). Background reference images were taken in the absence of a sample in the specimen holder. Reference images were taken intermittently through the imaging process to account for drift or alterations in the imaging apparatus over time. The interferometric data (cellular dry mass) was retrieved by comparison of the sample image to the reference image using QPM image processing. Cellular dry mass was calculated using this information and the refractive index of the imaging medium (conditioned medium as described above), which was measured using a refractometer.

Cell volume was quantified from the difference in apparent cell dry mass when images are taken in 2 different media with differing and known refractive indices. To do this, after imaging in conditioned media as described above media was replaced with pre-warmed conditioned medium containing 10% ficoll and re-imaged. The presence of ficoll increased the density and therefore the refractive index of the medium. The refractive indices of the two media were measured using a refractometer. See Popescu et al 2006 for the principles of QPM.

Cell Protein Content

Bichonic Acid (BCA) Assay

In the BCA assay the reduction of a copper containing substrate (by peptide bonds and the amino acids cysteine, tryptophan and tyrosine) produces a colorimetric change, the intensity of which can be quantified by measuring absorbance at 560nm in a spectrophotometer. The amount of copper reduced and therefore intensity of colour is proportional to the protein concentration in

the measured solution. To calculate the protein concentration of cell lysates, absorbance was compared to the absorbance of bovine serum albumin (BSA) standards of known concentrations quantified in parallel.

Cells cultured in 6-well dishes were gently washed 1x with PBS and lysed in 300μl radio-immunoprecipitation assay (RIPA) buffer (Table 2.4.5) + 0.05% sodium dodecyl sulphate (SDS) (BioRad) on ice, rotating for 30 minutes. Lysates were then transferred to labelled eppendorfs on ice. Lysate protein concentration was determined using a modified BCA Assay (Pierce), as follows: 25μl of sample was transferred to a well of a 96-well plate and, to this, 200μl of working BCA reagent (50:1 solution of reagents A:B) was added. After incubating the plate for 30 minutes at 60°c, protein concentration was determined by absorbance at 560nm using a Versamax spectrophotometer and SoftMax Pro Software (Molecular Devices) and comparison to the absorbance of bovine serum albumin (BSA) (Pierce) standards made in RIPA+0.05% SDS. Each well of the 6-well dish was lysed in 300ul lysis buffer, therefore:

Protein per well (mg) = lysate protein concentration (mg/ml) x 0.3

To calculate the amount of protein per cell, protein per well was normalised to the cell number per well of parallel 6-well cell culture plates. Cell number per well was quantified using a Z2 Coulter Counter (Beckman Coulter), as follows: Cells were gently washed 1x with phosphate-buffered saline (PBS) and removed from the dish with 500μl trypsin-EDTA. Trypsin activity was quenched with the addition of 500μl medium containing 3% FCS and the total volume transferred to 6ml Isoton II (Beckman Coulter) in an acuvette cup (Beckman Coulter). Each condition was assayed in triplicate.

Total Cell Protein (Alexa647-Succinimidyl Ester)

Cells were cultured on 13mm glass coverslips. Stocks of 10mg/ml Alexafluor-conjugated Succinimidyl Ester (Molecular Probes) were made up in dimethyl sulfoxide (DMSO) and stored at -20°c for up to 12 months. Coverslips were fixed in 4% PFA/PBS for 15 minutes at room temperature. After washing 2x in PBS cells were permeabilised in 100% ice-cold methanol for 10 minutes at room temperature before being washed a further 2 x in PBS and incubated in the dark at room temperature for 30 minutes in a 40ng/ml solution in PBS of

Alexafluor-conjugated Succinimidyl Ester to label cell primary amines. After this time, coverslips were washed 6x in PBS before being mounted on glass slides in mounting medium.

Succinimidyl esters react with primary amines, therefore labelling the N-terminus of amino acids, peptides and proteins and the R-group of lysines. The amount of cell-bound Alexa647-succinimidyl ester was taken as an indicator of cell protein content and was quantified as the total cell fluorescence intensity measured from widefield microscopy images taken using either widefield microscope described in section 2.6.

2.3 Molecular Biology

RNA extraction

After aspirating the cell culture medium and without washing the cells, 1ml Tri reagent was added directly to cells cultured on 10cm dishes. Cells were lysed by pipetting the sample up and down several times, avoiding bubbles. The homogenised samples were then transferred to 1.5ml eppendorfs, snap frozen in liquid nitrogen and stored at -80°c until use.

After thawing at room temperature, the homogenised samples were incubated at room temperature for 5 minutes to allow complete dissociation of nucleoprotein complexes. Then 200µl chloroform (VWR) was added to each sample in the eppendorf and the eppendorf shaken vigourously by hand for 15 seconds. The samples were then incubated at room temperature for 10 minutes before being centrifuged at 13000 RPM for 15 minutes at 4°c in a tabletop centrifuge (Biofuge). The mixture separates into a lower, pink phenol-chloroform phase and an upper aqueous phase that contains the RNA. The upper aqueous phase was removed (~400µl), transferred to a new tube and 500µl 100% isopropanol (VWR) added before incubating the samples at room temperature for 10 minutes. The samples were then centrifuged again at 13000 RPM for 10 minutes at 4°c. The supernatant was then removed from the tubes, leaving the RNA pellet, which was then washed by adding 600µl 75% ethanol and incubating at room temperature for 10 minutes. The samples were then vortexed briefly before being centrifuged at 7500g for 5 minutes at 4°c to re-

pellet the RNA. After aspirating the supernatant the RNA was left to air-dry and then resuspended in 12µl RNAse-free water. The concentration of RNA was determined using a nanodrop spectrophotometer (Thermoscientific) at OD^{260}. RNA was stored at -80°c until use.

Complementary DNA (cDNA) synthesis

To produce cDNA for quantitative RT-PCR, 500ng-1µg of RNA was reverse transcribed using the SuperScript™ II Reverse First-Strand Synthesis System (Invitrogen). Samples containing RNA, 1µl random hexamers and 1µl of dNTPs (10mM each dNTP) were made up to a total volume of 12µl using sterile, distilled water and then incubated at 65°c for 5 minutes and then rapidly chilled on ice for >1 minute. Then, 8ul of the Stock II Reaction mix (4µl 5x First-Strand Buffer, 2µl 0.1M Dithiotheitol (DTT), 0.5µl RNAseOUT™ (40U/µl), 0.5µl SuperScript™ II Reverse Transcriptase (200U), 1µl H2O) was added to each sample and mixed by pipetting up and down gently several times. The reactions were then incubated at 25°c for 10 minutes, then 42°c for 50 minutes. The reactions were then terminated by heating to 70°c for 15 minutes before being chilled on ice. Finally, the RNA in the sample was removed by addition of 0.5µl *E. coli* RNAseH (2U/µl) and incubation at 37°c for 20 minutes.

Quantitative Polymerase Chain Reaction (QPCR)

Quantitative PCR was performed using the MESA BLUE qPCR MasterMix Plus for SYBR® kit (Eurogentec) and Opticon2 DNA engine (MJ Research).

Relative transcript levels of target genes were normalised to B2M. The gene specific primers used to amplify target gene transcripts in this thesis are described in Table 2.3.1. For most reactions, gene specific primers were designed using the Roche Applied Science Assay Design Centre (Roche Applied Science), or, where specified, taken from published data.

To perform the qPCR: A master mix of 0.75µl primer stock solution (containing 10mM each of the forward and reverse primers in ddH_2O), 10µl 2x MESA Blue MasterMix and 7.5µl ddH_2O was made for η x reactions for each gene to be assayed in the experiment and mixed gently but thoroughly by pipetting. This 18µl volume of master mix was added to a well of the PCR plate, followed by 2µl cDNA template or 'No Template ddH_2O' control. All reactions were

performed in duplicate. The basic cycling parameters used for the qPCR are outlined in Table 2.3.2, although optimal annealing (A), extension (E) and primer dimer melting temperatures (TM) were determined empirically for each primer pair (Table 2.3.1). At the end of 40 cycles of amplification a dissociation curve was generated by measuring SYBR green fluorescence at 0.2°c intervals between 55°c and 95°c to check only one amplicon was detected by the PCR reaction. Relative quantitation of mRNA levels was made using the ΔΔCT method. This is an approximation method and assumes the normaliser gene and target gene are amplified with equivalent efficiencies (the proportion of cDNA strands amplified in every cycle).

Gene	Primer	Source	qPCR notes
B2M	F: 5' –TGACCGTGATCTTTCTGGTG- 3' R: 5' –ATTTGAGGTGGGTGGAACTG- 3'	Roche Applied Science, ProbeFinder	A 58°c, E 72°c, TM 77°c
FASN	F: 5' –GGCCACCTCAGTCCTGTTAT- 3' R: 5' –AGGGTCCAGCTAGAGGGTACA- 3'	Roche Applied Science, ProbeFinder	A 58°c, E 72°c, TM 77°c
HMGCoA Reductase	F: 5' –GACCTTTCTAGAGCGAGTGCAT- 3' R: 5' –GCTATATTCTCCCTTACTTCATCCTG- 3'	Roche Applied Science, ProbeFinder	A 58°c, E 72°c, TM 77°c
SREBP-2	F: 5' -CGCTCGCATTTCACTGAAGTAG- 3' R: 5' -GGCATAGAAGACGGCCTTCAC- 3'	(de Preux et al., 2007)	A 60°c, E 72°c, TM 77°c
SREBP-1a	F: 5' –CGAGGTGTGCGAAATGGAC- 3' R: 5' –GAAGCATGTCTGATGTCGGTCA- 3'	(de Preux et al., 2007)	A 58°c, E 72°c, TM 77°c
SREBP-1c	F: 5' –ACGGAGCCATGGATTGCACA- 3' R: 5' -CAAATAGGCCAGGGAAGTC- 3'	(de Preux et al., 2007)	A 60°c, E 72°c, TM 77°c

Table 2.3.1 Gene specific primers.

Stage	Condition	Number of Cycles
Hot Start	95°c, 10 minutes	1
Denaturation	95°c, 15 seconds	40
Annealing	58°c, 20 seconds	
Extension	72°c, 25 seconds	
Melt Primer Dimers	77°c, 1 second	

Table 2.3.2 Basic cycling conditions used for qPCR.

E. coli transformation by 'heat shock'

Aliquots containing 50µl of competent E. coli (DH5α strain) in 1.5ml eppendorf tubes were thawed on ice. The DNA to be transformed into the bacteria was then added directly to the thawed vials; typically this was ~20ng maxi prep DNA. After flicking several times to mix the DNA and bacteria the tubes were incubated on ice for 30-45 minutes before being heat-shocked at 42°c for 45 seconds and then immediately chilled on ice for 2-3 minutes. After this, 1ml of SOC medium (Invitrogen) was added to each tube and the tubes were incubated, shaking, at 37°c for 45 minutes. The bacteria were then pelleted by centrifugation at 6000 RPM for 2 minutes in a tabletop centrifuge and, after removing 750µl using a P1000 Gilson pipette, resuspended in the remaining 250µl of the supernatant. Usually, 50µl of this transformed bacterial suspension was spread onto LB agar plates and incubated overnight at 37°c.

The LB agar plates were made by melting LB Broth agar (10g tryptone, 5g yeast extract, 5g NaCl, 1ml IN NaOH, 15g agar or agarose, to a final volume of 1 liter in water), then leaving the melted agar until cooled to below 35°c before adding the appropriate antibiotic for selection (in all cases in this thesis, ampicillin to a final concentration of 100µg/ml) and pouring onto 10cm dishes (Sterilin). Plates were left to air dry in a sterile environment before use.

Growing up bacterial colonies and harvesting bacterial cultures using DNA maxi preps

Single bacterial colonies from the LB agar plates described above were picked and added to 4ml LB broth (10g tryptone, 5g yeast extract, 5g NaCl, 1ml IN NaOH, to a final volume of 1 litre in water) containing the antibiotic ampicillin (100µg/ml) for selection in a 5ml tube (Sterilin), loosely fastened, and incubated for ~8 hours, shaking, at 37°c. After this time, 1ml of this starter culture was used to inoculate 100ml LB broth containing the antibiotic ampicillin (100µg/ml) for selection and left overnight, shaking, at 37°c.

The bacteria from the overnight cultures were pelleted by centrifugation at 4000 RPM for 20 minutes at 4°c (Beckman Coulter, Model J-6M). Plasmid purification was carried out using the EndoFree Plasmid Maxi Kit (QIAGEN) according to the manufacturers instructions, except that the final DNA pellet was resuspended in 100µl sterile ddH_2O. The concentration of DNA was determined using a nanodrop spectrophotometer (Thermoscientific) from $Abs_{260/280}$. DNA was stored at -20°c.

DNA sequencing

DNA was sequenced externally by Source Bioscience. Samples were sent as follows: 15µl DNA (100ng/µl) and primers (3.2pmol/µl).

DNA plasmid constructs used in the thesis

The DNA constructs used in this thesis are as follows:

Plasmid	Vector	Description	Source	Published
pBabe-puroER^{TM}-mSREBP1a	pBabe-puroER^{TM}	Retroviral expression vector	Schulze lab (London Research Institute)	N/A
pBabe-puroER^{TM}-mSREBP2	pBabe-puroER^{TM}	Retroviral expression vector	Schulze lab (London Research Institute)	N/A
pBIRD-GFP	pBIRD	Retroviral expression vector	Raff lab (LMCB, UCL)	(Tang et al., 2001)

Table 2.3.3 DNA constructs used in the thesis

2.4 Western Blotting

Preparation of Protein Extracts from Whole Cell Lysates

Cells were washed gently 1x in ice-cold PBS, scraped in 1ml ice-cold PBS using a rubber bung and transferred to a 2ml eppendorf, all on ice. Cells were pelleted by centrifugation at 4°c for 5 minutes at 7000 RPM in a tabletop centrifuge and, after aspirating the supernatant, the cell pellet was snap-frozen in liquid nitrogen. Cell pellets were stored at -80°c before lysis. Cell pellets were lysed in RIPA buffer (Table 2.4.5) and protein concentration of the lysate was determined using the microplate BCA assay (Pierce, according to manufacturers instructions. After taking samples for the BCA assay, sample buffer (4x) was immediately added to the lysates to a final dilution of 1x. After the BCA assay, the protein concentration of the sample buffer containing

lysates was adjusted using 1x sample buffer and lysates were boiled for 5 minutes at 95°c.

Preparation of Protein Extracts from Nuclear and Cytoplasmic Fractions

Cells were washed gently 1x in ice-cold PBS, scraped in 1ml ice-cold PBS + protease inhibitors (Table 2.4.1) using a rubber bung and transferred to a 1.5ml eppendorf, all on ice. Cells were pelleted by centrifugation at 4°c for 5 minutes at 3000 RPM in a tabletop centrifuge (Biofuge) and, after aspirating the supernatant, the cell pellet was washed once with 500μl Buffer A (Table 2.4.2) and the centrifugation repeated. After aspirating the supernatant the cell pellet was resuspended in 4x pelleted cell volumes of Lysis Buffer (Buffer A + 0.5% NP40) and incubated on ice for 10 minutes. The suspension was flicked gently every 3 minutes during the incubation period to gently mix the contents. After centrifugation at 4°c for 10 minutes at 6000 RPM in a tabletop centrifuge the supernatant (cytoplasmic fraction) was transferred to a fresh eppendorf on ice and frozen at -80°c. The nuclear pellet was washed in 250μl of Buffer A and the centrifugation repeated. After aspirating the supernatant the nuclear pellet was resuspended in 1.5x pelleted cell volumes of Buffer C (Table 2.4.3) and incubated on ice for 15 minutes. The suspension was flicked gently every 5 minutes during the incubation period to gently mix the contents. After centrifugation at 4°c for 30 minutes at 13000 RPM in a tabletop centrifuge the supernatant (cytoplasmic fraction) was transferred to a fresh eppendorf on ice and frozen at -80°c. Before running an SDS-PAGE, sample buffer (4x) was added to the lysates to a final dilution of 1x and boiled for 5 minutes at 95°c.

Reagent	Source	Final Concentration
PBS	Internal	1x
β-glycerophosphate	Sigma	6.48mg/ml
Orthovanadate	Sigma	1mM
DTT	Sigma	0.5mM
Phenylmethanesulfonylfluoride (PMSF)	Sigma	0.5mM

Table 2.4.1 PBS + protease inhibitors.

Reagent	Source	Final Concentration
Hepes pH 7.9	Sigma	10mM
Magnesium chloride	Sigma	1.5mM
Potassium chloride	Sigma	10mM
Protease inhibitor cocktail	Sigma	1:50
β-glycerophosphate	Sigma	6.48mg/ml
Orthovanadate	Sigma	1mM
DTT	Sigma	0.5mM
Phenylmethanesulfonylfluoride (PMSF)	Sigma	0.5mM

Table 2.4.2 Buffer A.

Reagent	Source	Final Concentration
Hepes pH 7.9	Sigma	20mM
Glycerol	Sigma	25%
Sodium chloride	Sigma	0.5M
Magnesium chloride	Sigma	15mM
Ethylenediaminetetraacetic acid (EDTA)	Sigma	0.2mM
Protease inhibitor cocktail	Sigma	1:50
β-glycerophosphate	Sigma	6.48mg/ml
Orthovanadate	Sigma	1mM
DTT	Sigma	0.5mM
Phenylmethanesulfonylfluoride (PMSF)	Sigma	0.5mM

Table 2.4.3 Buffer C.

SDS-PAGE

Proteins were separated by SDS-PAGE, at room temperature (Table 2.4.4 for gel recipes). Proteins <30kDa were detected using 15% gels, 30-120kDa proteins using 10% gels and >120kDa proteins using 5% gels. PageRuler Plus Prestained protein ladder (Fermentas) was used for determination of protein molecular weights.

	Running Gel	Stacking Gel
30% Acrylamide/ 0.8% Bis	See text	17%
1M Tris (pH8.8)	37%	n/a
1M Tris (pH 6.8)	n/a	12%
20% SDS	0.10%	0.10%
10% Ammonium persulfate (APS)	0.040%	0.060%
TEMED	0.047%	0.12%

Table 2.4.4 SDS-PAGE gel recipes, showing final concentrations (to 2s.f.).

Protein Transfer and Immunoblotting

Proteins were transferred to a PVDF membrane (Immobilon) by wet transfer (Table 2.4.5), at 25V (0.5-1 Amp) for 2 hours at 4°c. Membranes were blocked for 1 hour at room temperature in 5% milk/TBS-T (Table 2.4.5) and incubated overnight at 4°c in primary antibody in block solution, rotating (Table 2.4.6). The following day, the membrane was washed for 3x 10 minutes in TBS-T and then incubated in secondary antibody in block solution (Table 2.4.6) for 2 hours at room temperature, rotating. After washing for 3x 10 minutes in TBS-T and 1x 5 minutes in TBS, membranes were developed using ECL/ ECL+ developing reagent (GE Healthcare, Table 2.4.6) and exposed using the ImageQuant LAS 4000 mini CCD camera system (GE Lifesciences). Where membranes required stripping and reprobing; membranes were incubated rocking for 1 hour in 1x stripping buffer (Table 2.4.5), then washed for 3x 5 minutes in TBS-T and reblocked for 1 hour in 5% milk/TBS-T, all at room temperature, before being incubated in primary antibody, as before.

Solution	Recipe
RIPA Lysis Buffer	100mM NaCl, 1% TritonX-100, 0.5% sodium deoxycholate, 0.1% SDS, 50mM Tris pH7.5, 1mM EGTA, 20mM NaF, 100μg/ml phenylmethanesulfonylfluoride (PMSF), 15μg/ml aprotinin, 1mM Na_3VO_4
Sample Buffer (4x)	200mM Tris pH6.8, 400mM DTT, 8% SDS, 0.2-0.4% Bromphenol Blue, 40% glycerol
Running Buffer (10x)	50mM Tris, 500mM Glycine, 0.1% SDS
Transfer Buffer (1x), for 10% and 15% gels	20% Methanol, 40mM Tris, 300mM glycine
Transfer Buffer (1x), for 5% gels	10% Methanol, 0.1% SDS, 40mM Tris, 300mM glycine
TBS-T (20x)	200mM Tris base pH8, 3M NaCl, 0.02% Tween-20
TBS (20x)	200mM Tris base pH8, 3M NaCl
5% Milk/ TBS-T	Skimmed milk powder in 1x TBS-T
Stripping Buffer (1x)	200mM glycine pH 2.5, 0.4% SDS

Table 2.4.5 Solutions used for protein extraction and Western blotting.

Antibody	Source	Dilution	Secondary Antibody	Develop Using	Mw (kDa)
pERK1/2	Sigma (M5670)	1:5000	α-mouse HRP	ECL	42/44
ERK1/2	Sigma (M8159)	1:10000	α-rabbit HRP	ECL	42/44
pS6K (thr389)	Cell Signalling Technology (CST) (9205S)	1:1000	α-rabbit HRP	ECL+	76
pAkt (ser473)	CST (193H12)	1:2000	α-rabbit HRP	ECL+	60
ERα (MC-20)	Santa Cruz (sc-542)	1:1000	α-rabbit HRP	ECL+	N/A
SREBP1 (2A4)	Neomarkers (MS-1207)	1:500	α-mouse HRP	ECL+	125/68
SREBP2	Abcam (ab30682)	1:500	α-rabbit HRP	ECL+	125/68
mSin3a (AK-11)	Santa Cruz (sc-767)	1:1000	α-rabbit HRP	ECL	150
GAPDH	Millipore (MAB374)	1:1000	α-mouse HRP	ECL	36
Vinculin	Sigma (V9131)	1:1000	α-mouse HRP	ECL	116
β-tubulin	Sigma (T4026)	1:2000	α-mouse HRP	ECL	55
α-rabbit HRP	GE Healthcare	1:2000	n/a	n/a	n/a
α-mouse HRP	GE Healthcare	1:2000	n/a	n/a	n/a

Table 2.4.6 Antibodies used for Western blotting.

2.5 Immunofluorescence and Fluorescent Labelling of Subcellular Components

Immunofluorescence

Cells were cultured on 13mm glass coverslips and fixed in 4% PFA (TAAB) in PBS for 15 minutes at room temperature. After washing 2x in PBS cells were permeabilised in dilutions of TritonX-100 (BioRad) in PBS, or ice-cold Methanol (VWR) at room temperature before blocking and incubating overnight at 4°c in primary antibody diluted in fresh blocking reagent, as described in Table 2.5.1. The following day, coverslips were washed 6x in PBS and incubated at room temperature for 1 hour in 3% BSA/PBS containing Alexafluor-conjugated secondary antibody (1:500) (Molecular Probes) plus Hoescht (1:5000). Coverslips were then washed 5x in PBS, 1x in ddH_2O and mounted on glass slides (VWR) in Fluoromount G mounting medium (Southern Biotech).

Imaging of fixed cell slides was performed depending on the cellular parameter subsequently quantified, as follows (detailed imaging protocols are described in section 2.6):

1. Organelle volume: Leica SPE confocal microscope.
2. Organelle number, area and fluorescence intensity: Zeiss Axioskop 2 widefield microscope.

Antibody	Source	Dilution	Permeabilise	Blocking solution	Secondary Antibody
α-TGN38	Sigma (T9826)	1:500	0.2% TritonX-100/PBS, 5 minutes	3% BSA/PBS	α-rabbit Alexa Fluor 488
α-fibrillarin	Abcam (ab4566)	1:500	0.2% TritonX-100/PBS, 10 minutes	3% BSA/PBS	α-mouse Alexa Fluor 488
α-GM130	BD Transducti-on (610822)	1:100	0.2% TritonX-100/PBS, 5 minutes	3% BSA/PBS	α-mouse Alexa Fluor 488
α-catalase	Gift from Prof. C. Danpure, UCL	1:500	0.3% TritonX-100/PBS, 5 minutes	3% BSA/PBS	α-guinea pig Alexa Fluor 555
α-LC3B	Nanotools (0231-100)	1:250	Ice-cold methanol, 5 minutes	3% BSA/PBS	α-mouse Alexa Fluor 488
α-KDEL	Stressgen	1:1000	0.2% TritonX-100/PBS, 5 minutes	3% BSA/PBS	α-mouse Alexa Fluor 488
α-ERα (MC-20)	Santa Cruz (sc-542)	1:50	0.5% TritonX-100/PBS, 5 minutes	10% BSA/ 0.1% Tween-20/ PBS	α-rabbit Alexa Fluor 488

α-SREBP1 (2A4)	Neomarkers (MS-1207)	1:150	0.1% TritonX-100/PBS, 5 minutes	3% BSA/PBS	α-mouse Alexa Fluor 488
α-SREBP2	Abcam (ab30682)	1:150	0.1% TritonX-100/PBS, 5 minutes	3% BSA/PBS	α-rabbit Alexa Fluor 488

Table 2.5.1 Antibodies used for immunofluorescence.

Fluorescent Labelling of Subcellular Compartments

Nucleus (Hoescht)

Cells were cultured on 13mm glass coverslips and fixed in 4% PFA/PBS for 15 minutes at room temperature. After washing 2x in PBS cells were permeabilised in 0.2% Tween-20/PBS for 5 minutes at room temperature, washed 2 x in PBS, 1 x in PBS plus Hoescht (1:10000) for 20 seconds, then a further 2 x in PBS before being mounted on glass slides in FluoromountG mounting medium.

Imaging of fixed cell slides was performed using a Leica SPE confocal microscope, as described in section 2.6.

Mitochondria (Mitotracker Green)

Cells were cultured on 13mm glass coverslips. Stocks of 1mM Mitotracker Green (Molecular Probes) were prepared in DMSO and stored at -20°c for up to 1 year. Working stocks were prepared by diluting the stocks to 50μM in DMSO and stored at -20°c for 1-2 months. Mitotracker was used at a final concentration of 100nM, by adding working stock directly to the medium of cells growing on coverslips. The cells were then incubated in the dark for 1 hour at 37°c, before being washed 2 x in PBS and fixed in 4% PFA/PBS at room temperature for 15 minutes. After permeabilisation in ice-cold acetone for 5 minutes at room temperature, the coverslips were washed 5 x in PBS and 1 x in H_2O, before being mounted on glass slides in ProLong Gold mounting medium (Invitrogen).

Imaging of fixed cell slides was performed using a Leica SPE confocal microscope, as described in section 2.6.

Lipid Droplets (Oil Red O)

Oil Red O stock solutions were made fresh for each experiment. The day preceding the experiment, Oil Red O powder was dissolved at a concentration of 5mg/ml in 100% isopropanol in a 37°c water bath for 1 hour, vortexing every 10 minutes, then passed through a 0.2μm filter and left at 4°c overnight. On the day of the experiment, the working solution was made by diluting the stock solution to a final concentration of 60% isopropanol, heating to 37°c and then leaving to cool at room temperature for 30 minutes before use.

Cells to be stained were cultured on 13mm glass coverslips and fixed in 4% PFA/PBS for 15 minutes at room temperature. Coverslips were then washed 1 x in H_2O and 1 x in 60% isopropanol for 20 seconds each before being incubated at room temperature with the working Oil Red O solution for 20 minutes. Coverslips were washed free of Oil Red O by rinsing 1 x in 60% isopropanol, then washing 3 x in H_2O, the middle wash containing Hoescht (1:10000) to stain the nuclei, before being mounted on glass slides in mounting medium.

Imaging of fixed cell slides was performed using a Zeiss Axioskop 2 widefield microscope, as described in section 2.6.

Plasma Membrane (Cell Mask and FM1-43)

1. Cell Mask:

Cells were cultured on 13mm glass coverslips. Staining solutions were prepared by diluting Cell Mask Orange stock solution (1:20000, final concentration 2.5μg/ml) (Molecular Probes) in warm conditioned medium. To label the cells, the coverslips were removed from the incubator, the culture medium aspirated and replaced with 500ul per well of the staining solution and the cells incubated in the stain solution for 5 minutes at 37°c. The stain solution was then removed, the coverslips washed 3 x with PBS and fixed in 4% PFA/PBS for 15 minutes at room temperature. After washing 2 x in PBS coverslips were mounted on glass slides in ProLong Gold mounting medium.

Imaging of fixed cell slides was performed using a Leica SP5 confocal microscope, as described in section 2.6.

2. FM1-43:

Cells were cultured on glass-bottomed dishes (Mattek, P35G-1.0-14-C). Stocks of 1mM FM1-43 (Molecular Probes) were prepared in ddH_2O and stored at -20°c. For prepare solutions for staining; FM1-43 stocks were diluted in warm conditioned medium, using medium that lacks phenol Red, at various concentrations (Surface Area=5μg/ml, 0-9 mins Endocytosis=2.5μg/ml, 0-60mins Endocytosis=10μg/ml, 0-60mins endocytosis with azide=2.5μg/ml). Cells were labelled live, whilst on the microscope stage (section 2.6). To label the cells, culture medium was removed from the cell culture dishes with a P1000 Gilson pipette and replaced with the FM1-43 staining solution, initially for 1 minute representing the time=0mins labelling. This was taken to represent labelling of the plasma membrane only. To image, the stain solution was removed with a P1000 Gilson pipette and replaced with imaging medium (plain DMEM lacking phenol Red) and the cells rapidly imaged.

For cell surface area experiments cell populations were seeded and treated in parallel and at each timepoint a single population was FM1-43 labelled and imaged, as for time=0mins above. Plasma membrane growth rates were calculated as follows:

Growth rate hr^{-1} (relative to size at t=0hrs):

$$= \frac{\text{Total cell fluorescence}_{time=t} - \text{Total cell fluorescence}_{time=0}}{t * \text{Total cell fluorescence}_{time=0}}$$

And:

$$\text{Growth rate } min^{-1} = \frac{\text{Growth rate } hr^{-1}}{60}$$

For plasma membrane endocytosis and recycling experiments, sequential labelling then imaging was repeated as necessary to quantify membrane internalisation over time.

Imaging was performed using spinning disc confocal microscopy as described in section 2.6.

2.6 Fluorescence Microscopy

Widefield Microscopy

Coverslips mounted on glass slides were imaged using either:

1. NIKON Eclipse Ti, with accompanying NIS elements software (Nikon). Images were taken using a 20x objective (0.8x NA)
2. Zeiss Axioskop 2 (Zeiss), with OpenLab software (Perkin Elmer). Images were taken using a 25x objective (0.8x NA)

Images were taken ensuring no saturation of pixel intensity.

Confocal Microscopy

Fixed Cell

Coverslips mounted on glass slides were imaged using either:

1. Leica TCS SPE Confocal Microscope, with accompanying Leica LAS AF software. Images were taken using a 63x (1.3 Numerical Aperture (NA)) or 40x (1.15x NA) objective, with a 1.5x zoom. Images were taken at 1024x1024 pixels therefore xy pixels had a 113.79nm (63x objective) or 179.21nm (40x objective) diameter. Optical sections were taken at 252nM intervals. Images were collected at 600Hz, with a 2 x frame average.
2. Leica TCS SP5 Confocal Microscope, with accompanying Leica LAS AF software. Images were taken using a 40x objective (1.3 NA), with 1.7 zoom. Images were taken at 1024x1024 pixels therefore xy pixels had a 222.8nm diameter. Optical sections were taken at 305nm intervals. Images were collected at 700Hz, with a 2x frame average.

For SPE and SP5 based imaging, fluorescence was excited and emission wavelengths collected as described in Table 2.6.1. Stacks of images were taken through the depth of the cell, ensuring no saturation of pixel intensity.

Live Cell

Spinning disc confocal microscopy was performed using a Perkin Elmer Ultraview Vox Confocal Imaging System with a Nikon Eclipse Ti microscope and using Volocity software. Cells growing on glass-bottomed dishes were placed on the microscope stage in a chamber supplied with a humidified gas mixture (90% air/ 10% CO_2) within a heated environmental chamber, set at 37°c, which also contained the body of the microscope and objective lens. Imaging was performed using a 40x or 20x objective and collected using a Hamamatsu C9100-13 CCD camera. Images were taken at 512x512 pixels therefore xy pixels had a 2.7μm diameter. Optical sections were taken at 0.5μm intervals. Differential Interference Microscopy (DIC) images were taken at the plane of best focus at the start of the experiment.

Fluorescent Marker	Laser (nm)
Hoescht	405
Alexa Fluor 488	488
Alexa Fluor 555	532
Oil Red O	532
Mitotracker Green	488
Cell Mask Orange	532
Tetramethylrhodamine Dextran (10k Mw)	532

Table 2.6.1 Wavelengths used to excite/ emission spectra wavelengths collected for fluorescence microscopy.

2.7 Image Quantification after Fluorescence Microscopy

Cell Surface Area (Cell Mask Orange)

Cell surface area was quantified from image stacks taken through the depth of Cell Mask Orange labelled cells using a Leica SP5 confocal microscope.

Image stacks were opened in ImageJ, Autothresholded from the brightest slice and made into binary images. Cell surface area was quantified as the sum of the cell surface area in the XYZ and XZY planes as follows: Cell surface area in the XYZ plane was taken as 2 x the thresholded cell area in the maximal projection of the image stack and in the XZY plane as the thresholded cell perimeter per slice of the image stack x interslice distance (z-spacing = 252nm). Cell area from maximal projections and cell perimeter per slice of image stacks were measured using the Analyse particles function, with the area and perimeter measurement functions activated within 'Set Measurements', respectively. Particles less than 10 pixels in size were excluded from measurements. This eliminated inclusion of background staining in the quantification.

Organelle Volume

Image stacks taken using fluorescence confocal microscopy (section 2.5) were opened in ImageJ (National Institute of Health), a region of interest (ROI) drawn around the organelle to be measured and the stack Autothresholded based on the brightest slice. The area of thresholded pixels in each slice was measured using the Analyse Particles function, with a minimal particle size of 10 pixels. This successfully excluded background staining from analyses. To obtain the volume of the organelle, the total area of pixel staining was multiplied by pixel depth. Organelle volume per unit of cell volume was calculated as the mean organelle volume/ mean cell volume measured using the CoulterCounter in a set of parallel experiments (section 2.2).

Organelle Area

Images taken using widefield microscopy (section 2.6) were opened in ImageJ. The 'Subtract Background' function was used to remove background, with a rolling ball radius of 50 pixels and no smoothing. Images were thresholded and

made binary. The threshold level was constant per experiment, but varied between experiments and the appropriate threshold was determined subjectively by eye. The Create Selection function was used to automatically outline the thresholded area and the contained area was then quantified using the Measurement function.

Organelle Number

Maximal projections of image stacks taken using fluorescence confocal microscopy (section 2.6) were generated in ImageJ and converted to 8-bit. The maximal projections were thresholded so minimal thresholded pixel intensity=100. The number of particles (organelles) was counted using the Analyse Particles function, with a minimal particle size of 10 pixels to exclude background staining. Organelle number per unit of cell volume was calculated as the mean organelle number/ mean cell volume measured using the CoulterCounter in a set of parallel experiments (section 2.2).

Where appropriate, mean cell volume was taken from CoulterCounter measurements and mean cell protein was taken from BCA measurements of parallel cell cultures and used to calculate mean organelle number per unit of cell volume/ protein.

Fluorescence Intensity

Image stacks taken using standard fluorescence confocal microscopy, spinning disc confocal microscopy or single images taken using widefield microscopy (section 2.6) were opened in ImageJ. For the confocal images, the Sum of Slice function was used for each stack to generate a single image whose pixel values represented the sum of pixel intensities at that location through the depth of the slice from the confocal images. Total fluorescence (corresponding to the plasma membrane and internalised plasma membrane for FM1-43 staining (section 2.5) or the amount of internalised fluorescent dextran (section 2.11) was determined per cell by quantifying the sum of pixel intensities within an ROI containing the cell of interest, corrected for background fluorescence by subtracting from each pixel within the ROI the mean non-cellular pixel value, i.e. background pixel value. The mean background pixel value was taken as the mean pixel value of two randomly drawn ROIs in regions of the image containing no cells, but as close to the cell being quantified as possible.

2.8 Transmission Electron Microscopy (TEM)

Cell Preparation and Imaging

After washing 2x in PBS, cells grown on 13mm glass coverslips were fixed in 2% PFA (EM Grade)/2% gluteraldehyde (TAAB, EM Grade) in 0.1M cacodylate for 30 minutes at room temperature. Post-fixation, cells were osmicated in the dark for 1 hour at 4°c in a 1:1 solution of 2% osmium tetroxide (TAAB): 3% potassium ferricyanide, washed 3 x in 0.1M cacodylate then incubated in 1% tannic acid/ 0.05M cacodylate for 40 minutes at room temperature, before washing a further 2 x in 0.05M cacodylate and 1 x in ddH_2O. The cells were then dehydrated in successive washes of 70% ethanol, 90% ethanol (3 minutes each) and 2 x 100% ethanol, (10 minutes each). Coverslips were embedded in EPON (Table 2.8.1) by first passing through a transition solvent of 1:1 polypropylene oxide (Fisher Scientific): EPON for 1 hour at room temperature, followed by 2 x 1 hour incubations at room temperature in 100% EPON at which point the coverslips were mounted cell side down on pre-polymerised EPON stubs and baked overnight at 60°c. The coverslips were removed from the cell embedded EPON stubs by freezing in liquid Nitrogen before ultrathin sections were cut from the EPON stubs and mounted on Formvar (Agar Scientific) coated grids. A systematic random sampling method was used in sectioning to ensure a representative sample population was obtained that would be suitable for stereological analysis. This involved taking sections every approximately 250nm, from a randomised starting height within the top of the EPON stub. To improve the contrast of images, sections were stained with lead citrate before imaging. Sections were inverted onto lead citrate droplets (in the presence of NaOH crystals to prevent moisture absorption by the droplets) and left for 15 minutes at room temperature, before being washed 5x in ddH_2O and left to air dry.

Imaging was performed on a Tecnai Spirit Transmission Electron Microscope (TEM) with iTem software (Olympus). Images were taken at 3860x2524 pixels and 16500 magnification. Sections were imaged at random to obtain a set of images for analysis that was representative of the cell population through the depth of the cell.

Reagent	Final Concentration	Source
Epon 812	48%	TAAB
Dodecenyl succinic anhydride (DDSA) (Distilled Grade)	19%	TAAB
Methyl nadic anhydride (MNA)	33%	TAAB
2,4,6-tris(Dimethylaminomethyl) phenol (DMP-30)	2%	TAAB

Table 2.8.1 EPON recipe.

Stereological Analysis of Transmission Electron Microscopy Images

Electron microscopy images were analysed within ImageJ. According to the principle of Delesse, area fraction is equivalent to volume fraction. Therefore organelle volume per cell was calculated as the organelle area per unit cell area x mean cell volume. Organelle and cell areas were estimated by tracing their respective perimeters within each image using the freehand draw tool in ImageJ and quantifying the contained areas. Lipid droplet number per cell was calculated using a modification of the method of Weibel and Gomez (Weibel, 1962), as follows:

$$\text{Number per unit volume} = \frac{K^{*}(\text{number per unit area}^{3/2})}{\beta^{*}\text{volume fraction}^{1/2}}$$

Where K is an arbitrary constant taken as 1 if the size distribution of the object is minimal, as is the case here, and β is the width to length ratio of the object, which I have taken as 1 as lipid droplets are approximately spherical.

2.9 Measuring De Novo Lipid Synthesis

Cells were seeded onto PLL, fibronectin (10μg/ml) and treated as described in section 2.1 'Protocol for Cell Cycle Arrest and Transfer to Defined Growth Factor-Free Conditions', using Minimal Medium. After treatment as indicated in the results for 4 hours, cells were incubated with 2.5μCi/well [2-^{14}C] pyruvate (250μM final concentration) (Perkin Elmer) for a further 4 hours. After washing 2x with PBS, cells were lysed in 1ml 0.5% TritonX-100/PBS. Lipids were extracted by successive addition of 2ml methanol, 2ml chloroform (VWR) and 1ml water, vortexing for 3-5 minutes between each addition. Phase separation was achieved by centrifuging the samples for 15 minutes at room temperature and 1500g. The lower organic phase was transferred to a scintillation vial and allowed to air dry at room temperature overnight. The lipids were dissolved in 5ml Ultima Gold LSC Cocktail (Perkin Elmer) and counts per minute quantified using a scintillation counter. Counts were normalised to the cell number of 6-well dishes seeded and cultured in parallel.

2.10 Endocytosis and Recycling of Cell Surface Protein (Cell Surface Protein Biotinylation)

Total Cell Surface Protein Endocytosis and Recycling

Biotin labelling solution was prepared immediately before the assay, as follows: 0.5mg/ml EZ-Link Sulfo-NHS-SS-Biotin (Pierce) was dissolved in ice-cold PBS/1mM $MgCl_2$/0.5mM $CaCl_2$ (PBS++), by rotating at 4°c for 15 minutes.

Cells cultured on 13mm glass coverslips were washed 2 x in ice-cold PBS++ to halt cell metabolism, including endocytosis and recycling, and incubated for 12 minutes on ice in biotin labelling medium, rotating gently. After this time, the labelling medium was aspirated and any remaining free biotin was quenched by 3 x 5 minute washes, on ice and rotating, in ice-cold Quenching Buffer (1mg/ml BSA/PBS++). After the final wash in Quenching Buffer, cells were washed 2 x on ice in ice-cold PBS++.

Endocytosis:

To perform the endocytosis assay the biotin labelled cells/coverslips were washed quickly 2 x in pre-warmed 37°c plain DMEM to rapidly warm them to 37°c so endocytosis would resume and the coverslips inverted onto 70ul of conditioned medium and incubated at 37°c. At specified times, coverslips were placed in ice-cold PBS++. At the end of the assay remaining cell surface biotin was cleaved by washing the cells 1 x in ice-cold Cleavage Buffer (Table 2.9.1) and then incubating the cells on ice and rotating for 2 x 15 minutes in ice-cold Cleavage Buffer. After aspirating the final Cleavage Buffer wash, remaining Cleavage Buffer was removed by washing the cells thoroughly 5 x in ice-cold PBS++. Subsequently, cells were fixed in 4% PFA/PBS for 20 minutes, washed 2 x in PBS and then permeabilised for 10 minutes in 0.2% TritonX-100, all at room temperature. Following fixation and permeabilisation, internalised and intracellular biotin was detected by incubating the cells/coverslips for 1 hour in 1:250 Alexa488-Streptavidin (Molecular Probes) at room temperature. After labelling, coverslips were washed 5x in PBS, 1x in ddH_2O and mounted on glass slides in FluoromountG mounting medium.

Recycling:

As for the endocytosis assay described above, the biotin labelled cells/coverslips were washed quickly 2 x in pre-warmed 37°c plain DMEM to rapidly warm them to 37°c so endocytosis would resume and the coverslips inverted onto 70ul of conditioned medium and incubated at 37°c for 45 minutes to allow internalisation and filling of the recycling path. After this time, coverslips were placed in ice-cold PBS++ and remaining cell surface biotin was cleaved by washing the cells 1 x in ice-cold Cleavage Buffer (Table 2.9.1) and then incubating the cells on ice and rotating for 2 x 15 minutes in ice-cold Cleavage Buffer. After aspirating the final Cleavage Buffer wash, remaining Cleavage Buffer was removed by washing the cells thoroughly 5 x in ice-cold PBS++. To perform the recycling assay, the coverslips were then washed quickly 2 x in pre-warmed 37°c plain DMEM to rapidly warm them to 37°c so trafficking would resume and the coverslips inverted onto 70ul of conditioned medium containing 50mM glutathione (pH adjusted back to 7-7.4 using sodium hydroxide (BDH)) and incubated at 37°c (the glutathione cleaved biotin that was returned to the

cell surface by recycling, preventing re-internalisation of the biotin by endocytosis). At specified times, coverslips were placed in ice-cold PBS++. At the end of the assay, any remaining cell surface biotin was cleaved using the protocol already described. Cells were then fixed and intracellular biotin labelled with Alexa488-Streptavidin as described for the endocytosis assay above.

Reagent	**Final Concentration**	**Source**
Glutathione	50mM	Sigma
EDTA	10mM	Sigma
NaCl	75mM	Sigma
BSA	1%	Sigma
NaOH	750mM	BDH
ddH_2O	N/A	MilliQ

Table 2.9.1 Cleavage buffer recipe.

Analysis:

Intracellular biotin was imaged using fluorescence widefield microscopy (Zeiss Axioskop 2) and quantified as total intracellular fluorescence per cell as described (sections 2.6 & 2.7). The mean fluorescence intensity per cell of cells after 0 minutes of endocytosis (Coverslips biotin labelled but not returned to 37°c before cell surface biotin was cleaved, i.e. cells where endocytosis and recycling of cell surface biotinylated proteins has not occurred) was subtracted from the mean intensity per cell at each timepoint, to control for uncleaved cell surface biotin.

2.11 Endocytosis and Recycling of Cell Surface Lipid (FM1-43)

The lipophilic styryl dye FM1-43 was used as a marker of plasma membrane endocytosis and recycling. Labelling was carried out and single cells imaged as described (sections 2.5 & 2.6). Fluorescence intensity was quantified as

described (section 2.7). Internalised membrane at time=t was quantified as follows:

Internalised membrane$_{time=t}$	=	Total cell fluorescence$_{time=t}$	–	Total cell fluorescence$_{time=0}$

Endocytosis rates (min^{-1}) were calculated from linear regression analysis on the internalised membrane across 0-9 minutes uptake. The rate at which FM1-43 accumulates in the cell is after endocytosis (min^{-1}), i.e. the rate when endocytic and recycling rates are in equilibrium representing the proportion of internalised membrane not recycled back to the cell surface, was calculated from linear regression analysis on the internalised membrane across 10-60 minutes uptake. Recycling rates (min^{-1}) were calculated by subtracting the rate of FM1-43 accumulation (10-60 minutes) from the rate of endocytosis. Rate analyses were performed on the mean data across all experiments performed.

2.12 Endocytosis and Recycling of Fluid-Phase (Fluorophore-Conjugated Dextran)

Microscopy Based Assay

Cells cultured on 13mm glass coverslips were inverted onto 70μl of tetramethylrhodamine dextran 10k Mw (2mg/ml) (Molecular Probes) in conditioned medium and incubated at 37°c. At specified times, coverslips were placed in ice-cold Ca^{2+} and Mg^{2+} free PBS (PAA) on ice and washed gently 10x with ice-cold Ca^{2+} and Mg^{2+} PBS. Subsequently, cells were fixed in 4% PFA/PBS on ice for 30 minutes, washed 3 x in PBS, the middle wash containing Hoescht (1:10000) to stain the nuclei and mounted on glass slides in mounting medium.

Internalised dextran was imaged using fluorescence confocal microscopy and quantified as total intracellular fluorescence per cell as described (sections 2.6 & 2.7). The mean fluorescence intensity per cell of control coverslips incubated for the length of the timecourse inverted onto 70ul of pre-chilled tetramethylrhodamine dextran 10k Mw (2mg/ml) in conditioned medium and on

ice was subtracted from the mean intensity per cell at each timepoint, to control for marker that became associated with the plasma membrane.

Rates of endocytosis and recycling of dextran were calculated from these values of total intracellular fluorescence per cell over time as described for FM1-43.

2.13 Statistical Analysis

All statistical analyses were performed using Prism4 (Graphpad). Analyses were performed as described in figure legends in the Results. Where Two-Way ANOVA was carried out, post hoc Bonferroni tests were applied. Where One-Way ANOVA was carried out, post hoc Newman-Keuls testing was performed when fewer than 5 comparisons were made and post hoc Tukey's testing was performed when greater than or equal to 5 comparisons were made.

Chapter 3: Results

Biogenesis Downstream of IGF-1 Stimulation or Raf/ MEK/ ERK Activation

Cell growth is classically associated with an increase in cell volume. This may involve a proportional increase in cell mass, organelle content and volume- as occurs in proliferating transit amplifying cell populations *in vivo* or when cells are proliferating exponentially in culture. These cells usually double their volume, mass and organelle content across the cell cycle before dividing to produce two daughter cells roughly equivalent to the starting mother cell. However, when the diversity in cell size, morphology and organelle content of different cell types *in vivo* is considered it is clear that non-uniform cell growth (where the addition of cell volume and organelle biogenesis occurs uncoupled) is also a frequent event. This is particularly well demonstrated by examples of differential organelle biogenesis within a single cell. For example, in an activated B cell the endoplasmic reticulum (ER) expands disproportionately to the accompanying increase in cell volume, which means ER density within the cell increases (Federovitch et al., 2005, Kirk et al., 2010, Rush et al., 1991). This is necessary for the mature B-cell to produce sufficient immunoglobulins during the immune response. The diversity in cell morphology across and within the development of different cell types shows that cell growth is distinctly more complex than the coordinate addition of cell mass and volume.

IGF-1 is classified as a Schwann cell growth factor because it drives addition of cell volume (Conlon et al., 2001, Echave et al., 2009). In contrast NRG-1 has not historically been considered as a growth factor because it cannot drive addition of Schwann cell volume (Conlon et al., 2001, Echave et al., 2009). However studies from our lab have shown that NRG-1 induces Schwann cell mitochondrial biogenesis, which increases mitochondrial volume in the cell (Echave et al., 2009); as NRG-1 does not drive an increase in cell volume, mitochondrial density increases. These results show that NRG-1 does have biogenic capabilities and therefore could be considered as a growth factor, even though it does not drive the addition of cell volume.

As outlined in the introduction, major signalling pathways activated downstream of both IGF-1 and NRG-1 are the PI3K/ Akt and the Raf/ MEK/ ERK pathways (Echave et al., 2009). In the Schwann cell, both IGF-1 and NRG-1 transiently activate equivalent and strong signalling through both ERK and Akt (Echave et al., 2009). However NRG-1 drives sustained ERK signalling whereas IGF-1 drives sustained Akt signalling (Echave et al., 2009). The ability of IGF-1 to drive addition of Schwann cell volume depends on the PI3K/ Akt pathway (Echave et al., 2009).

In light of the mitochondrial findings this thesis aimed to investigate biogenesis downstream of the PI3K/ Akt and ERK signalling pathways in further detail. To specifically activate ERK signalling; these studies used Schwann cells that stably express a tamoxifen (Tmx) inducible Raf kinase construct (NSΔRafER cells) (Samuels et al., 1993); application of Tmx (100nM) results in sustained Raf kinase activation. In this way it is possible to drive sustained and specific ERK signalling, without activation of PI3K/Akt (Samuels et al., 1993). The NSΔRafER cell system was used to compare the biogenic effects of ERK signalling to those of IGF-1 stimulation- a condition that drives PI3K/ Akt dependent addition of cell volume.

The basic experimental protocol used throughout was as follows: NSΔRafER cells were cell cycle arrested, using the DNA polymerase α inhibitor aphidicolin, in the presence of serum for 24hrs (Conlon and Raff, 2003, Conlon et al., 2001, Costa et al., 1992, Echave et al., 2009, Ikegami et al., 1978). The use of aphidicolin allowed the biogenic effects of Raf kinase or IGF-1 to be tested independently of effects each may have on cell cycle progression. This is important because if cells are dividing the biogenic effects are spread over an increasing number of cells and is difficult to follow. If cells are not dividing the biogenic effects are contained within single cells and can be more easily observed and quantified. Following this, cells were transferred to defined conditions (free from exogenous mitogens, growth factors and survival factors: Minimal Medium) plus aphidicolin for a further 24 hours. At this point, cells were treated with IGF-1 or the Raf kinase construct was activated using Tmx and assays conducted as indicated in the text, again in the presence of aphidicolin. Maintaining the cells in defined conditions free from exogenous mitogens, growth factors and survival factors (Minimal Medium) for 24 hours prior to Raf

kinase activation or IGF-1 stimulation provided a clean background against which the effects of these stimuli could be assayed. Variations in this protocol, both in cell type and/ or experimental conditions, are highlighted and described where they have been used.

3.1 The Addition of Mass and Volume can be Uncoupled During Cell Growth

The addition of cell volume is one parameter, and the classical descriptor, of cell growth. It is generally considered that cell mass correlates with cell volume, and the two parameters have traditionally been used interchangeably. As has been demonstrated in previous studies, IGF-1 drives an increase in Schwann cell volume, as shown in Figure 3.1 and 3.3 A (Conlon et al., 2001, Echave et al., 2009). Cell volume was quantified in two ways in these studies. First using the Coulter Counter (Figure 3.1) (Materials & Methods 2.2), which measures the volume of small particles by volume displacement as they pass through the instruments measuring aperture. The volume of trypsinised cells (because cells must be in suspension to pass through the coulter counter) was quantified after 24 hours IGF-1 stimulation or Raf kinase activation and compared to untreated control cells. Data previously published by the Lloyd lab showed the volumes quantified by this method are comparable to those of equivalent adherent cells quantified from confocal stacks of cells labelled with a fluorescent cytosolic dye, indicating that trypsinising cells does not significantly affect their volume and therefore that Coulter Counter measurements are a reliable quantitative measure of cell volume (Echave et al., 2007). In the second approach, cell volume was measured using Quantitative Phase Microscopy (QPM) and were performed in collaboration with the Kirschner Lab, Harvard Medical School (Figure 3.2 & 3.3 A) (Materials & Methods 2.2). QPM can be used to quantify the phase-shift of the light waves of a beam of light as they pass through a material, e.g. a cell. Cell volume can be calculated from the difference in the extent of the phase-shift when a cell is measured in two different media that have different refractive indices (in this case, conditioned medium and conditioned medium + 10% ficoll to increase the refractive index). QPM was performed on living, adherent cells grown on glass bottomed cell culture dishes, again after 24hrs +/- treatment- a schematic of the

image processing steps can be seen in Figure 3.2. Both methods gave equivalent results; that is, IGF-1 drives an ~1.3-fold increase in cell volume over 24 hours relative to control untreated cells whereas, and perhaps unsurprisingly given that NRG-1 does not drive addition of Schwann cell volume, sustained Raf kinase activation does not drive addition of Schwann cell volume (Figure 3.1 & 3.3 A).

In addition to cell volume, cell mass is also an important parameter of biogenesis and cell growth. QPM was used to quantify the dry organic mass of single cells; that is, the total mass of proteins, lipids, carbohydrates, nucleic acids and their derivatives, within the cell. Again, these experiments were performed in collaboration with the Kirschner Lab, Harvard Medical School. As for cell volume, the dry mass of living, adherent cells was quantified 24hrs +/- IGF-1 treatment or Raf kinase activation (Tmx treatment). As for cell volume, dry mass is calculated from the cell-induced phase-shift of the microscope light beam. Unlike cell volume, which uses the difference in cell-induced phase-shift between cells in media of two different refractive indices to calculate cell volume, cell dry mass can be calculated from the phase-shift induced by any one medium of known refractive index. Most surprisingly, in contrast to cell volume, Raf kinase was able to drive a comparable increase in cell mass to IGF-1; both IGF-1 stimulation and Raf kinase activation increased cell dry mass ~1.5-fold over 24 hours (Figure 3.3 B).

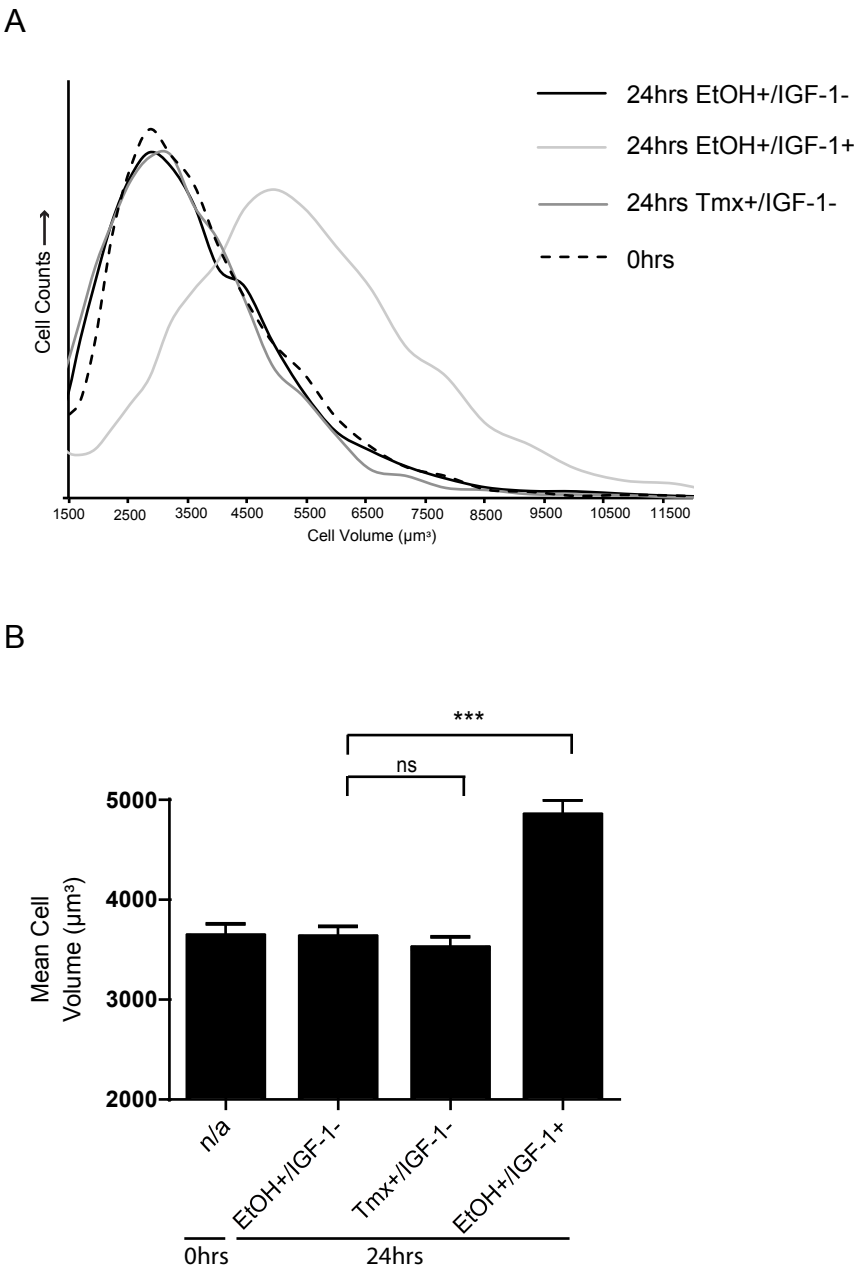

Figure 3.1 IGF-1 drives an increase in cell volume

Aphidicolin arrested NSΔRafER cells were treated as indicated and cell volume was quantified using a Coulter Counter

A) Representative frequency distribution of cell volumes in the measured populations (µm³)

B) Quantification of mean cell volume (µm³). Bar chart shows mean + standard error of the mean (SEM) of 8 experiments, performed in duplicate per condition per timepoint per experiment. Repeated Measures One-Way ANOVA $p<0.05$, select post hoc Tukey's as indicated on the graph.

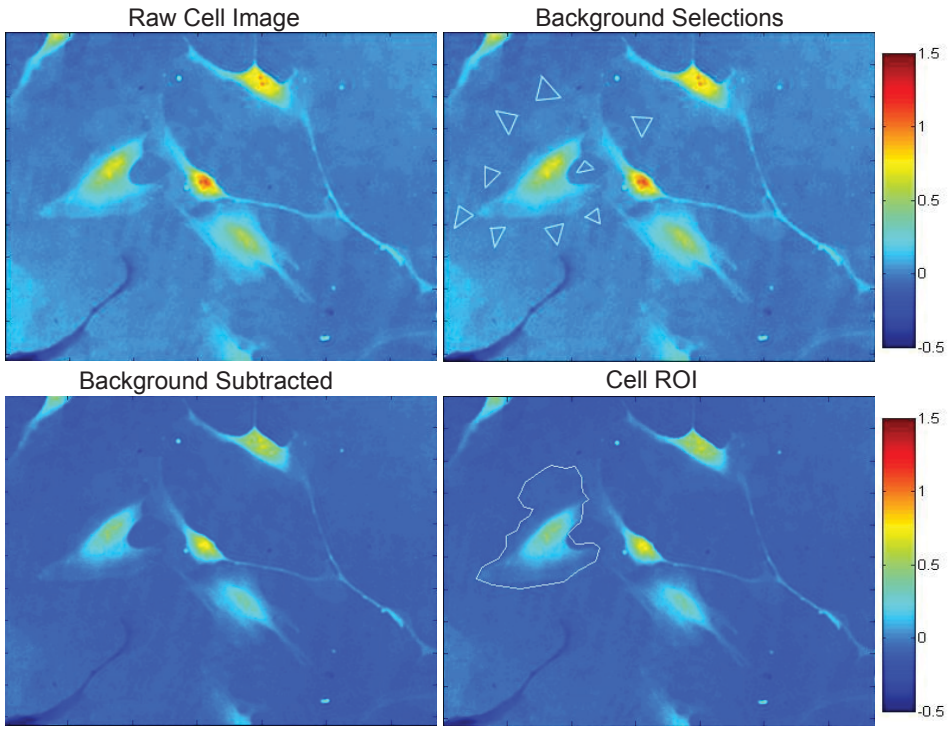

Figure 3.2 Image processing of raw Quantitative Phase Microscopy (QPM) images

Schematic showing the image processing of raw QPM data. Images were taken on a custom built Quantitative Phase Microscope and analysed in MetaMorph. Background selections were taken from non-cellular areas surrounding the cell of interest. These were used to remove tilts and background noise in the image, created by, for example, movement in the cell culture medium during image acquisition. Once this background had been subtracted the outline of the cell was carefully traced to generate the cell Region Of Interest (ROI). The cell induced phase shifts and, subsequently, cell dry masses and volumes were calculated from the cell ROI in the processed image.

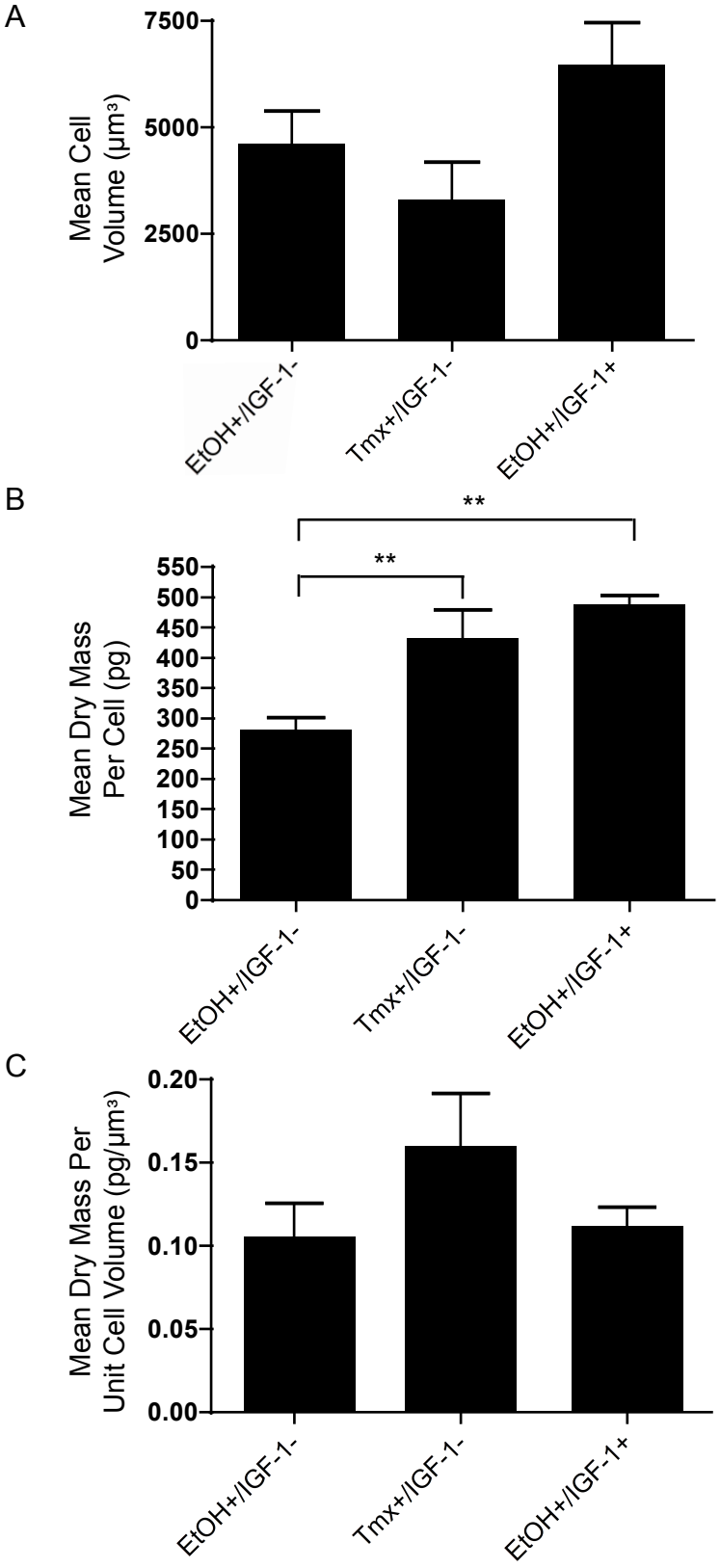

Figure 3.3 Cell mass and volume can be uncoupled during cell growth

Aphidicolin arrested NSΔRafER cells were treated as indicated and cell volume and dry mass quantified by Quantitative Phase Microscopy (QPM):
A) Mean cell volume (µm³). Bar chart shows mean +SEM from >12 cells quantified per condition.
B) Mean cell dry mass (pg). Bar chart shows mean +SEM of 4 experiments, minimum 20 cells quantified per condition per experiment. One-Way ANOVA $p<0.05$, post hoc Newman-Keuls as indicated on the graph.
C) Mean dry mass per unit of cell volume (pg/µm³). Bar chart shows mean +SEM from >12 cells quantified per condition.

To investigate this somewhat surprising finding further, and because a large proportion of cell dry mass is protein, the total protein mass per cell was quantified by two independent methods. First the standard Bicinchoninic Acid Assay (BCA) assay was used to measure the amount of protein per cell (Materials & Methods 2.2). The concentration of protein in cell lysates was measured using a modified BCA assay and normalized to the cell number in parallel cell culture dishes. The BCA is a colorimetric assay where the intensity of colour formation after the BCA reagent is added to a sample is proportional to the concentration of protein in the sample. The second approach to quantify protein per cell was to use a fluorophore-conjugated succinimidyl ester (S. Ester) to label fixed cell populations (Materials & Methods 2.2). The succinimidyl group reacts with primary amines, such as the N-terminus of proteins, peptides and amino acids and the R-group of lysines and therefore the amount of S. ester binding (fluorescence intensity per cell measured by microscopy) should reflect the amount of fixed protein, peptides and amino acids per cell. As can be seen in Figure 3.4 A, labeling resulted in staining throughout the cell with a clear increase in intensity in the central nuclear area of the cell, which would be predicted as this is the tallest part of the cell and contains the protein rich nucleus. To support the validity of using S. Ester labeling to quantify cell protein mass, the dry mass (by QPM) and then, after fixation, the protein mass (by S. Ester labeling) of the same cells were quantified and plotted against each other on a graph (Figure 3.4 B). Although dry mass is the sum of more than just cell protein content it would be expected that, within one cell population, there is a strong correlation between dry mass and protein per cell- because it would be predicted that the proportion of dry mass that is protein is relatively constant. As can be seen, the correlation between the QPM and S. Ester quantifications for individual cells is highly significant, supporting the use of the S. Ester technique to quantify cell protein content.

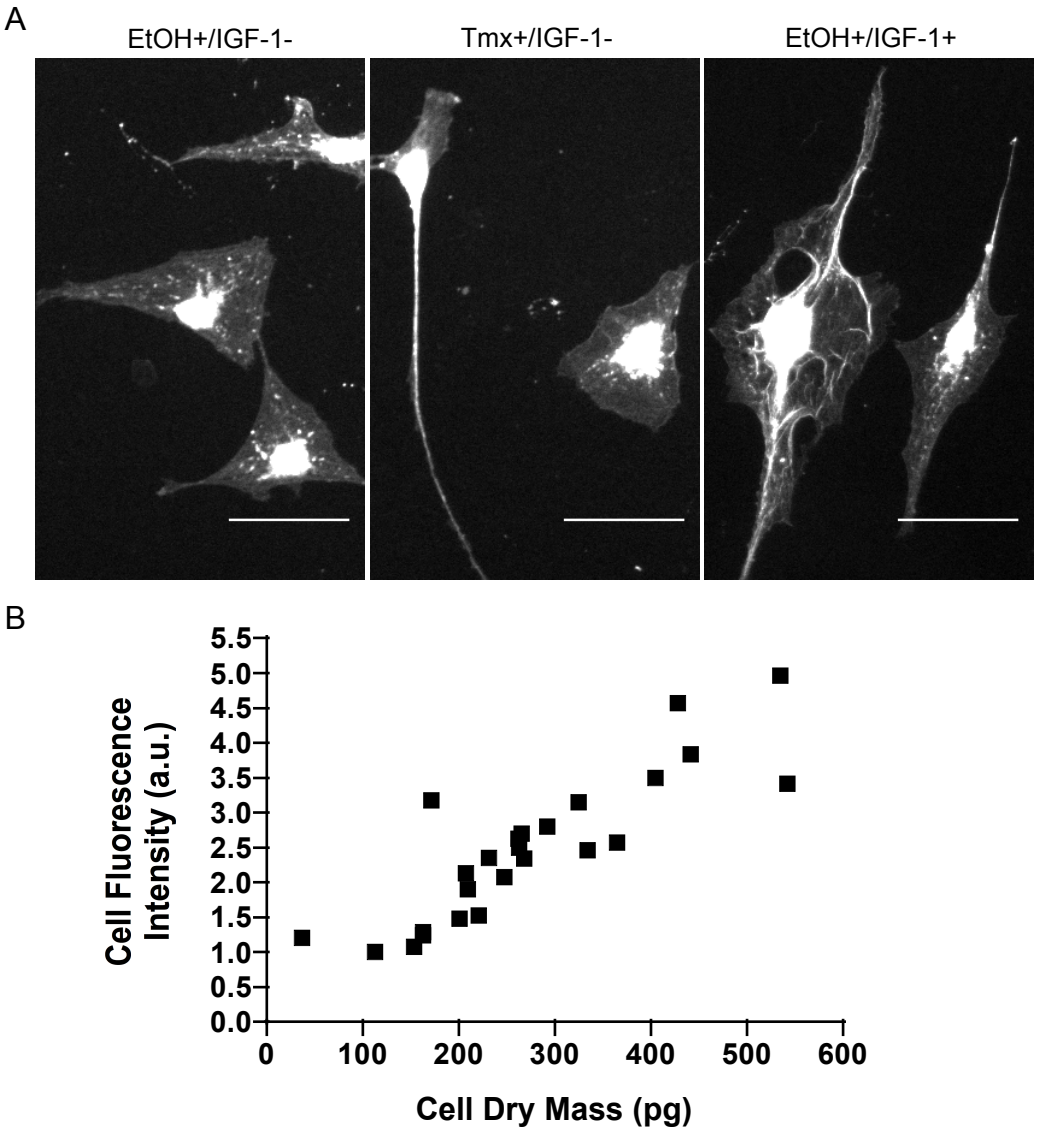

Figure 3.4 There is a strong correlation between cell dry mass, quantified by QPM, and protein mass, quantified by succinimidyl ester labelling

Aphidicolin arrested NSΔRafER cells (except where indicated below) were treated as indicated for 24hrs.

A) Representative widefield microscopy images after AlexaFlour647-succinimidyl ester labelling of fixed cells. Scale bar = 25μm.

B) Correlation between dry mass measured by QPM (pg) and the fluorescence intensity of the same cell quantified after subsequent succinimidyl ester labelling. Linear regression analysis, $p<0.0001$. Spearmans rank Correlation Coefficient, $p<0.001$.

As for cell volume and dry mass, the amount of protein per cell of NSΔRafER cells was quantified after 24hrs +/- IGF-1 or Tmx treatment (to activate Raf kinase). Both the BCA assay and S. ester labelling showed the same result; that is, in contrast to cell volume and consistent with the dry mass quantifications, activation of Raf kinase is at least as efficient as IGF-1 at driving an increase in protein mass. Compared to control (EtOH+/IGF-1-) cells, IGF-1 and Raf kinase activation each drove a significant ~1.3-1.5-fold increase in protein mass over 24 hours (Figure 3.5 A & 3.6 A). The increase in protein mass seen with Raf kinase activation was not an artefact of Tmx treatment because treating Schwann cells lacking the Tmx inducible Raf kinase construct with an equivalent dose of Tmx, did not drive an increase in cell protein mass (Figure 3.5 C & 3.6 B). Interestingly, cell protein content, as assayed by the BCA assay, is significantly greater in Raf kinase activated cells compared to IGF-1 treated cells (Figure 3.5 A). The same trend is seen with S. ester labeling, although it is not significant (Figure 3.6 A). Whether this is due to a difference in sensitivity of the two assays is not clear. If the difference is real, it is particularly interesting because IGF-1 tends to drive a slightly greater increase in dry mass than Raf kinase (Figure 3.3 A and 3.12 B). The difference in Figure 3.3 A is not significant, however this may be due to the relatively low cell numbers in this assay- these assays were performed in a limited timeframe as part of a collaboration, precluding further investigation of the finding.

The increase in protein mass and total dry mass downstream of IGF-1 is approximately proportional to the increase in cell volume and therefore the mass: volume ratio of the cell, i.e. mass density, does not significantly change (Figure 3.3 C & 3.5 B). In contrast, Raf kinase activation drives an increase in mass in the absence of an increase in cell volume and therefore the mass: volume ratio of the cell increases ~1.5-fold compared to control untreated cells (Figure 3.3 C & 3.5 B).

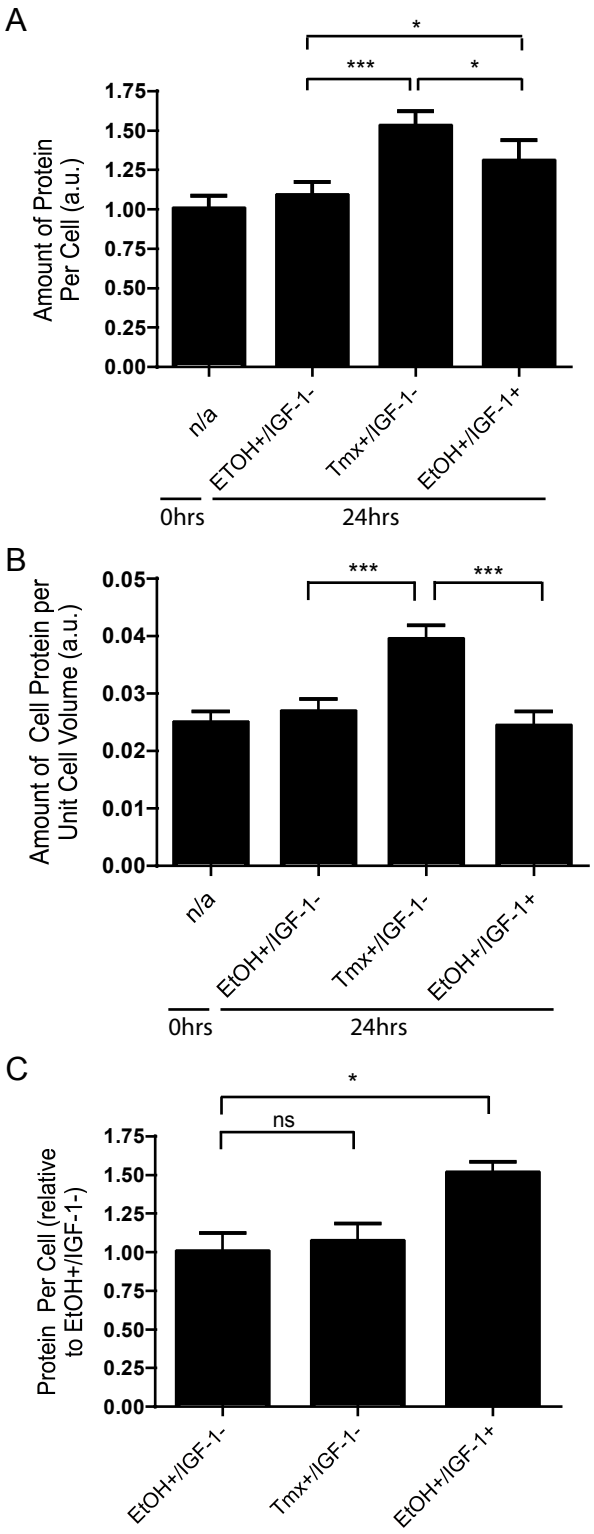

Figure 3.5 IGF-1 and Raf kinase activation drive an increase in cell protein mass

Aphidicolin arrested NSΔRafER cells (except where indicated below) were treated as indicated for 24hrs before protein per cell was quantified using the BCA Assay. Bar charts show mean +SEM.

A) Mean amount of protein per cell (a.u.). Mean of 8 experiments, performed in duplicate. One-Way ANOVA $p<0.0001$, post hoc Tukey's as indicated on the graph.

B) Mean amount of protein per unit cell volume (a.u.), experiments as in A). Repeated Measures One-Way ANOVA $p<0.05$, post hoc Tukey's as indicated on the graph.

C) Mean amount of protein per cell (a.u.) of aphidicolin arrested NS cells treated as indicated for 24hrs. Mean of 5 experiments, performed in duplicate. Repeated Measures One-Way ANOVA $p<0.05$, select post hoc Newman-Keuls as indicated on the graph.

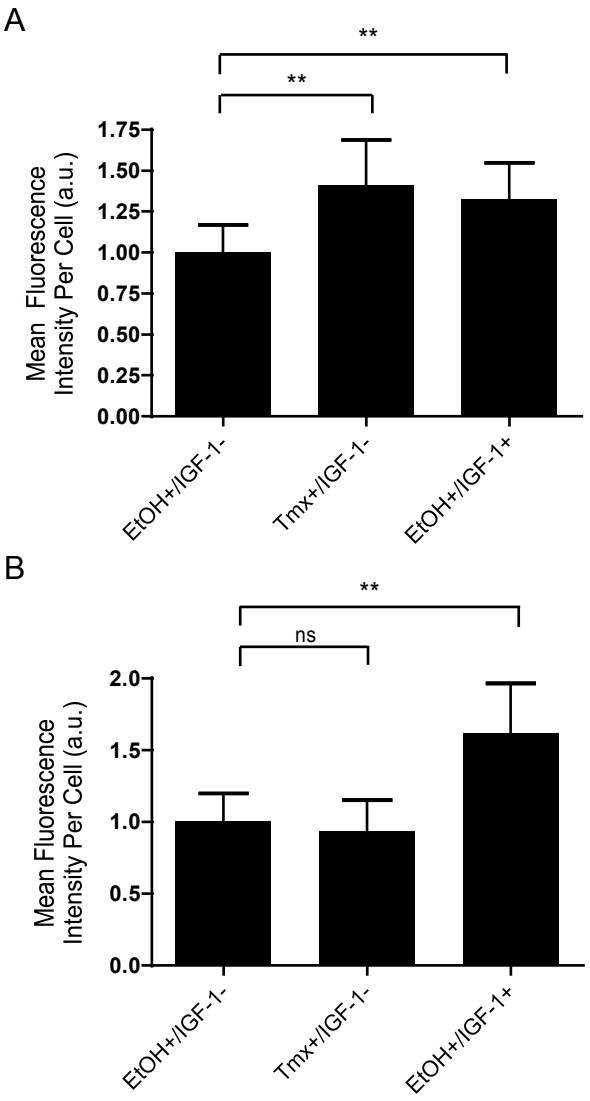

Figure 3.6 IGF-1 and Raf kinase activation drive an increase in cell protein mass

Aphidicolin arrested NSΔRafER cells (except where indicated below) were treated as indicated for 24hrs before protein per cell was quantified as fluorescence intensity per cell after AlexaFlour647-succinimidyl ester labelling of fixed cells. Bar charts show mean +SEM.
A) Mean fluorescence intensity per cell (a.u.) after succinimdyl ester labelling.
B) Mean fluorescence intensity per cell (a.u.) of aphidicolin arrested NS cells treated as indicated for 24hrs.
Mean of A) 6 and B) 3 experiments, minimum 50 cell quantified per experiment. Repeated Measures One-Way ANOVA, A) $p<0.01$ and B) $p<0.001$, select post hoc Newman-Keuls as indicated on the graphs.

In summary, the results shown here demonstrate that the addition of mass and volume can be uncoupled during cell growth. Whereas IGF-1 drives a proportional increase in cell mass and volume, sustained Raf kinase activation drives an increase in mass in the absence of an increase in cell volume. Therefore, whereas IGF-1 treated cells maintain a constant mass: volume ratio (density), the mass: volume ratio (density) of Raf kinase activated cells increases. These findings suggest that the addition of protein mass per se is insufficient to drive an increase in cell volume and therefore that another factor(s) must limit volume addition. In the context of this system, it raises the question of what other factor(s) IGF-1 regulates to drive cell volume addition.

3.2 IGF-1 dependent Cell Volume Addition is PI3K and mTORC1 Dependent, but MEK Independent

The level of phosphorylated Akt is an indicator of the activation state of the PI3K/ Akt pathway and the level of phosphorylated S6 Kinase (S6K) is an indicator of mTORC1 activation (mTORC1 is a major downstream effector of Akt). As described in the Introduction (Section 1.7), the PI3K/ Akt and mTORC1 pathway are central regulators of cell growth and are activated downstream of IGF-1 (Engelman et al., 2006). The Raf/ MEK/ ERK signalling pathway also activates biogenic pathways (Section 1.7) and, as shown by the results above, cell growth (addition of mass). Although there is no evidence that Raf kinase activation can activate PI3K/ Akt, there is evidence that ERK signalling activates mTORC1, through phosphorylation and inhibition of the negative regulator of mTORC1, TSC2, as well as direct phosphorylation of the Raptor subunit of mTORC1 (Carriere et al., 2008, Carriere et al., 2011, Ma et al., 2005). To determine the activation state of these pathways after IGF-1 treatment or Raf kinase activation in Schwann cells, Western blot analysis was performed over a timecourse after IGF-1 or Tmx treatment (Figure 3.7).

Consistent with published data, Western blot analysis showed that IGF-1 drives sustained activation of the PI3K/ Akt/ mTORC1 pathway (Figure 3.7 A i pAkt (ser 473) and iii pS6K (thr 389)) (Echave et al., 2009). Activation persists at 24 hours after IGF-1 treatment, which is the endpoint for most growth/ size assays in this study. In contrast, and again consistent with published data,

Western blot analysis showed that IGF-1 only transiently activates ERK signalling; levels of pERK1/2 return to basal control levels within 1 hour of IGF-1 treatment (Figure 3.7 A ii) pERK1/2) (Echave et al., 2009).

Confirming the activity of the RafER construct, sustained activation of Raf kinase drove sustained activation of ERK signalling, as shown by Western blot (Figure 3.7 A ii pERK1/2, Tmx+/IGF-1-). This figure also demonstrates that a single dose of Tmx was sufficient to activate the Raf kinase construct and downstream ERK signalling for at least 24 hours. Raf kinase activation drove a possible transient activation of S6K, seen at 10 minutes and 1 hour post-Tmx treatment (Figure 3.7 A iii pS6K (thr 389)). This activation declined over time, returning almost to control levels by 6 hours post-Tmx treatment. There is some evidence that activated ERK can phosphorylate and activate mTORC1 and this may explain the levels of pS6K seen here (Carriere et al., 2008, Carriere et al., 2011, Winter et al., 2011). Tmx treatment of normal Schwann cells lacking the Tmx-inducible Raf kinase construct showed that activation of these pathways was not an artefact of Tmx treatment (Figure 3.7 B). Raf kinase did not activate signalling through Akt (Figure 3.7 A i pAkt (ser 473)).

The PI3K/ Akt/ mTORC1 pathway is a central regulator of cell growth that is critical for nutrient uptake, biogenesis and cell volume addition in numerous systems *in vitro* and *in vivo* (Bohni et al., 1999, Echave et al., 2009, Gao and Pan, 2001, Kwon et al., 2001, Leevers et al., 1996, Montagne et al., 1999, Porstmann et al., 2005, Porstmann et al., 2008, Ruvinsky et al., 2005, Shima et al., 1998, Wullschleger et al., 2006). Consistent with a central role for the PI3K/ Akt/ mTORC1 pathway in cell growth as described in the Introduction, published data from our lab has shown that addition of Schwann cell volume downstream of IGF-1 is dependent upon sustained signalling through the PI3K/ Akt/ mTORC1 pathway (Echave et al., 2009). To confirm this result in these studies, cells were treated with IGF-1 (or Tmx) +/- inhibitors against PI3K and mTORC1: ZSTK474 (500nM), an ATP-competitive inhibitor of class I PI3Ks and Rapamycin (0.15µg/µl), an allosteric inhibitor of mTORC1. Inhibitors were added to cells 30 minutes prior to IGF-1 or Tmx, to ensure any signalling through these pathways was blocked before the addition of the factors. Cell volume was quantified 24 hours later, using the Coulter Counter. Western blot analyses showed that ZSTK474 and Rapamycin effectively blocked signalling

through Akt and S6K respectively at the concentrations used in these assays (Figure 3.8 C, ZSTK474 & 3.9 C, Rapamycin). Use of either of these inhibitors significantly blocked IGF-1 dependent cell volume addition (Figure 3.8 ZSTK474 & 3.9 Rapamycin) (Materials & Methods 2.1). There is no statistically significant effect of either inhibitor on the cell volume of control or Raf kinase activated cells, although the trend was for cell volume to be reduced in both conditions with either inhibitor (Figure 3.8 & 3.9).

ERK signalling has previously been shown to be dispensible for IGF-1 driven cell volume addition (Echave et al., 2009). To confirm this result, ERK signalling was blocked using PD184352 (0.75μM), an allosteric inhibitor of MEK1/2, the upstream activator of ERK1/2 (Materials & Methods 2.1). As for the PI3K and mTORC1 inhibitors, PD184352 cells were pre-treated with the inhibitor for 30 minutes before factors (IGF-1 or Tmx) were added and cell volume was quantified after a further 24 hours. As shown in Figure 3.10, inhibition of ERK signalling did not block IGF-1 dependent cell volume addition. Western blot analysis of pERK1/2 showed the inhibitor is active at the concentration used in the assays (Figure 3.10 C).

In conclusion, IGF-1 dependent cell volume addition depends on signalling through PI3K and mTORC1 but is refractory to inhibition of MEK. Correlating with these results, IGF-1 stimulation drives sustained activation of the PI3K/Akt/mTORC1 pathway but only transient activation of MEK/ERK signalling.

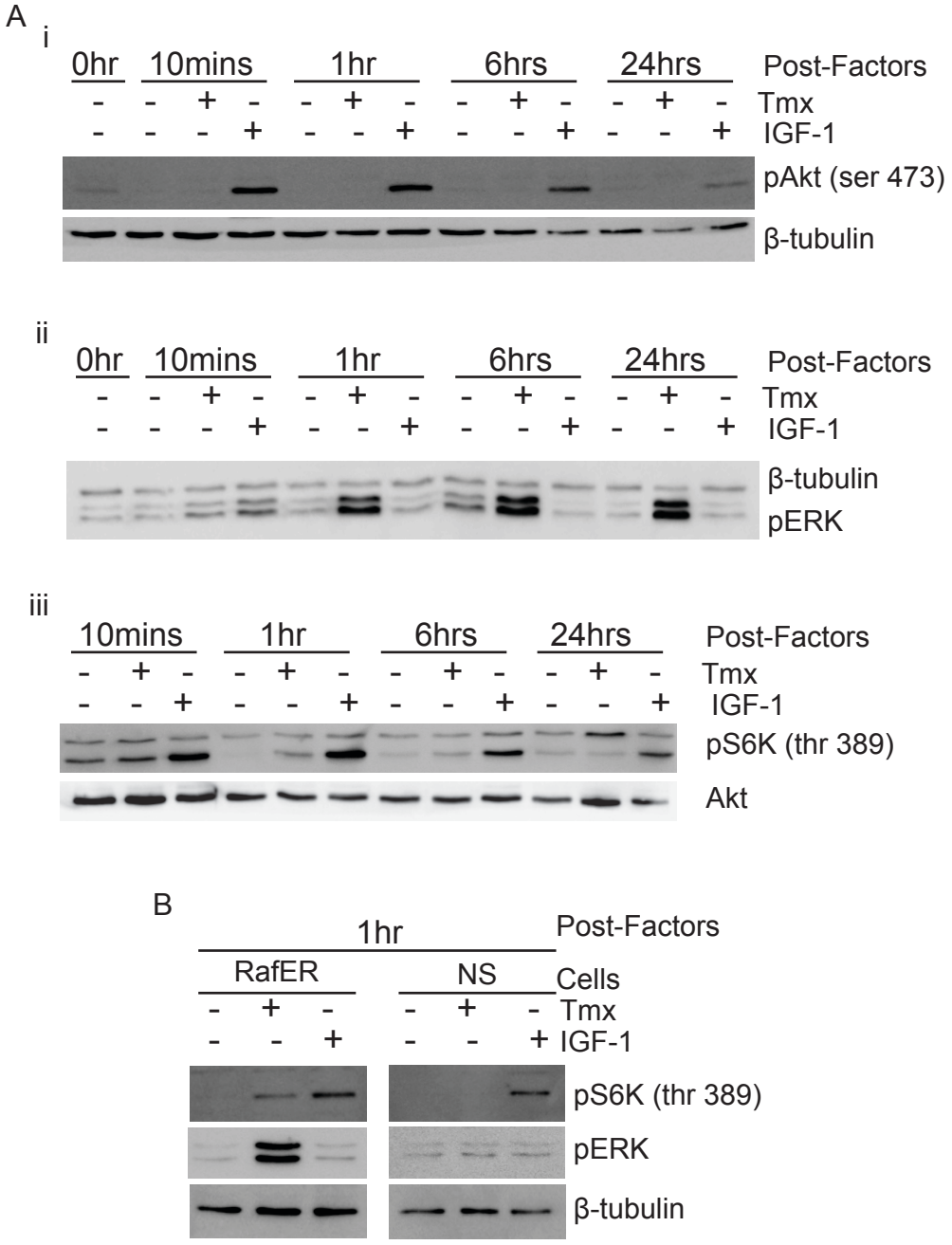

Figure 3.7 IGF-1 drives sustained signalling through the PI3K/Akt/mTORC1 pathway and Raf kinase activity drives sustained pERK activation

A) Aphidicolin arrested NSΔRafER cells were treated as indicated and then cell lysates collected for western blot analysis of protein levels of: i) pAkt (ser473), ii) pS6K (thr389), iii) pERK. Akt or β -tubulin were used as a loading control.
B) Aphidicolin arrested NSΔRafER or NS cells were treated as indicated and then cell lysates collected for western blot analysis of pERK and pS6K (thr389) protein levels. β-tubulin was used as a loading control.

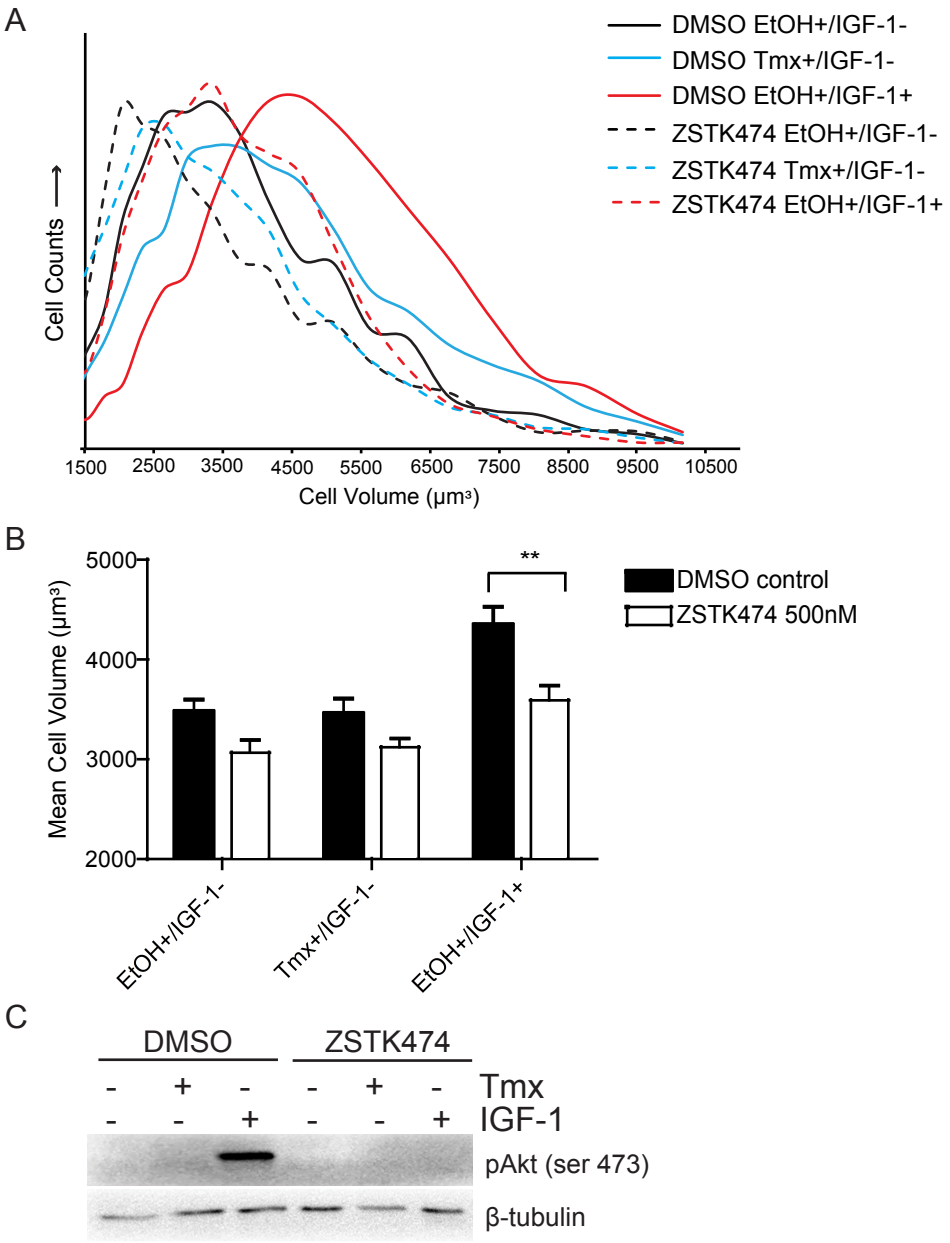

Figure 3.8 IGF-1 dependent cell volume addition is PI3K dependent

Aphidicolin arrested NSΔRafER cells were treated as indicated for 24hrs (cell volume) or 1hr (western blot) +/-ZSTK474, an inhibitor of class I PI3Kinases before:
A) Cell volume was quantified using a Coulter Counter, shown as a representative frequency distribution of cell volumes in the measured populations (µm³).
B) Cell volume was quantified using a Coulter Counter, shown as quantification of mean cell volume (µm³). Bar chart shows mean +SEM of 4 experiments, each experiment performed in duplicate. Repeated measures two-way ANOVA, between growth conditions $p<0.01$, DMSO vs inhibitor $p<0.01$. Post hoc Bonferroni as shown on the graph.
C) Western blot analysis was performed on cell lysates to show the inhibitor was working.

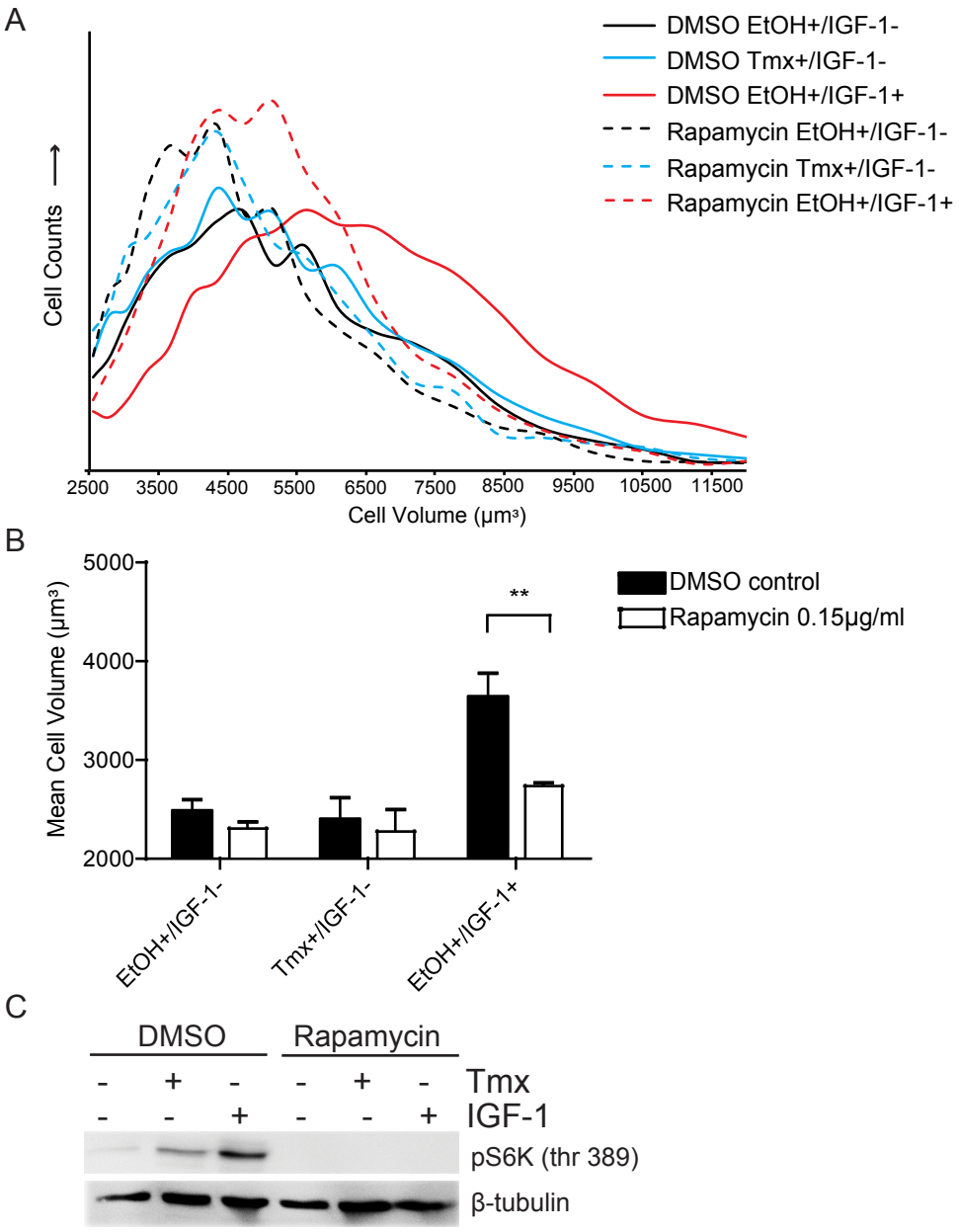

Figure 3.9 IGF-1 dependent cell volume addition is mTORC1 dependent

Aphidicolin arrested NSΔRafER cells were treated as indicated for 24hrs (cell volume) or 1hr (western blot) +/-Rapamycin, an inhibitor of mTORC1 before:
A) Cell volume was quantified using a Coulter Counter, shown as a representative frequency distribution of cell volumes in the measured populations (µm³).
B) Cell volume was quantified using a Coulter Counter, shown as quantification of mean cell volume (µm³). Bar chart shows mean +SEM of 3 experiments, each experiment performed in duplicate. Repeated measures two-way ANOVA, between growth conditions $p<0.01$, DMSO vs inhibitor $p<0.01$. Post hoc Bonferroni as shown on the graph.
C) Western blot analysis was performed on cell lysates to show the inhibitor was working.

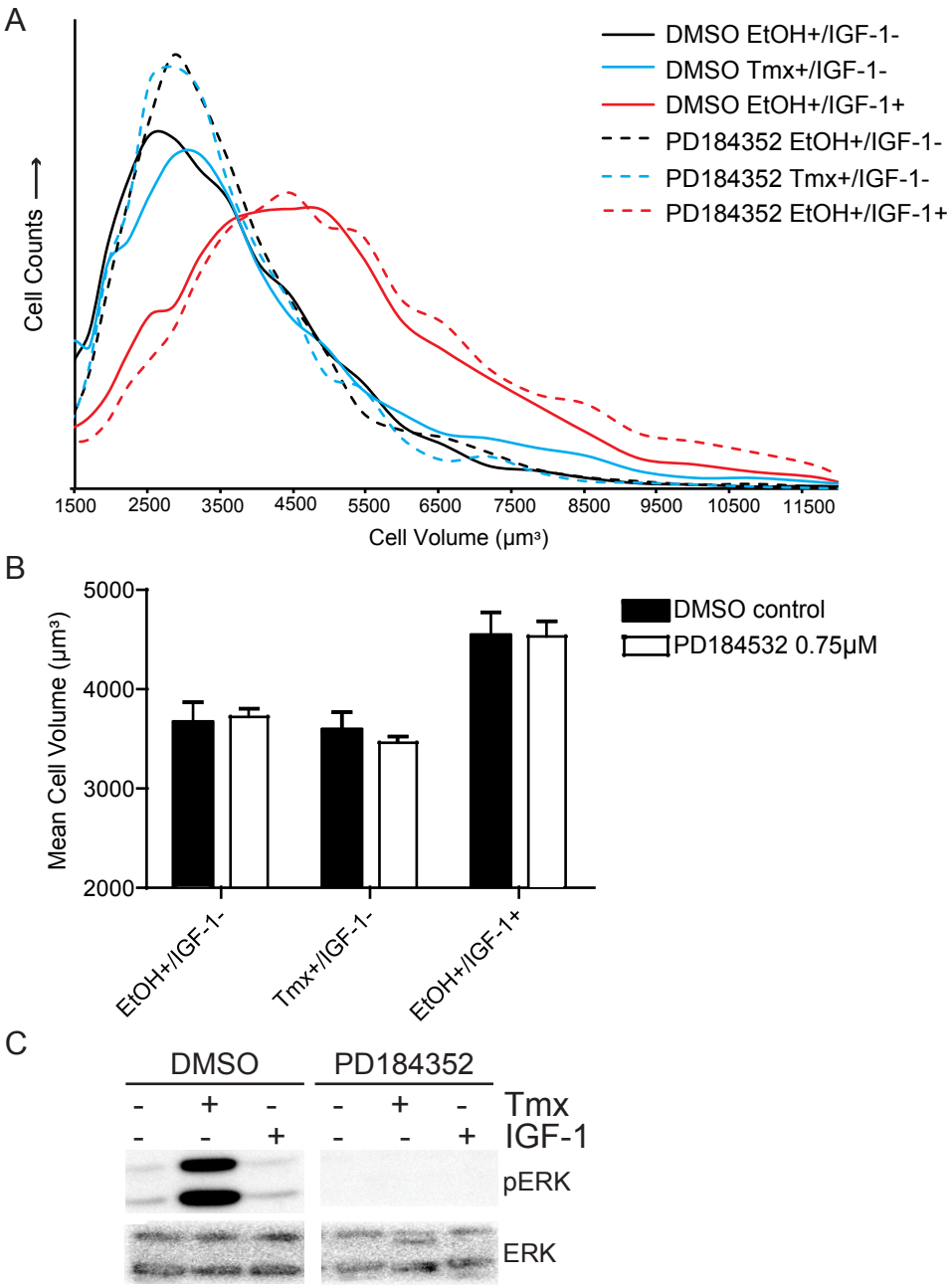

Figure 3.10 IGF-1 dependent cell volume addition is MEK independent

Aphidicolin arrested NSΔRafER cells were treated as indicated for 24hrs (cell volume) or 1hr (western blot) +/- PD184352, an inhibitor of MEK before:
A) Cell volume was quantified using a Coulter Counter, shown as a representative frequency distribution of cell volumes in the measured populations (µm³).
B) Cell volume was quantified using a Coulter Counter, shown as quantification of mean cell volume (µm³). Bar chart shows mean +SEM of 5 experiments, each experiment performed in duplicate. Repeated measures two-way ANOVA, between growth conditions $p<0.01$, DMSO vs inhibitor $p>0.05$. Post hoc Bonferroni as shown on the graph.
C) Western blot analysis was performed on cell lysates to show the inhibitor was working.

3.3 Addition of Mass is PI3K, mTORC1 and MEK Dependent

As demonstrated in the preceding Section IGF-1 and Raf kinase differentially activate distinct signalling pathways; namely signalling through Akt, mTORC1 and ERK. It was therefore important to determine whether IGF-1 and Raf kinase rely differentially on activity through each of these signalling pathways to drive addition of cell mass. To do this cells were treated with inhibitors against PI3K, mTORC1 and MEK for 24hrs +/- IGF-1 or Tmx (as for cell volume in the above section) and the amount of protein per cell quantified using S. Ester labelling, as described in Section 3.1.

As for cell volume, IGF-1 dependent addition of protein mass required signalling through PI3K and mTORC1 (Figure 3.11 A & B, respectively), correlating with sustained activation of the PI3K/ Akt/ mTORC1 pathway. Interestingly and in contrast to the addition of cell volume, the addition of protein mass downstream of IGF-1 also required signalling through the MEK/ERK pathway. As shown in Figure 3.12, inhibition of MEK blocked IGF-1 dependent addition of protein mass, as assayed by two independent methods: S. Ester labelling and quantification of cell protein mass (Figure 3.12 A), as well as QPM quantification of cell dry mass (Figure 3.12 B) (QPM in collaboration with the Kirschner Lab, Harvard Medical School). This is despite the fact that IGF-1 only transiently activated ERK signalling, which may suggest that a basal flux of activity through this pathway is required for addition of protein.

This result is particularly interesting because it demonstrates that cell volume can be added independently of cell mass during cell growth- because inhibiting MEK blocks IGF-1 induced addition of mass, but not volume. Therefore in the presence of the MEK inhibitor cells continue to add volume but do not add mass. Given that the results in Section 3.1 have already shown that cell mass can be added independently of cell volume during cell growth (downstream of specific Raf kinase activation), this means that both mass and volume can be independently regulated during cell growth.

Unsurprisingly, given that activation of Raf kinase in this inducible system drives sustained and specific ERK signalling, addition of mass downstream of Raf kinase was also MEK dependent (Figure 3.12). Interestingly, although Raf kinase activation did not activate signalling through PI3K (as indicated by levels

of pAkt, Figure 3.7 A), addition of protein mass downstream of Raf kinase required PI3K (Figure 3.11 A). Addition of protein mass downstream of Raf kinase also required mTORC1 (Figure 3.11 B), which was only transiently activated following Raf kinase activation (Figure 3.7 A iii pS6K). These results suggests basal signalling through PI3K and mTORC1 may be required for the addition of protein mass.

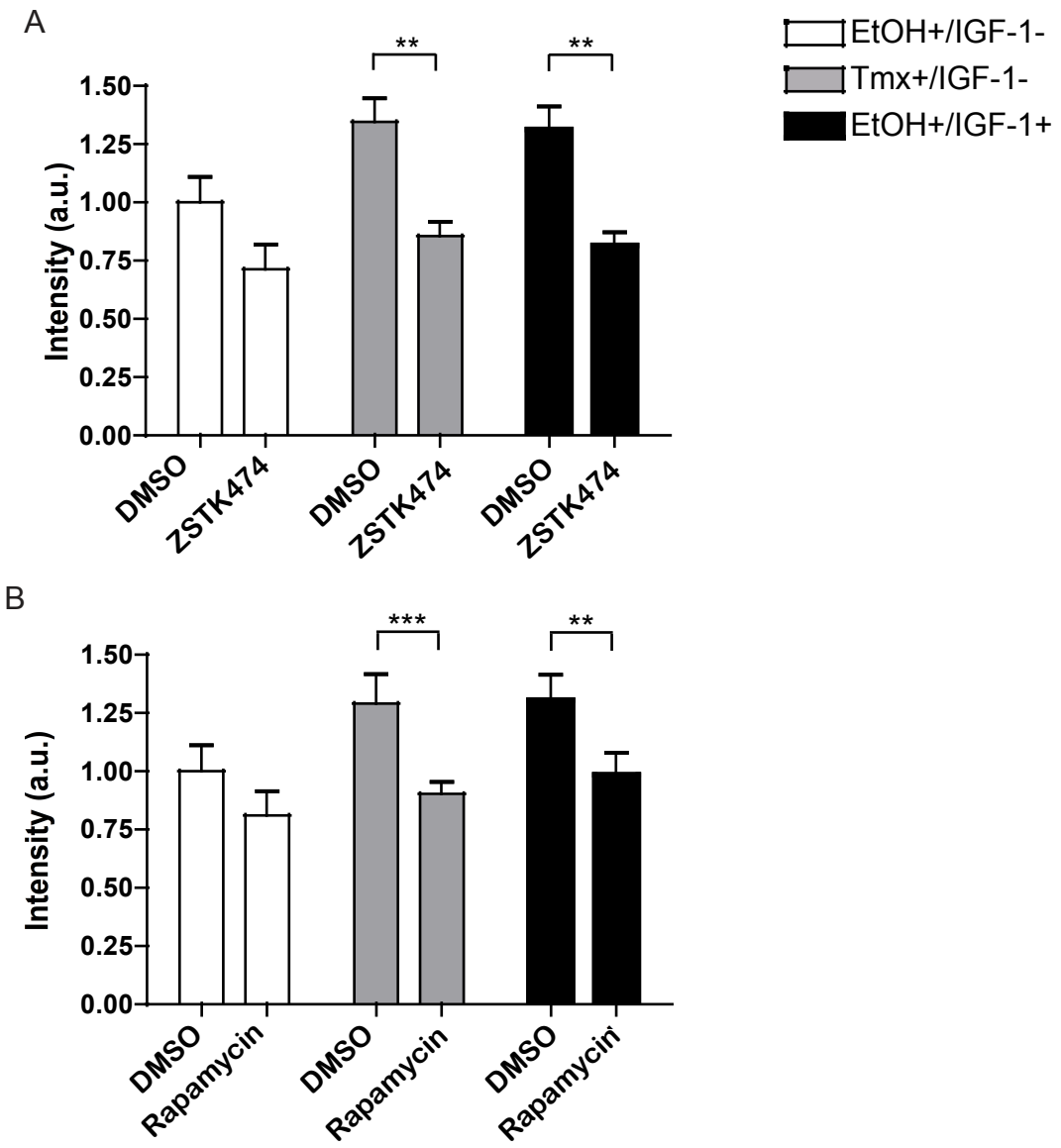

Figure 3.11 Addition of mass is PI3K and mTORC1 dependent

Aphidicolin arrested NSΔRafER cells were treated +/- inhibitors as indicated for 24hrs before mean amount of protein per cell (a.u.) was quantified (as total fluorescence intensity per cell after AlexaFlour647-succinimidyl ester labelling of fixed cells).
A) +/- ZSTK474, an inhibitor of class I PI3Kinases.
B) +/- Rapamycin, an inhibitor of mTORC1.
Bar charts show mean +SEM of A), B) 4 experiments, minimum 50 cells quantified per condition per experiment. Repeated Measures Two-Way ANOVA A) and B) DMSO vs inhibitor $p<0.001$. Post hoc Bonferroni as indicated on the graphs.

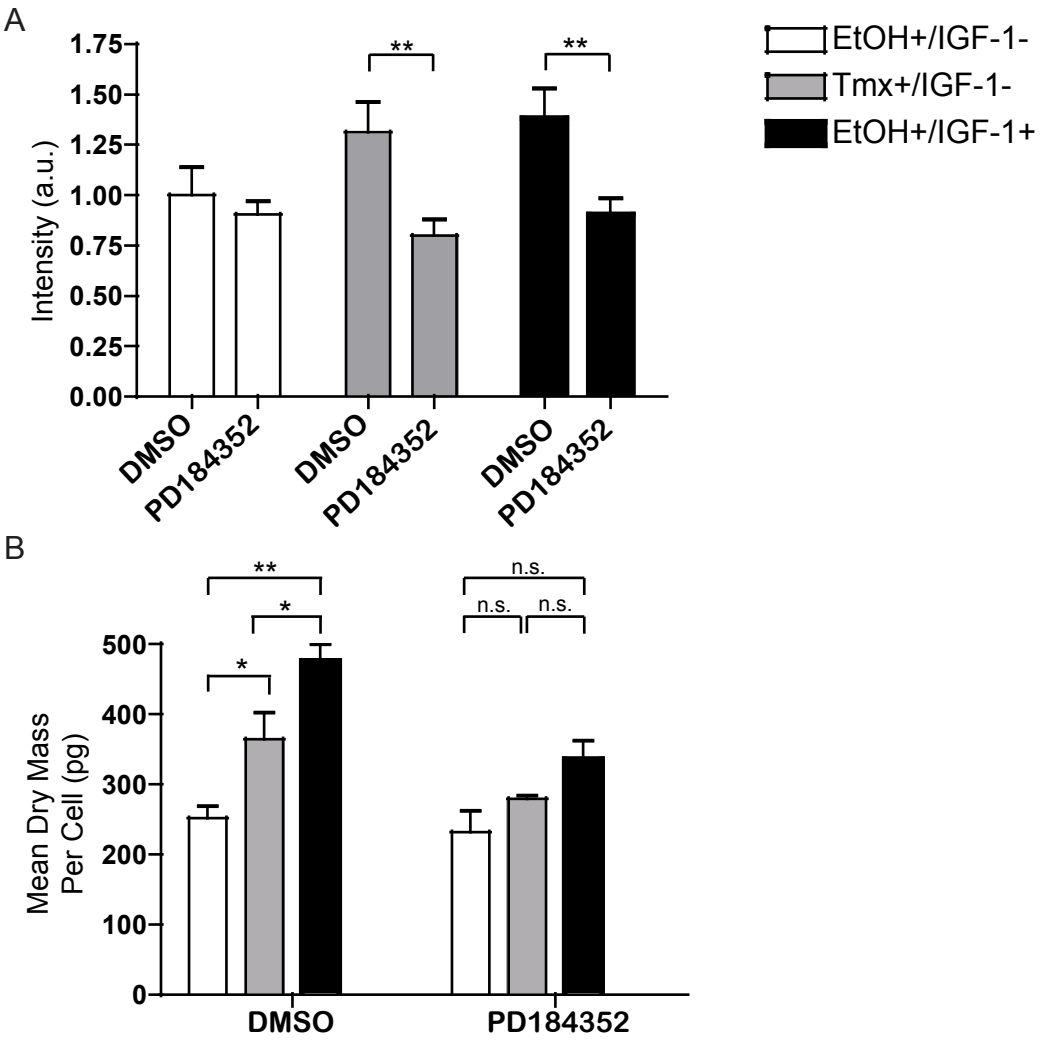

Figure 3.12 In contrast to cell volume, addition of mass is MEK dependent

Aphidicolin arrested NSΔRafER cells were treated as indicated for 24hrs +/-PD184352, an inhibitor of MEK, before:
A) Mean amount of protein per cell (a.u.) was quantified as total fluorescence intensity per cell after AlexaFlour647-succinimidyl ester labelling of fixed cells. Bar chart shows mean +SEM of 4 experiments, minimum 50 cells quantified per condition per experiment.
B) Mean dry mass per cell (pg) was quantified by QPM. Bar chart shows mean +SEM of 2 experiments, minimum 20 cells quantified per condition per experiment.
Repeated measures Two-Way ANOVA, A) DMSO vs inhibitor $p<0.001$, B) Between growth conditions $p<0.05$. Post hoc Bonferroni as indicated on the graph.

To confirm the specificity of the inhibitors with respect to the pathways (PI3K, mTORC1 and ERK) assayed in these experiments, Western blot analyses were performed against markers of each pathway +/- each inhibitor. As expected, inhibiting PI3K (ZSTK474) or mTORC1 (Rapamycin) did not block ERK signalling (Figure 3.13 A pERK1/2). Similarly, inhibiting MEK (PD184352) did not significantly block signalling through PI3K downstream of IGF-1 (Figure 3.13 B pAkt). However, the Western blot analysis suggested that inhibiting MEK reduced IGF-1 dependent S6K activation (Figure 3.13 A i pS6K). This requires further investigation, but it might suggest MEK/ ERK signalling contributes to mTORC1 activation downstream of IGF-1. If so, it would be interesting to determine if reduced signalling through mTORC1 contributes to the inhibition of IGF-1 dependent cell mass addition when MEK is inhibited (Figure 3.12). Moreover, given that the IGF-1 dependent addition of both mass and volume is prevented when mTORC1 signalling is blocked using Rapamycin (Figure 3.9, 3.11 & 3.13), it is interesting to speculate whether a partial block through this pathway is sufficient to block addition of mass, whereas a complete block is required to inhibit volume addition. Inhibiting MEK did block the transient activation of mTORC1 downstream of Raf kinase (Figure 3.13 A i pS6K). This is as predicted because Raf should drive specific signalling through MEK/ ERK and therefore MEK/ ERK should mediate Raf kinase dependent activation of mTORC1.

Both Rapamycin and ZSTK474 reduced signalling through mTORC1 to below the basal levels seen in control cells (Figure 3.13 A i pS6K (thr 389)). Although this might suggest non-specific inhibition of mTORC1 by ZSTK474, it is more likely that basal PI3K activity is required even for basal mTORC1 activity. Indeed, ZSTK474 was chosen because it has very low levels of non-specific mTORC1 inhibition compared to other PI3K inhibitors; in a different cell culture system, it was found that ZSTK474 inhibited PI3K at as little as 100nM whereas, in the same system, a 100μM concentration blocked only 40% of mTORC1 activity (Kong and Yamori, 2007). Given that 100nM was the concentration used in this study, it is unlikely that the inhibitor is acting directly on mTORC1.

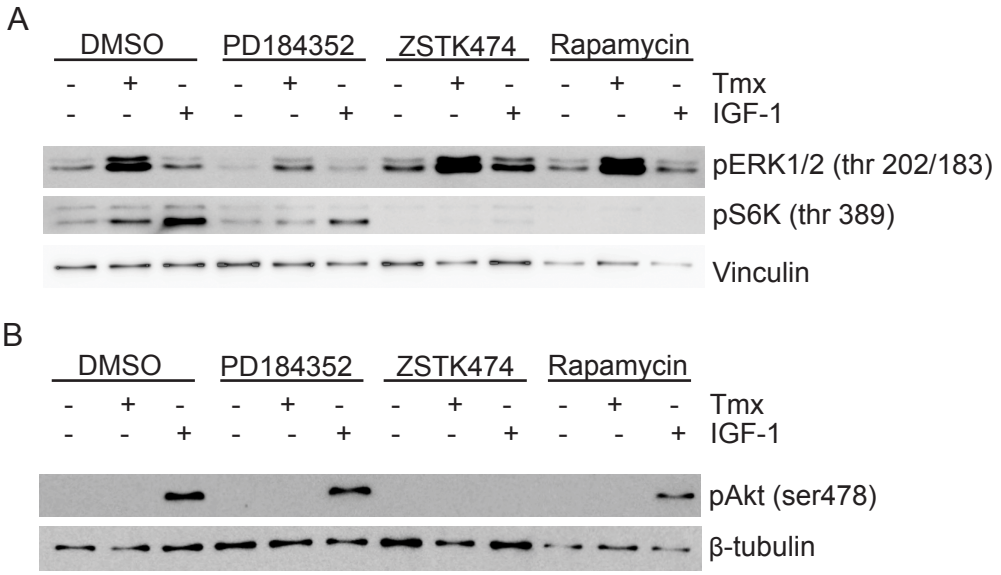

Figure 3.13 Inhibitors used are specific, with respect to the analysed pathways

Aphidicolin arrested NSΔRafER cells were treated +/- inhibitors as indicated for 24hrs before cell lysates were collected and western blot analysis performed to confirm the specificity of the inhibitors used, with respect to the:
A) MEK (pERK) and mTORC1 (pS6K) pathways.
B) PI3K/Akt (pAkt) pathway.

Basal signalling through mTORC1 is inhibited by both ZSTK474 and Rapamycin and both these inhibitors block Raf kinase dependent addition of protein mass- despite the fact Raf kinase activation did not activate signalling through PI3K (as indicated by levels of pAkt, Figure 3.7 A) and only transiently activated S6K (Figure 3.7 A iii pS6K). This is consistent with a hypothesis that a basal flux through mTORC1 is required for the addition of protein mass.

In conclusion, as for cell volume, IGF-1 dependent addition of cell mass is PI3K and mTORC1 dependent. However, in contrast to cell volume, the addition of mass also requires signalling through MEK. Similarly, Raf kinase dependent addition of cell mass requires PI3K, mTORC1 and MEK. As Raf kinase drives addition of mass in the absence of an increase in cell volume and IGF-1 treatment can drive volume addition when the addition of protein mass is blocked (MEK inhibition), this means the addition of cell mass and volume can be separated and independently regulated. Unlike cell volume addition, the dependence on PI3K, mTORC1 and MEK to add cell mass does not correlate with activation of signalling through these pathways by IGF-1 and Raf kinase. This may suggest that a basal flux of signalling through these pathways is necessary for a cell to add mass upon receipt of a specific growth stimulus.

Organelle Biogenesis Downstream of IGF-1 and Raf Kinase Activation: A Cell Biological Approach

The above results demonstrate that both Raf kinase activation and IGF-1 treatment drive Schwann cell biogenesis, but in distinct ways; both cause addition of protein mass however only IGF-1 drives addition of cell volume. This suggests the addition of protein mass per se is insufficient to drive an increase in cell volume. If so, additional factors must limit cell volume addition.

To begin to investigate what other factor(s) IGF-1 regulates to drive cell volume addition a cell biological approach was taken to compare biogenesis downstream of IGF-1 stimulation and Raf kinase activation. A combination of fluorescence and electron microscopy was used to compare organelle size and morphology 24 hours after IGF-1 stimulation or Raf kinase activation, i.e. the time at which cell volume and mass were assayed in the preceding sections.

3.4 IGF-1 Stimulation and Raf Kinase Activation Drive the Addition of Mitochondrial Volume and an Increase in Endoplasmic Reticulum (ER) Labelling

The mitochondria are described as the powerhouse of the cell; they are the sites of aerobic respiration synthesising ATP for the cell's bioenergetic requirements. In addition, the mitochondria provides the substrates for biosynthesis of fatty acids and amino acids to drive de novo lipogenesis and protein synthesis, respectively (DeBerardinis et al., 2008a, Deberardinis et al., 2008b, Vander Heiden et al., 2009, Lynen, 1966). Indeed, growing evidence suggests this latter function is the primary function of mitochondria in rapidly growing cells where there is excess glucose (DeBerardinis et al., 2008a, Deberardinis et al., 2008b, Vander Heiden et al., 2009). The excess glucose provides sufficient fuel to drive glycolysis at a fast enough rate to produce much of the cells ATP requirement. This means mitochondrial resources can be diverted from ATP production to providing substrates for biosynthesis. Given that IGF-1 and Raf kinase are driving cell growth, i.e. biogenesis, it was interesting to investigate the mitochondrial load in these cells.

To quantify the amount of mitochondria per cell the mitochondrial-specific fluorescent dye Mitotracker Green was used to label the mitochondria and the total volume of mitochondria per cell was determined from image stacks taken through the depth of the cell by fluorescence confocal microscopy (Materials & Methods 2.5-2.7) (Casley et al., 2002, Echave et al., 2009). Unlike many mitochondrial dyes the fluorescence of Mitotracker Green is reported to be relatively independent of mitochondrial membrane potential, which means labelling should be independent of mitochondrial activity and therefore reflect only the mitochondrial content of the labelled cells. Mitotracker Green (100nM) was added to the medium of live cells for 1hr at 37°c, 24 hours after IGF-1 treatment or Raf kinase activation, and the cells were then fixed and processed for confocal microscopy. Using this technique it can be seen that both Raf kinase activation (Tmx+/IGF-1-) and IGF-1 stimulation (EtOH+/IGF-1+) drove an ~1.3- to 1.5-fold increase in mitochondrial volume per cell over 24 hours compared to control, untreated (EtOH+/IGF-1-) cells (Figure 3.14 A & B). To confirm the increase in mitochondria per cell downstream of Raf kinase activation was not an artefact of Tmx treatment, mitochondrial volume was also

quantified after treating normal Schwann cells lacking the Tmx inducible Raf kinase construct with Tmx or IGF-1. As shown in Figure 3.15, only IGF-1 drove an increase in mitochondrial volume in these cells, suggesting the increase in the amount of mitochondria after Raf kinase activation in the NSΔRafER cells was not an artefact of Tmx treatment.

Consistent with the findings of Echave et al, the increase in mitochondrial volume was proportional to the increase in cell volume downstream of IGF-1 and therefore mitochondrial density in the cell was unchanged compared to control (Echave et al., 2009). As Raf kinase increases mitochondrial volume per cell in the absence of an increase in cell volume, there was an ~1.5-fold increase in mitochondrial density per cell compared to control and IGF-1 stimulated cells (Figure 3.14 B ii). This is also consistent with the finding that NRG-1, which drives sustained activation of the Raf/ MEK/ ERK signalling pathway, drives mitochondrial biogenesis (Echave et al., 2009).

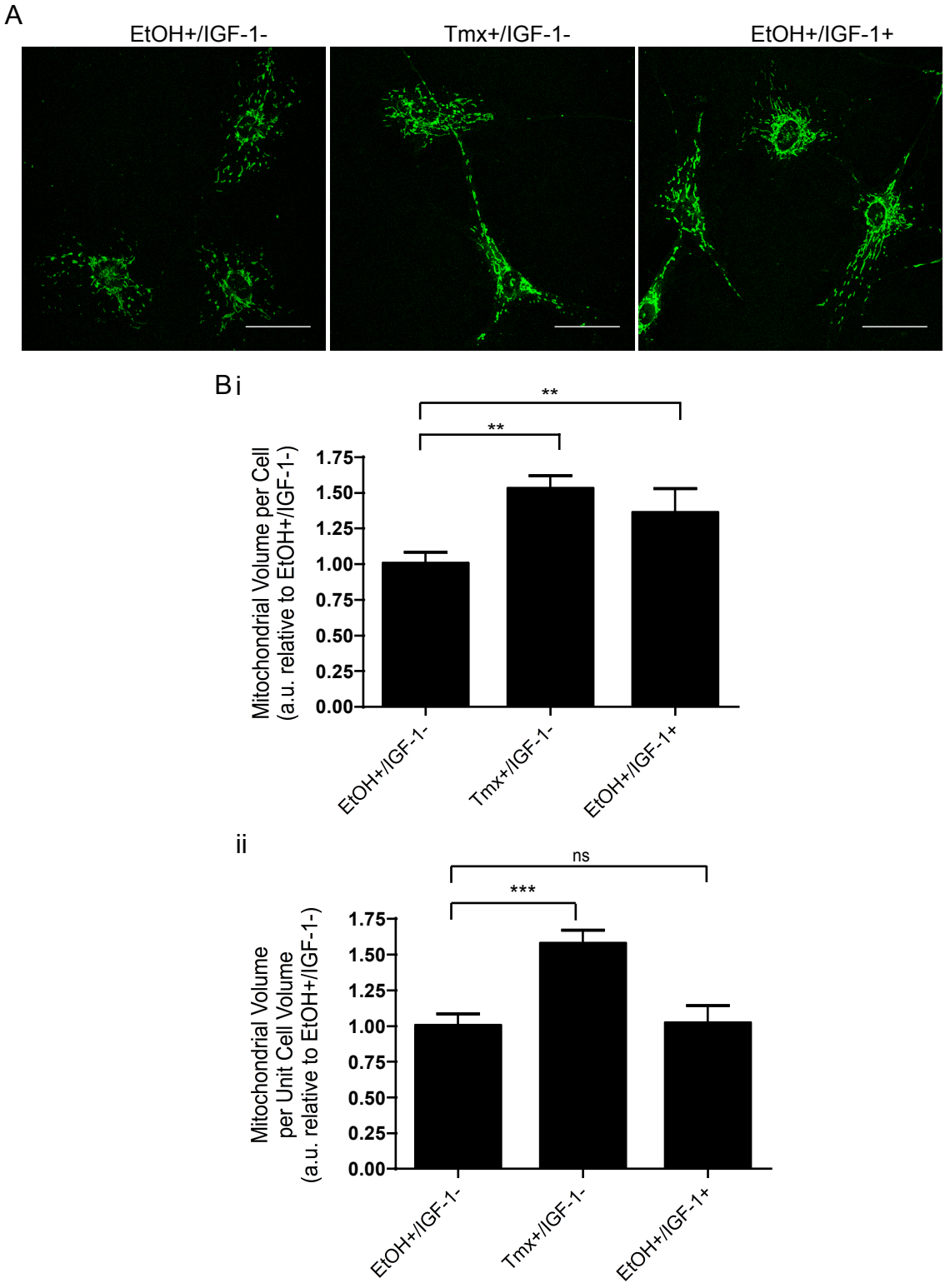

Figure 3.14 IGF-1 stimulation and Raf kinase activation drive addition of mitochondrial volume

Aphidicolin arrested NSΔRafER cells were treated as indicated for 24hrs then stained with MitotrackerGreen to label mitochondria. Organelle volume was quantified from confocal microscopy image stacks.
A) Representative maximal projection images of labelled mitochondria.
B) Mean total mitochondrial volume per cell (a.u.). Scale bar = 25μm.
C) Mean mitochondrial volume per unit of cell volume (a.u.). The cell volume of parallel cell cultures was quantified using a Coulter Counter.
Bar charts show mean +SEM of 6 experiments, minimum 35 cells quantified per condition per experiment. Repeated Measures One-Way ANOVA A) p,0.01 and B) p<0.001. Select post hoc Newman-Keuls as indicated.

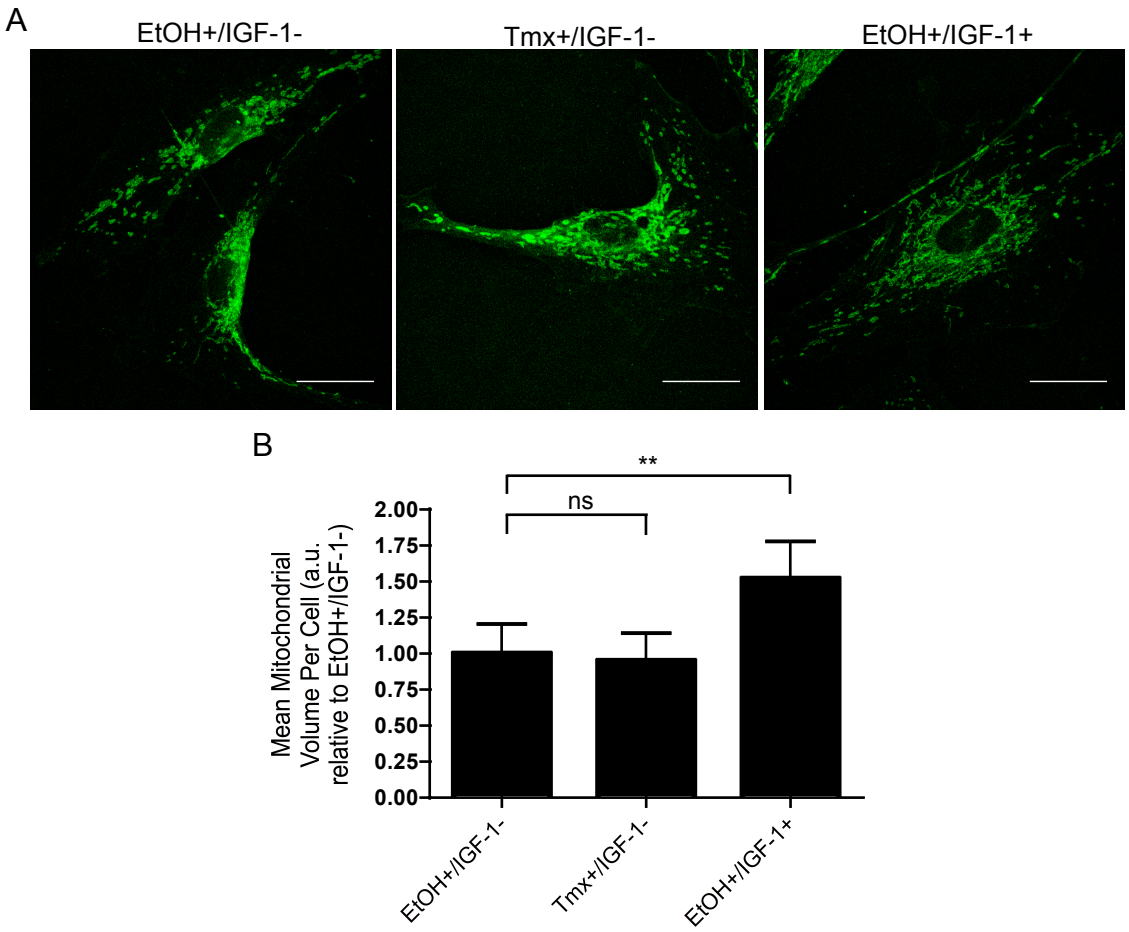

Figure 3.15 Raf kinase dependent increase in mitochondrial volume is not an artefact of tamoxifen treatment

Aphidicolin arrested NS cells were treated as indicated for 24hrs then stained with Mitotracker Green to label mitochondria:
A) Representative maximal projection images of labelled mitochondria. Scale bar = 25μm.
B) Mean total mitochondrial volume per cell (a.u.). Bar chart shows mean +SEM of 6 experiments, minimum 35 cells quantified per condition per experiment. Repeated Measures One-Way ANOVA $p<0.01$. Select post hoc Newman-Keuls as indicated.

Quantifying mitochondrial volume from light microscopy images may be problematic because the diameter of many mitochondria is less than 100nm and therefore below the resolution of the light microscope. This leads to an overestimation of mitochondrial volume per cell. More critically, the extent of overestimation may be different in different cell conditions if there is variation in mitochondrial diameter and/ or the proximity of mitochondria to one another within the cytoplasm between conditions. Therefore, to confirm the results obtained by light microscopy, mitochondrial volume was also quantified from electron microscopy (EM) images using stereology (Materials & Methods 2.8). Cells were treated for 24hrs +/- IGF-1 or Tmx, as for the Mitotracker assays, and then fixed and processed for Transmission Electron Microscopy. Briefly; cells were fixed, delipidated and dehydrated before being embedded in an EPON resin. The resin was then sectioned at 250nM intervals, starting from a random height within the sections. Each section contained slices from a number of cells and sections through the depth of the resin were chosen at random for imaging and subsequent analysis. These steps ensured a random sample of cell sections were analysed. Mitochondrial volume was quantified by calculating the mean proportion of the cell area occupied by mitochondria in the imaged cells (area fraction), which is equivalent to the mean proportion of the cell volume occupied by mitochondria (volume fraction) according to the principle of Delesse. The volume of mitochondria in μm^3 was obtained by multiplying the volume fraction with the mean cell volume of parallel culture dishes.

The EM results confirmed the light microscopy results. That is, both IGF-1 stimulation and Raf kinase activation drove an ~1.5-fold increase in the total mitochondrial volume per cell (Figure 3.16 A & B i) and, because Raf kinase increases mitochondrial volume in the absence of an increase in cell volume, mitochondrial density per cell increased (Figure 3.16 B ii). IGF-1 drove a proportional increase in mitochondrial and cell volume and so mitochondrial density does not change relative to control untreated cells (Figure 3.16 B ii).

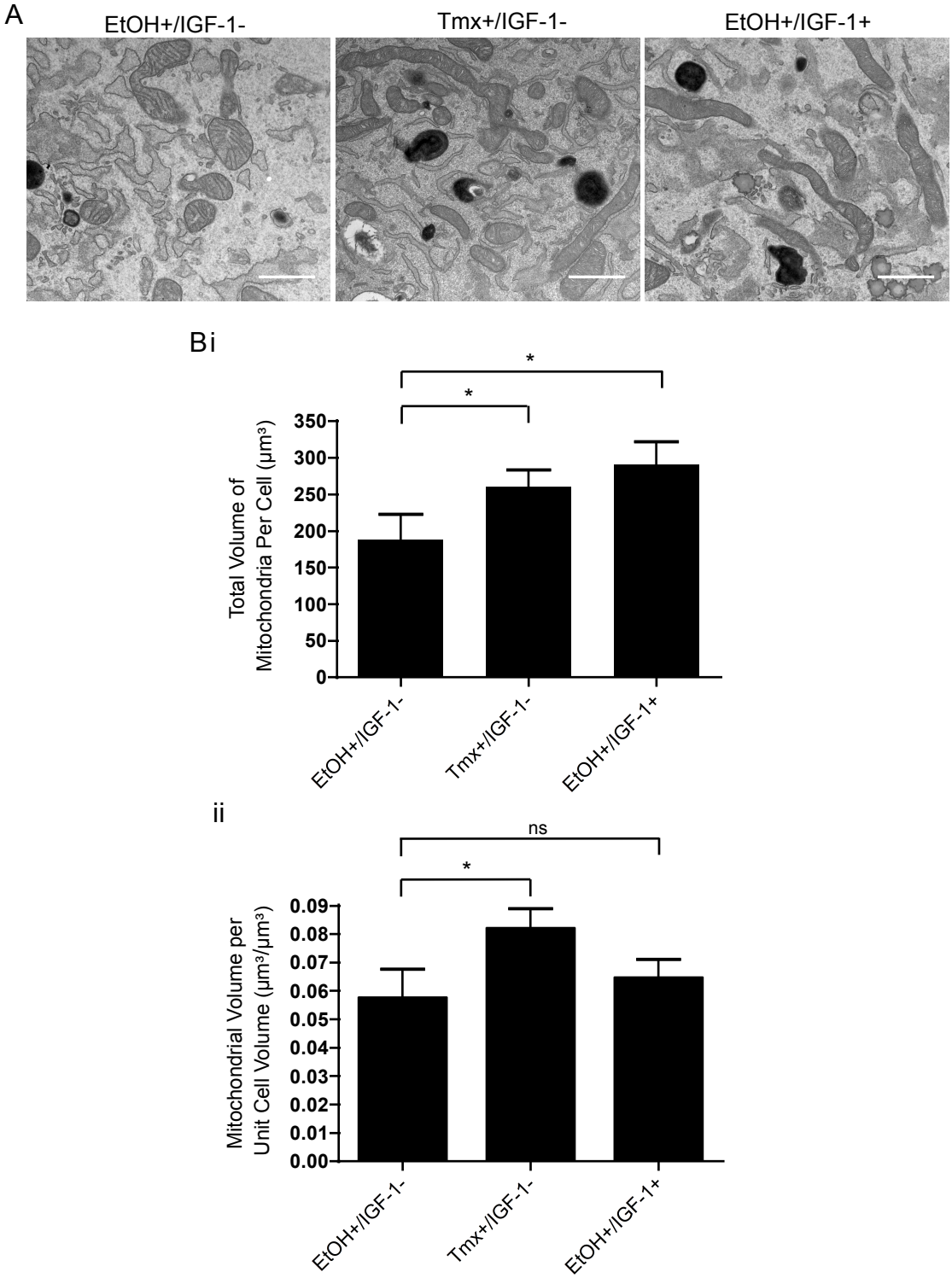

Figure 3.16 IGF-1 stimulation and Raf kinase activation drive the addition of mitochondrial volume

Aphidicolin arrested NSΔRafER cells were treated as indicated for 24hrs then fixed for transmission electron microscopy (TEM). Stereology was used to quantify mitochondrial volume and volume density per cell.
A) Representative TEM images showing sections taken from the mid-height of the cell. Scale bar =100nm.
B) Mean total mitochondrial volume per cell (μm^3),
C) Mean mitochondrial volume per unit of cell volume ($\mu m^3/\mu m^3$).
Bar charts show mean +SEM of 3 experiments, minimum 80 images quantified per condition per experiment. Repeated Measures One-Way ANOVA B) and C) $p<0.05$. Post hoc Newman-Keuls as indicated.

Another organelle central to biosynthesis is the endoplasmic reticulum (ER). The ER is composed of smooth (SER) and rough (RER) that function primarily in lipid and protein metabolism respectively. The SER is a major site of lipid synthesis as well as being involved in other aspects of metabolism including calcium homeostasis. The RER is the site of protein synthesis and primary modifications of integral membrane proteins and proteins destined for export and secretion. To label the ER and provide an indication of the relative size of this organelle in different conditions, cells were fixed after 24hrs +/- IGF-1 treatment or Raf kinase activation and immunostained for fluorescence microscopy with an α–KDEL antibody (Materials & Methods 2.5). 'KDEL' is a 4 amino acid ER retention signal contained in many resident ER proteins (e.g. grp94 (SER) and BiP (RER)) and therefore the amount of KDEL per cell should be an indicator of the amount of ER per cell; this technique cannot distinguish between the amount of SER and RER. Labelled cells were imaged using fluorescence widefield microscopy and fluorescence intensity per cell was quantified to indicate the amount of ER in the cell (Materials & Methods 2.6 & 2.7). As can be seen in Figure 3.17 both Raf kinase activation (Tmx+/IGF-1-) and IGF-1 stimulation (EtOH+/IGF-1+) resulted in an ~1.5-fold increase in KDEL+ fluorescence per cell compared to control (EtOH+/IGF-1-) over 24hrs, suggesting an increase in the amount of ER in the cell.

In conclusion, these results demonstrate that IGF-1 and Raf kinase drive an increase in the amount of mitochondria and ER in the cell. In other words, the increase in mass downstream of these stimuli is correlated with an increase in the mass of certain organelles. Given the central role both these organelles have in cellular biosynthesis, these findings are consistent with the increase in mass downstream of IGF-1 and Raf kinase activation.

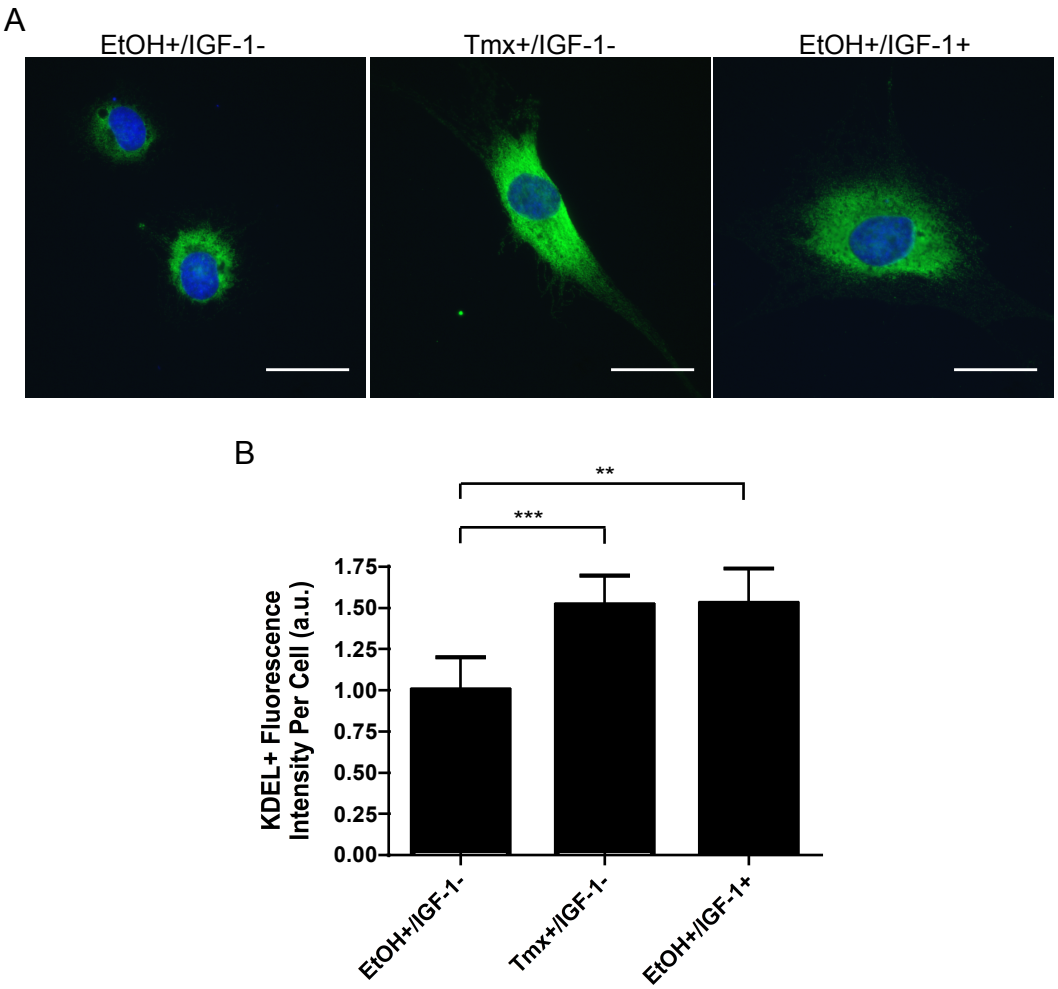

Figure 3.17 IGF-1 stimulation and Raf kinase activation drive an increase in the KDEL receptor, suggesting an increase in the size of the endoplasmic reticulum

Aphidicolin arrested NSΔRafER cells were treated as indicated for 24hrs, before anti-KDEL receptor immunofluorescence to label the endoplasmic reticulum (ER). Total fluorescence intensity was quantified from widefield microscopy images of labelled cells in ImageJ.
A) Representative widefield microscopy images of labelled ER. Scale bar = 25μm.
B) Mean fluorescence intensity per cell (a.u.). Bar chart shows mean +SEM of 3 experiments, minimum 30 cells quantified per condition per experiment. Repeated Measures One-Way ANOVA, $p<0.001$. Post hoc Newman-Keuls as indicated on the graph.

3.5 The Nucleus and Trans-Golgi Network do not show Gross Morphological Changes after IGF-1 or Raf Kinase Activation

It has been proposed that cells maintain a constant nuclear: cytoplasmic (N:C) ratio and this is a mechanism of cell size control (Umen, 2005). If so, it would be predicted that nuclear volume increases as cell volume increases to maintain a constant N:C ratio. However several studies suggest this is not the case. In budding yeast a constant N:C is not maintained as cells grow across the cell cycle (Jorgensen et al., 2007). In addition, although serum treatment drives an increase in both nuclear volume and cell volume in primary Schwann cells and fibroblasts, the increase in nuclear volume is not proportional to the increase in cell volume and so N:C decreases (Echave et al., 2007). It is not clear how nuclear size is related to function. It was therefore interesting to determine whether Raf kinase activation or IGF-1 stimulation affect nuclear volume. To quantify nuclear volume Hoescht was used to label the nuclei of fixed cells and nuclear volume was calculated from image stacks taken through the depth of the cell by fluorescence confocal microscopy (Materials & Methods 2.5-2.7). As shown in Figure 3.18, neither Raf kinase activation (Tmx+/IGF-1-) or IGF-1 stimulation (EtOH+/IGF-1+) significantly changed nuclear volume compared to control (EtOH+/IGF-1-) over 24 hours. As it has previously been shown that serum drives an increase in Schwann cell nuclear volume (Echave et al., 2007), cells were also treated with medium containing serum (3% FCS (foetal calf serum)) to try to determine whether the lack of significant change in nuclear volume downstream of IGF-1 or Raf kinase was real or simply due to a detection problem. Consistent with previous findings, 3% FCS increased nuclear volume by ~1.25-fold compared to control (Figure 3.18). However, it is possible that IGF-1 and/ or Raf kinase drive a change in nuclear volume that is below the detection resolution of this technique.

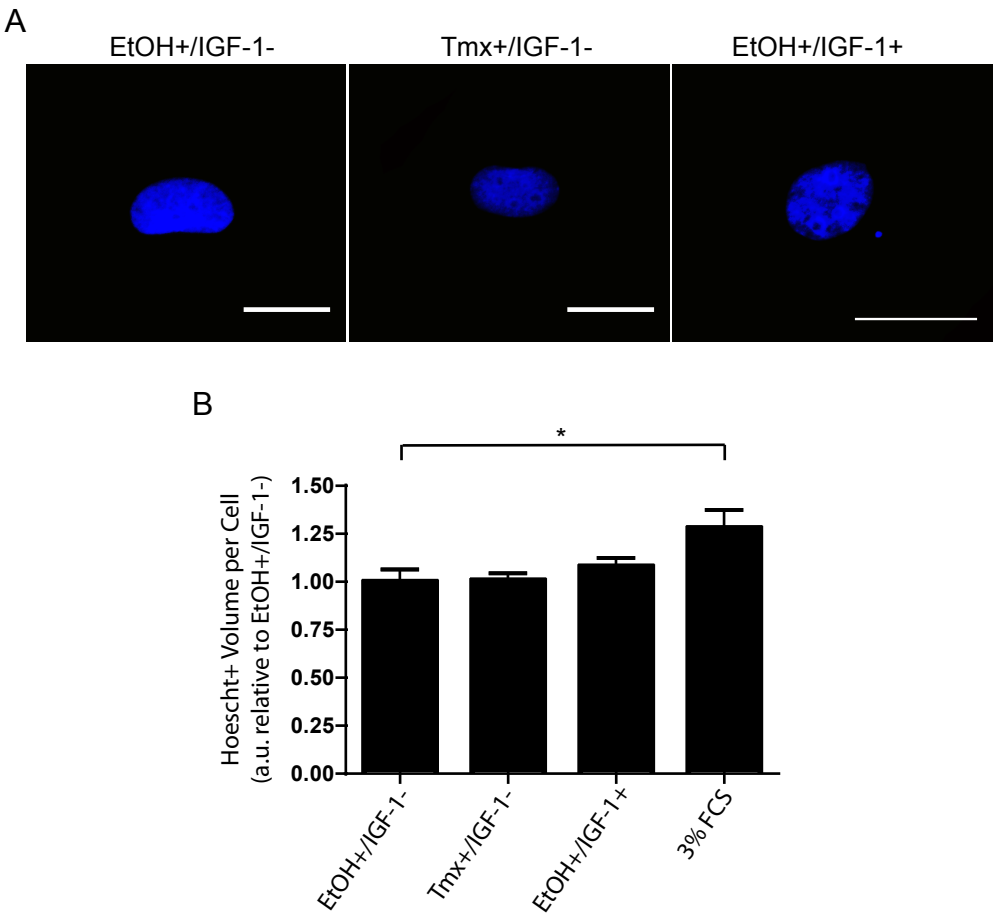

Figure 3.18 There is no significant change in nuclear volume after IGF-1 stimulation or Raf kinase activation

Aphidicolin arrested NSΔRafER cells were treated as indicated for 24hrs before Hoescht staining to label the nuclei. Organelle volume was quantified from image stacks taken by confocal microscopy.
A) Representative maximal projection images of labelled nuclei. Scale bar = 25μm.
B) Mean total nuclear volume per cell (a.u.). Bar chart shows mean +SEM of 4 experiments, minimum 30 cells quantified per condition per experiment. Repeated Measures One-Way ANOVA, $p<0.05$. Post hoc Newman-Keuls as indicated on the graph.

The Golgi apparatus receives proteins and lipids from the ER and modifies, sorts and packages them for delivery to their correct cellular location, or for secretion. The Golgi can be sub-divided into 4, approximately distinct, domains. The cis-Golgi is where cargo (proteins and lipids) are first received from the ER; cargo then moves more or less progressively through the medial, trans and, finally, the trans-Golgi network (TGN) and is appropriately modified, for example by glycosylation, as it moves. The TGN is primarily the sorting and distribution centre of the Golgi where, once correctly packaged, vesicles containing the modified cargo bud off and travel to the plasma membrane or other subcellular compartments. Given that IGF-1 and Raf kinase increase protein mass and possibly the amount of ER in the cell, it was interesting to determine whether there was a corresponding increase or change in Golgi architecture. Such a change might be necessary for processing an increased amount of nascent protein traffic, if this occurs, downstream of IGF-1 and Raf kinase activation, for example. To identify any changes in TGN architecture cells were fixed after 24hrs +/- Raf kinase activation or IGF-1 treatment and immunostained for fluorescence microscopy with an α–TGN38 antibody (Materials & Methods 2.5). TGN38 is an integral TGN membrane protein that has a role in formation of exocytic vesicles from the TGN and cycles between the TGN and plasma membrane- and it is regularly used as a marker of the TGN. Estimated TGN volume was quantified from image stacks taken through the cell by fluorescence confocal microscopy (Materials & Methods 2.6 & 2.7). As shown in Figure 3.19, although there is a trend for Raf kinase activation (Tmx+/IGF-1-) and IGF-1 stimulation (EtOH+/IGF-1+) to increase TGN volume compared to control (EtOH+/IGF-1-), this is not significant- potentially due to the relatively large variability in TGN size between cells in the same growth factor condition. It must be noted, as for the mitochondria, individual TGN vesicles and stacks can be smaller than the resolution of the light microscope; such differences in TGN volume will not be detected by this method.

In conclusion, neither nuclear and TGN volume are not significantly altered in IGF-1 treated or Raf kinase activated cells, compared to control; however, these results need to be interpreted with some caution.

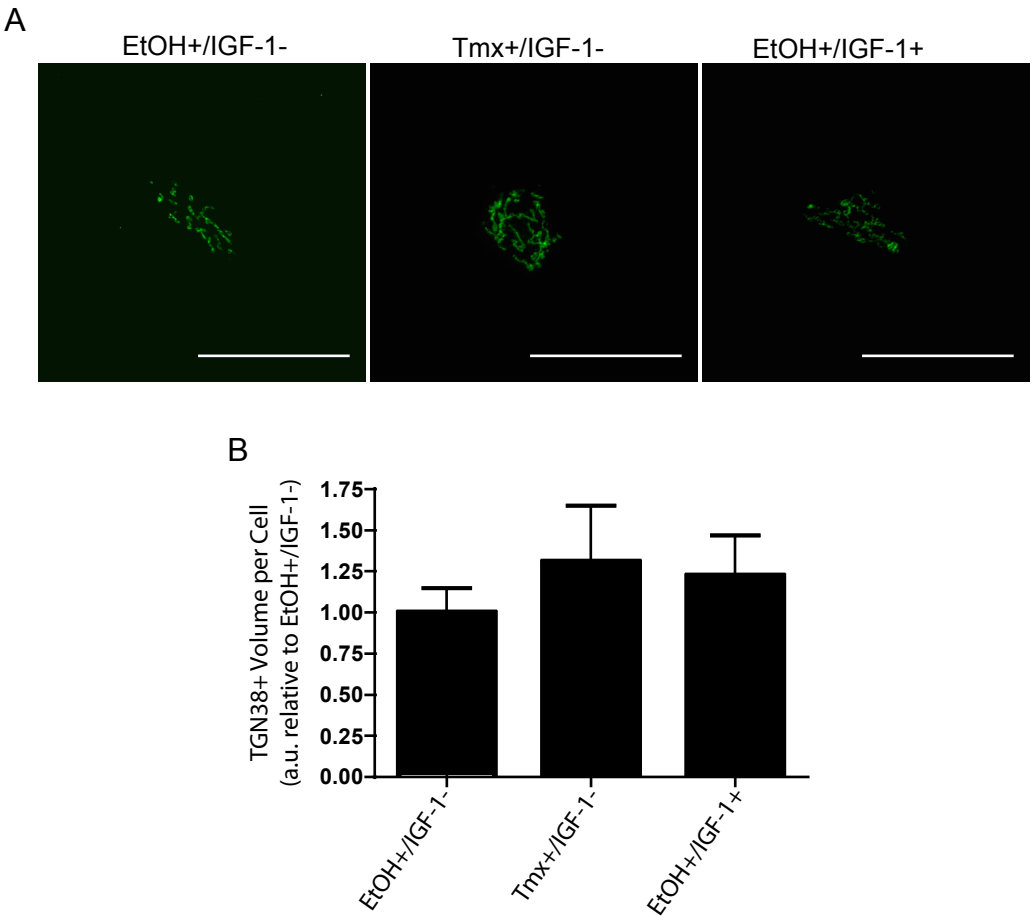

Figure 3.19 IGF-1 stimulation and Raf kinase activation do not drive a significant change in trans-Golgi network (TGN) volume

Aphidicolin arrested NSΔRafER cells were treated as indicated for 24hrs, before anti-TGN38 immunofluorescence to label the TGN. Organelle volume was quantified from image stacks taken by confocal microscopy.
A) Representative widefield microscopy images of labelled TGN. Scale bar = 25μm.
B) Mean TGN volume per cell (a.u.). Bar chart shows mean +SEM of 5 experiments, minimum 30 cells quantified per condition per experiment. Repeated Measures One-Way ANOVA, $p>0.05$.

3.6 The cis-Golgi and Organelles Associated with Lipid Metabolism Increase Downstream of IGF-1

To continue to characterise the cellular and morphological effects of IGF-1 and Raf kinase activation, the morphology, number and/ or volume of three other organelles- the cis-Golgi, lipid droplets and peroxisomes- were then analysed. As described above, the Golgi apparatus has four distinct domains. The cis-Golgi is the first of these and the site where proteins and lipids are received from the ER and begin to be further modified and processed. As before, cells were treated for 24hrs +/- Raf kinase activation or IGF-1 treatment before being fixed and immunostained for fluorescence microscopy. The cis-Golgi was labelled using an α–GM130 antibody (Materials & Methods 2.5). GM130 facilitates membrane fusion events within the cis-Golgi and therefore helps maintain the organelle's structure. Cis-Golgi volume was quantified from image stacks taken through the cell by fluorescence confocal microscopy (Materials & Methods 2.6 & 2.7). As shown in Figure 3.20, IGF-1 stimulation (EtOH+/IGF-1+), but not Raf kinase activation (Tmx+/IGF-1-) appeared to drive a significant change in cis-Golgi volume compared to control (EtOH+/IGF-1-) over 24 hours. Again, as for both the mitochondria and TGN, the diameter of cis-Golgi cisternae can be smaller than the resolution of the light microscope and therefore this method will not detect sub-resolution changes in cis-Golgi volume between the conditions tested. This means the quantified volumes may be under- or over- estimated for any condition and therefore, if the error is in a different direction or of a different magnitude between the three conditions (Control, Raf kinase or IGF-1), the IGF-1 specific difference may have been over- or under- estimated.

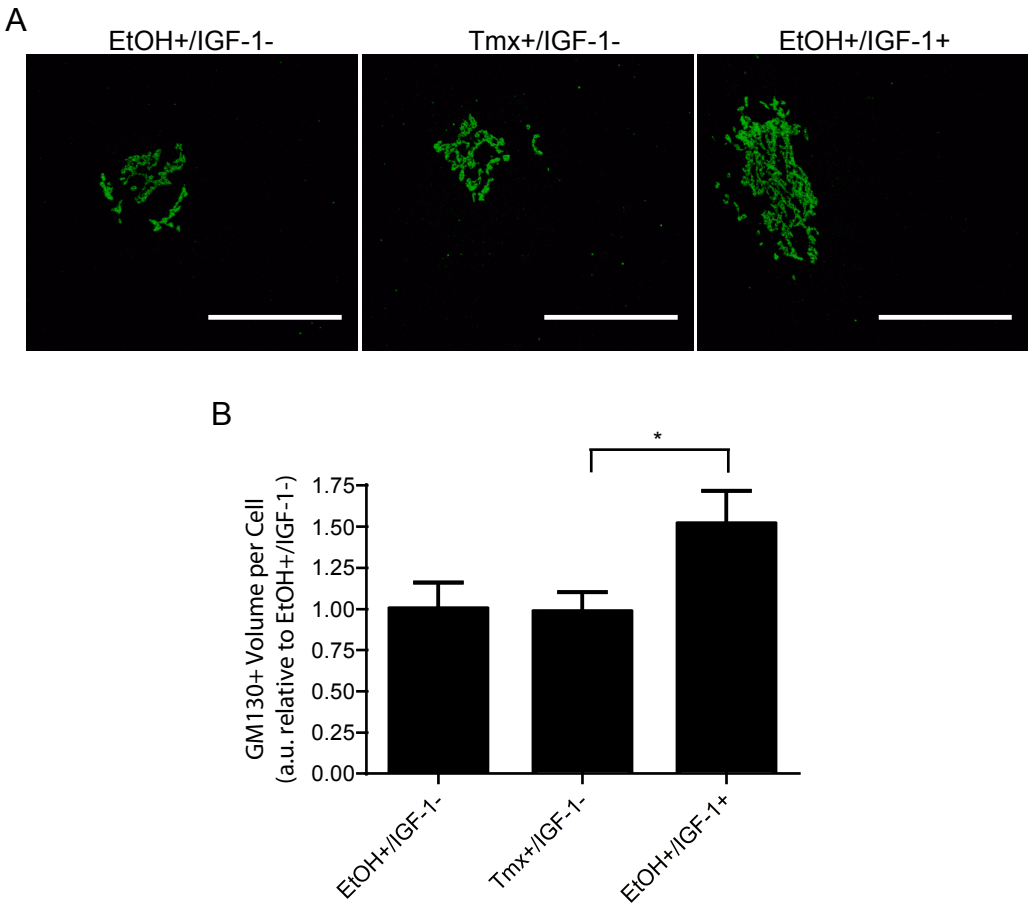

Figure 3.20 IGF-1 stimulation drives an increase in cis-Golgi volume

Aphidicolin arrested NSΔRafER cells were treated as indicated for 24hrs, before anti-GM130 immunofluorescence to label the cis-Golgi. Organelle volume was quantified from image stacks taken by confocal microscopy.
A) Representative maximal projection images of labelled cis-Golgi. Scale bar = 25μm.
B) Mean total cis-Golgi volume per cell (a.u.). Bar chart shows mean +SEM of 4 experiments, minimum 30 cells quantified per condition per experiment. Friedman test $p<0.05$, post hoc Dunn's test as indicated.

Lipid droplets consist of a core of neutral lipids, primarily triacylglycerols (TAGs) and sterol esters, surrounded by a phospholipid monolayer containing many proteins that metabolise and transport lipids to/ from the lipid droplet surface (Walther and Farese, 2009). To label the lipid droplets, cells were fixed before being incubated with Oil Red O, which is a neutral lipid stain and therefore labels the lipid droplet core. Oil Red O emits red fluorescence and so the number of lipid droplets per cell was quantified in ImageJ from fluorescence widefield microscopy images of labelled fixed cells (Materials & Methods 2.5). The processed images used for quantification of lipid droplet number per cell are shown in Figure 3.21 A. As for the previous organelle analyses, cells were analysed 24 hours after IGF-1 or Tmx treatment. Quantification of the number of lipid droplets per cell (Figure 3.21 B) showed that IGF-1 stimulation (EtOH+/IGF-1+) but not Raf kinase activation (Tmx+/IGF-1-) resulted in a 2-fold increase in the number of lipid droplets per cell compared to control (EtOH+/IGF-1-). To confirm these results lipid droplets were identified and quantified by stereology from electron micrographs of sectioned cells (sections were ~250nm thick) (Materials & Methods 2.8). Two types of lipid droplets were identified by EM (Figure 3.22 A) and to distinguish between them for quantification purposes they were termed ‘Lipid Bodies’ and ‘Electron Dense Lipid Droplets’. Quantification of the number of lipid droplets per cell (by stereological analysis of electron micrographs, Materials & Methods 2.8) showed that over 24 hours IGF-1 stimulation caused a 2-fold increase in the number of Lipid Bodies per cell (Figure 3.22 B i). There was also a trend for the number of Electron Dense Lipid Droplets to increase specifically downstream of IGF-1, however this trend is not statistically significant. The number of lipid droplets per cell quantified by EM was greater than the number quantified by Oil Red O staining. This may be because Oil Red O staining is less sensitive at labelling lipid droplets than the direct identification of lipid droplets by EM. It may also be because, as noted from the EM images (data not shown), lipid droplets were often found clustered in the Schwann cells; if their proximity to one another is below the resolution of the light microscope they would be identified from Oil Red O staining as one larger droplet, when in fact they are a group of multiple droplets.

The size of lipid droplets is know to be highly heterogeneous and can range from <1-100μm in diameter, depending on cell type and cell state (Walther and Farese, 2009). To determine whether there was a difference in the size of individual lipid droplets between IGF-1, Raf kinase and control cells the mean volume per lipid droplet was also quantified from EM images using stereology. The results show there was no significant difference in the mean size of either type of lipid droplet between the three conditions (Figure 3.22 B ii). As shown in Figure 3.22 B iii, because the number of Lipid Bodies per cell increased specifically downstream of IGF-1 and there was no difference in the volume of individual droplets between conditions, the total volume of Lipid Bodies per cell increased 2-fold in the presence of IGF-1 over 24 hours, compared to Raf kinase activated (Tmx+/IGF-1-) or control (EtOH+/IGF-1-) cells. There was no significant difference in the total volume of Electron Dense Lipid Droplets per cell between the conditions. These results show that IGF-1 stimulation, but not Raf kinase activation results in an increase in the number and total volume of lipid droplets per cell over 24hrs, compared to control untreated cells.

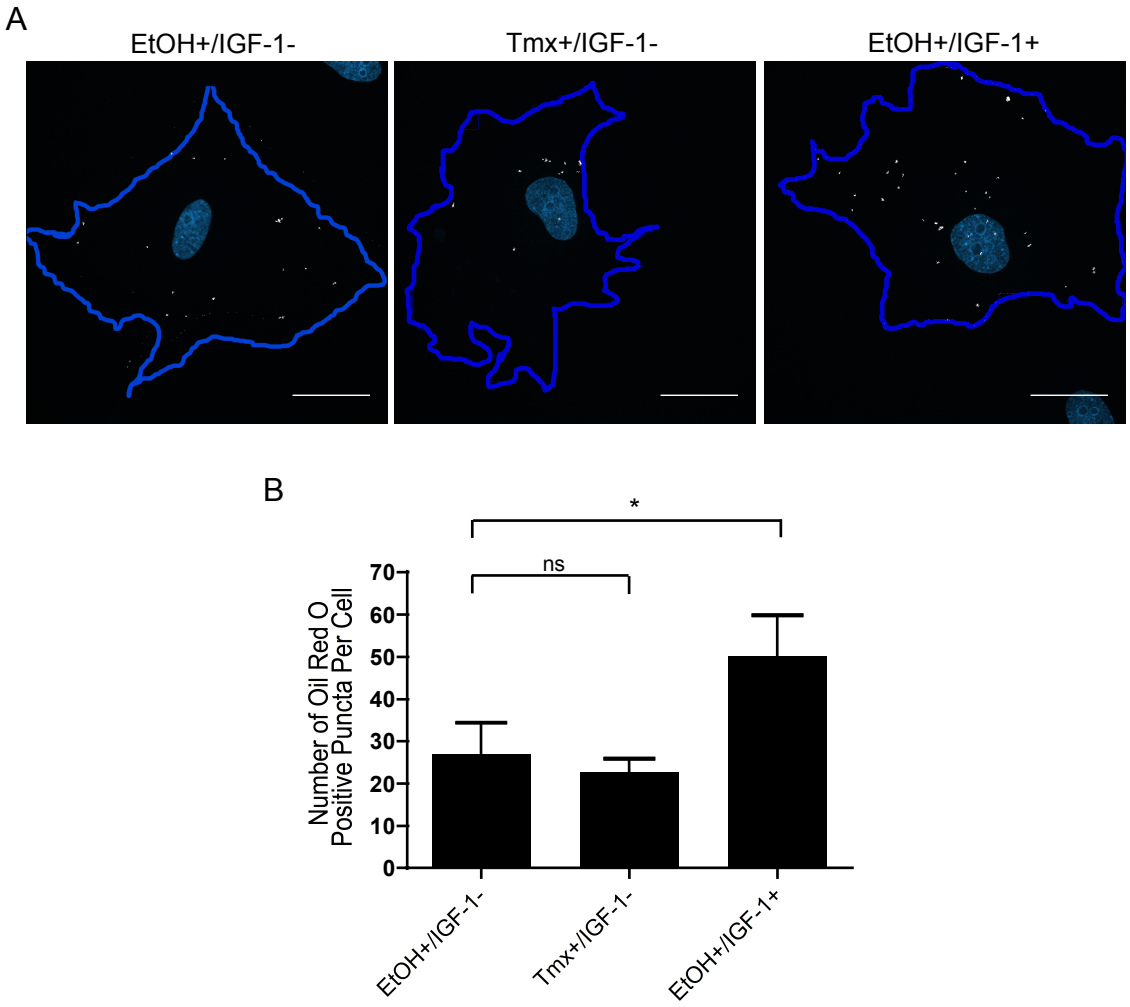

Figure 3.21 IGF-1 drives an increase in the number of lipid droplets per cell

Aphidicolin arrested NSΔRafER cells were treated as indicated for 24hrs then stained with Oil Red O to label the lipid droplets.
A) Representative maximal projections of Oil Red O staining. Scale bar = 25μm.
B) The mean number of lipid droplets per cell was quantified from images as shown in A) using ImageJ. Bar chart shows mean of 5 experiments, minimum of 20 cells quantified per condition per experiment. Repeated Measures One-Way ANOVA, $p<0.05$. Select post hoc Newman-Keuls as indicated on the graph.

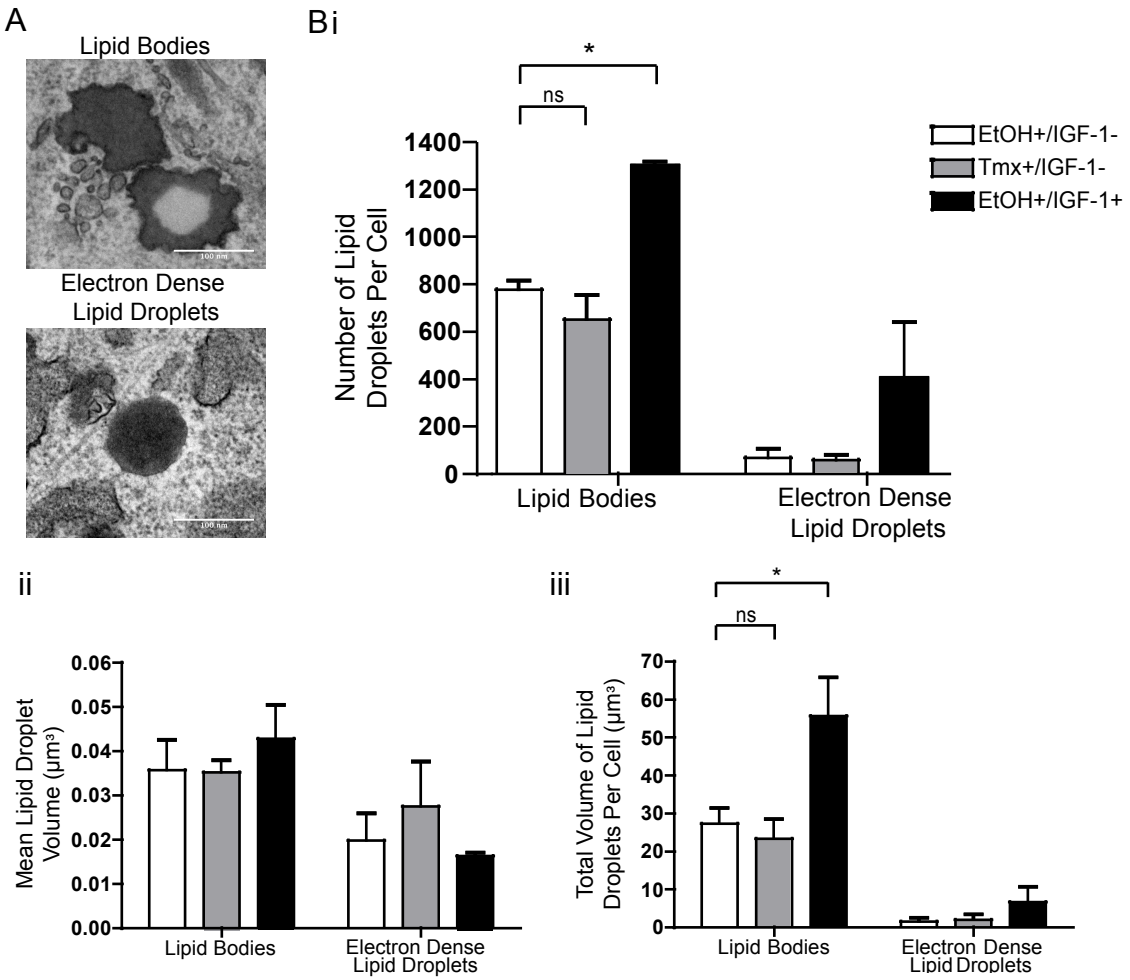

Figure 3.22 IGF-1 drives an increase in the number and total volume of lipid droplets per cell

Aphidicolin arrested NSΔRafER cells were treated as indicated for 24hrs then fixed for transmission electron microscopy (TEM). Stereology was used to quantify the number and volume of lipid droplets per cell.
A) Representative TEM images of the morphology of the two types of lipid droplets identified in Schwann cells.
B) i) Mean number of lipid droplets per cell, ii) Mean volume of individual lipid droplets (μm^3) and iii) Mean total volume of lipid droplets per cell (μm^3).
Bar charts show mean +SEM of 3 experiments, minimum of 80 images quantified per condition per experiment. Repeated Measures Two-Way ANOVA B) and D) Between growth conditions $p<0.01$, Between lipid droplet types $p<0.01$ and C) Between growth conditions $p>0.05$, Between lipid droplet types $p<0.05$. Select post hoc Bonferroni as indicated on the graphs.

Finally, to quantify the number of peroxisomes per cell, cells were fixed after 24hrs +/- Raf kinase activation or IGF-1 treatment and immunostained for fluorescence microscopy with an α–catalase antibody to label the peroxsiomes (Materials & Methods 2.5). Catalase is a peroxisomal matrix protein (also found in lower concentrations in the cytoplasm) involved in the redox function of the peroxisome. The number of peroxisomes per cell was quantified in ImageJ from maximal projection images taken by fluorescence confocal microscopy (Figure 3.23 A & B i) (Materials & Methods 2.6 & 2.7). As for the number of lipid droplets per cell, IGF-1 (EtOH+/IGF-1+) but not Raf kinase activation (Tmx+/IGF-1-) caused a 2-fold increase in the number of peroxisomes per cell (Figure 3.23 B i). This increase is greater than the increase in cell volume downstream of IGF-1 and therefore the density of peroxisomes within the cell increased (Figure 3.23 B ii). This may indicate a central role for peroxisomes in IGF-1 dependent cell metabolism.

Interestingly, the IGF-1 dependent increase in peroxisome number, like cell volume, depended on mTORC1; pre-treatment of the cells with rapamycin, an mTORC1 inhibitor, blocked the increase in peroxisome number after IGF-1 stimulation (Figure 3.24). Consistent with a close link between peroxisome number and cell volume downstream of IGF-1, inhibiting MEK using PD184352- which did not block IGF-1 dependent cell volume addition- also did not block the IGF-1 dependent increase in peroxisome number (Figure 3.25). Interestingly, because MEK inhibition blocked IGF-1 dependent addition of cell mass, this result also suggests peroxisome number does not contribute significantly to cell mass. These findings cannot distinguish whether peroxisomes act upstream or downstream of IGF-1 dependent cell volume addition but they may suggest peroxisome number and cell volume are closely linked downstream of IGF-1.

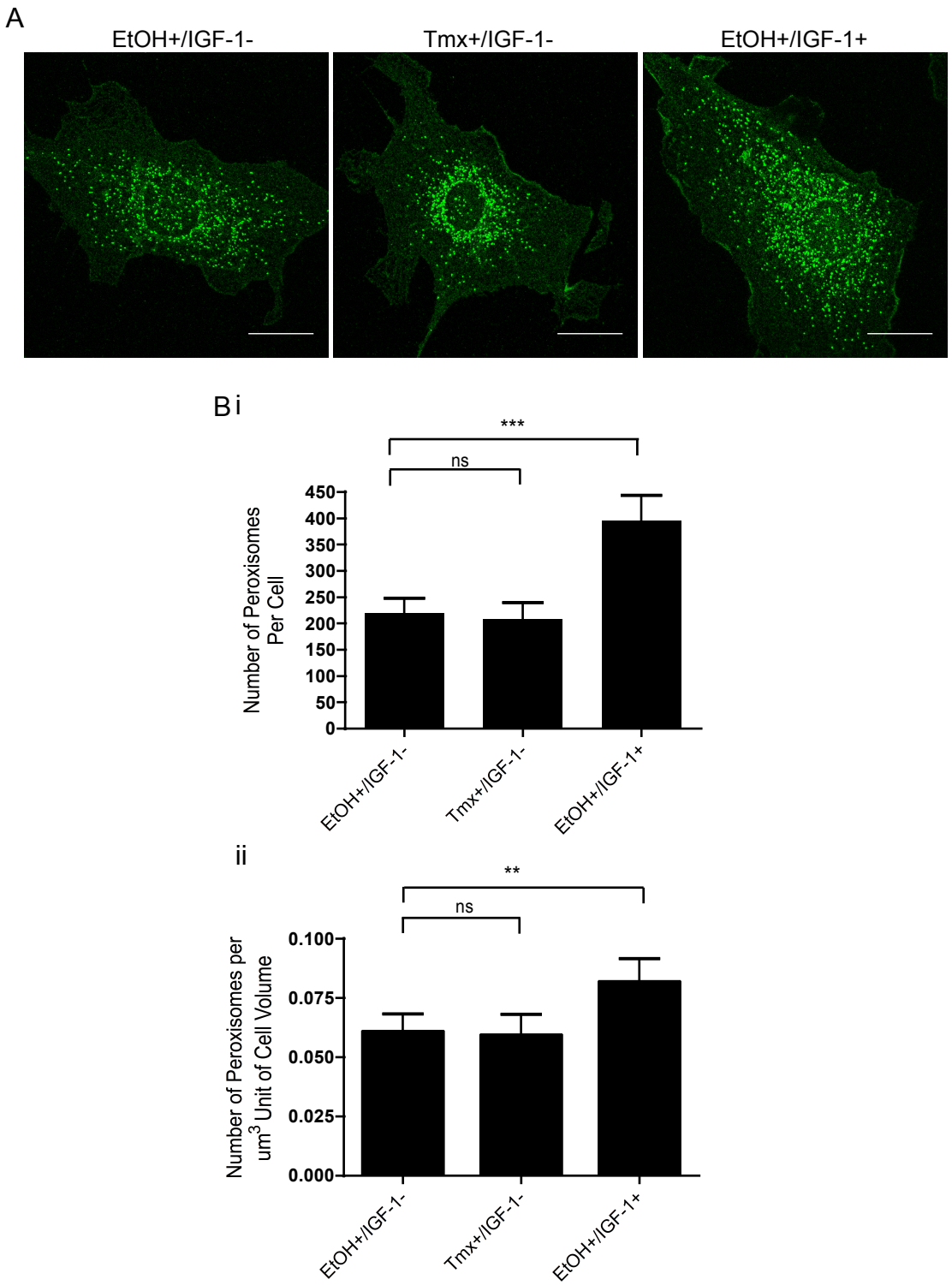

Figure 3.23 IGF-1 drives an increase in peroxisome number per cell

Aphidicolin arrested NSΔRafER cells were treated as indicated for 24hrs before anti-catalase staining to label the peroxisomes.
A) Representative maximal projection images of labelled peroxisomes. Scale bar = 25μm.
B) Mean number of peroxisomes per cell quantified from images as shown in A) in ImageJ.
C) Mean number of peroxisomes per μm^3 cell volume.
B) and C) Bar charts showing mean +SEM of 3 experiments, minimum of 25 cells quantified per condition per experiment. Repeated Measures One-Way ANOVA B) $p<0.001$ and C) $p<0.01$. Select post hoc Newman-Keuls as indicated on the graph.

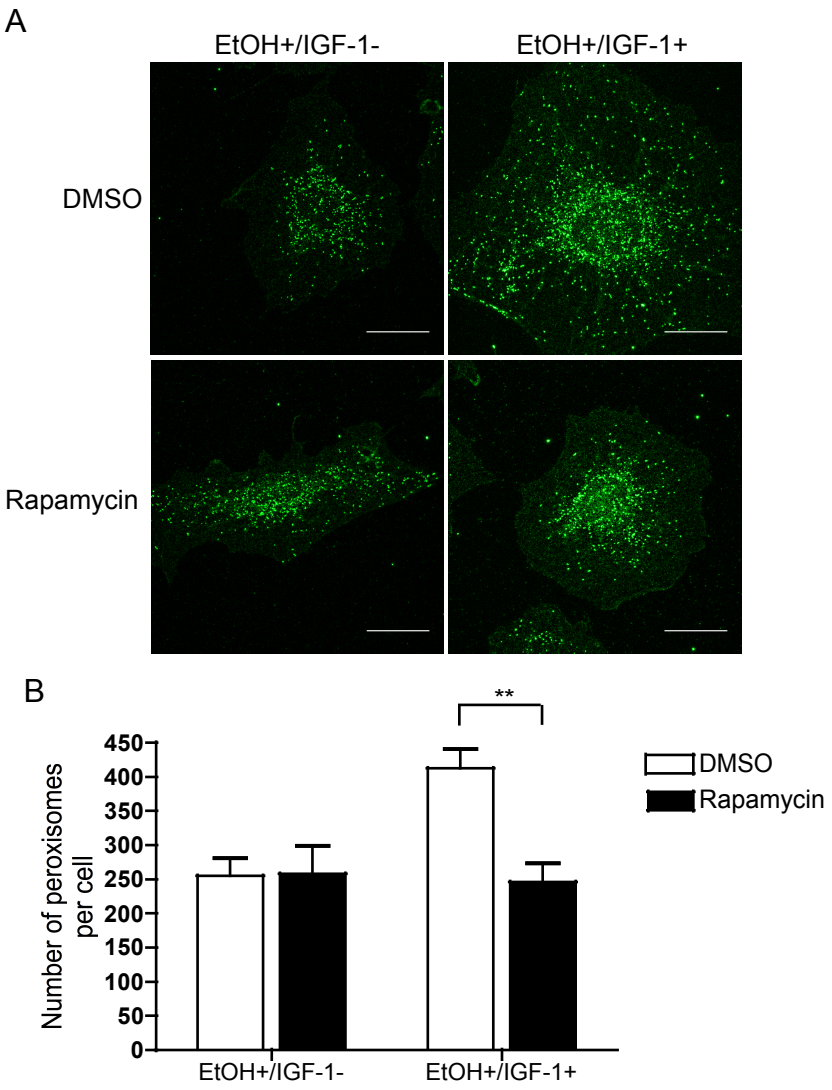

Figure 3.24 IGF-1 drives an mTORC1 dependent increase in peroxisome number per cell

Aphidicolin arrested NSΔRafER cells were treated as indicated +/- Rapamycin (to inhibit mTORC1) for 24hrs before anti-catalase staining to label the peroxisomes.
A) Representative maximal projection images of labelled peroxisomes. Scale bar = 25μm.
B) Mean number of peroxisomes per cell quantified from images as shown in A) in ImageJ. Bar chart shows mean +SEM of 3 experiments, minimum of 25 cells quantified per condition per experiment. Repeated Measures Two-Way ANOVA, interaction $p<0.01$. Post hoc Bonferroni as indicated on the graph.

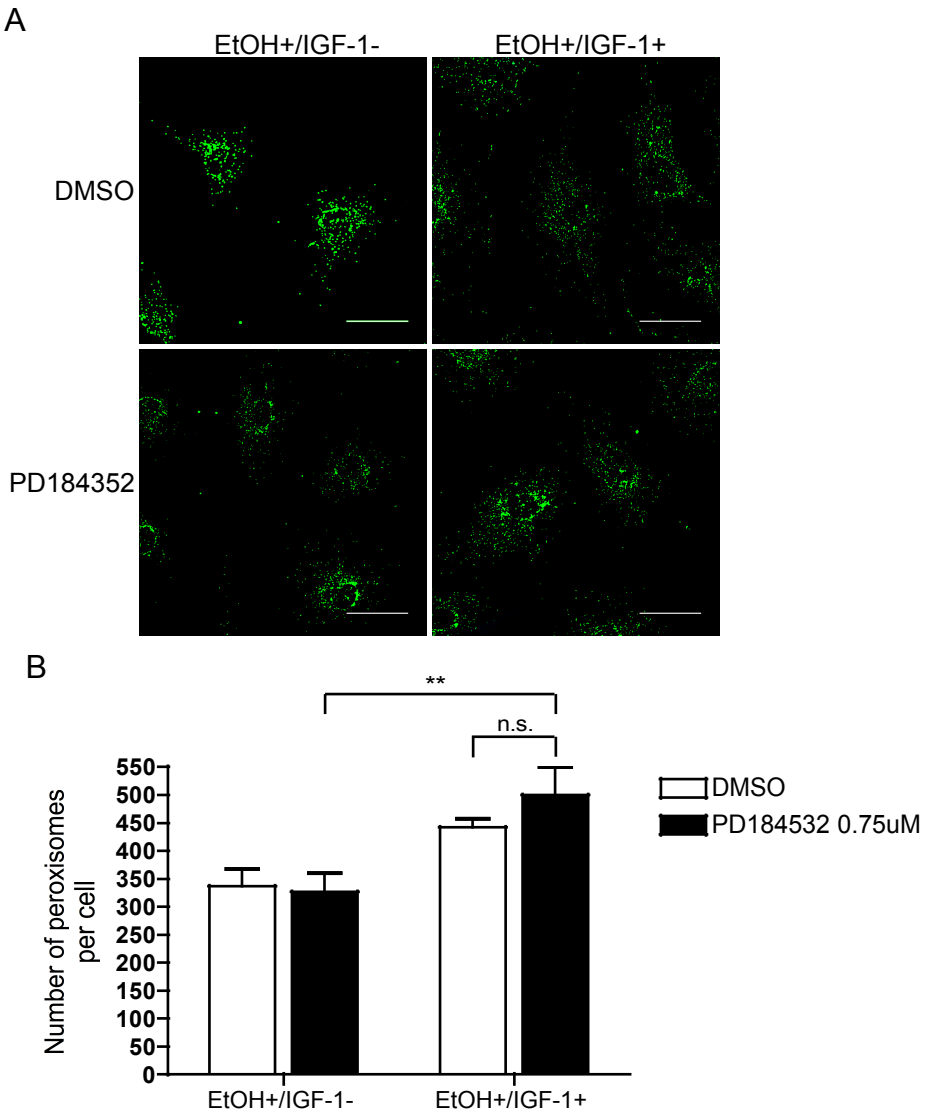

Figure 3.25 IGF-1 drives a MEK independent increase in peroxisome number per cell

Aphidicolin arrested NSΔRafER cells were treated as indicated +/- PD184352 (to inhibit MEK) for 24hrs before anti-catalase staining to label the peroxisomes.
A) Representative maximal projection images of labelled peroxisomes. Scale bar = 25μm.
B) Mean number of peroxisomes per cell quantified from images as shown in A) in ImageJ. Bar chart shows mean +SEM of 4 experiments, minimum of 25 cells quantified per condition per experiment. Repeated Measures Two-Way ANOVA Growth factors $p<0.01$, post hoc Bonferroni not shown.

In conclusion: the results presented in this Section demonstrate that IGF-1, but not Raf kinase, drives an increase in the number and total volume of lipid droplets, the number of peroxisomes and appears to increase the amount of cis-Golgi per cell, over 24hrs. These organelles all have roles in cell lipid metabolism. Given that IGF-1, but not Raf kinase, also drives an increase in cell volume, this may suggest that altered lipid metabolism has a role in IGF-1 dependent cell volume addition.

3.7 Chapter 3: Summary

The findings described in this chapter can be summarised as follows:

- The addition of cell mass and volume can be uncoupled during cell growth, demonstrating they are independently regulated processes: In the Schwann cell, IGF-1 drives coordinate addition of cell mass and volume, whereas Raf kinase activation drives an increase in cell mass in the absence of an increase in cell volume.
- IGF-1 dependent addition of cell volume is PI3K and mTORC1 dependent, but MEK independent- as previously published.
- The addition of protein mass downstream of IGF-1 or Raf kinase is PI3K, mTORC1 and MEK dependent.
- The finding that MEK is required for IGF-1 dependent addition of cell protein, but not volume demonstrates that cell volume can be added in the absence of an increase in cell protein mass during cell growth. This again highlights that mass and volume can be uncoupled during cell growth and therefore can be independently regulated.
- Organelle size and/ or number does not necessarily correlate with cell mass or volume or the size and number of other organelles, but is likely regulated in response to specific signals. Mitochondrial volume and the amount of ER appear to increase downstream of both Raf kinase and IGF-1. In contrast, only IGF-1 drives an increase in the cis-Golgi, lipid droplets and number of peroxisomes in the cell, suggesting the addition of cell volume may be associated with specific changes in cell lipid metabolism.

3.8 Chapter 3: Discussion

3.8.1 The Addition of Mass, Volume and Organelle Content can be Uncoupled During Cell Growth

The findings presented in this Chapter demonstrate that the addition of protein mass and volume are separable processes that can be independently regulated during cell growth. Given that it is often assumed that mass and volume increase co-ordinately during cell growth- and consequently that measures of mass and volume can be used interchangeably to describe growth- these results have important implications for the way we describe, study and think about cell growth. When describing cell growth we must be clear whether we are referring to cell mass (e.g. cell protein mass) or cell volume. Ideally, we would also describe how this relates to changes in cell organelle content. In addition, because they are separable and therefore can be independently regulated, to understand both the upstream signalling and the downstream effector mechanisms that control cell mass and volume, requires the addition of cell mass and volume to be studied in isolation. Given that this study has shown how mass and volume can be uncoupled downstream of IGF-1 and Raf kinase in the Schwann cell, this model system is an ideal and tractable system in which to continue such studies. Importantly, this study demonstrates that the addition of volume is, in itself, a regulated process not necessarily driven simply by the synthesis of more 'stuff' (protein). Although intuitively it might be expected that cell protein mass and volume would co-vary as proteins synthesised during cell growth will take up space, i.e. volume, the results presented in this study demonstrate that this assumption does not hold true. This raises two basic, yet important, biological questions: what drives the addition of cell volume in the absence of an increase in protein? And, reciprocally, how can the addition of protein mass *not* drive an increase in cell volume?

Considering the first question: in the experiments presented in this Chapter, when MEK is inhibited in Schwann cells, IGF-1 can still drive a comparable addition of cell volume, even though the addition of cell protein mass is blocked. Although the use of an inhibitor is undoubtedly an artificial manipulation, the result nonetheless clearly demonstrates that it is possible to add volume in the absence of an increase in protein mass and, therefore, raises

the question: what drives the increase in cell volume? Both in terms of what is added to the cell to effect the increase and also what molecular mechanisms are required to drive the increase. It is also a second clear demonstration that the addition of protein is not the principle driver of cell volume addition- because volume can still be added when the addition of protein mass is prevented. One attractive candidate as a factor that is essential for the addition of cell volume is cell lipid. To add cell volume during cell growth it seems inevitable that lipids are required to fuel membrane biogenesis, including the increase in plasma membrane. This implies that there is a increase in lipid synthesis and the amount of lipid per cell. If this process continues to occur when MEK is inhibited, in the presence of IGF-1, this might be sufficient to drive expansion of membranous organelles, the plasma membrane and, as a result, cell volume. Certainly the results of these studies indicate a role for cell lipid metabolism in IGF-1 driven growth, as the cis-Golgi, lipid droplets and peroxisomes all increase specifically downstream of IGF-1- correlating with the increase in cell volume- and all three of these organelles have roles in cell lipid metabolism. Important membrane lipids are synthesised and/ or modified in the cis-Golgi and peroxisomes; sphingomyelins are synthesised and lipids are glycosylated in the cis-Golgi and ether phospholipids (plasmalogens) are synthesised in the peroxisomes (Colley, 1997, Jeckel et al., 1990). In addition, as a site of fatty acid oxidation, the peroxisomes are also involved in fatty acid breakdown and remodelling. Finally, lipid droplets are not simply storage sites for excess lipids as was once thought, but interact dynamically with organelles including the ER and plasma membrane to regulate cell lipid metabolism (Martin and Parton, 2006, Walther and Farese, 2009). Strikingly, as for cell volume, the IGF-1 dependent increase in peroxisomes was not blocked when MEK is inhibited. However, as for cell volume, it was blocked when mTORC1 was inhibited. These findings further correlate the addition of cell volume with, potentially, cell lipid metabolism (the addition of cis-Golgi and lipid droplets was not investigated after MEK or mTORC1 inhibition). A possible role for the peroxisomes in IGF-1 dependent cell growth will be discussed in more detail later in this Discussion.

If lipogenesis is necessary for the addition of cell volume, it is important to address whether it is also sufficient to drive addition of cell volume, or whether other factors are also required. For example, activation of specific

biogenic pathways may be required to ensure synthesised lipids are assembled into functional membranes, such as the plasma membrane- in other words, that this process is specifically regulated. The role of lipogenesis in IGF-1 mediated cell growth is explored in Chapter 5 of this thesis and the regulation of plasma membrane size is investigated further in Chapter 4. It may also be that the addition of cell volume requires the addition of other molecules, such as water. Water comprises 70% of the weight of the cell and net water movement into or out of the cell can result in rapid and significant changes to cell volume, therefore it seems highly plausible that regulation of water transport could have a role in the regulation of cell volume during cell growth (Luby-Phelps, 2000). These factors will be discussed in more detail at the end of Chapter 5. Based on the points raised in this section, it is tempting to speculate that, when MEK is inhibited, IGF-1 continues to drive the addition of cell volume because IGF-1 continues to drive both the biogenesis of cell membranes (particularly the plasma membrane, which as the limiting membrane of the cell can restrict volume addition) and the uptake of water, which together drive the addition of cell volume.

If the addition of lipids is sufficient to drive the membrane biogenesis that is necessary to increase cell volume, this implies that certain membranes and organelles can increase without increasing the total amount of protein in the cell- because it was possible to increase volume in the absence of an increase in total protein mass. It is possible, however, that although the total amount of protein in the cell did not increase in IGF-1 treated cells when MEK was inhibited, existing cell protein may have been redistributed to de novo membranes and/ or organelles and this may be required for the synthesis of these structures. This may be particularly important during mitochondrial biogenesis, as evidence from studies in *S. cerevisiae* suggests that the synthesis and assembly of certain mitochondrial membrane proteins and phospholipids are coupled (Gebert et al., 2011, Gohil and Greenberg, 2009). Moreover, this coupling is essential for the addition of either to mitochondrial membranes. This means that if the addition of either the lipids or the proteins is disrupted, mitochondrial membrane biogenesis is inhibited. This study did not address whether mitochondria still increase downstream of IGF-1 when MEK is inhibited, however previous findings from our lab have shown that mitochondrial gene transcription is blocked following inhibition of MEK, which suggests that

the increase in mitochondrial volume may be blocked (Echave et al., 2009). It would be useful to characterise in greater detail, using a combination of fluorescent imaging and electron microscopy, the composition and structure of IGF-1 treated cells where MEK/ ERK signalling has been inhibited. This could include, for example, quantification of mitochondrial volume. Such an analysis would help address the cellular changes that occur and therefore may be required for the addition of cell volume. As a final and brief point to consider when thinking about the regulation of cell protein in the presence of MEK inhibition, it is important to note that although total protein mass does not increase if MEK is inhibited, the turnover of proteins, e.g signalling proteins, is not necessarily blocked and this turnover may be required for the addition of cell volume, e.g. to regulate flux through important signalling pathways.

To consider the second question: how can the addition of protein mass not drive the addition of cell volume? As shown by this study, activation of Raf kinase drives an increase in cell protein mass, and the density of specific organelles such as the mitochondria, without increasing cell volume. This means that increasing protein mass per se is insufficient to drive an increase in cell volume and demonstrates that the addition of cell volume is itself an independently regulated process. In other words, increases in cell volume are not simply a passive consequence of synthesising any macromolecule (protein), which then pushes out on the edges of the cell to increase cell volume either directly, or, in the case of soluble macromolecules such as cytosolic proteins, because water is drawn into the cell by osmosis as a result of increases in the concentration of soluble proteins in the cell (as will be discussed further below). One question raised by this finding is: where in the cell is the protein mass added such that it does not drive an increase in cell volume? Given that the amount of mitochondria and ER increase after Raf kinase activation, these organelles are likely to be the repository for a certain amount of the added protein. The mitochondria represent only 8.5% of the volume of the cell in Raf kinase activated cells, compared to 6.5% in control treated cells, explaining why this increase does not drive a significant increase in cell volume. The analyses performed in this study do not indicate what the increase in ER represents in terms of cell volume; if it is significant, then presumably other parts of the cell are reduced to compensate – perhaps, for example, cytosolic volume is reduced.

Interestingly, a microarray performed in our lab with the NSΔRafER Schwann cells used in this study demonstrated that Raf kinase induces large changes in gene expression and an increase in the amount of RNA in the cell, consistent with protein biogenesis (Unpublished observations and (Parrinello et al., 2008). Moreover, subsequent analyses of protein expression demonstrated that Raf kinase activation increases the expression of a number of secreted proteins (Napoli et al., 2012). Although secreted proteins are only present in the cell transiently- as they are synthesised on rough ER (RER), transported through the ER and Golgi systems and then transported to the plasma membrane in secretory vesicles- an increase in the synthesis of such proteins may also contribute to the increase in cell protein mass. Would this be expected to result in an increase in cell volume? Perhaps, if the volume of the ER and Golgi increased to cope with the increased secretory traffic. However, as described above, although the amount of ER does seem to increase, this does not result in an increase in cell volume. As this study found no significant increase in the amount of cis-Golgi or trans Golgi network (TGN) downstream of Raf kinase activation (although there was a trend for TGN volume to increase in Raf kinase activated cells, compared to control) this may suggest any increase in secretory traffic could be processed without an increase in the size of the Golgi. Alternatively, as considered in the results, it may be that Golgi volume does increase, but the light microscopy based assay used in this study was not sensitive enough to detect the increase, because the size of individual Golgi cisternae is below the resolution of the light microscope.

Aside from the organelles, proteins can also be added to cytoskeletal structures- to the actin cortex, the microtubules and the nuclear lamina. These were not investigated in this study. As microtubule length has been shown to regulate cell length and cortical actin regulates cell shape and size, this suggests that if Raf kinase activation does increase the amount of cytoskeletal components, the resulting 3D-structures are more dense, as they do not significantly affect cell volume (Picone et al., 2010, Salbreux et al., 2012). It may be, for example, that there is an increase in the number of microtubules in the cell to facilitate an increase in secretory traffic to the plasma membrane.

Finally, an interesting question to consider is whether Raf kinase drives an increase in the amount of soluble cytosolic proteins and/ or the size of the

cytosolic precursor amino acid pool. If so, this would be expected to increase intracellular osmolarity and therefore, in order to prevent this resulting in uptake of cell water and an increase in cell volume (assuming the increase would be detectable) Raf kinase activated cells would have to activate compensatory mechanisms to decrease intracellular osmolarity, i.e. by driving the loss of inorganic ions and organic osmolytes. An additional factor that also needs to be considered if Raf kinase drives an increase in the concentration of cytosolic proteins is that there is a hypothesis stating that cells sense 'macromolecular crowding' (changes in the behaviour of molecules at high concentrations) to regulate water uptake and, consequently, cell volume (Burg, 2000, Lang, 2007). If Raf kinase increases the concentration of soluble protein to the point where crowding would be predicted to be an issue, this suggests either the hypothesis is invalid (at least in these conditions), or mechanisms downstream of Raf kinase overcome the crowding.

3.8.2 The Biological Implications of Uncoupling the Addition of Cell Mass, Volume and Organelle Content

The findings presented in the Chapter have clearly shown that mass, volume and organelle biogenesis can be uncoupled. The mass and volume of the cell reflects the sum of the organelles and cytosol (and therefore the macromolecules and water) and hence, the differential regulation of cell mass and volume reflects the differential regulation of organelle and cytosolic content. Organelle biogenesis is metabolically expensive and is therefore tightly regulated according to need, which means that the uncoupling of cell mass and volume and, linked to this, differences in organelle content are likely to reflect differences in the needs, functions and/ or metabolic activity of a cell.

In the Schwann cell, proliferation *in vitro* is absolutely dependent on ERK signalling and *in vivo* strong and sustained ERK signalling drives Schwann cell dedifferentiation and proliferation (Echave et al., 2009, Napoli et al., 2012). In contrast, as demonstrated in this study and in other studies both *in vitro* and *in vivo*, PI3K regulates Schwann cell size (volume) (Collins et al., 2012, Cotter et al., 2010, Echave et al., 2009, Macklin, 2010, Maurel and Salzer, 2000). *In vivo*, the addition of Schwann cell volume must be able to occur in the absence of cell division. This is because a significant amount of Schwann cell growth occurs when the cells are quiescent (although they remain poised to re-enter

the cell cycle, e.g. following nerve injury, to facilitate nerve regeneration) and therefore must occur without stimulating the mitogenic pathway. In the case of myelinating Schwann cells, for example, it is only once the cells are aligned with an axon and are quiescent that myelination occurs and the cell grows to its final size. Therefore it is advantageous, and likely even necessary, to have cell volume addition and cell proliferation regulated by distinct signalling pathways- the PI3K pathway and the ERK pathway, respectively. Although the growth and proliferative pathways may not be as distinct in many other cell types (where growth and proliferation is more frequently found coupled), their separation in the Schwann cell provides the opportunity to investigate biogenesis and cellular changes associated with each process independently.

Although the Raf kinase system used in this thesis is artificial, it seems reasonable to assume that at least some of the cellular changes that occur after Raf kinase activation represent changes associated with preparation for cell proliferation. Most interesting in this regard is the increase in mitochondrial volume. This is reminiscent of the increase in mitochondria seen after stimulation with the mitogen NRG1, which also drives strong and sustained ERK signalling (Echave et al., 2009). It is interesting to speculate, as in Echave et al, that the increase in mitochondrial density is necessary to provide the ATP to fuel the energetically expensive process of proliferation. Considering the addition of Schwann cell volume: *in vivo*, like PI3K signalling, lipogenesis is required for Schwann cell myelination and for the cells to grow to their final size and *in vitro*, IGF-1 promotes lipogenesis in myelinating Schwann cell cultures (Collins et al., 2012, Liang et al., 2007, Verheijen et al., 2009). Therefore, following the discussion in the above Section 3.8.1, it is tempting to speculate that the IGF-1 driven increase in the amount of cis-Golgi, lipid droplets and peroxisomes is necessary for lipogenesis, which drives the addition of cell volume. In this regard, as stated in Section 3.8.1 and as will be discussed in further detail later in this Discussion, the peroxisomes are particularly interesting because their number correlates with the addition and inhibition of cell volume downstream of IGF-1. It also seems reasonable to hypothesise that the increase in mitochondria observed after IGF-1 treatment, as well as providing ATP to fuel cell growth, also provides biosynthetic precursors required to drive macromolecular synthesis required for volume addition, e.g. to drive lipogenesis. It does seem likely that cell proliferation will also require a certain

amount of lipogenesis, even in the absence of associated cell volume addition, in order to produce the necessary increase in plasma membrane. In this study, however, there was not evidence that Raf kinase activated de novo lipogenesis. This may be because the cells were cell-cycle arrested, circumventing the requirement for plasma membrane addition. It is also possible that the increase in plasma membrane required during cell division does not require, in the absence of cell volume addition, a significant increase in lipogenesis.

The observations regarding cell organelle content described above suggest that at least some of the changes in organelle content observed downstream of Raf kinase activation and IGF-1 treatment in the Schwann cell could be consistent with the known function of each of these pathways *in vivo*. Examples of biogenic stimuli driving organelle biogenesis to control cell function have been directly studied in other cell types; ER expansion in the B cell is necessary for the production of immunoglobulins required to fight infection in an immune response, for example, and melanosome biogenesis in melanocytes protects cells against the mutagenic effects of ultraviolet radiation (UVR) (Federovitch et al., 2005, Rush et al., 1991, Schiaffino, 2010). Moreover, beyond the function of any one cell type, the ability to differentially regulate cell mass, volume and organelle content downstream of distinct signalling pathways must also help provide the flexibility to generate the diversity in cell size, morphology and organelle content across different cell types *in vivo* that is necessary for cells to carry out cell type specific functions efficiently. Differential cell growth can, for example, help drive the expansion of a large lipid droplet in adipocytes so that they can function effectively as an organism's energy storage depot and can help drive specific expansion of the Golgi network in secretory cells so that they can efficiently modify the sufficient amounts of proteins and lipids for secretion (Koga and Ushiki, 2006, Zweytick et al., 2000).

3.8.3 Regulating Cell Mass, Volume and Organelle Content

Cells undergo continuous organelle and macromolecular turnover, as described in the Introduction, and the mass, volume and organelle content (size) of the cell is determined by the balance between the rate at which each of these components is accumulated/ synthesised and the rate at which each is lost/ degraded. This means that to understand how Raf kinase and IGF-1 drive an increase in cell mass, volume and/ or organelle content, it will be necessary

to understand how they regulate these opposing processes to drive net accumulation. This was not addressed in the current study. Given that both stimuli drive an increase in protein mass, the obvious starting point for such investigations would be to quantify the rates of protein synthesis and degradation downstream of Raf kinase and IGF-1. This could be done relatively easily using radiolabelled amino acids. In addition, because nucleolar size and cell ribosome number are closely coupled to the rate of protein synthesis (because ribosome biogenesis is metabolically costly), these could also be quantified as indicators of protein synthesis rates (Grewal et al., 2007, Grewal et al., 2005, Rudra and Warner, 2004, Warner, 1999, Wullschleger et al., 2006).

Interestingly, there is evidence that protein synthesis and degradation is coupled downstream of growth factor signalling in sympathetic neurons (Franklin and Johnson, 1998, Kirkland and Franklin, 2007). In the presence of the growth factor NGF, neurite outgrowth was resistant to the inhibition of protein synthesis (protein synthesis was inhibited to varying extents using different concentrations of the protein synthesis inhibitor cycloheximide), because there was a corresponding inverse change in the rate of protein degradation (Kirkland and Franklin, 2007). The authors propose this coupling helps ensure robust growth in the face of inevitable stochastic fluctuations in the rate of protein synthesis *in vivo*. It would be very interesting to use the Schwann cell system to determine if coupling is a general feature of cell growth control and to use the experimentally tractable Schwann cell system to address the molecular mechanism by which this occurs; for example, to determine whether there is direct crosstalk between the synthetic (ribosomes) and degradative (proteasomes and/ or lysosomes) machinery, or whether there is coordinated control of both by upstream growth factor activated signalling pathways. It would also be very interesting to determine whether coupling is limited to protein biogenesis, or if the synthesis and degradation of lipids, and even organelles, is also coupled. If so, coupling may be a universal mechanism regulating all aspects of cell growth.

Considering the increase in protein mass induced by IGF-1 and Raf kinase activation a little further: although both stimuli increase cell protein mass, they may increase distinct subsets of proteins. In other words, the proteome of the cell may be very different following each stimulus. Such differences may be

significant to the distinct functions of the cell following IGF-1 treatment or Raf kinase activation. High throughput proteomic comparisons of the two conditions, as well as analyses of the proteins induced following each stimulus could be performed by SILAC combined with mass spectrometry analyses. These analyses may shed light on the mechanisms by which IGF-1 and Raf kinase increase cell protein mass, as well as any differences in these mechanisms between the two conditions and, therefore, could be important for understanding cell growth control downstream of these stimuli.

Beyond considering macromolecular synthesis and degradation, it is important to understand how biogenic stimuli regulate organelle biogenesis, which is a largely poorly understood part of cell growth control. The finding that Raf kinase and IGF-1 regulate the size and/ or number of several organelles provides an ideal opportunity to study how growth factor activated signalling pathways activate the gene expression and biosynthetic programmes required to synthesise organelles. A study from our lab has already begun to address how growth factor activated signalling regulates Schwann cell mitochondrial biogenesis (Echave et al., 2009). In this study, Echave et al 2009 demonstrated that the transcription factor oestrogen-related receptor α (ERRα) is induced co-operatively by the extracellular factors IGF-1 and NRG1 and that this is critical for the induction of mitochondrial gene expression downstream of these factors. Mitochondria are a good model organelle for studying growth factor activated organelle biogenesis because a number of transcription factors and co-activators that regulate mitochondrial biogenesis have been identified, including ERRα and the transcriptional co-activator peroxisome proliferator-activated receptor γ co-activator α (PGC1α), which is considered to be a master regulator of mitochondrial biogenesis (Hock and Kralli, 2009, Ventura-Clapier et al., 2008). This, together with the relative ease with which mitochondrial volume and mitochondrial DNA replication can be quantified, means it is straightforward to investigate the effects of specific biogenic stimuli on mitochondrial biogenesis. It would be very interesting to determine whether IGF-1 and Raf kinase increase mitochondrial volume via common transcriptional regulators, in addition to ERRα, as well as whether these signals converge only at these transcriptional regulators, or further upstream. As well as improving our understanding of mitochondrial biogenesis downstream of these stimuli, this will also provide information on how conserved the mechanisms driving

mitochondrial biogenesis are between distinct growth factor activated signalling pathways.

3.8.4 Organelles Driving the Addition of Cell Mass and Volume

As has been touched upon in Sections 3.8.1 and 3.8.2, the relationship between the organelles and the mass and volume of the cell is complex, because the organelles do not just represent the mass and volume of the cell at any one point in time; many organelles are also the machinery required to drive future changes in cell mass and volume. Considering the findings of this study, the relationship between the mitochondria, ER and cell protein mass may represent a particularly noteworthy example of this. Raf kinase and IGF-1 both drive an increase in protein mass, mitochondrial volume and, seemingly, the amount of ER. The ER and mitochondria, as already discussed, are likely to represent part of the increase in protein mass. However, their functions are also likely to play an important role in driving the increase in cell protein, which will include contributing to the synthesis of more mitochondria and ER. This is because the mitochondria provide the ATP and biosynthetic precursors for macromolecular synthesis and the rough ER (RER) is where integral membrane proteins, secreted and ER and Golgi proteins are synthesised. Moreover, the RER expands in response to increased demand for protein (Federovitch et al., 2005, Kirk et al., 2010, Schuck et al., 2009). However, it must be noted that this study did not distinguish between smooth ER (SER) and RER and so it is not actually possible to conclude whether it is the RER, the SER, or both that seems to increase downstream of Raf kinase activation. The two types of ER can be distinguished by electron microscopy and this could be exploited to perform such quantifications. It would be interesting to perform these analyses not just in terms of considering the addition of protein mass, but also considering the addition of cell volume downstream of IGF-1. This is because the SER is a primary site of lipid synthesis and so it would be very interesting to determine if the amount of SER increases specifically downstream of IGF-1, which would further link cell volume addition and cell lipid metabolism.

As has been raised earlier in this Discussion, the findings of this study suggest there may be a specific role for peroxisomes in the addition of cell volume because, like cell volume, the number of peroxisomes increases downstream of IGF-1, but not Raf kinase activation. Furthermore, like cell

volume, this increase is not blocked by inhibition of MEK, but is blocked by inhibition of mTORC1. Although the role of peroxisomes in cell volume addition has not been investigated, the pathologies of several inherited peroxisome biogenesis disorders- namely those associated with impaired ether phospholipid synthesis- include hypomyelination and stunted growth, suggesting peroxisomes may function in cell growth, potentially including cell volume addition (Chrast et al., 2011, Wanders et al., 2010). The steps in peroxisome biogenesis are increasingly well understood- 34 peroxin (PEX) genes important in peroxisome biogenesis have been identified and characterised and this could be exploited to address whether peroxisomes have a functional role in cell volume regulation- particularly because knockout mice and cell lines exist for a number of these, which would facilitate loss-of-function studies (Lazarow, 2003, Liu et al., 2012). If peroxisomes have a role in cell volume regulation during cell growth, this finding would be important not only because it would be the first time this organelle has been directly associated with the regulation of cell growth, but also because the peroxisomes may then provide a novel therapeutic target for diseases of cell overgrowth, e.g. cancers.

3.8.5 Signalling Pathways Driving Cell Growth

The findings of this study suggest that PI3K and mTORC1 are necessary for the addition of Schwann cell volume and protein mass. This is consistent with findings *in vivo*, which show that loss of signalling through this pathway leads to hypomyelination and therefore reduced cell size in myelinating Schwann cells (Cotter et al., 2010, Macklin, 2010, Maurel and Salzer, 2000). In fact, the PI3K/ Akt/ mTORC1 pathway appears to be ubiquitously important in cell growth control; inhibition of this pathway prevents cell growth, and hyperactivation of the pathway can drive cell growth, across multiple diverse systems *in vitro* and *in vivo* (Chan et al., 2011, Collins et al., 2012, Echave et al., 2009, Flores et al., 2008, Lai et al., 2004, Leevers et al., 1996, Maurel and Salzer, 2000, Peng et al., 2003, Porstmann et al., 2005, Porstmann et al., 2008). However, many of the studies in which activating PI3K/ Akt/ mTORC1 signalling was shown to drive hypertrophy were performed *in vivo*, or in the presence of serum *in vitro* (Abe et al., 2010, Flores et al., 2008, Lai et al., 2004, Meikle et al., 2008, Peng et al., 2003, Porstmann et al., 2008, Zhou et al., 2009). In both cases, this means extracellular factors were present that might

have cooperated with the hyperactivated signal to drive cell growth- in other words, the PI3K/ Akt/ mTORC1 pathway may not actually be sufficient to drive cell growth. The primary Schwann cell system used in this study can be exploited to address this issue, as- using expression constructs for different pathway components- the pathway can be activated in conditions free from potentially confounding extracellular growth factors. This approach has already been used to show that activating Akt (by overexpressing a tamoxifen inducible Akt construct) is sufficient to drive addition of Schwann cell volume, but it is not known if it can also drive addition of cell mass (Echave et al., 2009). Moreover, it is not known whether the addition of volume and/ or mass can be further narrowed down to mTORC1 downstream of Akt. It may be that, as has been found in mouse liver, Akt drives mTORC1-independent effects that are required for mTORC1-dependent biogenesis to manifest (Wan et al., 2011, Yecies et al., 2011). Addressing these questions are important to determine the intrinsic roles of activated PI3K, Akt and mTORC1 in cell growth.

After considering the specific functions of these upstream growth factor activated signalling molecules, the next question is: what signalling pathways are activated downstream of PI3K/ Akt, mTORC1, and also ERK, to drive biogenesis? Given that both IGF-1 and Raf kinase activation increase Schwann cell protein mass, it would be very interesting to determine whether there is a role for c-Myc. Myc is known to drive protein biogenesis, associated with an increase in rRNA levels, ribosome and nucleolar density and protein synthesis, and both ERK and Akt have been shown to stabilise the inherently unstable c-Myc protein (Chan et al., 2011, Grewal et al., 2005, Iritani and Eisenman, 1999, Johnston et al., 1999, Kim et al., 2000, Pierce et al., 2004, Saucedo and Edgar, 2002, Schreiber-Agus et al., 1997, Sears, 2004, Schuhmacher et al., 1999, Wu and Johnston, 2010). ERK can phosphorylate and stabilise c-Myc directly, whereas Akt phosphorylates and inhibits the kinase GSK3β, which phosphorylates c-Myc and, as a result, targets it for ubiquitination and degradation (Sears et al., 2000, Sears, 2004). Consistent with a potential role for c-Myc in the Schwann cell, levels of the c-Myc protein increase downstream of hyperactive Ras, which activates both PI3K/ Akt and ERK signalling (Collins et al., 2012). Interestingly, dMyc drives an increase in ribosomal density and nucleolar size in the *Drosophila* wing imaginal disc (Betschinger et al., 2006, Grewal et al., 2005). Given that ribosome number is meant to correlate tightly

with rates of protein synthesis, this may suggest protein density increases downstream of dMyc in these cells- reminiscent of effect of activating Raf kinase in this system. Therefore it is particularly interesting to speculate whether there is a specific role for c-Myc downstream of Raf kinase activation in the Schwann cell.

Finally, this study did not investigate whether IGF-1 and sustained Raf kinase activation can synergise to drive biogenesis. Preliminary experiments suggest the two do not synergise on cell volume (data not shown). This is consistent with the finding that NRG1, which drives strong and sustained ERK signalling and does not drive addition of Schwann cell volume, does not enhance IGF-1 driven Schwann cell volume addition (Conlon et al., 2001). However, the two signals might co-operate to drive the addition of protein mass, i.e. the biogenic effect they both promote. This would be reminiscent of the finding that IGF-1 and NRG1 synergise to drive mitochondrial biogenesis in the Schwann cell, as well as the finding that IGF-1 and loss of the tumour suppressor protein Rb synergise to drive enhanced addition of cell mass and volume (Collins et al., 2012, Echave et al., 2009). Such synergistic and additive effects can help provide the flexibility to produce diverse cell growth *in vivo*, including differential organelle biogenesis, cell mass and volume, in response to activation of different combinations of signalling pathways.

3.8.6 Conclusion

The findings of this study demonstrate that both cell mass and volume can be separately and independently regulated. Ultimately, this means it is possible to independently regulate the addition of different organelles and cytosol, which allows cells to adapt to changes in the extracellular environment and to carry out different cellular functions. It is tempting to speculate, for example, that the increase in mitochondrial volume observed downstream of Raf kinase activation, increases the cells capacity to produce ATP and therefore prepares the cells for the energetically expensive process of cell proliferation, which is also induced by ERK signalling. From a physical perspective, it is perhaps surprising that both protein mass and volume can be added in the absence of the other. Whilst the findings presented in this Chapter have not provided definitive answers to how this is achieved, they have provided a number of relevant points of discussion- including the potential role

for lipids in the addition of cell volume, and where in the cell protein might be added such that it does not increase cell volume. A complete understanding of cell growth control will require understanding the mechanisms by which biogenic stimuli regulate both macromolecular synthesis and organelle biogenesis to drive cell growth. Given that this study has identified that Raf kinase activation and IGF-1 regulate both processes, these questions could be addressed in this tractable and powerful primary Schwann cell system.

Chapter 4: Results

Plasma Membrane Growth and the Dynamics of Plasma Membrane Turnover

It is inevitable that sustained cell volume addition will require expansion of the plasma membrane. The aim of the second part of this thesis was to study the mechanisms that regulate plasma membrane size and expansion during cell growth. The experimental conditions used in these studies differed slightly from those used in the preceding chapter. Namely, serum was used as a growth factor instead of IGF-1. Serum is more potent, promoting greater and more sustained growth; aphidicolin-arrested Schwann cells treated with serum (3% FCS) for 24hrs have ~2-fold greater increase in cell volume and protein mass than the equivalent cells treated with IGF-1 (Collins et al., 2012, Conlon et al., 2001). Plasma membrane growth and dynamics in cells growing in the presence of serum were compared to cells that are growth factor deprived and, as a result, do not add mass or volume (Collins et al., 2012, Conlon and Raff, 1999, Echave et al., 2007, Edinger and Thompson, 2002, Franklin and Johnson, 1998, Kirkland and Franklin, 2007, Lum et al., 2005a, Vander Heiden et al., 2001). Serum-treated versus growth factor-starved conditions represent the two extremes of cell growth and biogenesis. This meant they were more likely to provide a tractable system in which plasma membrane dynamics could be investigated.

The basic experimental system is as described in Part 1. That is, cells were cell cycle arrested in the presence of serum (3% FCS) for 24hrs using the DNA polymerase α inhibitor aphidicolin. Then cells were transferred to defined conditions, in the absence of exogenous mitogens, growth factors and survival factors (SATO Medium), plus aphidicolin for a further 24 hours. At this point cells were treated with serum or maintained in SATO, still in the presence of aphidicolin, and assays conducted as indicated in the text. Using aphidicolin allowed the biogenic effects of serum to be investigated independently of effects on the cell cycle. As the effect of Raf kinase activation was not a focus of this research, these experiments used normal Schwann cells, i.e. lacking the Tmx-inducible Raf kinase construct.

4.1 Serum Drives Cell Growth: Cells in the Presence of Serum Add Mass, Volume and Plasma Membrane

Serum is rich in extracellular factors, including growth factors. It also contains abundant nutrients, for example lipoproteins, that are the substrates for bioenergetics and biogenesis in the cell. The growth and biogenic capabilities of serum can be demonstrated by quantifying cell volume and protein mass over time after aphidicolin-arrested cells in defined conditions (SATO) are treated with medium containing 3% foetal calf serum (3% FCS). As shown in Figure 4.1 & 4.2, serum was able to drive an ~1.7-fold increase in cell volume over 24 hours as measured by Coulter Counter analysis. If the cell culture medium was not changed this increase plateaued between 24 and 36 hours post-serum addition (Figure 4.1 A dotted line). Presumably this is because extracellular growth factors and nutrients in the serum were utilised by the cell and, as a result, were depleted from the extracellular medium. If the cell culture medium was replaced with fresh 3% FCS medium at 24 hours, cell volume addition continued (Figure 4.2 B). Previous findings from our lab and others have shown cells will not grow in the absence of extracellular growth factors and/or activation of biogenic pathways by genetic manipulation. Consistent with this, Schwann cells that remained in defined, growth factor free conditions did not add cell volume (Figure 4.1 & 4.2, SATO) (Collins et al., 2012, Conlon and Raff, 1999, Echave et al., 2007, Edinger and Thompson, 2002, Franklin and Johnson, 1998, Kirkland and Franklin, 2007, Lum et al., 2005a, Vander Heiden et al., 2001).

In addition to driving an increase in cell volume, serum was able to drive an ~1.5-fold increase in protein mass over 24 hours (Figure 4.3, '3% FCS') (Conlon and Raff, 2003). In contrast, cells deprived of growth factors did not add protein mass (Figure 4.3, 'SATO'). The amount of protein per cell was quantified using two approaches; first using the standard BCA assay (Figure 4.3 A) and second by S. Ester labelling (Figure 4.3 B) (Both methods as described in Results 3.1 and Materials & Methods 2.2).

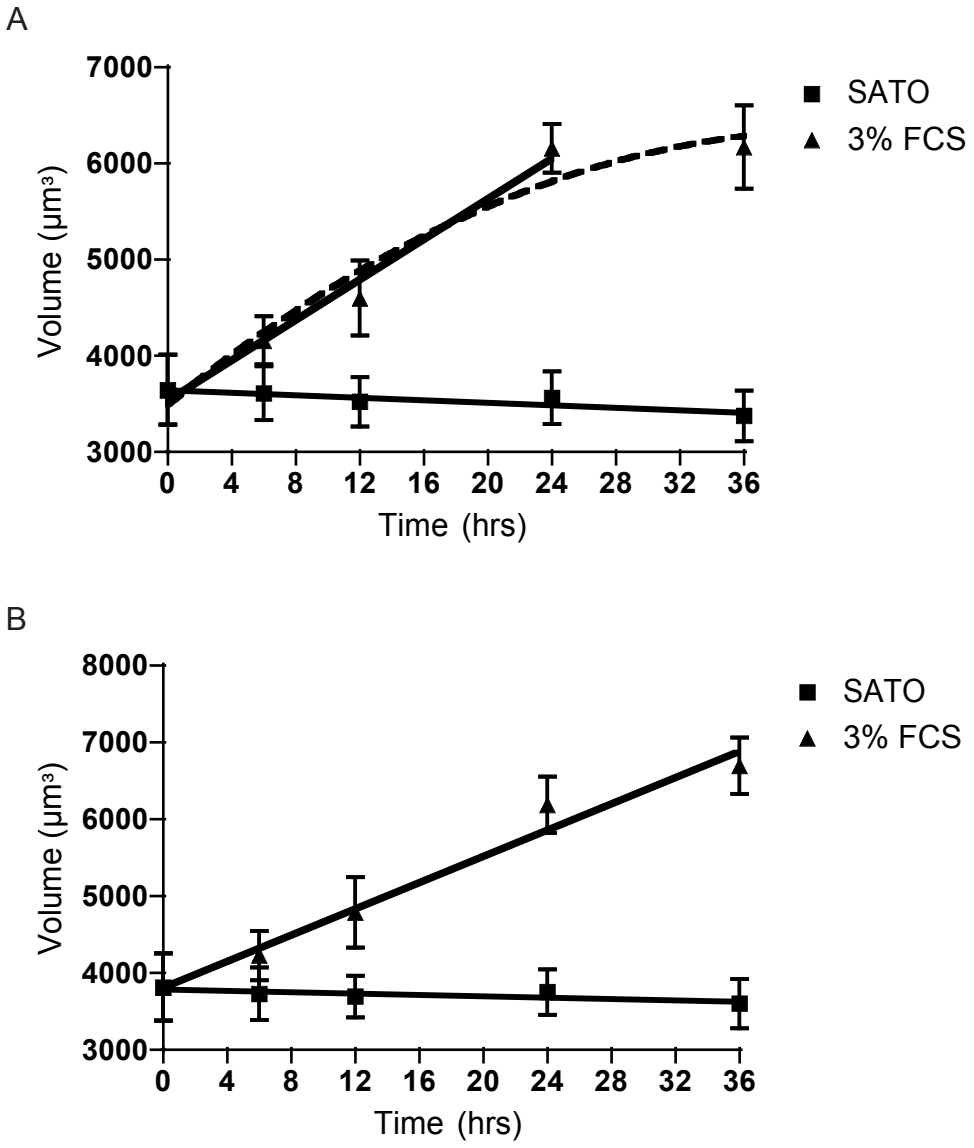

Figure 4.1 Serum drives the linear addition of cell volume

Aphidicolin arrested NS cells were treated as indicated before cell volume was quantified using a Coulter Counter. Graphs show mean +SEM.
A) Mean cell volume over time (µm³), no media change at 24hrs.
B) Mean cell volume over time (µm³), media change at 24hrs.
Graphs show mean +SEM of A) 7 and B) 4, performed in duplicate per timepoint per condition. Linear regression analysis A) 3% FCS $p<0.05$, SATO $p>0.05$ and B) 3% FCS $p<0.05$, SATO $p<0.05$.

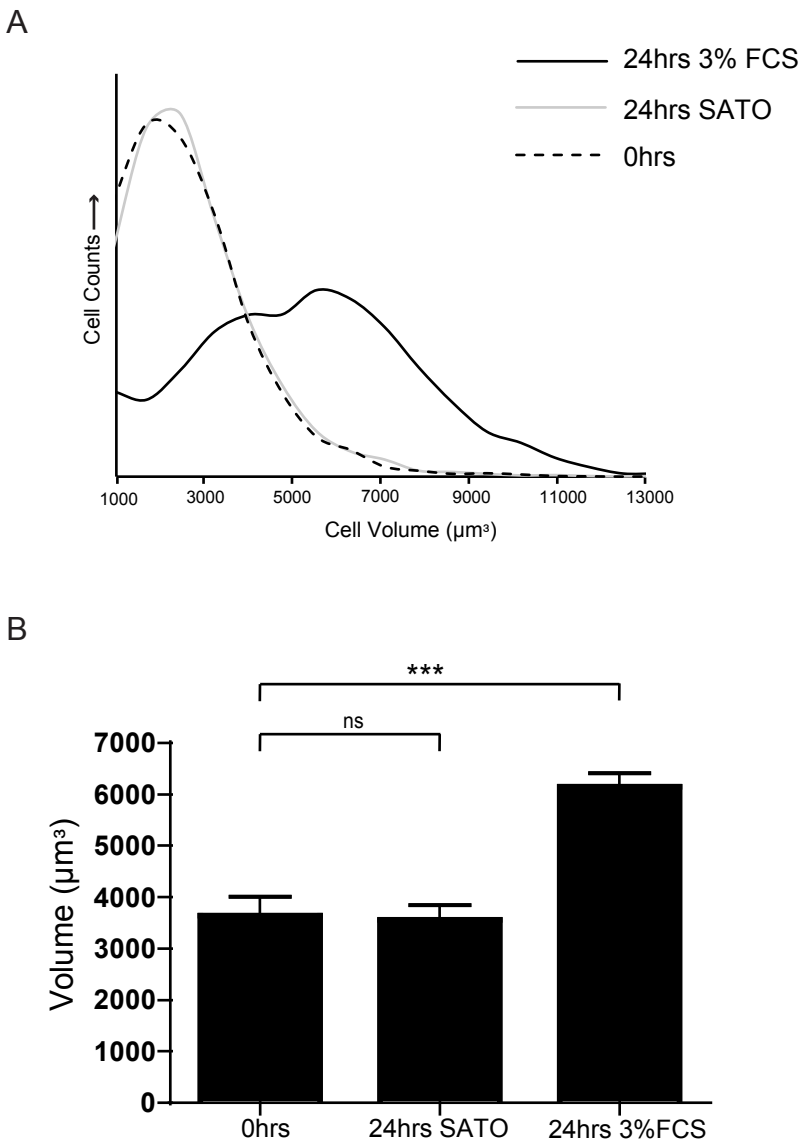

Figure 4.2 Serum drives addition of cell volume

Aphidicolin arrested NS cells were treated as indicated before cell volume was quantified using a Coulter Counter.
A) Representative frequency distribution of cell volumes in the measured populations (µm³).
B) Mean cell volume (µm³). Bar chart showing mean +SEM of 7 experiments, performed in duplicate, and t-test with Bonferroni correction for multiple hypothesis testing.

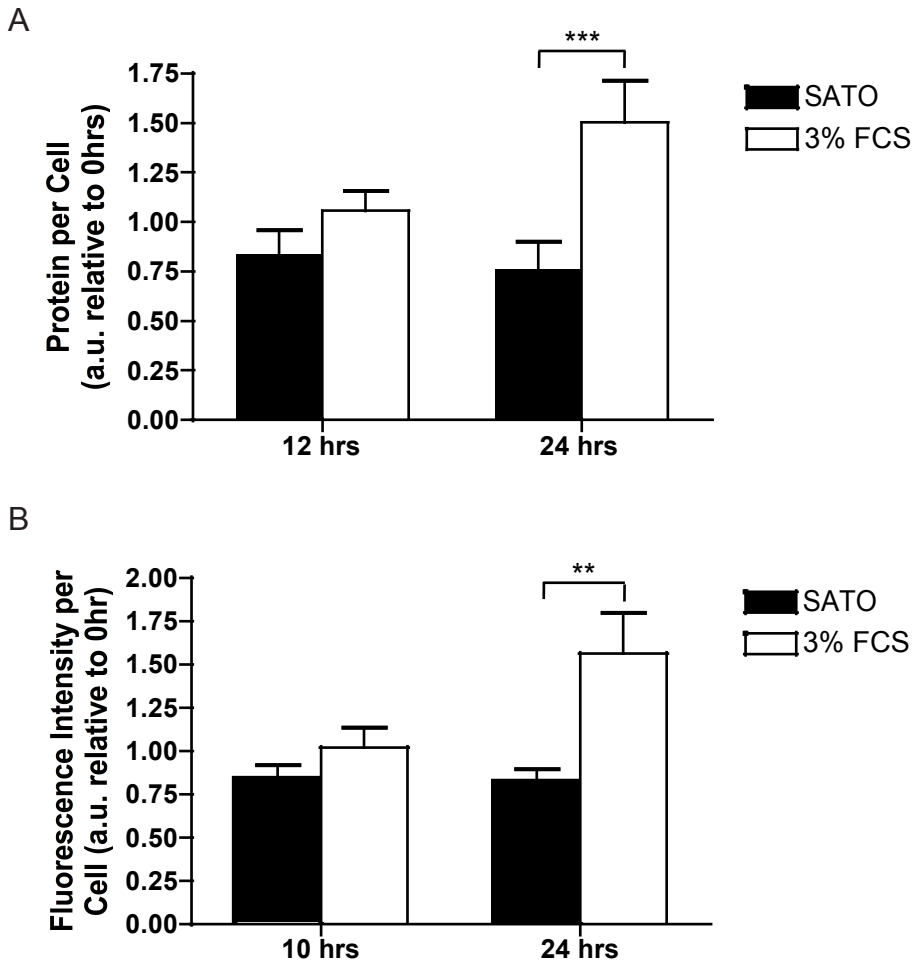

Figure 4.3 Serum drives addition of cell protein mass

Aphidicolin arrested NS cells were treated as indicated before mean amount of protein per cell was quantified:
A) By the BCA assay (a.u.). Bar chart shows mean +SEM of 7 experiments, performed in duplicate per timepoint per condition.
B) As fluorescence intensity per cell after AlexaFlour647-succinimidyl ester labelling of fixed cells (a.u.). Bar chart shows mean +SEM of 4 experiments, minimum of 50 cells quantified per condition per timepoint per experiment.
Repeated Measures Two-Way ANOVA A) SATO vs 3%FCS $p<0.0001$, Interaction $p<0.01$ and B) SATO vs 3%FCS $p<0.01$, Interaction $p<0.05$, post hoc Bonferroni as indicated on the graphs.

To determine the effect of serum and growth factor starvation on plasma membrane size, two different approaches were used to quantify plasma membrane size as cells were growing in the presence of serum or shrinking due to growth factor starvation. In the first approach an amphipathic fixable fluorescent dye, Cell Mask Orange, was used to label the plasma membrane of live cell populations. The cells were then fixed and imaged by confocal fluorescence microscopy; images were taken at 252nm intervals through the depth of the cell. An outline of the cell surface was generated *in silico* from the image stacks and cell surface area was estimated from this outline (Materials & Methods 2.5 & 2.6) (Figure 4.4). The image of the cell surface created by this method is a simplification of the real cell surface as sub-light resolution membrane architecture and folds of the plasma membrane cannot be detected. This means such folds will not be quantified. This limitation is more acute in the Z-plane where the resolution of the light microscope is approximately twice the distance as it is in the XY-plane. As the morphology of cells in serum and SATO are very different, there may be a difference in the size of the experimental error associated with the cell surface area measurements between these conditions. To control for this, cell surface area was quantified at 2 hours, as well as 24 hours, +/- serum treatment. After 2 hours cells in serum have already begun to take on a different morphology to those in SATO; however if the cells are changing surface area over the 24 hour assay one would predict these differences would be greater at 24 hours than 2 hours.

There was no detectable difference in the cell surface area of the growing (3% FCS) and starved (SATO) cells 2 hours +/- serum addition and no difference in cell surface area compared to 0 hours (Figure 4.4 B). This suggested that the difference in cell morphology between serum treated and starved cells does not cause a detectable, artefactual difference in cell surface areas quantified by this method; at least whilst the cells are similar sizes. Across 24 hours, the surface area of cells growing (adding cell volume and protein mass) in the presence of serum increased ~1.5-fold, indicative of an increase in plasma membrane size (Figure 4.4 B). In contrast, the cells that remained in the absence of extracellular growth factors maintained a constant cell surface area (Figure 4.4 B), consistent with the inability of these cells to grow (add cell volume and protein mass).

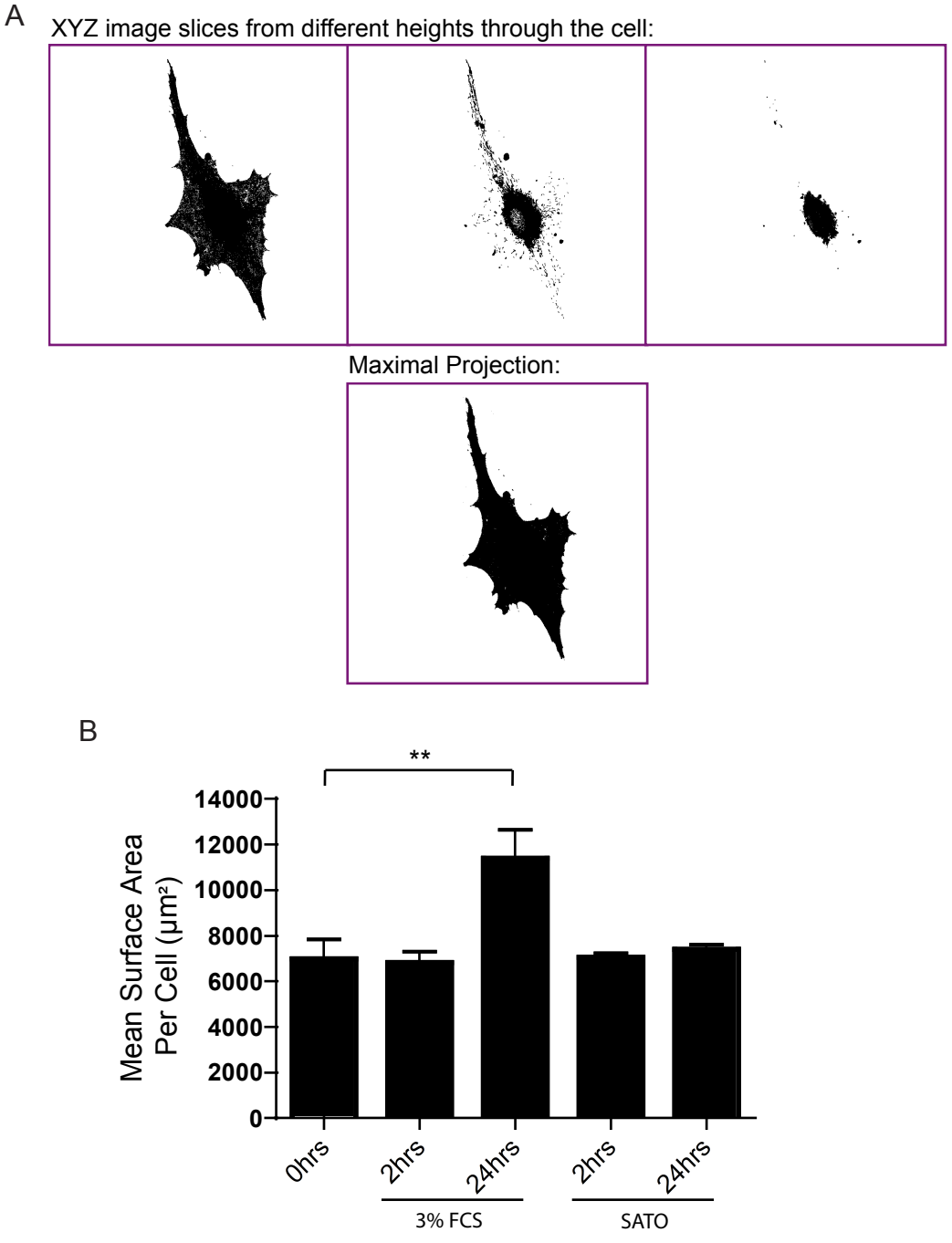

Figure 4.4 Serum drives addition of plasma membrane

Aphidicolin arrested NS cells were treated as indicated before the plasma membrane dye CellMask Orange was used to label the cell surface of fixed cells. Cell surface area was quantified in ImageJ from image stacks of labelled cells taken by fluorescence confocal microscopy.
A) Representative images of CellMask Orange labelled cells used for quantification of:
B) Mean cell surface area (µm²). Graphs shows mean +SEM of 3 experiments, minimum of 15 cells quantified per timepoint per condition per experiment. Repeated Measures One-Way ANOVA $p<0.01$, post hoc Tukey's as indicated on the graph.

It is possible that the apparent change in surface area of the growing cells could be the result of the unfolding of plasma membrane ruffles rather than an increase in the actual amount of membrane. To address this possibility a second and more direct method was used to quantify plasma membrane size. The bulk of the plasma membrane, like all biological membranes, is composed of lipid. The fluorescent lipophilic probe FM1-43 inserts non-specifically into lipid membranes (i.e. insertion is unaffected by which lipid species make up the membrane) and once inserted into one leaflet of a lipid bilayer (e.g. the outer leaflet of the plasma membrane) it does not flip-flop into the other leaflet (Betz et al., 1996, Gaffield and Betz, 2006). Therefore, the size of the plasma membrane can be inferred as the total fluorescence intensity per cell after a brief labelling of the cells with FM1-43. It is the amphiphilic nature of the molecule that prevents FM1-43 flipping between the leaflets of the bilayer; it has two aliphatic hydrophobic tails that insert into the inner hydrophobic region of the membrane and a hydrophilic dicationic head that anchors in the membrane surface (Betz et al., 1996, Gaffield and Betz, 2006). Cell fluorescence intensity was quantified from spinning disc confocal images of live aphidicolin-arrested Schwann cell populations after briefly labelling the cells 10 and 24hrs +/- serum (3% FCS) treatment in FM1-43 containing medium (Materials & Methods 2.6 & 2.7).

As can be seen in Figure 4.5, consistent with the Cell Mask data, serum caused an increase in fluorescence intensity per cell over 24 hours, demonstrating that the size of the plasma membrane increased over this time. In contrast, and again consistent with the Cell Mask data, cells starved of serum appeared to maintain a constant plasma membrane size over the same time period; because the fluorescence intensity per cell remained unchanged. The FM1-43 results indicated plasma membrane size increased ~2.25-fold over 24 hours in the presence of serum. This is greater than the increase quantified using the Cell mask approach (~1.5-fold). As already detailed, the Cell Mask assay simplifies the cell surface morphology and cannot account for sub-light microscopy resolution membrane structures or plasma membrane folds, which means the Cell mask quantification likely underestimates plasma membrane size per unit of cell surface. In contrast, FM1-43 will label both these structures and this may explain the larger increase in size quantified using this approach.

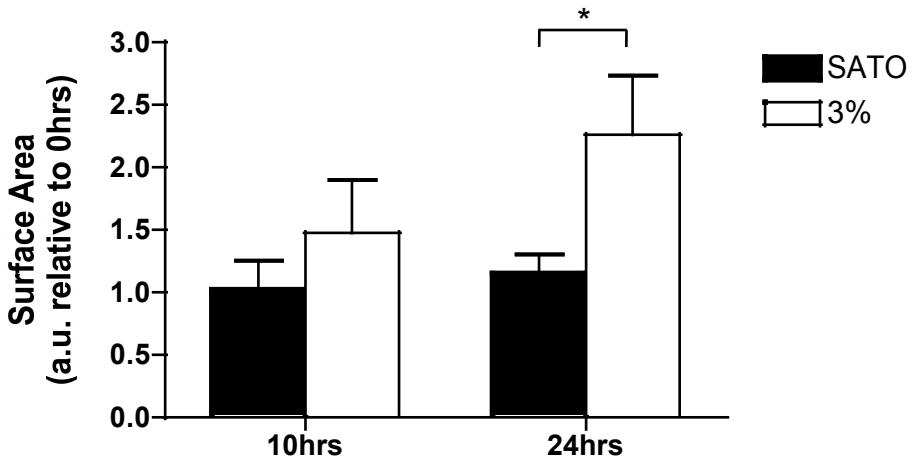

Figure 4.5 Serum drives addition of plasma membrane

Aphidicolin arrested NS cells were treated as indicated before the plasma membrane of live cells was briefly labelled using the fluorescent lipophilic dye FM1-43 and imaged using spinning disc fluorescence confocal microscopy. Total cell fluorescence intensity was taken to represent plasma membrane size, shown as plasma membrane size over time (a.u.). Graphs shows mean +SEM of 5 experiments. Minimum of 10 cells quantified per timepoint per condition per experiment. Repeated Measures Two-Way ANOVA (10 vs 24 hrs), interaction $p<0.05$, post hoc Bonferroni as indicated on the graph.

Taken together the results described in this Section confirm that serum is a powerful Schwann cell growth factor that drives a significant increase in cell volume, protein mass and plasma membrane size over time. In the absence of serum and any growth factor stimulus Schwann cells do not add volume, protein mass or plasma membrane.

4.2 Starved Cells Upregulate the Catabolic Process of Autophagy

The results above show that Schwann cells are unable to add protein mass, volume or plasma membrane in the absence of serum or growth factors, suggesting that anabolic processes may be suppressed in these conditions. In fact, studies have shown that growth factor withdrawal usually has an even more dramatic effect on cell metabolism than simply suppression of anabolic processes; when extracellular factors are removed cells are unable to take up and utilise sufficient extracellular nutrients and become catabolic, undergoing autophagy to produce the nutrients to prolong survival (Edinger and Thompson, 2002, Lum et al., 2005a, Lum et al., 2005b).

A simple assay was used to determine whether autophagy is induced upon growth factor starvation in the Schwann cell: autophagosomes are cleared by fusion with, and degradation by, the lysosome and so the rate of autophagy can be inferred by the extent of autophagosome accumulation in the cell after lysosome function is inhibited. Therefore, chloroquine was used to inhibit the lysosome and autophagosome load per cell was quantified from immunofluorescence microscopy images of cell labelled with an autophagosome marker (α-LC3b) (Materials & Methods 2.5-2.7 & Figure 4.7 A)). Autophagosome load was quantified as the amount of LC3b positive area per cell. As shown in Figure 4.6 & 4.7 B, chloroquine treatment induced a significant increase in the LC3b positive area per cell, both in cells that are in the presence of serum (3% FCS) or those in the absence of serum (SATO). This suggested Schwann cells undergo autophagy both in the presence or absence of serum. However the increase in the LC3b positive area, and therefore autophagic flux, was greatest in the serum-deprived cells (SATO); more than 3-fold greater than the increase seen in the presence of serum (3% FCS). Indeed, serum deprivation increased the autophagy rate to an even

greater extent than treatment with Rapamycin, an inducer of autophagy (Figure 4.7 B). In the growth factor starved cells, mTORC1 activity was not evident- as would be predicted given the absence of growth factor signalling (Figure 4.6 B).

These results show that the rate of autophagy is higher in serum starved (i.e. growth factor starved) cells than in growing (serum treated) cells or cells treated with an inducer of autophagy. This finding is consistent with studies in other cell types, which have shown that cells in the absence of growth factors cannot take up and utilise sufficient nutrients to maintain cell metabolism and instead undergo autophagy, using the products of this catabolism to drive necessary biosynthetic and bioenergetic reactions (Edinger and Thompson, 2002, Lum et al., 2005a, Lum et al., 2005b).

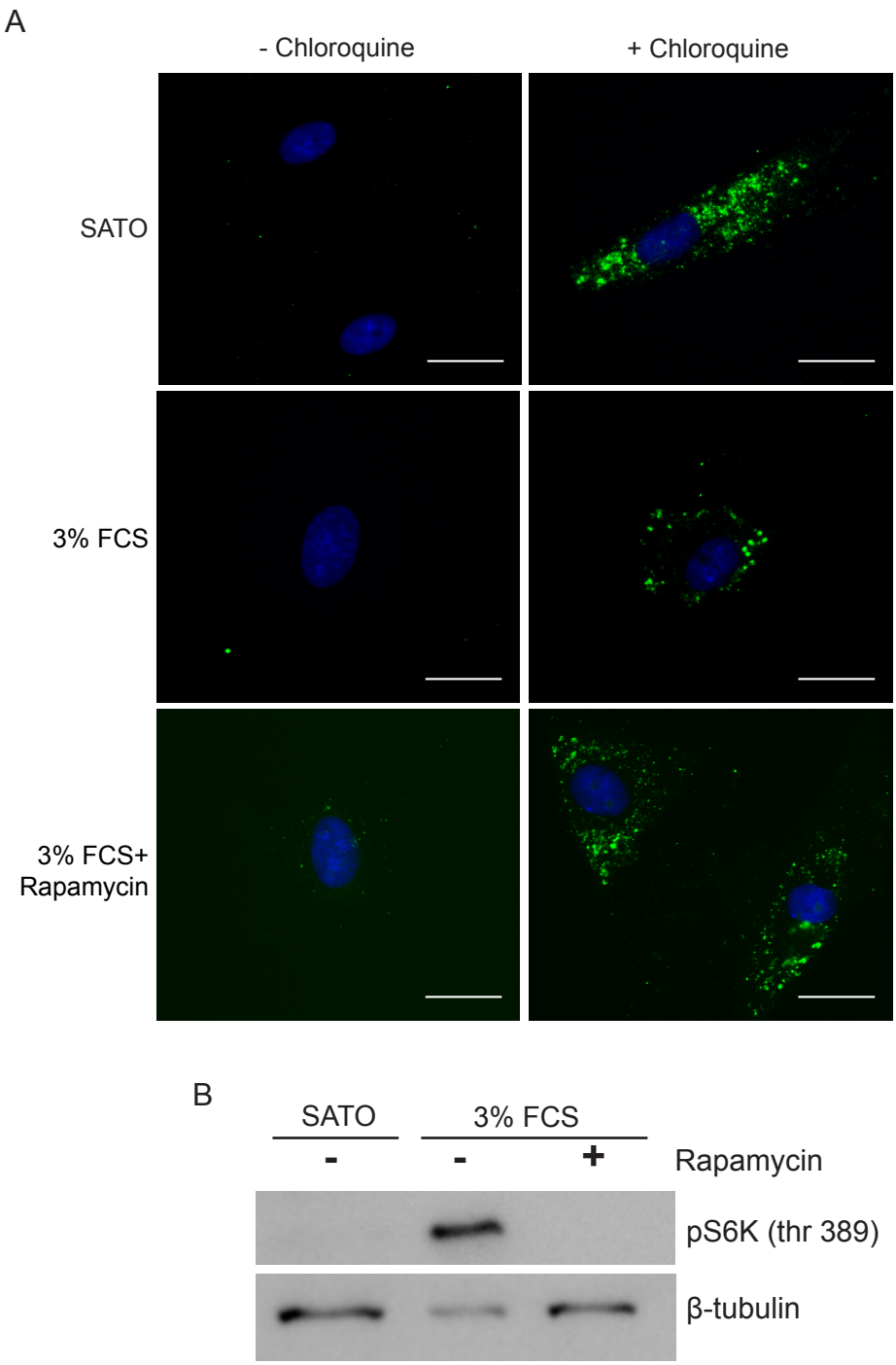

Figure 4.6 Serum suppresses autophagy

Aphidicolin arrested NS cells were treated as indicated before:
A) Anti-LC3b staining to label the autophagosomes. Shown are representative widefield microscopy images of labelled autophagosomes. Scale bar = 25μm.
B) 10hrs +/- serum/ Rapamycin treatment, cell lysates were collected for western blot analysis of protein levels of pS6K (thr389). β -tubulin were used as a loading control.

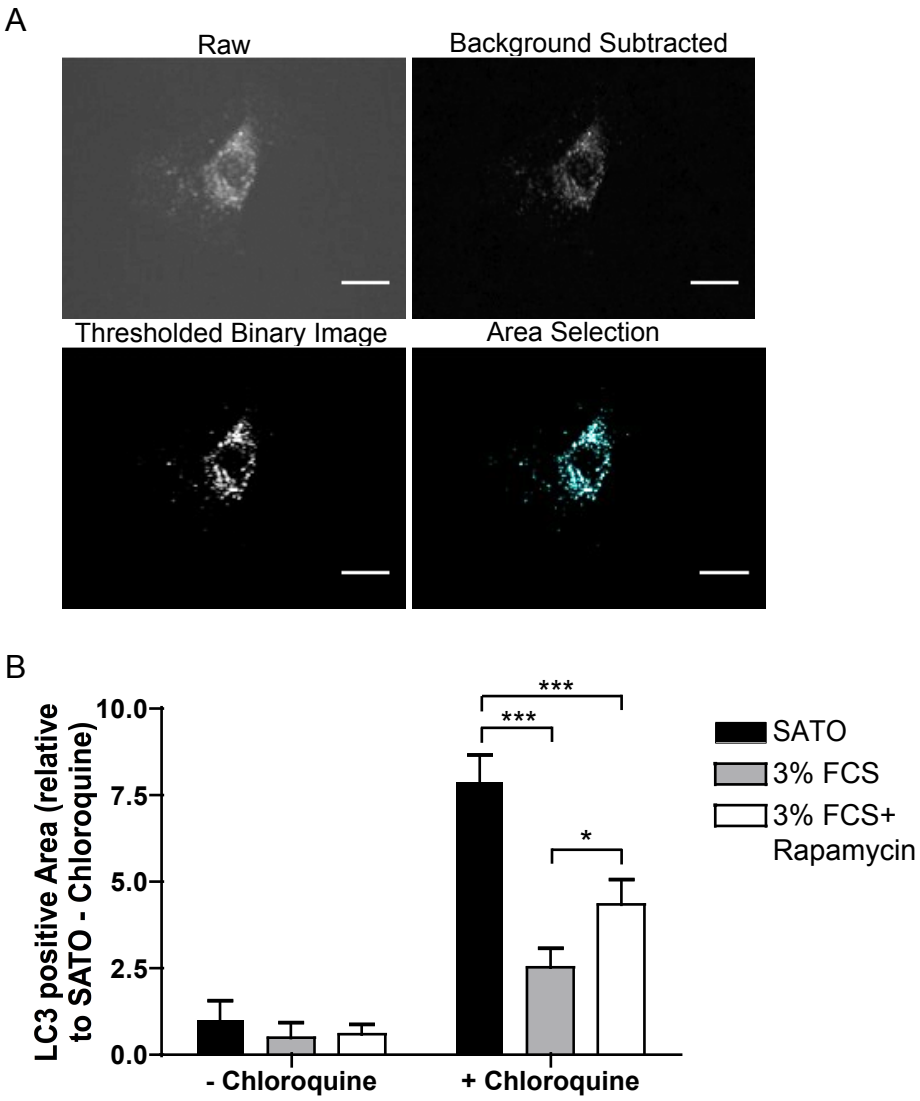

Figure 4.7 Serum suppresses autophagy

Aphidicolin arrested NS cells were treated as indicated before anti-LC3b staining to label the autophagosomes.
A) Schematic demonstrating the processing and analysis of raw images performed in ImageJ for quantification of:
B) Mean LC3b positive area per cell. Bar chart shows mean +SEM of 5 experiments. Minimum of 50 cells quantified per condition per experiment. Repeated Measures Two-Way ANOVA, interaction $p<0.001$, post hoc Bonferroni as indicated.

4.3 Endocytosis and Recycling Rates of Membrane Lipids are Equivalent and Rapid in Starved and Growing Cells

The plasma membrane is dynamic and membrane turnover is critical for regulation of extracellular signalling, uptake of nutrients and other substrates and maintaining the integrity of the barrier the plasma membrane forms between the intra- and the extra- cellular environment. Given its importance it is unsurprising that membrane turnover is a carefully regulated process. Membrane dynamics vary between cell types, although differences may also be skewed by the method of quantification as well as what membrane parameter, i.e. protein, lipid or fluid-phase, is quantified (Burgert and Thilo, 1983).

The size of the plasma membrane is determined by the balance between the rate of membrane removal and membrane delivery. For the plasma membrane to grow there must be net delivery of membrane, which can be achieved by increasing the rate of membrane delivery, reducing the rate of membrane removal or both (Figure 4.8). It may even be achieved when membrane delivery and removal both increase or decrease, as long as the change in delivery relative to removal results in net delivery of membrane. For the plasma membrane to maintain a constant size the rate of membrane removal and delivery must be in equilibrium. Although the mechanisms by which plasma membrane size can be rapidly altered (for example upon stretch in alveolar or bladder epithelial cells) have been well studied, the mechanisms by which sustained expansion of the plasma membrane occurs during growth has not. Given that Schwann cells in the presence of serum add plasma membrane whereas starving cells maintain a constant plasma membrane size over 24hrs (Section 4.1, Figure 4.4 & 4.5), comparing these conditions seemed a tractable system in which to begin to investigate the mechanics of plasma membrane growth.

The plasma membrane is removed and delivered by both vesicular and non-vesicular mechanisms (Figure 4.8). Proteins move primarily via the vesicular pathways and lipids via both vesicular and non-vesicular routes (Prinz, 2010). Vesicular transport consists of a complex system of endocytic (removal) and exocytic (delivery) pathways. The exocytic pathways can be broadly divided into the exocytosis of *de novo* material (the secretory pathway), or material derived from previously endocytosed material (recycling exocytosis);

within these two categories multiple specific and overlapping pathways exist (Chieregatti and Meldolesi, 2005, Grant and Donaldson, 2009). This is true also for endocytic pathways (Conner and Schmid, 2003). As vesicular trafficking is a major mechanism of membrane removal (endocytosis) and delivery (exocytosis), these pathways were the focus of initial analyses. More specifically, the rates of endocytosis and recycling (of previously endocytosed material) were quantified. Although the terms 'endocytosis' and 'recycling' each encompass a range of specific pathways, global rates of endocytosis and recycling can be quantified using markers carried by (as far as is known) all pathways. As lipids are the major component of all cell membranes, the rates of endocytosis and recycling of membrane lipids were quantified first.

Immediately after the addition of serum there will be a period of rapid endocytosis of activated nutrient and extracellular factor receptors. As this rapid rate of plasma membrane turnover is only transient it cannot represent the plasma membrane dynamics that contribute to long-term sustained serum-driven plasma membrane growth. Therefore, the rates of plasma membrane endocytosis and recycling were quantified 10 hours +/- the addition of serum (3% FCS) when this transient increase in membrane turnover should have passed. The rate of plasma membrane lipid endocytosis and recycling was quantified using the lipophilic styryl dye FM1-43 used in Section 4.1 to quantify plasma membrane size. As already described, FM1-43 inserts non-specifically into lipid membranes and does not flip-flop between the leaflets of a bilayer. FM1-43 moves with the membrane it is inserted in, which means when the dye inserts into plasma membrane it will be endocytosed with that membrane. This can be quantified as the increase in fluorescence intensity, i.e. the amount of FM1-43, per cell. Importantly, FM1-43 is fluorescent only in a hydrophobic environment, e.g. lipid membranes, which means fluorescence intensity of a labelled cell should reflect only labelled membrane- any dye internalised within the lumen of endocytic vesicles should not fluoresce.

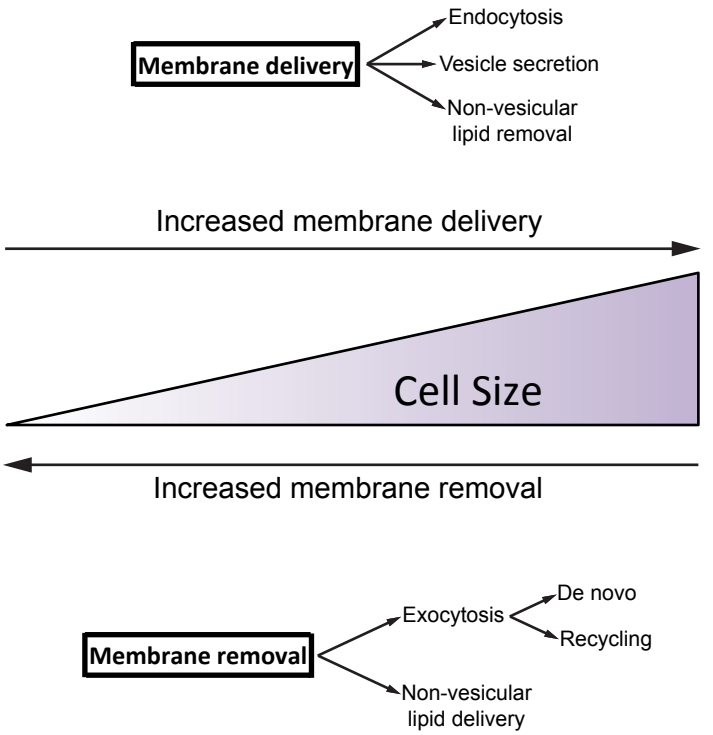

Figure 4.8 Regulation of plasma membrane size

The size of the plasma membrane is determined by the balance between the processes that deliver membrane (exocytosis and non-vesicular lipid delivery) and those that remove membrane (endocytosis, vesicular secretion and non-vesicular lipid removal).

The initial rate of increase in fluorescence per cell over time reflects the rate of lipid endocytosis. Then, as recycling of previously endocytosed material begins, the rate of accumulation of fluorescence slows to a lower rate that reflects the equilibrium between the rate of endocytosis and the rate of recycling (Figure 4.9). The rate of lipid recycling is calculated by subtracting the equilibrium rate from the initial rate of endocytosis. FM1-43 is frequently used to study the endocytosis and recycling of synaptic vesicle membrane and has also been used in other cell types (Bertrand et al., 2006, Gaffield and Betz, 2006, Hao and Maxfield, 2000). It is important to note one caveat of this technique; the FM1-43 inserted into the lipid membrane is in dynamic equilibrium with the surrounding medium and diffuses within the lipid leaflet it is inserted in. Therefore if labelled membrane destined for recycling passes through a membrane compartment that contains a lower concentration of FM1-43 before being recycled, some dye will exit the membrane destined to be recycled (data from (Griffiths et al., 1989) suggests this will be the case). This means the amount of FM1-43 leaving the cell in the recycled membrane will not equal the amount that entered the cell in the equivalent size of endocytosed membrane- it will be less and therefore the size of the recycled membrane will be underestimated (Hao and Maxfield, 2000). How significant this error is and whether the size of the error is different in the growing and starving cells was not investigated within these studies.

For these assays, aphidicolin-arrested Schwann cells were incubated with FM1-43 containing medium 10 hours +/- serum treatment and the rate of plasma membrane lipid endocytosis and recycling determined from the increase in total cell fluorescence intensity of specific cells over time: the fluorescence intensity of a cell was quantified from live cell spinning disc confocal microscopy images taken through the cell's depth, as it was for imaging FM1-43 labelled cells in the plasma membrane size assays (Materials & Methods 2.10).

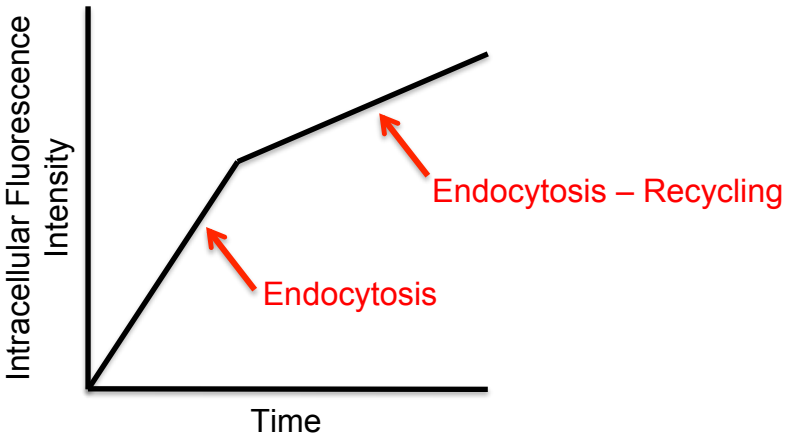

Figure 4.9 Accumulation of fluorescence intensity over time represents membrane endocytosis and recycling

When cells are continuously incubated in FM1-43 containing medium, FM1-43 is non-specifically incorporated into the plasma membrane. As incorporation is independent of membrane lipid composition the cell fluorescence intensity represents the size of the lipid membrane labelled with the probe. The FM1-43 will then move with the membrane as it is internalised by endocytosis and then recycled back to the plasma membrane. The initial rate of increase in intracellular fluorescence intensity (total cell fluorescence intensity - total cell fluorescence intensity at t=0mins, i.e. the fluorescence intensity of the labelled plasma membrane) reflects the rate of lipid endocytosis. As recycling of previously endocytosed membrane begins, the rate of accumulation of intracellular fluorescence slows to a new and lower rate that represents the balance between the rate of endocytosis and the rate of recycling exocytosis. The rate of recycling is calculated by subtracting the equilibrium rate from the rate of endocytosis.

Plotting the accumulation of intracellular fluorescence intensity against time showed there was no significant difference in the accumulation of fluorescence intensity (representing cell surface derived plasma membrane lipid) between the starved and growing cells (Figure 4.10 A i). This is shown more clearly when the initial and secondary rates are plotted on separate graphs (Figure 4.10 A ii & iii, respectively) and when the endocytosis and recycling rates are calculated from the best fit lines (Figure 4.10 B). These results indicate that growth factor starved (SATO) and growing (3% FCS) cells endocytose and recycle plasma membrane lipids at equivalent rates (Figure 4.10). From this data, measurable recycling began between 5 and 10 mins after endocytosis; demonstrated by the shift from the initial more rapid rate of increase in fluorescence intensity to the second lower rate (Figure 4.10 A i). This is consistent with findings in other cell types for the turnover of both membrane lipids and specific membrane proteins (Hao and Maxfield, 2000, Koval and Pagano, 1990, Maxfield and McGraw, 2004, Mayor et al., 1993, Scharschmidt et al., 1986).

At 10 hours post-factor addition the growing cells have ~1.5-fold more plasma membrane than the starved cells, according to the FM1-43 data described in Section 4.1 (Figure 4.5). Therefore, because the starved and growing cells seemed to move equivalent amounts of membrane lipid, the starved cells endocytose and recycle a greater proportion of their membrane lipid than the growing cells (Figure 4.11). Expressing turnover relative to plasma membrane size showed that membrane turnover is rapid, as the equivalent of the total cell surface lipid is internalised once every ~15-20 minutes (Figure 4.11). Although studies in other cell types give a wide range of values for the rate of membrane internalisation, these rates found certainly fall within the range found by other studies in a range of cell types (1-20 times per hour) (Burgert and Thilo, 1983, Hao and Maxfield, 2000). These results indicated that even in growth factor starved cells the highly energetic, ATP-dependent processes of membrane lipid trafficking were maintained at high rates-equivalent to those of cells growing in serum (3% FCS). This was somewhat surprising given that growth factor deprived cells were highly autophagic and unable to grow, suggesting they are nutrient deprived and catabolic, and therefore might be predicted to downregulate ATP-dependent processes such as membrane trafficking compared to anabolic, growing cells (3% FCS).

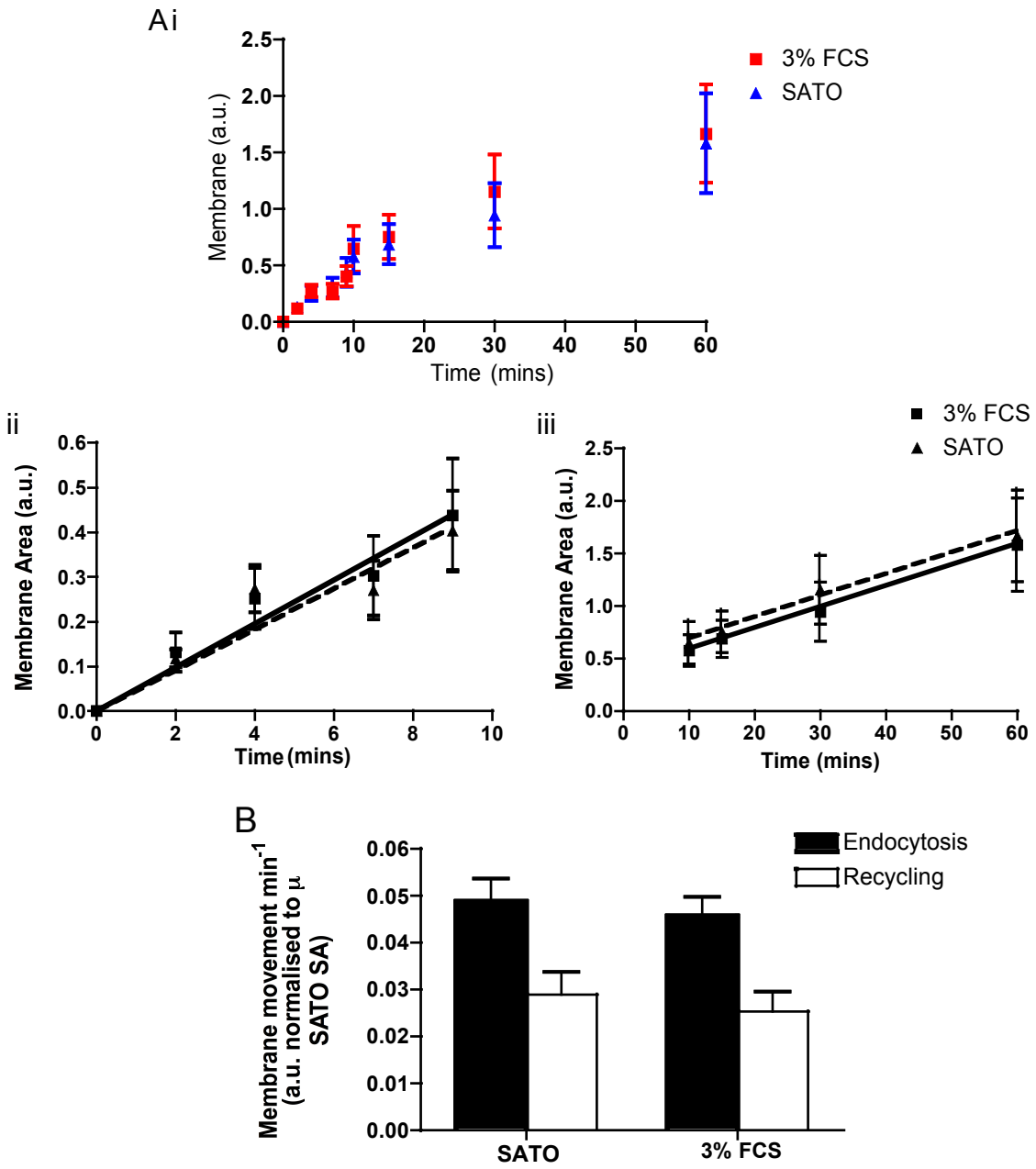

Figure 4.10 Endocytosis and recycling rates of membrane lipids are similar in starved and growing cells (serum-starved and serum-treated cells)

Aphidicolin arrested NS cells were treated as indicated for 10hrs then incubated in FM1-43 containing medium to label the plasma membrane and, over time, internalised plasma membrane. Labelled cells were imaged at timepoints as indicated using live cell spinning disc confocal microscopy. Endocytosis and recycling rates were calculated from the change in total cell fluorescence intensity over time. Graphs show mean +SEM.
A) Intracellular accumulation of FM1-43 derived fluorescence over time, i) 0-60 mins (the combined graph of ii) and iii)), ii) 0-9 mins, iii) 10-60 mins. Mean of ii) 7, iii) 8 experiments, 1 cell quantified per condition per experiment. Linear Regression Analysis and Two-Way ANOVA (Time: 0-9, or, 10-60 mins) of ii) and iii) all have minimum significance of $p<0.01$.
B) Bar charts to show endocytosis and recycling rates, calculated from the graphs shown in A). Two-Way ANOVA, endocytosis vs recycling $p<0.01$, post hoc Bonferroni as indicated.

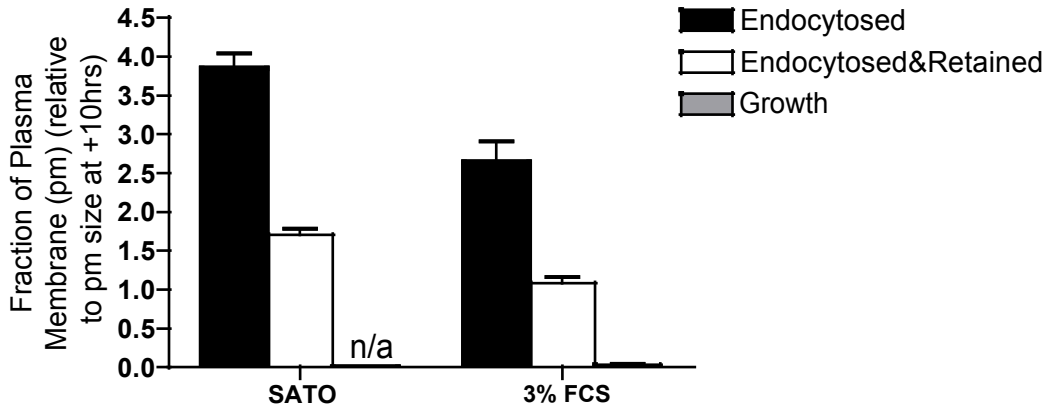

Figure 4.11 The whole plasma membrane turns over faster in starved cells compared to growing cells (serum-starved vs serum-treated cells)

Aphidicolin arrested NS cells were treated as indicated for 10hrs then incubated in FM1-43 containing medium to label the plasma membrane and, over time, internalised plasma membrane. Labelled cells were imaged at timepoints as indicated using live cell spinning disc confocal microscopy. Endocytosis and recycling rates were calculated from the change in total cell fluorescence intensity over time and normalised to plasma membrane size in each condition.

Bar chart shows mean +SEM. Endocytosis and recycling rates were calculated from the graphs shown in 5.10, normalised to fluroescence intensity at 0mins for each cell quantified. Growth rate was calculated from data in figure 4.9. Two-Way ANOVA, endocytosis vs recycling $p<0.001$, SATO vs 3% FCS $p<0.001$, interaction $p<0.01$, post hoc Bonferroni as indicated on the graph.

**Note added in proof – we now realise that, given that these are not specific inhibitors, these results must be interpreted with care. We can say that these inhibitors block ATP and show that dye uptake is an active process.*

To confirm that FM1-43 was being internalised in an ATP-dependent manner, consistent with internalisation via endocytosis, the assay was performed in the presence of inhibitors of respiration to block ATP production and subsequently deplete ATP within the cells. Inhibitors were added to the cells 30 minutes prior to the start of the assay to allow time for cellular ATP levels to become depleted*. Inhibition of oxidative phosphorylation using sodium azide completely blocked intracellular accumulation of FM1-43 (fluorescence intensity) in the starving cells (SATO) and reduced the uptake of FM1-43 in the growing cells (3% FCS) (Figure 4.12 A). These results suggested the starving cells are more reliant on oxidative phosphorylation (aerobic respiration) to produce ATP than the growing cells, consistent with findings in other cell culture systems (DeBerardinis et al., 2008a, Gomes et al., 2011a, Lunt and Vander Heiden, 2011). Blocking both oxidative phosphorylation and glycolysis, by treating cells with sodium azide together with sodium fluoride (to inhibit glycolysis), blocked FM1-43 accumulation in both the starving (SATO) and growing (3% FCS) cells (Figure 4.12 B). The latter assay had to be performed over a shorter time period (0-9 minutes) as when both oxidative phosphorylation and glycolysis are blocked, the cells rapidly looked very sick, had extensive membrane blebs and died. The results of both assays show FM1-43 is internalised in an ATP-dependent manner, consistent with internalisation of the dye via endocytosis.

In summary: the results presented in this Section demonstrate that the rate of ATP-dependent endocytosis and recycling of plasma membrane lipid is equivalent in starved (SATO) and growing (3% FCS) cells. Moreover this rate is very rapid, with the whole plasma membrane lipid content internalised once every 15-20 minutes. The rate of membrane turnover was more than 75x greater than the calculated rate of serum-induced plasma membrane growth. Moreover, the standard error on the calculated endocytic and recycling rates was 2- to 6-fold greater than the plasma membrane growth rate. This means that any shift in the balance between these rates which may be responsible for driving plasma membrane expansion in the growing cells would be too small to be detected using this assay (Figure 4.11 B). Therefore, the rapidity of membrane turnover precludes using this type of kinetic approach to determine the mechanism of plasma membrane growth.

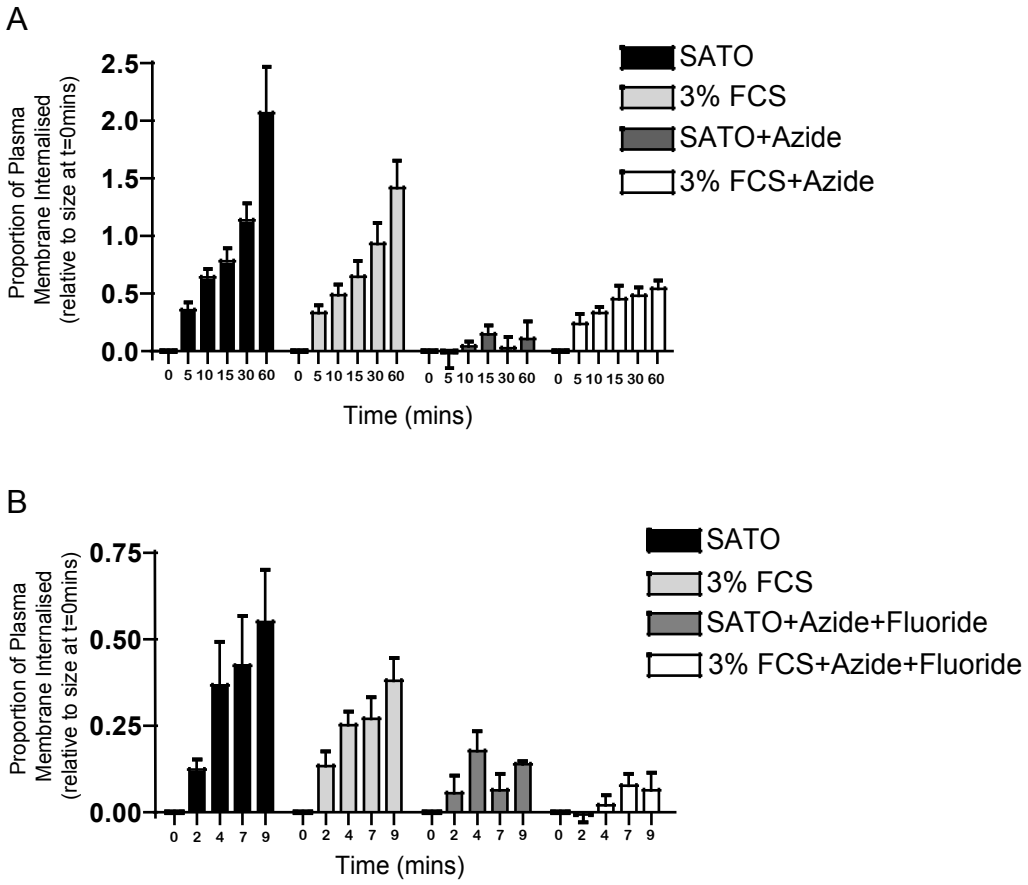

Figure 4.12 Intracellular accumulation of FM1-43 is ATP-dependent

Aphidicolin arrested NS cells were treated +/- serum as indicated for 9.5hrs then treated +/- inhibitor for 30mins before being incubated in FM1-43 containing medium to label the plasma membrane and, over time, internalised plasma membrane. Labelled cells were imaged at times as indicated using live cell spinning disc confocal microscopy. Graphs show intracellular accumulation of FM1-43 derived fluorescence over time, relative to plasma membrane size.
A) 0-60mins +/- sodium azide.
B) 0-9mins +/- sodium azide/sodium fluoride.
Graphs show mean +SEM of A) 4 and B) 5 experiments, 1 cell quantified per condition per experiment. Regression analysis, null hypothesis=regression curves are the same A) SATO vs SATO+azide $p<0.0001$, 3% FCS vs 3% FCS+azide $p<0.01$ B) SATO vs SATO+azide $p<0.01$, 3% FCS vs 3% FCS+azide $p<0.0001$.

4.4 Fluid-Phase Endocytosis and Recycling Rates are Similar in Starved and Growing Cells

It was somewhat surprising that ATP-dependent membrane lipid turnover was as rapid in the starved cells as in the growing cells, given that they are autophagic, slowly losing volume and predicted to be nutrient starved. To further investigate these findings, an alternative method was used to quantify plasma membrane trafficking; quantification of the rates of fluid-phase endocytosis and recycling. Fluid-phase represents the volume/ contents of trafficked vesicles. Fluid-phase endocytosis and recycling was quantified using fluorescently labelled 10kDa dextran, a classic fluid-phase marker. Similar to FM1-43, dextran should be non-specifically endocytosed and recycled with the contents of endocytic vesicles. The rates of fluid-phase endocytosis and recycling can be determined by quantifying the accumulation of dextran in cells over time, as they were for membrane lipid. These assays were performed 10hrs +/- serum treatment (as before): Schwann cells grown on coverslips were incubated in cell culture medium containing fluorescently labelled dextran for various times before being fixed. Mean fluorescence intensity per cell at each timepoint, representing the amount of dextran accumulated within the cell within that time, was quantified from maximal projection fluorescence confocal microscopy images of labelled cells (Materials & Methods 2.6 & 2.11).

As shown in Figure 4.13 A, fluorescently labelled dextran accumulated in the cells over time. Importantly, consistent with uptake being via endocytosis, accumulation of intracellular fluorescence was an active process because it was blocked when cells were kept at 4°c (Figure 4.13 B). Consistent with the membrane lipid turnover results, recycling of previously endocytosed material began to occur after 5-10mins (as demonstrated by the shift from the higher to lower rate of fluorescence intensity accumulation). Figure 4.14 A shows that endocytosis (the initial rate of fluorescence accumulation) was equivalent in starved and growing cells (SATO and 3% FCS, respectively). The second rate was slower in the growing cells, which suggests recycling occurs faster as the initial rates were equivalent. However, when the endocytosis and recycling rates were quantified, the difference was not significant (Figure 4.14 B).

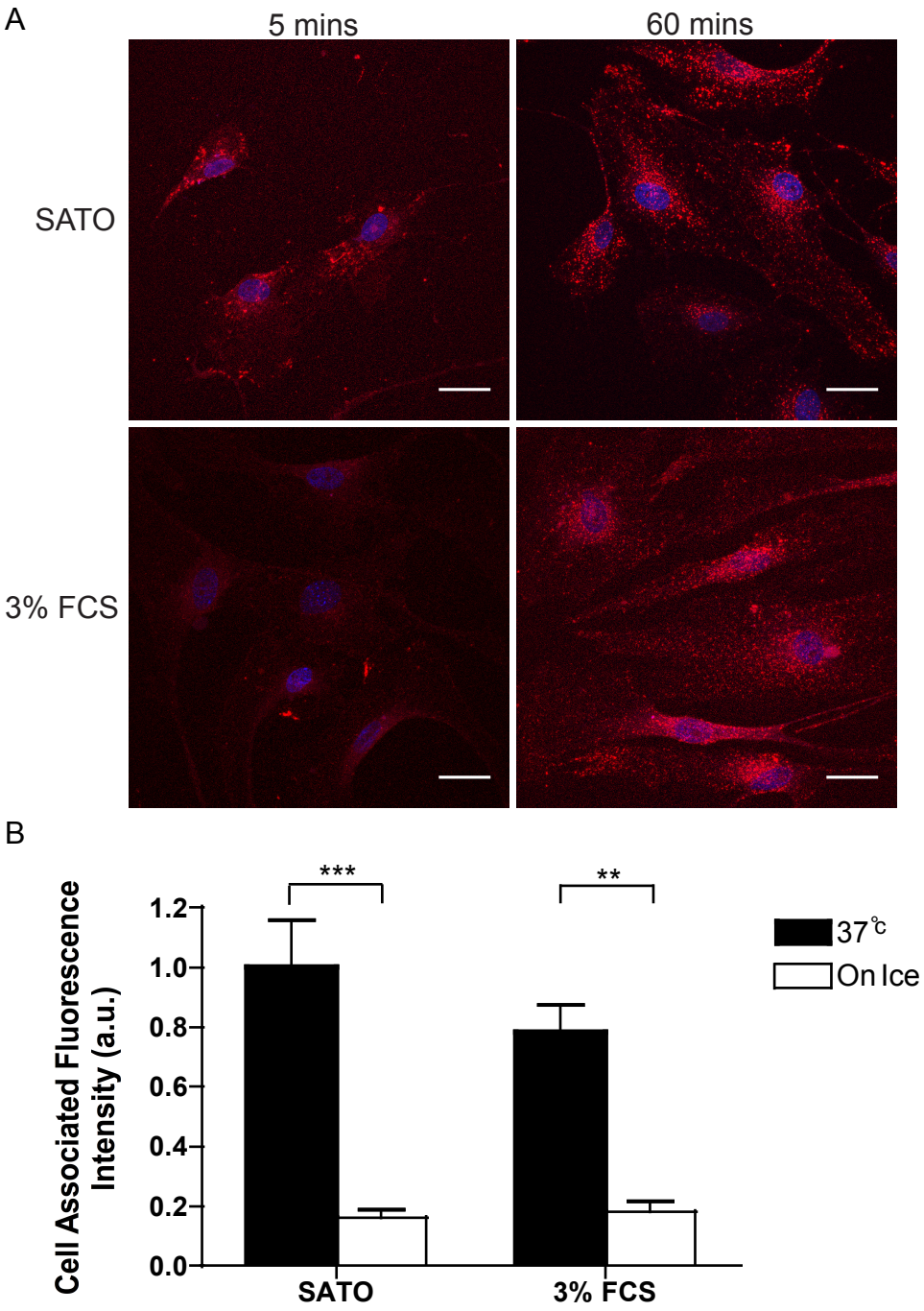

Figure 4.13 Fluid-phase endocytosis and recycling rates are similar in starved and growing cells (serum-starved and serum-treated cells)

Aphidicolin arrested NS cells were treated as indicated for 10hrs then incubated in fluorophore-conjugated dextran containing medium. Intracellular fluorescence intensity increases over time as dextran is endocytosed.
A) Representative maximal projection images of labelled cells over time, scale bar = 25µm.
B) Dextran accumulation over 60mins at 37°c versus 4°c, to show uptake is an active process. Mean of 5 experiments, minimum 25 cells quantified per condition per timepoint per experiment. Bar chart shows mean +SEM. Repeated Measures Two-Way ANOVA, 37°c vs On Ice $p<0.001$, post hoc Bonferroni as indicated on the graph.

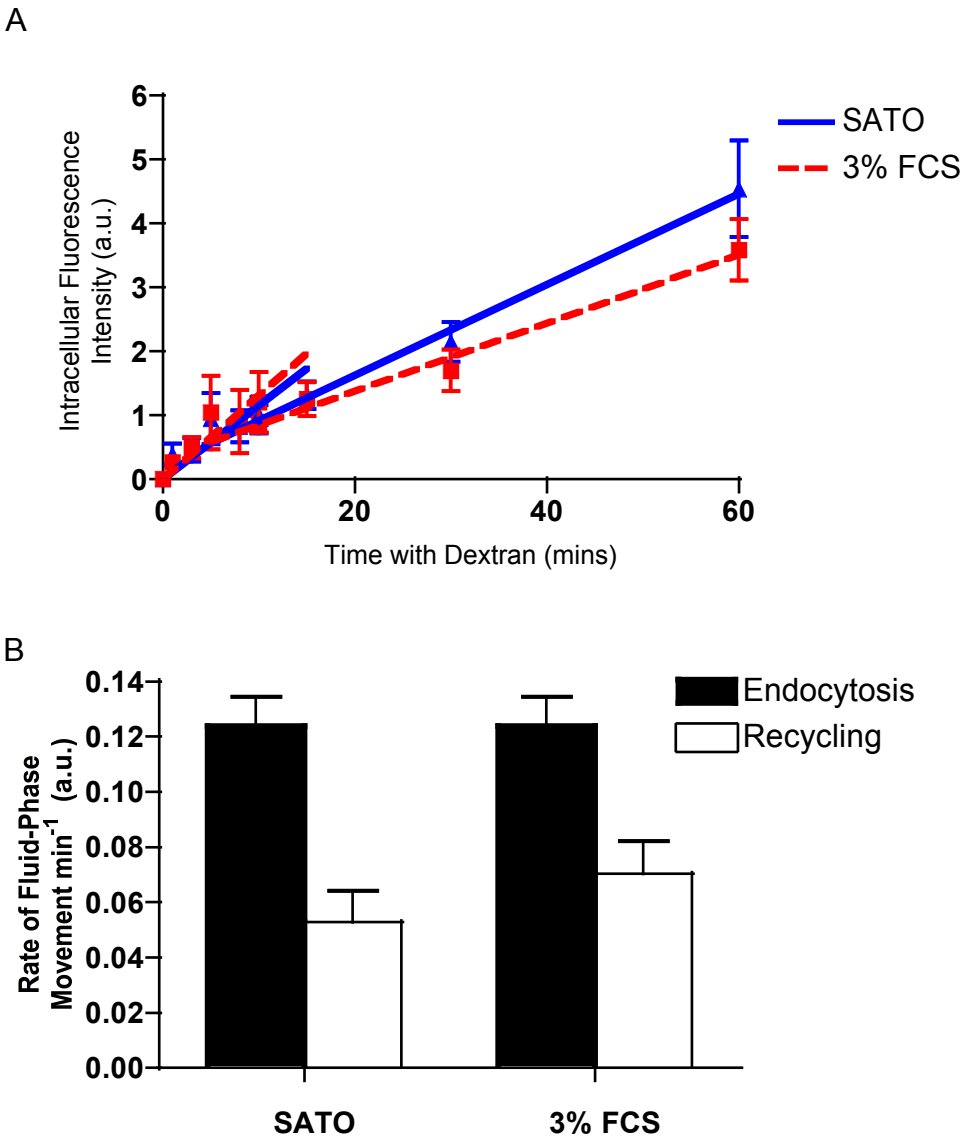

Figure 4.14 Fluid-phase endocytosis and recycling rates are similar in starved and growing cells (serum-starved and serum-treated cells)

Aphidicolin arrested NS cells were treated as indicated for 10hrs then incubated in fluorophore-conjugated dextran containing medium, as in the previous figure. Endocytosis and recycling rates were calculated from the increase in intracellular fluorescence intensity over time. Graphs show mean +SEM.

A) Intracellular fluorescence intensity over time. Mean of 3 (0-10 mins), 5 (10-60 mins) experiments, minimum 25 cells quantified per condition per timepoint per experiment. The linear regression analyses performed on this data were used to calculate:

B) Mean endocytosis and recycling rates in 3% FCS and SATO. Repeated Measures Two-Way ANOVA, Endocytosis vs Recycling $p<0.001$, post hoc Bonferroni as indicated on the graph.

In conclusion, using this second approach to quantify membrane trafficking (quantifying the turnover of fluid phase) confirmed that starved and growing cells appeared to endocytose and recycle material at similar rates.

4.5 Membrane Protein Endocytosis and Recycling Rates are Similar in Starved and Growing Cells

Proteins, like lipids, are a critical component of cell membranes; they are necessary for all functions of the plasma membrane, from nutrient uptake to signalling and substrate adhesion. It is therefore unsurprising that the expression, localisation and turnover of plasma membrane proteins is carefully regulated. The mechanisms regulating the plasma membrane trafficking of many specific proteins have been well studied; especially those of extracellular factor and nutrient receptors, such as the epidermal growth factor receptor (EGFR) and transferrin receptor (TfnR), respectively. It is also known that different proteins have different trafficking kinetics and, in the case of receptors, are often regulated by ligand concentration and receptor activation. How the kinetics of individual proteins relates to the global rate of plasma membrane protein turnover is unclear.

The results presented in Sections 4.3 and 4.4 indicate that both fluid-phase and lipid turnover at the plasma membrane is similar in starved (SATO) and growing (3% FCS) Schwann cells. However, this does not mean the global rate of protein endocytosis and recycling at the plasma membrane are equivalent. It is possible that the behaviour of plasma membrane proteins may be uncoupled from that of the membrane lipid and fluid-phase. For example, in receptor mediated endocytosis (one of the major endocytic pathways) proteins are often clustered prior to being internalised, which increases the ratio of the protein: lipid in the endocytosed vesicle compared to the plasma membrane. Given that certain signalling pathways, such as mTORC1, activated downstream of serum (i.e. in the growing cells) are known to positively regulate this form of endocytosis (Galvez et al., 2007, Hennig et al., 2006, Pelkmans et al., 2005) it was interesting to determine how the global rate of plasma membrane protein endocytosis and recycling compare between the starving and growing cells.

Two simple assays were developed to track and quantify membrane protein endocytosis and recycling, respectively. These assays use the common technique of cell surface biotinylation where an amine-reactive biotin probe is used to label cell surface proteins. Cell surface biotinylation was performed on ice to prevent uptake of the biotin into the cell during labelling. To quantify total membrane protein endocytosis labelled, cells were then incubated at 37°c to allow trafficking, including endocytosis, to resume. As labelled proteins were endocytosed, biotin accumulated within the cells. At 0, 4, 8, 12 and 20 minutes after warming, cells were placed on ice to stop trafficking and remaining cell surface biotin was cleaved and removed. Cells were fixed, intracellular biotin was detected using Alexafluor488-Streptavidin and the amount of biotin per cell quantified as fluorescence intensity per cell from fluorescence widefield microscopy images (Materials & Methods 2.9). Turnover was quantified following 10 hours +/- serum treatment in aphidicolin-arrested Schwann cells, as for the membrane lipid and fluid-phase assays.

As shown in Figure 4.15 A, label accumulated in distinct puncta over time, consistent with internalisation via endocytosis and trafficking within the vesicular endomembrane system. Similar to the membrane lipid and fluid-phase assays, when intracellular fluorescence intensity was plotted against time the initial rate of accumulation was taken to represent the rate of total protein endocytosis. As shown by the close correlation in intracellular fluorescence intensity between starved (SATO) and growing (3% FCS) cells over the first 12 minutes of the assay (Figure 4.15 B), the starved and growing cells internalised membrane protein at a similar rate.

Only proteins on the cell surface at the start of the assay are biotin labelled. This means that as the assay proceeds, the proportion of label distributed between the intracellular recycling membranes and the cell surface equilibrates, which means there will be no further increase in the amount of label inside the cell, as is seen in Figure 4.15 B. Moreover, intracellular intensity will fall (Figure 4.15 B) as endocytosed labelled proteins are degraded.

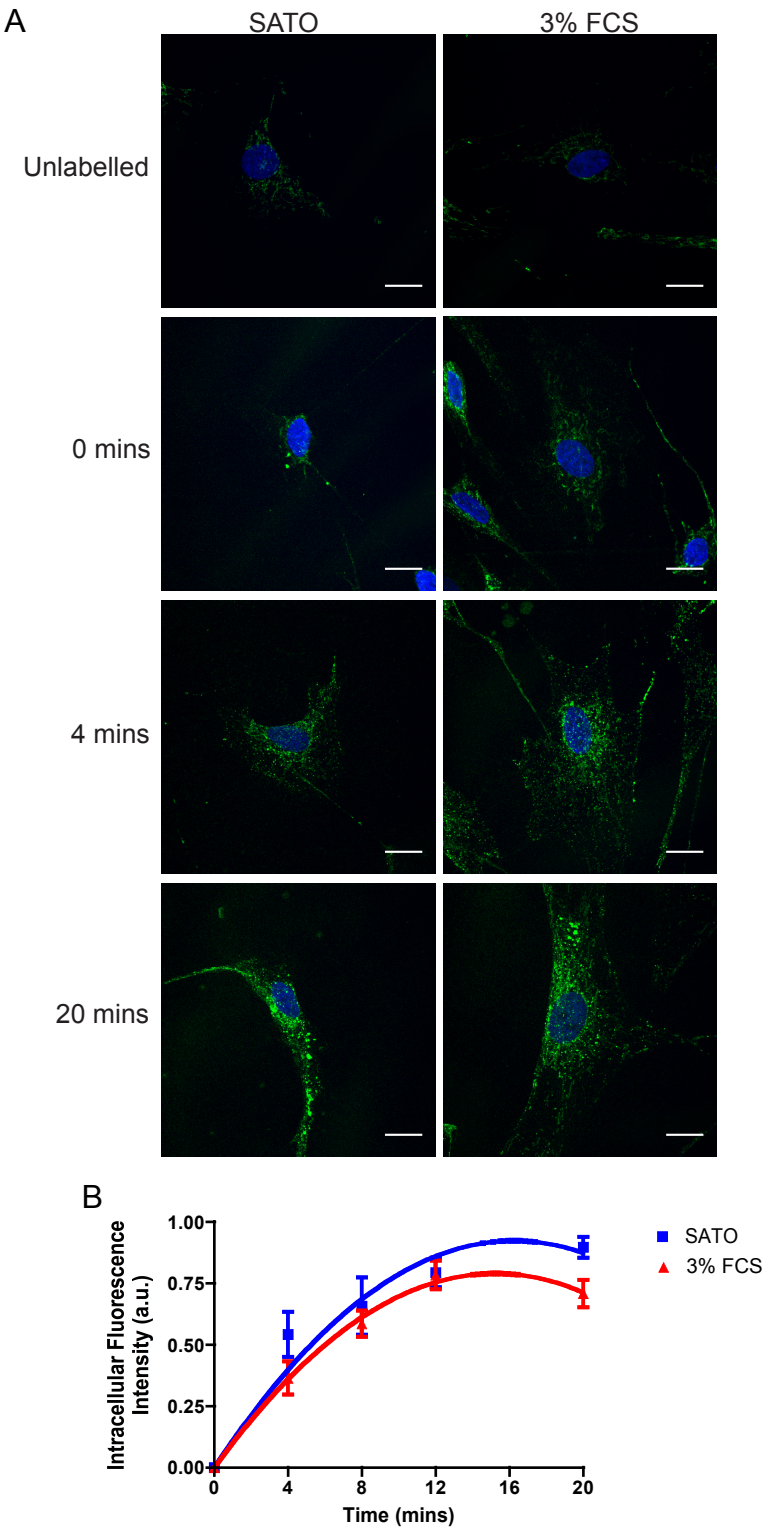

Figure 4.15 The rate of total membrane protein endocytosis is similar in starved and growing cells (serum-starved and serum-treated cells)

Aphidicolin arrested NS cells were treated as indicated for 10hrs before cell surface biotinylation to label cell surface proteins. The kinetics of biotin internalisation after returning labelled cells to 37°C was taken to represent the kinetics of cell surface protein internalisation.
A) Representative widefield microscopy images of intracellular biotin accumulation over time. Cells were fixed at various timepoints and intracellular biotin was detected using fluorophore-conjugated streptavidin and used to quantify:
B) Fluorescence intensity over time. Graph shows mean +SEM of 7 experiments. Minimum of 25 cells quantified per condition per timepoint per experiment. F-test comparison of the non-linear regression analyses performed for 3% FCS and SATO, $p>0.05$.

To quantify the rate of total membrane protein recycling, a modified version of the endocytic assay was developed. Cells were labelled as for the endocytic assay and then returned to 37°c for 45 minutes to allow loading of the recycling compartment with labelled protein. The 45 minute timepoint was chosen because the membrane lipid and fluid-phase results show recycling begins before this time (beginning between 5 and 10 minutes after endocytosis, Figure 4.10 & 4.14). In addition, as there are both fast and slow recycling compartments, by loading the cells for 45 minutes the intention was to label both the slow and fast compartments so that the quantified rate of recycling is more reflective of the global rate of protein recycling. After 45 minutes, cells were placed on ice to prevent further trafficking and remaining cell surface biotin cleaved. The cells were then returned to 37°c to once again allow trafficking, including recycling, to resume. Cleavage buffer (reduced glutathione) was added to the cell culture medium when cells were returned to 37°c so that, as labelled proteins were recycled to the cell surface, their biotin label was cleaved and lost from the cells. At 0, 4, 8, 12 and 20 minutes after warming, cells were placed on ice to prevent further trafficking and any residual cell surface biotin was again cleaved and removed. Remaining intracellular biotin was labelled, imaged and quantified as for the endocytic assay.

As shown in Figure 4.16 A, cells were heavily labelled at the start of the assay, with label concentrated in distinct puncta throughout the cell- consistent with localisation in the endomembrane system including recycling compartments. Over time label was lost from the cells. As for the endocytic assay, intracellular fluorescence intensity was taken to represent the amount of labelled protein in the cell. Therefore, the rate of loss of intensity over time represented the loss of labelled protein. This occurs by recycling, but is also likely to include loss resulting from degradation of labelled proteins. Plotting intracellular fluorescence intensity over time showed that the rate of loss of label was similar in the starved (SATO) and growing (3% FCS) cells, suggesting the total rate of loss (by recycling and/ or degradation) of endocytosed membrane protein was equivalent in the two conditions (Figure 4.16 B). These results, together with the results from the preceding sections, suggest that the global rates of endocytosis and recycling are similar for membrane lipid, protein and fluid-phase in growing (3% FCS) and starved (SATO) cells.

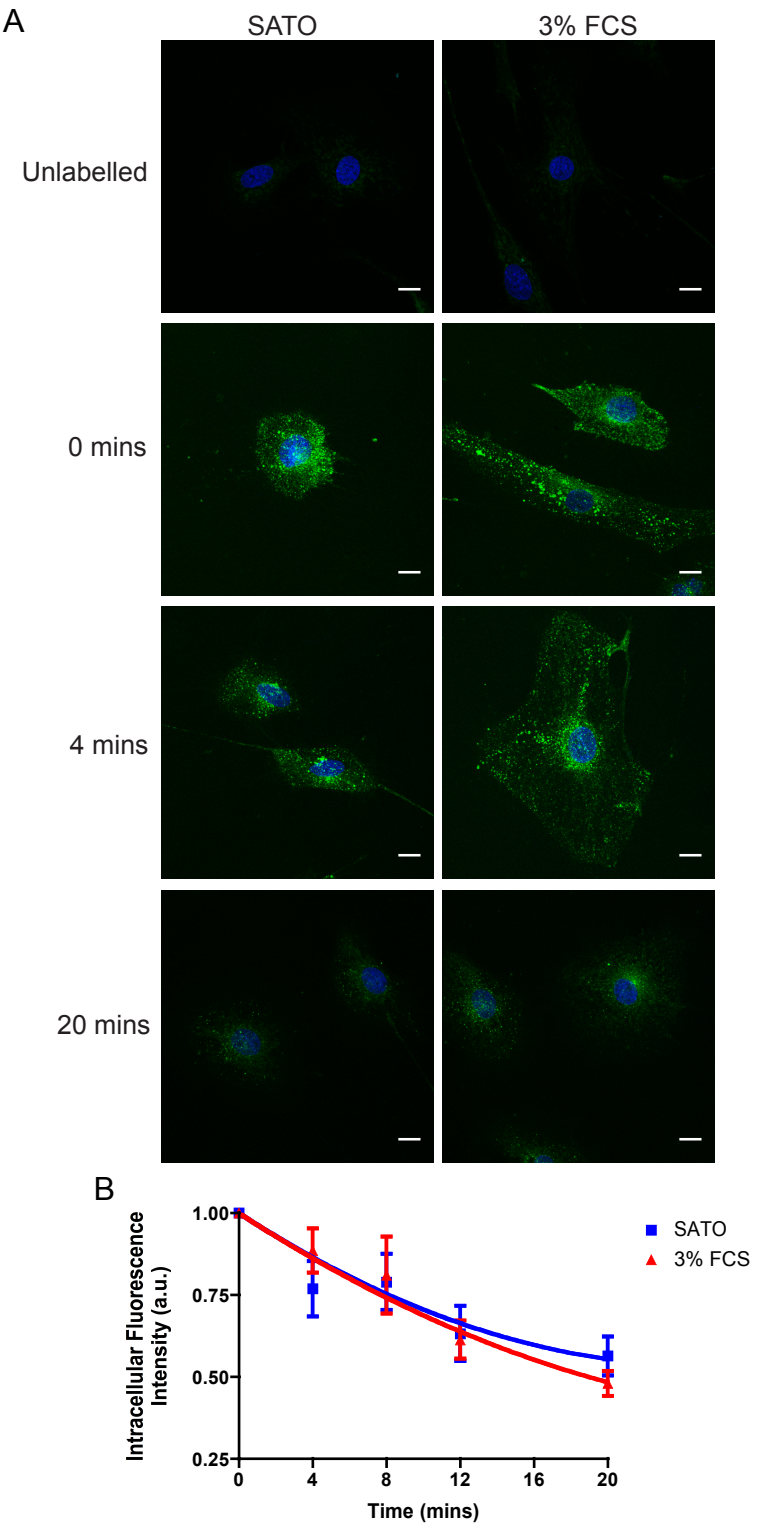

Figure 4.16 The rate of membrane protein recycling is similar in starved and growing cells (serum-starved and serum-treated cells)

Aphidicolin arrested NS cells were treated as indicated for 10hrs then cell surface biotinylated and returned to 37°c to load the recycling compartment with biotin labelled proteins before remaining cell surface biotin was removed. The subsequent loss of intracellular biotin after cells were again returned to 37°c was taken to represent the kinetics of cell surface protein recycling.
A) Representative widefield microscopy images of loss of intracellular biotin over time. Cells were fixed at various timepoints and intracellular biotin was detected using fluorophore-conjugated streptavidin and used to quantify:
B) Fluorescence intensity over time. Graph shows mean +SEM of 4 experiments. Minimum of 25 cells quantified per condition per timepoint per experiment. F-test comparison of the linear regression analyses performed for 3% FCS and SATO, $p>0.05$.

4.6 Chapter 4: Summary

The findings described in this chapter can be summarised as follows:

- Serum, a rich source of extracellular growth factors and nutrients, drives Schwann cell growth: Cells in the presence of serum add cell volume, protein mass and plasma membrane.

  In the absence of serum and extracellular growth factors, cells cannot add protein mass or plasma membrane and lose cell volume.

  As expected, starved cells display significantly higher rates of autophagy than growing cells. This is consistent with published data demonstrating that growth factor starved cells cannot maintain sufficient nutrient uptake to fuel metabolism and, as a result, catabolise intracellular contents by autophagy to provide the nutrients to prolong survival.
- Despite these biogenic differences, cells growing in the presence of serum and cells that are growth factor starved maintain equivalent and highly rapid rates of ATP-dependent membrane lipid endocytosis and recycling. Moreover, because the starved cells have a smaller plasma membrane than the growing cells, the starved cells internalise a larger proportion of the cell surface per unit time than the growing cells. The equivalent of the whole lipid membrane is internalized approximately four times per hour, compared to approximately 2.5 times per hour.
- The rates of fluid-phase and membrane protein endocytosis and recycling appear to be equivalent in starved and growing cells. This emphasizes the common kinetics of membrane trafficking in these biogenically distinct conditions.

4.7 Chapter 4: Discussion

The plasma membrane has the potential to both constrain and facilitate increases in cell volume. As cell volume is added during cell growth, it seems inevitable that the plasma membrane must expand, because the plasma membrane is the limiting membrane of the cell. The mechanisms driving this process are poorly understood and so this Chapter aimed to use the *in vitro* Schwann cell culture system to address the regulation of plasma membrane expansion during cell growth. These studies used a kinetic approach to compare the rates of plasma membrane endocytosis and recycling in cells which were growing and adding plasma membrane with those that were starved and maintaining a constant plasma membrane size in order to try to identify changes in the kinetics of membrane turnover that might be responsible for driving the expansion of the plasma membrane observed in the growing cells. As it transpired, the speed of membrane turnover precluded using this approach to identify the mechanism driving plasma membrane growth. This is because the speed of membrane turnover was so much greater than the rate of plasma membrane growth, which meant that- using the techniques available- the change in the balance between the rate at which membrane was added and membrane was removed that was responsible for driving plasma membrane growth was not detectable. Nonetheless, in addition to highlighting the speed of membrane turnover, these studies led to the striking observation that starved cells maintain a rate of cell surface endocytosis and recycling that is equivalent to the growing cells and is therefore incredibly rapid. The significance of these finding will be considered in the following Discussion.

4.7.1 Plasma Membrane Growth

Expansion and retraction of the plasma membrane can cause changes in cell surface area, however they cannot explain the persistent increase in plasma membrane required in proliferating cells, or during sustained membrane growth, such as in developing and elongating neurons and myelinating glia. These latter examples are two of the most dramatic examples of plasma membrane growth. A typical motor neuron axon with a 1μm diameter that is growing at 0.5mm a day must add ~1μm^2 membrane a minute and the membrane of a myelinating Schwann cell can increase up to 10,000-fold in just 10 weeks in rodents (Pfenninger, 2009, Webster, 1971). Consistent with this,

the FM1-43 data from this study indicates that serum drives an increase in the absolute amount of Schwann cell plasma membrane, and not just unfolding of existing membrane.

It was not possible to use the kinetic approach employed in this study to understand the quantitative regulation of plasma membrane growth downstream of serum. This regulation remains poorly understood in all cases where changes in plasma membrane size have been studied. However, for systems where rapid changes in plasma membrane size are induced, the membrane trafficking pathways that are required to effect changes in plasma membrane size are better understood. Strikingly, the pathways involved differ depending on the system. For example, whereas Golgi-derived secretory membranes drive growth of axons and dendrites, membrane expansion at the latter stages of mitosis and during *Drosophila* spermatocyte cytokinesis depends on membrane recycling (Boucrot and Kirchhausen, 2007, Dyer et al., 2007, Pfenninger, 2009, Prager-Khoutorsky and Spira, 2009, Ye et al., 2007). In *Drosophila* cellularisation, which divides the syncytial blastoderm into single membrane-enclosed cells, both Golgi-derived and recycling membranes are required (Lecuit and Wieschaus, 2000, Pelissier et al., 2003). Therefore plasma membrane size can be altered by distinct mechanisms in different cell types, in response to diverse stimuli. Studying the trafficking pathways responsible for driving plasma membrane growth may be more difficult in the Schwann cell growth model, as the increase in plasma membrane size during cell growth occurs more slowly over a longer period of time. In addition, the results of studies using inhibitor and/ or molecular approaches to block any one trafficking pathway to determine if this has an effect on plasma membrane growth are likely to be difficult to interpret, for two main reasons. First, because membrane trafficking has pleiotropic functions and so, for example, although endocytosis removes plasma membrane and therefore may be predicted to antagonise plasma membrane growth, endocytosis may also be required to drive plasma membrane growth because it is required for nutrient uptake and/ or efficient signalling through growth factor receptor activated signalling pathways. Second, there is some evidence that if one trafficking pathway is inhibited, others may be upregulated to compensate, therefore potentially leading to a false negative conclusion (Cupers et al., 1994). However, the studies of situations of rapid changes in plasma membrane size clearly show that a range of mechanisms

can be activated in different situations to drive changes in plasma membrane size.

As the membrane turnover rates are equivalent in growing and starved cells, this suggests that growth factor activated signalling pathways do not affect the constitutive rate of plasma membrane turnover. However, reports using both inhibitor and silencing techniques have shown that growth factor activated signalling pathways, such as mTORC1 and integrins, can regulate the constitutive activity of different vesicular trafficking pathways. mTORC1, for example, promotes clathrin-mediated endocytosis (CME) and integrin signalling has been shown to promote caveolae-mediated endocytosis, but not CME, in HeLa cells (Galvez et al., 2007, Hennig et al., 2006, Pearse and Robinson, 1990, Pelkmans et al., 2005). Given that inhibitors and genetic silencing techniques often block basal as well as stimulated flux through the relevant signalling pathways, it is possible that a basal flux through growth factor activated signalling pathways is maintained in the starved cells and that this is required to maintain membrane turnover. Quantifying the rates of trafficking through various endocytic and exocytic routes after inhibiting different growth factor activated signalling pathways, such as PI3K/ Akt, mTORC1 and/ or ERK, in the presence and absence of serum, could address whether any of these pathways have a role in regulating plasma membrane turnover in the Schwann cell. Interestingly, if mTORC1 activity does induce rapid and sustained CME downstream of serum, this implies there must be a corresponding upregulation of exocytic pathways/ downregulation of other endocytic pathways to compensate for the loss of plasma membrane caused by the increased rate of CME. A complementary approach, to address the regulation of trafficking pathways downstream of growth factor activated signalling, would be to determine whether these pathways regulate the expression, localisation and/ or activity of trafficking machinery, such as the Rab proteins- as this large family of small GTPases regulate diverse steps in vesicular transport (Somsel Rodman and Wandinger-Ness, 2000). For example, Rab4 and Rab11 have both been shown to regulate recycling exocytosis, a process that delivers membrane to the cell surface. Therefore it is interesting to speculate whether the activity of Rab4 and Rab11 could be promoted by growth factor activated signalling pathways to increase the rate of recycling exocytosis, to drive delivery of membrane to the cell surface and plasma membrane expansion.

In contrast to growth factors directly regulating plasma membrane expansion, an alternative hypothesis is that plasma membrane size increases as an indirect consequence of other aspects of growth factor induced cell growth. For example, it has been proposed that plasma membrane tension is maintained at a constant set point, with deviations from this set point driving compensatory changes in membrane area to return to the set point (Morris and Homann, 2001). If this is true, perhaps growth factor induced increases in cell volume push out on the plasma membrane and increase the membrane tension, thus inducing changes in the rates of plasma membrane trafficking to drive the increase in plasma membrane size, e.g. by inducing the release of membrane-bound vesicles to increase the rate of membrane delivery to the cell surface. If plasma membrane growth is regulated simply as an indirect consequence of increases in cell volume, then understanding the mechanisms driving plasma growth could potentially be addressed in any system where cell volume changes. In other words, initial mechanistic studies could be addressed in a system where cell volume changes more rapidly and extensively than during cell growth, e.g. as a result of changes in extracellular osmolarity. Such a system is more experimentally tractable than a cell growth system where the changes in cell volume are smaller and longer term. Any findings from such studies could then be tested in a cell growth system. A limited number of studies have addressed how endocytosis and exocytosis rates change upon osmotic shock (Morris and Homann, 2001). However, they have not addressed the specific signalling pathways and vesicular pathways involved and therefore further mechanistic studies are required and could prove highly informative (Morris and Homann, 2001).

This Discussion, so far, has considered the mechanisms of plasma membrane growth in terms of the pathways by which membrane is delivered and removed during changes in plasma membrane size. It has not addressed how membrane synthesis is coordinated with plasma membrane expansion. Although short term and/ or small increases in plasma membrane size may be provided by mobilisation of intracellular membrane stores, e.g. from endosomes (Dyer et al., 2007), sustained or large changes in plasma membrane area must be accompanied by membrane biogenesis. Consistent with this, phagocytosis in Human Embryonic Kidney 293 (HEK 293) cells leads to the induction of de novo cholesterol and phospholipid synthesis that matches the amount of

internalised membrane (Castoreno et al., 2005). Similarly, proper development of the extensive Schwann cell myelin sheath requires de novo lipogenesis and expression of the regulators of this process peak during myelination (Leblanc et al., 2005, Verheijen et al., 2009). Growth factor and growth factor activated signalling pathways are known to drive lipid uptake and de novo lipogenesis and it seems likely this is required to drive membrane biogenesis and may be sufficient to induce volume addition under these conditions- the role of lipogenesis in cell growth is investigated in Chapter 5 of this thesis (Duvel et al., 2010, Li et al., 2010, Peterson et al., 2011, Porstmann et al., 2005, Porstmann et al., 2008, Smith et al., 2008, Yellaturu et al., 2009a, Du et al., 2006, Luu et al., 2012, Demoulin et al., 2004, Hegarty et al., 2005, Zhou et al., 2004).

4.7.2 The Rapid Rate of Plasma Membrane Turnover

The most striking aspect of plasma membrane turnover is the speed at which it occurs. The plasma membrane is a remarkable structure. To be an effective barrier between the intra- and extra- cellular environments, plasma membrane integrity must be maintained at all times. Yet despite this, as the interface between these two environments, the plasma membrane must be dynamic; it is the only site of communication and substance exchange between the inside and outside of the cell.

This study found that the equivalent of the total cell surface lipid is internalised once every 15-20 minutes in both starved and growing cells. A limited number of studies have quantified membrane internalisation rates in other cell types and the results are in line with the findings of this study (ranging between 3-60 minutes, depending on the parameter and cell type quantified) (Burgert and Thilo, 1983, Griffiths et al., 1989, Hao and Maxfield, 2000, Steinman et al., 1976, Thilo and Vogel, 1980). Remarkably, because single membrane lipids can move by non-vesicular as well as vesicular routes, which would not be detected with the FM1-43 based assay used in this study, the quantification of membrane lipid internalisation made in this study is in fact quite likely an underestimate of the true rate (Prinz, 2010). The proportion of membrane lipid that moves via non-vesicular pathways is not well understood, however some studies have found that the movement of cholesterol and phosphatidylcholine to and from the plasma membrane is only minimally affected by inhibition of vesicular pathways (Hao et al., 2002, Kaplan and

Simoni, 1985, Prinz, 2010, Sleight and Pagano, 1983). This suggests the contribution of non-vesicular pathways to total membrane lipid addition/ removal may be significant, although it cannot be excluded that in these examples non-vesicular pathways were upregulated to compensate for the inhibition to vesicular transport.

Rapid membrane lipid turnover may prove to be a robust and constitutive feature of cell biology, because it is maintained even in the starved cells in this study. Moreover, because this rapid rate is maintained in starved cells where other ATP-dependent processes will be downregulated to conserve cellular resources, this suggests that rapid membrane trafficking must be a critical and fundamental cellular process. Which aspect(s) of membrane function require the rapid rate of membrane turnover observed in these studies? Although the answer to this question remains unknown, it is possible to speculate on possible reasons a rapid rate of plasma membrane turnover may be required. It may be that membrane proteins and lipids undergo high rates of damage and therefore must be replaced at a high frequency. Although lipids can be remodelled in situ within membranes, it may be more efficient- particularly for those lipids in the outer leaflet of the membrane and therefore a distance from the cytosolic lipolytic and lipogenic enzymes- for the lipids to be internalised via endocytosis and then remodelled, for example replacing damaged fatty acids, or fatty acids that have undergone inappropriate oxidation, which would affect the packing and therefore liquidity of the plasma membrane. Another possibility is that the high rate of membrane turnover allows the cell to respond rapidly to changes in the intra-/ extra- cellular environment that require a change in membrane composition, i.e. because the machinery that replaces the membrane is already active, it is only the specific lipids/ proteins trafficked to/ from the plasma membrane that will need to be altered, upon the receipt of the relevant cellular signal. It has been postulated that the rapid ‘futile-cycling’ of triacylglycerols to free fatty acids and glycerol and back again, as well as the rapid glycolytic cycle observed in aerobic cells is, in part, also to provide the flexibility to respond to changes in the cellular environment (DeBerardinis et al., 2008a, Watt and Steinberg, 2008) and therefore this hypothesis is consistent with other aspects of cellular function. It is also highly plausible that at least some of the membrane functions that require a rapid rate of membrane turnover may differ between the starved and growing cells, because the metabolism of these cells

differs and several functions of membrane turnover are directly related to cell metabolism. For example, maintaining nutrient transporter mediated nutrient uptake requires membrane endocytosis and exocytosis. Growth factor signalling activates this process and so it will be active in the growing cells. In contrast, due to the absence of growth factor activated signalling, growth factor starved cells significantly downregulate nutrient transporter expression and internalisation (and therefore atrophy as they activate autophagy in order to provide the nutrients to drive cell metabolism), which suggests this function makes a significantly lower contribution to membrane turnover in the starved cells (Edinger and Thompson, 2002, Leto and Saltiel, 2012). It is not only nutrient transporter endocytosis and exocytosis that might be predicted to differ between the starved and growing cells. Many growth factor receptors, for example, are endocytosed upon ligand binding and this can be necessary to promote growth factor signalling (Pearse and Robinson, 1990).

Given that the rate of certain functions of membrane turnover are likely to differ between the starved and growing cells, it might be predicted that the growth factor starved and growing cells are likely to traffic individual protein and/ or lipid components at very different rates. Somewhat surprisingly, preliminary studies investigating the rate of internalisation of specific proteins in the Schwann cell system suggest that the plasma membrane expression of the transferrin receptor, IGF-1 receptor and N-cadherin are similar in starved and growing cells, relative to total cell protein (data not shown). Although these experiments need to be repeated to verify and quantify the results, they are surprising. The transferrin receptor is a nutrient transporter that has been shown to be downregulated upon growth factor withdrawal in haematopoietic cells and there is no IGF-1 to bind and stimulate the endocytosis of the IGF-1 receptor in the growth factor starved cells (Edinger, 2007, Edinger and Thompson, 2002, Wieman et al., 2009, Wieman et al., 2007). Moreover, both the transferrin and IGF-1 receptors are classically endocytosed by CME, which is promoted by mTORC1 activity and mTORC1 signalling is activated only in the growing cells (Galvez et al., 2007, Hennig et al., 2006, Pelkmans et al., 2005). Therefore, it might have been predicted that the rate of internalisation of these proteins would be lower in the growth factor starved cells. Interestingly, one study has reported that when CME was inhibited by starvation, nutrient receptors were internalised via alternative pathways (Boucrot et al., 2010); the receptors

became localised in internalised tubules of plasma membrane that were not visible in the fed cells. Perhaps a similar process is maintaining the internalisation of the transferrin and IGF-1 receptors in the starved Schwann cell.

Interestingly, membrane trafficking is not the only cellular process that appears to persist at a constitutive and rapid rate. A recent study compared the metabolism of rapidly growing and proliferating fibroblasts with those that were quiescent, in very low serum conditions (Lemons et al., 2010). This study found that several aspects of cell metabolism, including catabolic processes such as fatty acid and protein synthesis that might be expected to occur at a higher rate in the rapidly growing cells, were equivalent in the two conditions. However, the rates of degradation and secretion of lipids and proteins were higher in quiescent fibroblasts, compared to growing fibroblasts, resulting in no net growth. These findings of Lemons et al, together with the findings of this study, highlight the clear difference between the absolute rates of any cellular process and the rate of cell growth. Any biosynthetic process, e.g. lipid synthesis, may occur at a rapid rate. However, it will only result in net biogenesis and cell growth if the rate of the opposing process, in this case lipid degradation, is not equally as fast.

4.7.3 The Rate of Plasma Membrane Trafficking is Equivalent in Starved and Growing Cells

It was surprising that the rate of membrane lipid endocytosis and recycling is equivalent in starved and growing cells; membrane endocytosis and exocytosis is ATP-dependent and starved cells inhibit/ reduce the rate of ATP-dependent processes that are not absolutely required, in order to conserve cellular energy and resources. Adaptive changes that can optimise cellular energy balance are observed in the starved Schwann cells in this study, which emphasises that these cells are energetically and biogenically challenged. Growth factor/ nutrient starved cells have been shown to rely more on mitochondrial oxidative phosphorylation to produce cellular ATP, than growing cells (DeBerardinis et al., 2008a, Gomes et al., 2011a, Gomes et al., 2011b, Gomes and Scorrano, 2011, Hardie, 2011). This is because oxidative phosphorylation is significantly more efficient than glycolysis at producing ATP. Consistent with increased reliance on the oxidative pathway, FM1-43 uptake

was blocked in the starved cells when oxidative phosphorylation was inhibited, whereas in the growing cells inhibition of both oxidative phosphorylation and glycolysis was required. In addition to increased dependence on oxidative phosphorylation, the starved cells also upregulate autophagy, which can provide the substrates to fuel necessary cell metabolism (Altman et al., 2009, Edinger and Thompson, 2002, Lum et al., 2005a, Rathmell et al., 2000, Yu et al., 2010). Together, these findings indicate the starved cells are undergoing adaptations to conserve cellular resources and optimise ATP productions. Therefore, the fact that ATP-dependent membrane turnover in these cells is maintained at an equivalent rate to in the growing cells, demonstrates that maintaining membrane turnover rates must be a critical cellular process- although the reason for this is not clear, as was discussed in Section 4.7.2.

4.7.4 Conclusion

The findings presented in this Chapter demonstrate that the turnover of the plasma membrane is incredibly dynamic and rapid in both starved and growing cells. As this ATP-dependent process is maintained at a rapid rate in starved cells that are undergoing adaptive changes to conserve cellular resources, it suggests the rapid rate is critical for cell function. This suggests there is a fundamental function of membrane turnover that is required in both starved and growing cells. This may be the replacement of effete membrane lipids and proteins or it may be that maintaining rapid turnover is required to enable rapid responses to changes in the extracellular environment, for example. However, given that aspects of cell metabolism, such as nutrient uptake and growth factor activated signalling, that differ between the starved and growing cells require membrane turnover, it is possible that certain functions of membrane turnover differ in importance between the two conditions. Strikingly, the equivalent rate of membrane turnover in starved and growing cells suggests that the global rate of membrane turnover is constitutive and unaffected by activation of growth factor activated signalling pathways. However, these pathways have previously been shown to regulate specific trafficking paths. This suggests either that the basal flux through these signalling pathways, which is maintained in the starved cells, is sufficient to maintain these trafficking pathways and/ or that regulation of these pathways has no impact on the global rate of trafficking. Understanding the relationship

between cell metabolism, bioenergetics and plasma membrane turnover and growth requires an understanding of the mechanisms regulating membrane trafficking in both starved and growing cells, as well as the critical functions of membrane turnover that require turnover rates to be maintained at such a rapid rate.

Chapter 5: Results

The Role of Lipogenesis in Cell Volume Addition

The results presented in Chapter 3 ('Biogenesis Downstream of IGF-1 Stimulation or Raf/ MEK/ ERK Activation') demonstrated that IGF-1 and Raf kinase differentially regulate organelle size and morphology. Given that it is likely that lipids need to produced to add volume during cell growth (to facilitate the expansion of membranous organelles and the plasma membrane), it was interesting to note that organelles associated with lipid metabolism, namely the peroxisomes and lipid droplets, are specifically increased downstream of IGF-1. This suggested that addition of cell volume, even over the short (24 hour) time period of these assays, would require specific alterations in cell lipid metabolism.

Several lines of evidence support this hypothesis: first, IGF-1 has been shown to drive lipogenesis through PI3K/ Akt dependent expression of the SREBPs, the master regulators of de novo lipogenesis (Du et al., 2006, Luu et al., 2012, Smith et al., 2008). Second, Akt has been shown to drive an mTORC1/ SREBP/ de novo lipogenesis dependent increase in cell volume in human epithelial cells (Porstmann et al., 2008). Finally and importantly, IGF-1 dependent addition of Schwann cell volume is PI3K/ Ak/ mTORC1 dependent (Section 3.2) (Echave et al., 2009). Therefore, the remainder of these studies focused on investigating the role of lipogenesis in the regulation of cell volume and IGF-1 dependent cell volume addition.

As in Chapter 3, these investigations used the NSΔRafER cells. This meant lipogenic pathways could be studied in Raf kinase activated cells, where mass is added in the absence of an increase in cell volume, as well as in IGF-1 treated cells, where cells are adding mass and volume. It was hoped this would help discern whether there is a specific role for lipogenesis in the regulation of cell volume during Schwann cell growth. The basic experimental protocol was also as in Chapter 3, except where specified in the text. Briefly: cells were cell cycle arrested, using aphidicolin, in normal Schwann cell medium (3% FCS) for 24hrs before being transferred to Minimal Medium plus aphidicolin for a further 24 hours and then treated with IGF-1 or Tmx (to activate the Raf kinase construct).

5.1 IGF-1, but not Raf Kinase Activation, Induces Expression of Genes that Drive Fatty Acid and Sterol Synthesis

The defined cell culture medium (Minimal Medium) used in these studies is essentially free from exogenous lipids, which means any increase in the amount of cellular lipids must result from de novo lipogenesis, i.e. synthesis of lipids from non-lipid sources (Section 1.5.2). As stated above, the master regulators of de novo lipogenesis are the SREBP family of bHLH-zip transcription factors (Section 1.5.2). To determine whether IGF-1 was regulating SREBP expression in the Schwann cell, as it has been shown to do in other systems, western blot analysis was performed against the SREBPs.

There are three SREBP proteins encoded by two genes: SREBP-1a and -1c (encoded by SREBP1) and SREBP-2 (encoded by SREBP2). As described in the Introduction (Section 1.5.2), the SREBPs are synthesised as inactive precursors (~125 kDa) that are retained in the endoplasmic reticulum until an activation signal drives their translocation to the Golgi where they are cleaved to release the N-terminal active transcription factor (~68 kDa), which enters the nucleus and can activate transcription.

The antibodies used in this study recognise epitopes in the N-termini of the proteins and therefore recognise both the precursor and mature SREBPs. The SREBP-1 antibody recognises both the SREBP-1a and -1c isoform and therefore the two were not distinguished in these analyses. Cells were collected 1 and 4 hours +/- IGF-1 treatment or Raf kinase activation (Tmx) and cytoplasmic and nuclear fractions extracted for Western blot analysis. As can be seen in Figure 5.1, by 1 hour post-factor addition, IGF-1 treatment drove an increase in the level of mature, nuclear SREBP-2 (~1.5-fold), compared to control and Raf kinase activated cells and, by 4 hours post-factor addition, this was also seen for SREBP-1 (~1.7-fold). These results suggested that IGF-1 was activating the SREBP pathway. The timings are consistent with the findings of other studies, which have shown that IGF-1 and/ or Akt can induce accumulation of nuclear SREBPs within 2 hours (Du et al., 2006, Luu et al., 2012, Porstmann et al., 2008). The different kinetics of SREBP-1 and -2 activation may indicate their activation is- at least in part- via distinct mechanisms. There also appeared to be a small, transient increase in the level of mature, nuclear SREBP-2 downstream of Raf kinase activation compared to

control, however this was not sustained (Figure 5.1- 1 hour). SREBP-1c and SREBP-2 are themselves SREBP target genes; consistent with an increase in the mature proteins, there is an increase in the precursor proteins downstream of, in particular, IGF-1.

It is interesting to note the multiple bands of the mature SREBP-2- particularly in the IGF-1 treated cells. The SREBPs can be modified in a number of ways (phosphorylation, sumoylation, acetylation and ubiquitination), which can positively and negatively regulate their transcriptional activity and stability (Introduction Section 1.5.2) (Giandomenico et al., 2003, Hirano et al., 2003, Kotzka et al., 2004, Kotzka et al., 2000, Roth et al., 2000, Sundqvist et al., 2005). Given that the ratio between the bands is particularly affected in the IGF-1 treated cells it is interesting to speculate whether IGF-1 drives such post-translational modifications.

To analyse the transcriptional activity of the SREBPs, the mRNA expression levels of two SREBP target genes, Fatty Acid Synthase (FASN) and HMGCoA Reductase (HMGCoR), were quantified by RT-qPCR. FASN and HMGCoR are rate-limiting enzymes for fatty acid and sterol synthesis, respectively, and whose expression is regulated in large part at the level of transcription. Consistent with the increase in the level of mature SREBP protein downstream of IGF-1, IGF-1 treatment increased the mRNA expression of both FASN (~3.5-fold) and HMGCoR (~1.8-fold) 6 hours post-factor addition, compared to control cells (Figure 5.2, EtOH+/IGF-1+). This was not seen downstream of Raf kinase activation, although there was a trend for the mRNA expression of HMGCoR- the classic SREBP-2 target- to be slightly increased compared to control (Figure 5.2 B Tmx+/IGF-1-). This suggests the slight increase in SREBP-2 downstream of Raf kinase has no significant effect on the expression of these downstream target genes. Together, these results demonstrate that IGF-1 activates a transcriptional program leading to the expression of genes that drive de novo fatty acid and sterol synthesis. However, it was important to determine whether IGF-1 dependent expression of these genes has a functional effect on these processes.

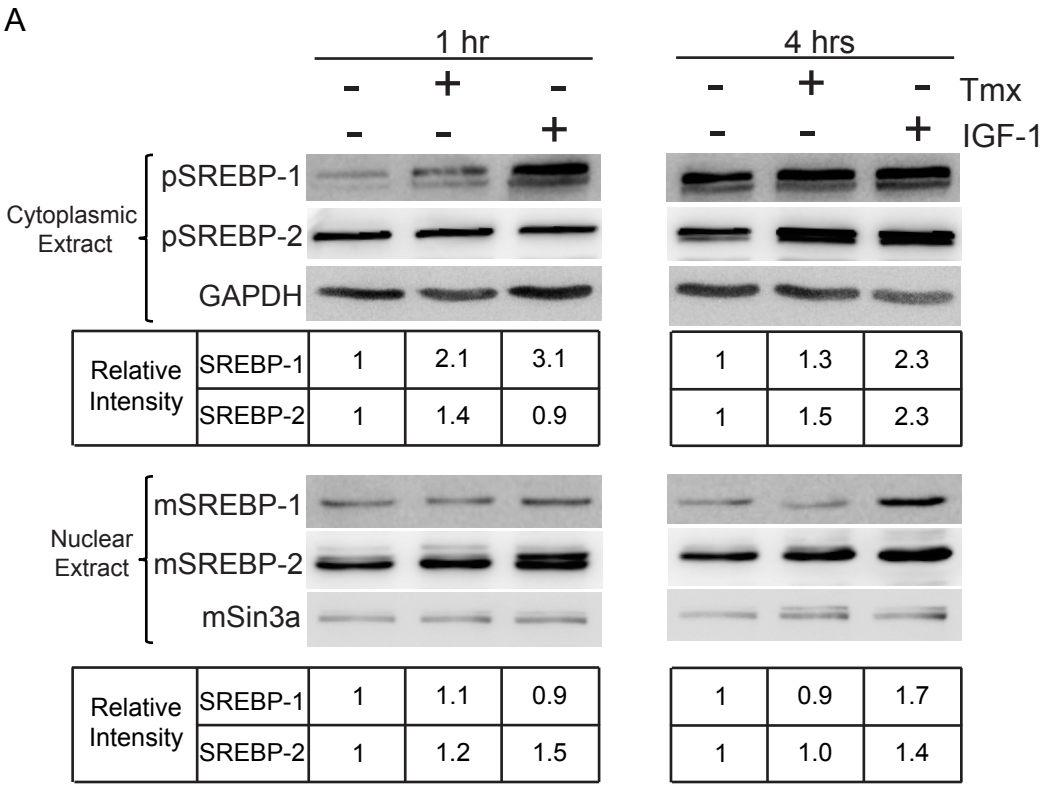

Figure 5.1 IGF-1 increases the amount of cytoplasmic precursor and nuclear mature SREBP proteins

Aphidicolin arrested NSΔRafER cells were treated as indicated. Cells were then collected and cytoplasmic and nuclear extracts separated and lysed before western blot analysis was performed against SREBP-1 and SREBP-1. mSin3a and GAPDH were used as nuclear and cytoplasmic loading controls, respectively. The cytoplasmic and nuclear extracts were from the same experiment for each timepoint. Quantifications show the mean fold-change to control (-Tmx, -IGF-1), normalised to the loading control, from 2-5 experiments.

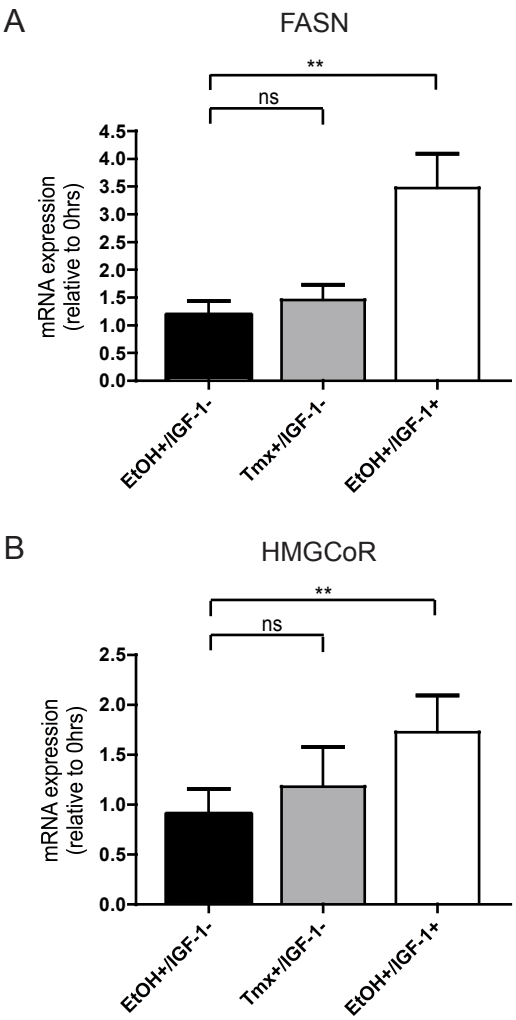

Figure 5.2 IGF-1 increases the mRNA expression of key SREBP target genes that drive de novo fatty acid and sterol synthesis

Aphidicolin arrested NSΔRafER cells were treated as indicated for 6hrs before total RNA was extracted. mRNA levels of the indicated genes was analysed by RT-qPCR and normalised to B2M as a loading control; mRNA expression levels are expressed relative to time 0hrs.
A) FASN mRNA expression levels.
B) HMGCoR mRNA expression levels.
Bar charts show mean +SEM of A) and B) 6 experiments. One-Way Repeated Measures ANOVA, A) and B) $p<0.01$. Select post-hoc Newman-Keuls as indicated on the graphs.

The main extracellular precursors for de novo lipogenesis present in the Schwann cell medium are glucose, glutamine and pyruvate. To indicate the rate of de novo lipogenesis from extracellular substrates, the incorporation of radiolabelled pyruvate into cellular lipids was quantified, as follows: Cells were treated with IGF-1 or Tmx, to activate Raf kinase, for 4 hours before [2-^{14}C] pyruvate (2.5μCi/well) was added to the cell culture medium for a further 4 hours. Cellular lipids were then extracted and the amount of radioactivity incorporated into the lipid fraction was quantified by scintillation counting. This value was normalised to the cell number of cells from parallel cell culture dishes to determine incorporation per cell. The rate of pyruvate incorporation into lipid was assayed between 4 & 8 hours post-factor addition because by 4 hours post-factor addition there is accumulation of both SREBP-1 and -2 in the nucleus downstream of IGF-1 (Figure 5.1) and, importantly, the nuclear SREBP appears to be active, as indicated by the induction of SREBP targets critical for de novo lipogenesis (Figure 5.2). Therefore it was hypothesised that if the rate de novo lipogenesis increases downstream of this, then it would be increased between 4 and 8 hours post-factor addition. As can be seen in Figure 5.3, IGF-1 (EtOH+/IGF-1+) drove a 3-fold increase in the incorporation of radiolabel into cellular lipids, compared to control (EtOH+/IGF-1-) and Raf kinase activated (Tmx+/IGF-1-) cells. Moreover, there was no significant difference in incorporation between Raf kinase and control conditions, consistent with the lack of significant increase in the mRNA expression of the SREBP targets FASN and HMGCoR that are required for de novo lipogenesis (Figure 5.2).

Although the contribution of the different extracellular substrates to de novo lipogenesis (e.g. pyruvate, glucose, glutamine and acetate) does not always change co-ordinately in response to activation of distinct signalling pathways, the results presented here are consistent with the findings of other studies that have shown that IGF-1 and/ or Akt/mTORC1 (activated in response to IGF-1 in the Schwann cell and required for IGF-1 driven Schwann cell volume addition, Figure 3.7, 3.8 & 3.9) increase the incorporation of glucose, glutamine and acetate into cellular lipids (Hagiwara et al., 2012, Porstmann et al., 2008, Smith et al., 2008, Wise et al., 2008).

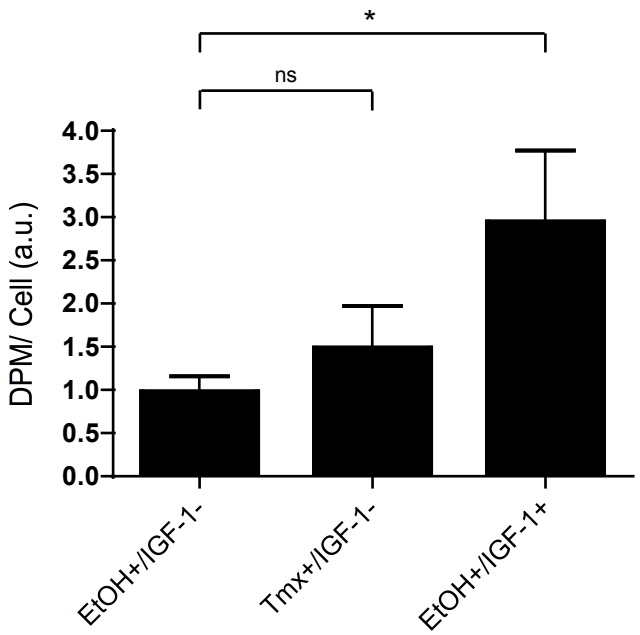

Figure 5.3 IGF-1 increases de novo lipogenesis from extracellular pyruvate

Aphidicolin arrested NSΔRafER cells were treated as indicated for 4hrs before [2-^{14}C] pyruvate was added to the cell culture medium. Cells were left for a further 4hrs before cell lipids were extracted and the incorporation of radiolabel into cellular lipids measured by scintillation counting. Bar chart shows ^{14}C incorporation into the lipid phase (as Disintegrations per Minute (DPM)) normalised to cell number and shows the mean +SEM of 3 experiments. One-Way Repeated Measures ANOVA, $p<0.05$, post-hoc Newman-Keuls as indicated on the graph.

In conclusion: IGF-1 drives expression of the mature nuclear forms of SREBP-1 and SREBP-2 and their downstream targets FASN and HMGCoR, rate limiting enzymes in de novo lipogenesis. This is consistent with published findings from other groups (Du et al., 2006, Luu et al., 2012, Smith et al., 2008). Although Raf kinase drives a slight increase in mature nuclear SREBP-2, there is no significant effect of downstream mRNA expression of FASN and HMGCoR. Consistent with this, IGF-1, and not Raf kinase activation, increased the incorporation of extracellular radiolabeled pyruvate, a precursor substrate for de novo lipogenesis, into cellular lipids. These findings correlate with the IGF-1 specific increase in cell volume and suggest de novo lipogenesis might be required for IGF-1 dependent cell volume addition.

5.2 IGF-1 Dependent Cell Volume Addition Requires SREBP-2 and is Inhibited by Inhibitors of De Novo Lipogenesis

To investigate a functional role for the SREBPs in the regulation of cell volume, siRNAs were used to knock down SREBP-1 and SREBP-2 prior to IGF-1 treatment/ Raf kinase activation. Transfection complexes were applied for 18 hours to cells seeded in normal Schwann cell medium (containing 3% FCS). The cells were then medium changed into Minimal Medium plus aphidicolin for 24 hours before factors (IGF-1 or Tmx) were added in fresh Minimal Medium plus aphidicolin. Cell volume was quantified using the Coulter Counter after a further 24 hours. RNA was collected at the end of the assay to quantify knockdown efficiency by RT-qPCR (Materials & Methods 2.3). The two SREBP-1 isoforms (SREBP-1a and -1c) were not individually targeted in this study; the siRNAs silence both isoforms. Two distinct oligos that recognise opposite ends of each SREBP mRNAs were used to reduce the chance of drawing conclusions based on off-target effects.

As can be seen in Figure 5.4 A, silencing SREBP-2 significantly inhibited cell volume addition downstream of IGF-1 and also reduced the volume of control (EtOH+/IGF-1-) and Raf kinase activated cells (Tmx+/IGF-1-). This suggests SREBP-2 is required for the maintenance and IGF-1 dependent addition of cell volume. Figure 5.4 B i demonstrates SREBP-2 mRNA expression was reduced to ~20% of the scrambled control for all three

conditions, using either oligo. Confirming that the siRNAs were not also non-specifically silencing SREBP-1, the mRNA expression of SREBP-1a was not reduced by the SREBP-2 siRNA oligo's (Figure 5.4 B ii). Consistent with a role for de novo lipogenesis in the regulation of cell volume downstream of SREBP-2, silencing SREBP-2 using either siRNA oligo inhibited mRNA expression of HMGCoR in all three conditions (Figure 5.5 A). The mRNA levels of FASN were also reduced by both siRNA oligo's in IGF-1 treated cells (Figure 5.5 B, EtOH+/IGF-1+), suggesting that SREBP-2 is required for FASN expression downstream of IGF-1. Given that cell volume was reduced in all three conditions, this may suggest sterol synthesis has a more significant role than fatty acid synthesis in the maintenance of cell volume. Differences in the extent to which target gene mRNA is reduced after SREBP-2 silencing between the different growth factor conditions (control, Raf kinase activation and IGF-1 treatment) and the two siRNA oligos may reflect differences in SREBP-2 activity between the growth factor conditions and/ or efficacy of SREBP-2 knockdown.

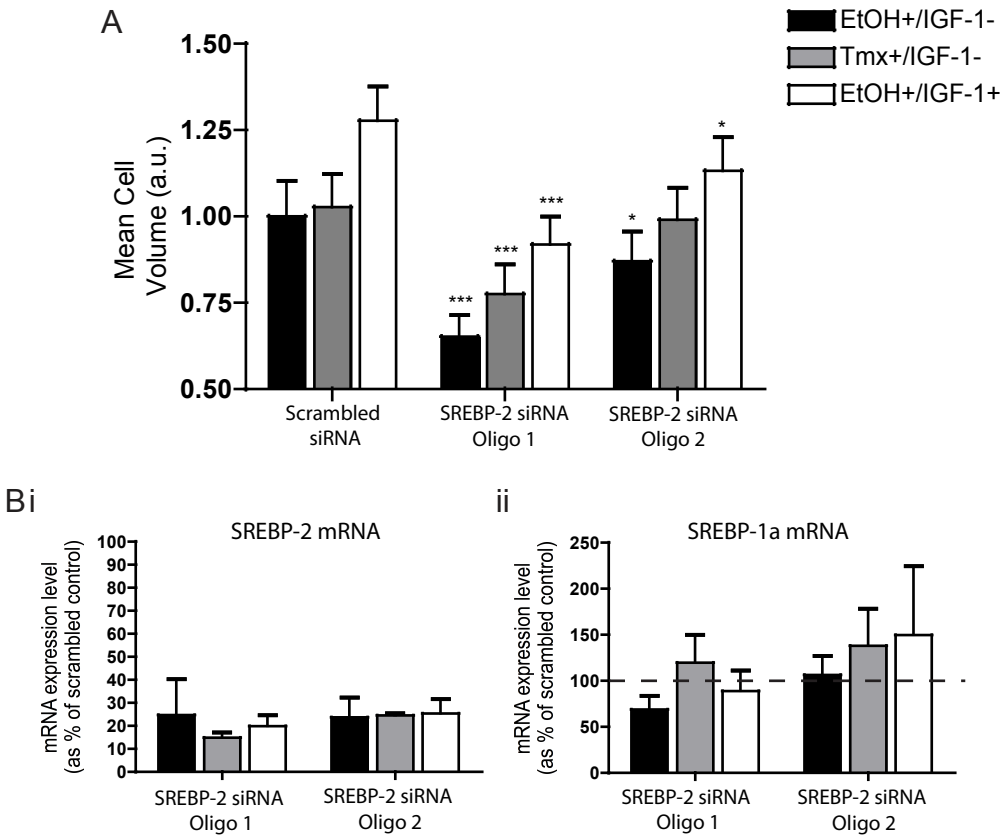

Figure 5.4 siRNA knockdown of SREBP-2 blocks IGF-1 dependent cell volume addition and reduces the volume of control (no factor) and Raf kinase activated cells

NSΔRafER cells were transfected with siRNAs as indicated in normal (3% FCS) Schwann cell medium for 18hrs then transferred into defined (no factor) conditions plus aphidicolin for 24hrs before factors (Tmx or IGF-1) were added as indicated for a further 24hrs. Final cell volume was quantified using a Coulter Counter.

A) Quantification of mean cell volume. Bar chart shows mean +SEM of 3 experiments. Two-Way ANOVA, siRNA $p<0.001$. Post hoc Bonferroni compared to Scrambled control, for each growth factor condition, as indicated on the graph.

B) i) SREBP-2 and ii) SREBP-1a mRNA expression level analysed by RT-qPCR and normalised to B2M as a loading control. Total RNA was collected at the end of the assay when cell volume was quantified.

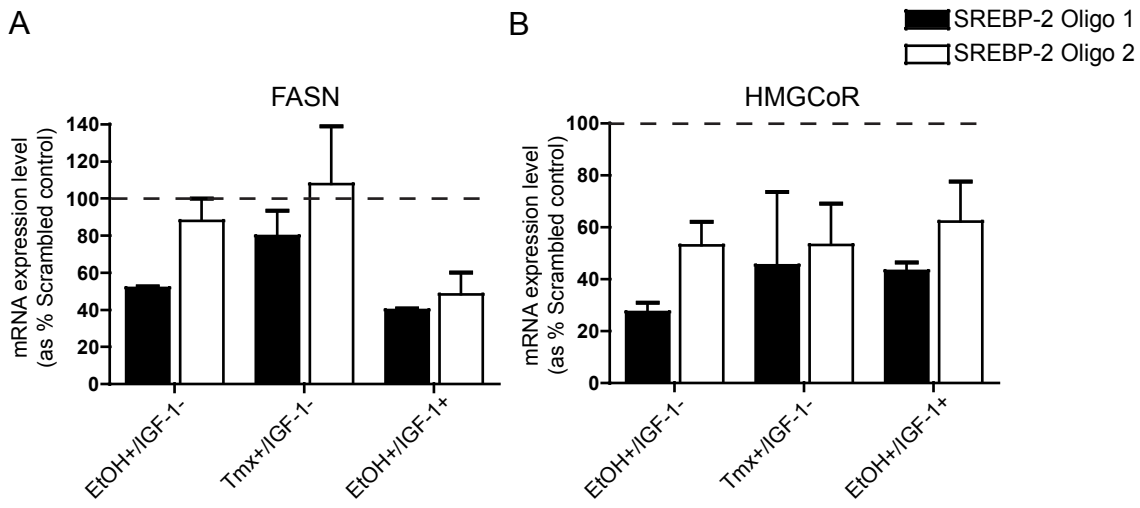

Figure 5.5 mRNA levels of the SREBP targets FASN & HMGCoR after siRNA knockdown of SREBP-2

NSΔRafER cells were transfected with siRNAs as indicated in normal (3% FCS) Schwann cell medium for 18hrs then transferred into defined (no factor) conditions plus aphidicolin for 24hrs before factors (Tmx or IGF-1) were added as indicated for a further 24hrs before total RNA was extracted. mRNA levels of the indicated genes were analysed by RT-qPCR and normalised to B2M as a loading control. Bar charts show mean mRNA expression level as % of the Scrambled control. Dashed line represents 100%, i.e. expression in the Scrambled control.
A) FASN mRNA.
B) HMGCoR mRNA.
Bar charts show mean +SEM of 3 experiments.

In contrast to SREBP-2, siRNAs targeting SREBP-1 had no significant effect on IGF-1 dependent cell volume addition, or the cell volume of control (EtOH+/IGF-1-) or Raf kinase activated cells (Tmx+/IGF-1-) (Figure 5.6 A). Silencing SREBP-1 reduced SREBP-1a mRNA expression to ~20-60% and SREBP-1c to ~10-50% of the scrambled controls (Figure 5.6 B). Similarly, knockdown of SREBP-1 did not reduce the mRNA expression levels of FASN or HMGCoR (Figure 5.7). The increases in FASN and HMGCoR mRNA expression seen in some growth factor conditions and/ or one or other siRNA oligo may reflect differences in the efficacy of SREBP-1 knockdown combined with compensation by SREBP-2 activity. Together, these results may suggest SREBP-1 is dispensable for the regulation of Schwann cell volume. This is not implausible, given that the different isoforms have been shown to be differentially regulated and to differentially regulate target genes in different cell types (Amemiya-Kudo et al., 2002, Horton et al., 2002, Horton et al., 2003a, Shimano et al., 1997a). In adipocytes, for example, SREBP-1c does not drive lipogenic gene expression (Sekiya et al., 2007, Shimomura et al., 1998). However it is possible there was not sufficient knockdown of SREBP-1 at the protein level. The amount of cell material required for the SREBPs to be detected at the protein level limited this investigation- it is not clear whether this is due to low levels of SREBP-1 expression, or poor antibody quality. This analysis is required to conclude whether SREBP-1 is non-essential for cell volume regulation in the Schwann cell. It is also possible the loss of one or other SREBP-1 isoform was compensated by the enhanced activity of SREBP-2- as occurs in the liver of mice that have lost functional SREBP-1a and -1c (Shimano et al., 1997b).

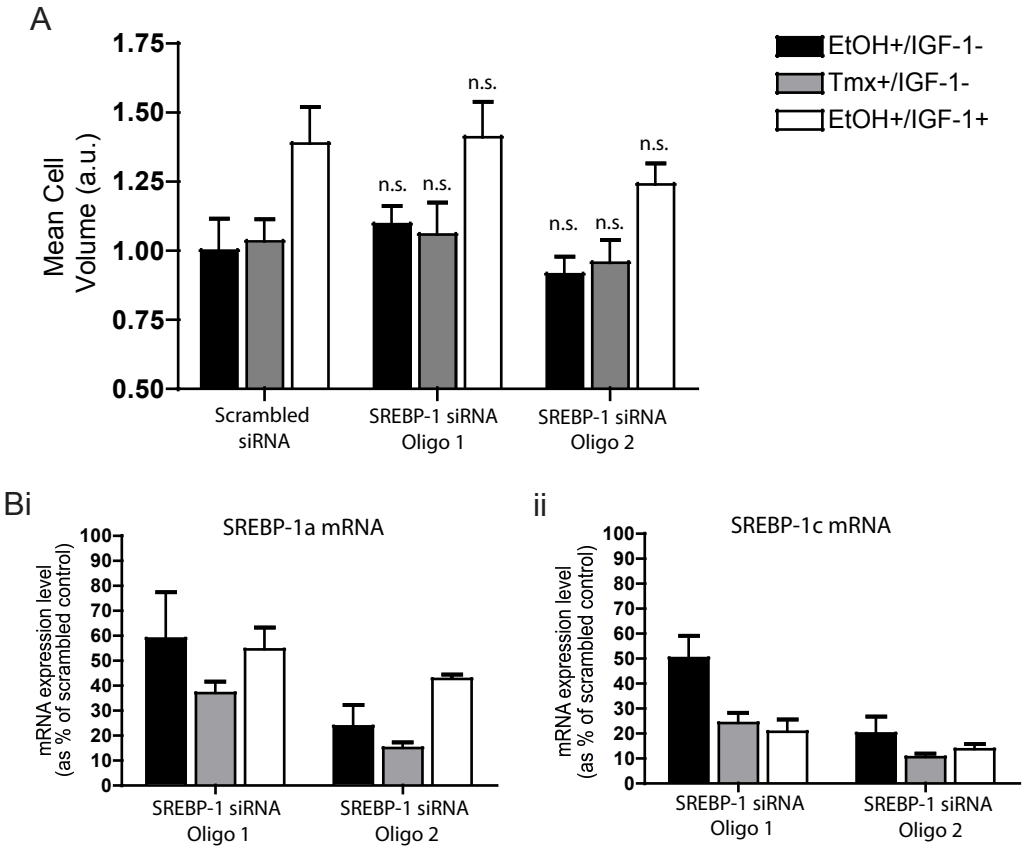

Figure 5.6 siRNA knockdown of SREBP-1 does not inhibit cell volume

NSΔRafER cells were transfected with siRNAs as indicated in normal (3% FCS) Schwann cell medium for 18hrs then transferred into defined (no factor) conditions plus aphidicolin for 24hrs before factors (Tmx or IGF-1) were added as indicated for a further 24hrs. Final cell volume was quantified using a Coulter Counter.
A) Quantification of mean cell volume. Bar chart shows mean +SEM of 3 experiments. Two-Way ANOVA, Growth Factor $p<0.001$. Post hoc Bonferroni compared to Scrambled control, for each growth factor condition, as indicated on the graph.
B) i) SREBP-1a and ii) SREBP-1c mRNA expression level analysed by RT-qPCR and normalised to B2M as a loading control. Total RNA was collected at the end of the assay when cell volume was quantified.

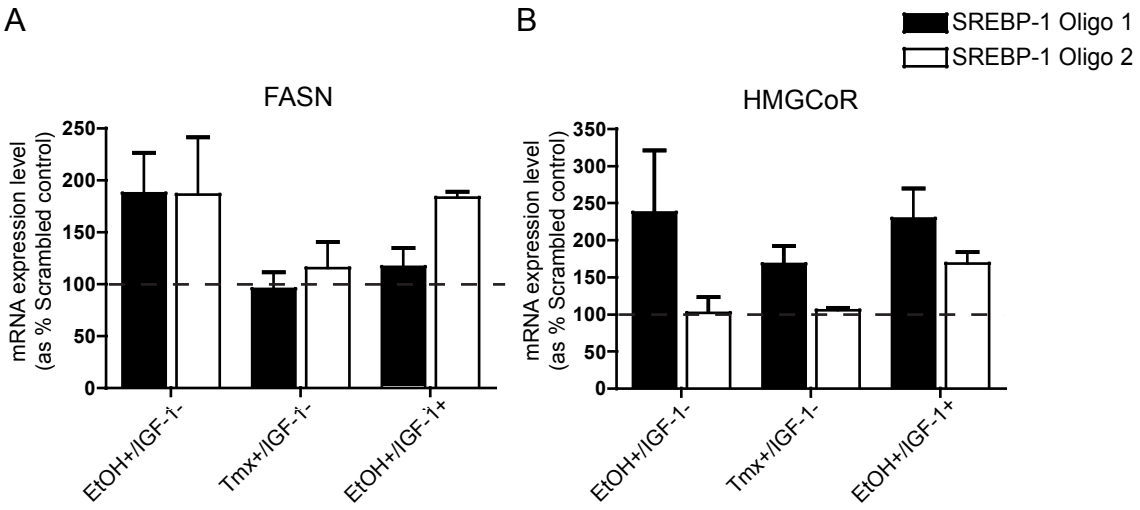

Figure 5.7 mRNA levels of the SREBP targets FASN & HMGCoR after siRNA knockdown of SREBP-1

NSΔRafER cells were transfected with siRNAs as indicated in normal (3% FCS) Schwann cell medium for 18hrs then transferred into defined (no factor) conditions plus aphidicolin for 24hrs before factors (Tmx or IGF-1) were added as indicated for a further 24hrs before total RNA was extracted. mRNA levels of the indicated genes were analysed by RT-qPCR and normalised to B2M as a loading control. Bar charts show mean mRNA expression level as % of the Scrambled control. Dashed line represents 100%, i.e. expression in the Scrambled control.
A) FASN mRNA.
B) HMGCoR mRNA.
Bar charts show mean +SEM of 3 experiments.

HMGCoR catalyses the rate limiting step of sterol synthesis- the production of mevalonate. Other isoprenoids can also be synthesised from mevalonate, which have roles including being used for post-translational protein modification (prenylation). To investigate more directly a role for HMGCoR in the regulation of cell volume, the HMGCoR inhibitor simvastatin was used. Simvastatin (5μm) was added to cells 30 minutes prior to the addition of factors (IGF-1 or Tmx) and cell volume was assayed after a further 24 hours. As shown in Figure 5.8 A, simvastatin significantly inhibited IGF-1 (EtOH+/IGF-1+) dependent cell volume addition and reduced the volume of control (EtOH+/IGF-1-) and Raf kinase activated (Tmx+/IGF-1-) cells, suggesting that HMGCoR is indeed required both to maintain and add cell volume.

To try to determine whether there is also a role for de novo fatty acid synthesis in the regulation of cell volume in these conditions, the effect of two inhibitors of this pathway were also analysed: Cerulenin (7.5μg/ml), which inhibits FASN and HMGCoR to block both fatty acid and sterol/ isoprenoid synthesis, and C75 (3μg/ml), which inhibits FASN to specifically block fatty acid synthesis. Reassuringly, like simvastatin, cerulenin significantly blocked IGF-1 dependent cell volume addition (Figure 5.8 B). Cerulenin also appeared to reduce the volume of control (EtOH+/IGF-1) and Raf kinase activated (Tmx+/IGF-1-) cells, but these reductions are not statistically significant. IGF-1 dependent cell volume addition was also slightly but significantly blocked using C75, but the volume of control or Raf kinase activated cells was unaffected (Figure 5.8 C). These results are consistent with a role for de novo lipogenesis in the regulation of Schwann cell volume, although it must be noted that the efficacy of the inhibitors was not tested.

The results using cerulenin and C75 are also difficult to interpret because these inhibitors made the cells incredibly unhealthy- this was apparent when cell protein mass was quantified using the fluorescent S. Ester label (Section 3.1); cells treated with cerulenin and, in particular, C75 were highly vacuolar with ‘strings’ of labelling through the cell (Figure 5.9). Although this may be a direct consequence of blocking fatty acid synthesis, it also raised the concern these inhibitors were having indirect toxic side effects. Cells treated with simvastatin showed protein staining and morphology similar to the control cells.

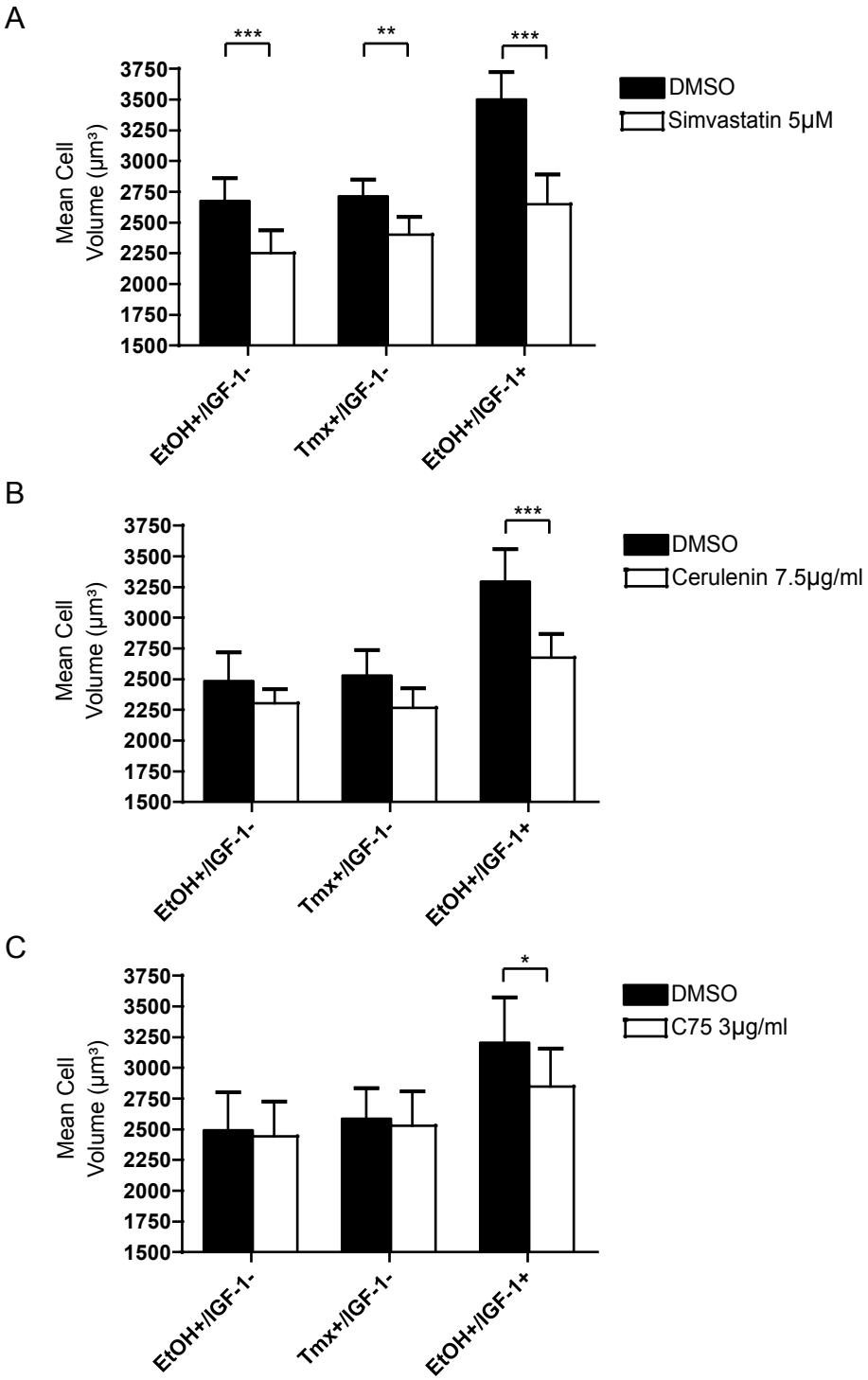

Figure 5.8 Addition of volume is blocked by inhibitors that block fatty acid and/ or sterol synthesis

Aphidicolin arrested NSΔRafER cells were treated as indicated +/- inhibitors for 24hrs before cell volume was quantified using a Coulter Counter. Bargraphs show mean cell volume +SEM.
A) +/- Simvastatin (5µM), an inhibitor of HMGCoR.
B) +/- Cerulenin (5µg/ml), an inhibitor of FASN and HMGCoR.
C) +/- C75 (3µg/ml), an inhibitor of FASN.
Bar charts show mean +SEM of A) and C) 4 and B) 5 experiments. Repeated Measures Two-Way ANOVA A) DMSO vs Inhibitor $p<0.001$, Interaction $p<0.001$, B) DMSO vs Inhibitor $p<0.001$, Interaction $p<0.05$ and C) DMSO vs Inhibitor $p<0.05$. Post hoc Bonferroni as indicated on the graphs.

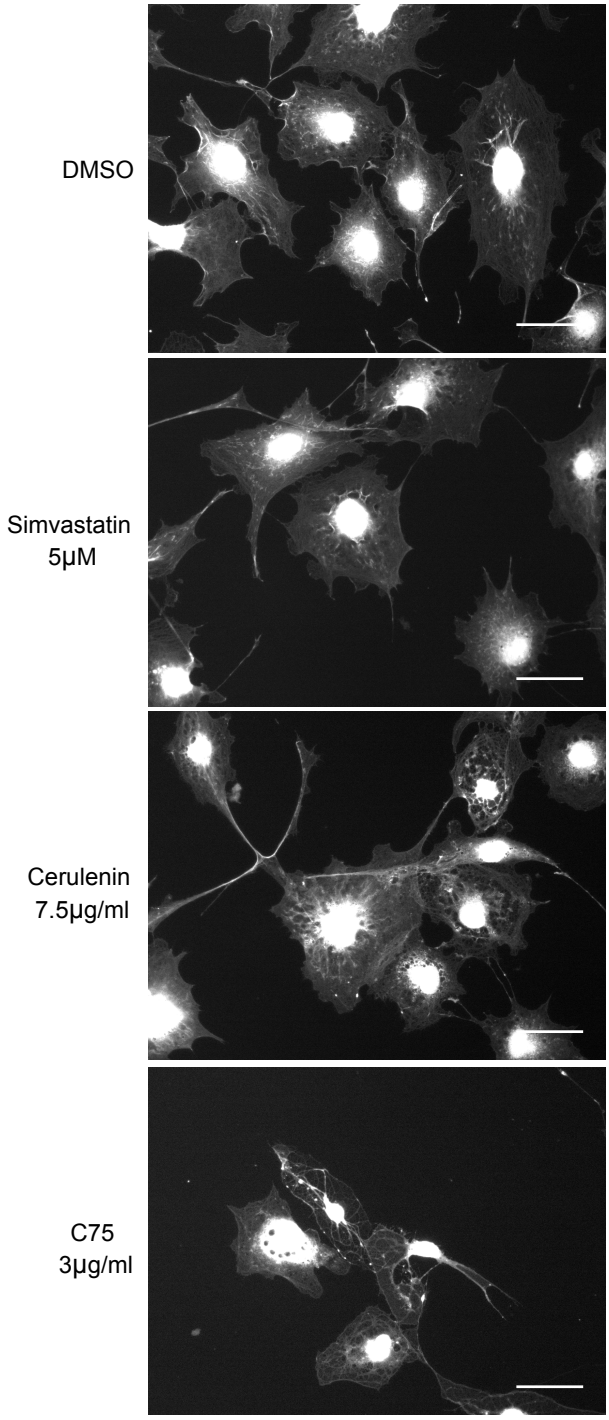

Figure 5.9 Cells look unhealthy in the presence of fatty acid synthesis inhibitors

Aphidicolin arrested NSΔRafER cells were treated +/- inhibitors as indicated for 24hrs +IGF-1 before being fixed and labelled with AlexaFlour647-succinimidyl ester. Total fluorescence intensity per cell was then quantified and taken to represent mean amount of protein per cell (a.u.). Representative widefield microscopy images of labelled cells. Scale bar = 25μm.

When cell protein mass was quantified from S. Ester labelling, it was found that cerulenin and C75 treatment significantly inhibited Raf kinase dependent addition of protein mass (Figure 5.10 B & C, Tmx+/IGF-1-). Cerulenin also significantly inhibited the addition of protein mass in the presence of IGF-1 (Figure 5.10 B, EtOH+/IGF-1+). Although C75 appeared to block IGF-1 dependent addition of protein mass, this was not statistically significant (Figure 5.10 C, EtOH+/IGF-1+). It is possible that de novo fatty acid synthesis is linked to the addition of cell protein mass as well as cell volume; for example, de novo lipogenesis may be required to maintain proper organelle membranes and is therefore indirectly required for the addition of protein mass during cell growth. However, non-specific toxic side effects of the inhibitors may also block cell protein mass.

In contrast to cerulenin and C75, simvastatin had no effect on protein mass (Figure 5.10 A). The finding that simvastatin blocked IGF-1 dependent cell volume addition, yet did not prevent IGF-1 dependent addition of protein mass, demonstrates once again that the addition of cell mass and volume can be uncoupled and therefore regulated independently during cell growth.

To summarise: SREBP-2 is required for the maintenance (control and Raf kinase activated cells) and IGF-1 dependent addition of Schwann cell volume. Consistent with this, chemically inhibiting HMGCoR also blocks the maintenance and IGF-1 dependent addition of Schwann cell volume. In contrast, SREBP-1 appears to be dispensable for the regulation of Schwann cell volume- however further investigations are required to confirm these results. It is possible that the regulation of protein mass is linked to fatty acid synthesis, but these findings require more careful investigation.

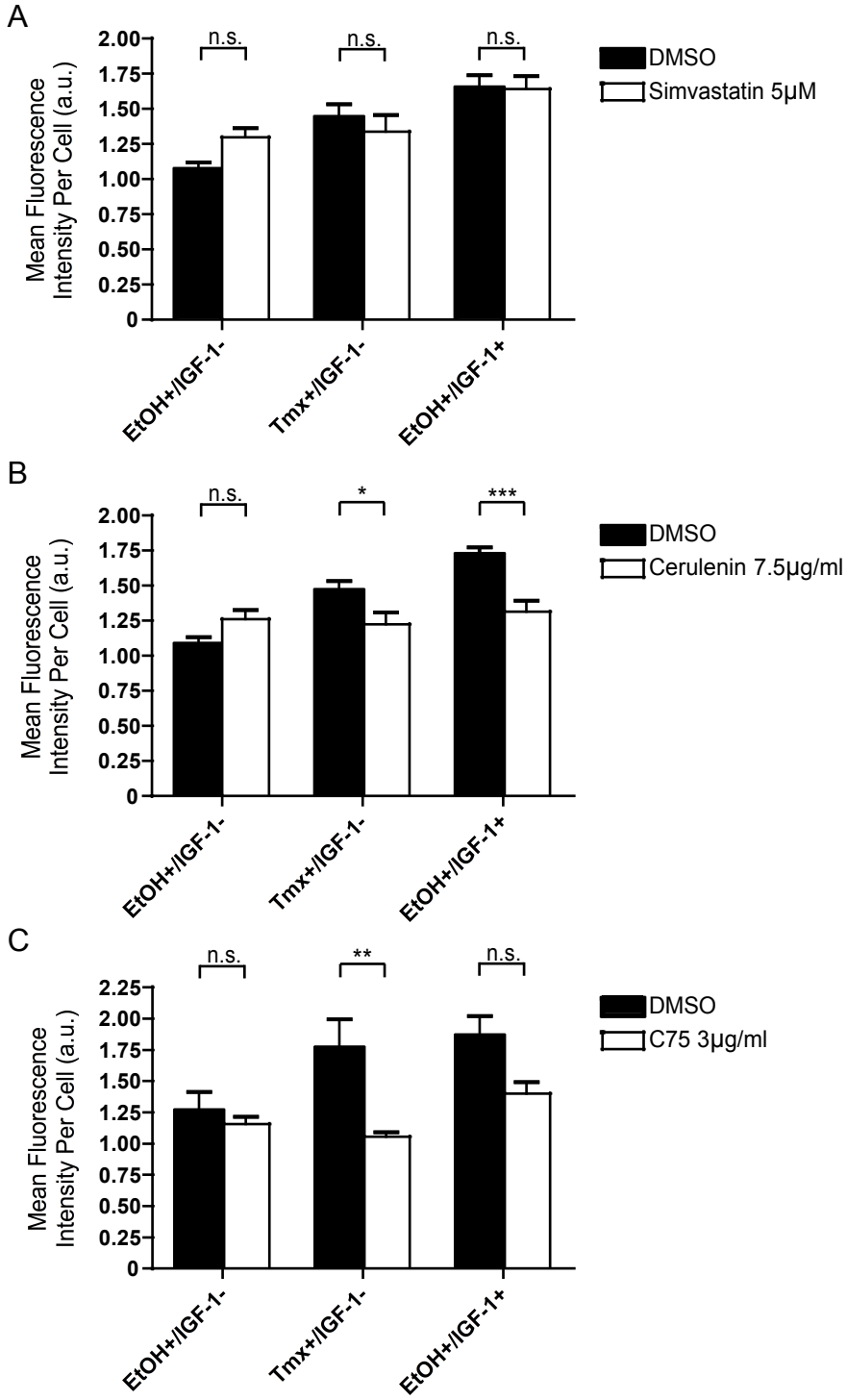

Figure 5.10 Addition of protein mass is blocked by inhibitors that block fatty acid synthesis

Aphidicolin arrested NSΔRafER cells were treated as indicated +/-inhibitors for 24hrs before being fixed and labelled with AlexaFlour647-succinimidyl ester. Total fluorescence intensity per cell was then quantified and taken to represent mean amount of protein per cell (a.u.).
A) +/- Simvastatin (5μM), an inhibitor of HMGCoR.
B) +/- Cerulenin (5μg/ml), an inhibitor of FASN and HMGCoR.
C) +/- C75 (3μg/ml), an inhibitor of FASN.
Bar charts show mean +SEM of 5 experiments, minimum 50 cells quantified per condition per experiment. Repeated Measures Two-Way ANOVA A) Growth Factor $p<0.001$, B) Growth Factor $p<0.001$, DMSO vs Inhibitor $p<0.05$, Interaction $p<0.001$ and C) Growth Factor $p<0.05$, DMSO vs Inhibitor $p<0.001$. Post hoc Bonferroni as indicated on the graphs.

5.3 Expression of Constitutively Active SREBP-2 or SREBP-1a is not Sufficient to Drive Addition of Cell Volume

The above results demonstrate that SREBP-2 is necessary for IGF-1 dependent cell volume addition. This raised the question of whether driving SREBP activity is sufficient to drive cell volume addition- either in the absence of any growth factor signalling, or in the presence of Raf kinase activation where certain biogenic pathways are already activated (those leading to the addition of protein mass).

Although this study did not find a role for SREBP-1 in the addition or maintenance of Schwann cell volume, this may because SREBP-1 (1a and -1c) were not sufficiently knocked down. In addition, even if there is not a role for endogenous SREBP-1 in the regulation of Schwann cell volume, this does not mean driving sustained activation of the protein would not have an effect. Moreover, SREBP-1a is the most potent transcriptional activator of the three SREBPs (Bengoechea-Alonso and Ericsson, 2007, Shimano et al., 1997a). Therefore, the response of Schwann cells to activation of both SREBP-1a and SREBP-2 with or without simultaneous activation of Raf kinase and/ or IGF-1 activation was investigated.

To do this, stable cell lines expressing a 4-hydroxytamoxifen (Tmx) inducible form of the mature SREBP-1a or SREBP-2 protein were generated in both normal Schwann cells and the NSΔRafER cells. The constructs were generated by the Schulze laboratory (London Research Institute) and contain the N-terminal domain of human SREBP-1a or SREBP-2 fused to a modified hormone-binding domain of the oestrogen receptor- the modification means the domain selectively binds to Tmx and does not bind it's natural ligand, 17β-oestradiol (Figure 5.11) (Littlewood et al., 1995). Stable cell lines were generated by retroviral transduction. The nomenclature that will be used to describe these cell lines throughout this section is as follows: Normal Schwann cells expressing the constructs are 'NS' and the NSΔRafER cells are 'NR' and these descriptions will be followed by ER.mSREBP1a or ER.mSREBP2 as appropriate. Expression of the SREBP fusion constructs in the NR cells means that upon Tmx addition, both Raf kinase and the expressed SREBP are activated.

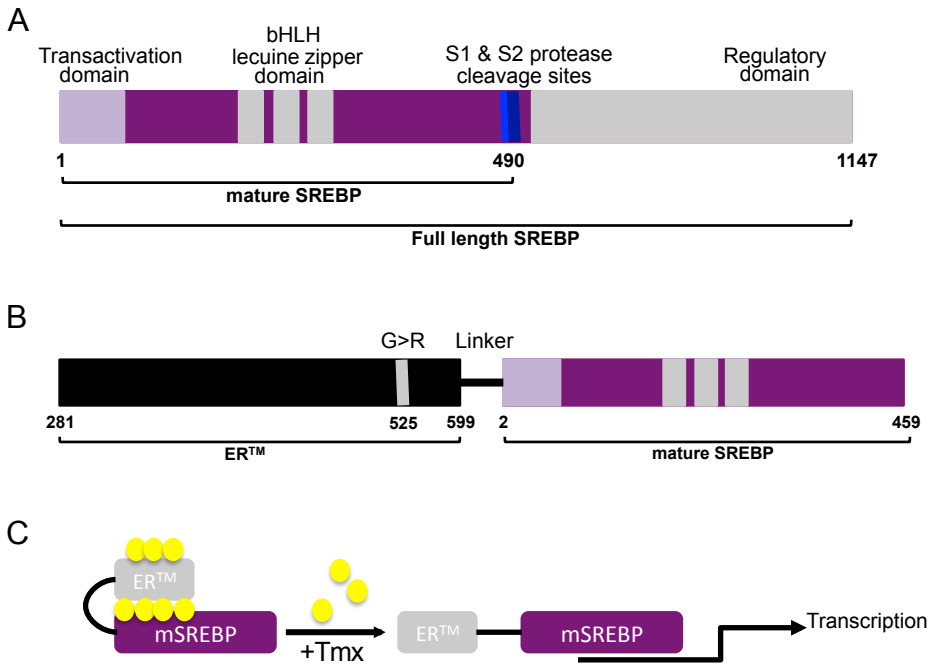

Figure 5.11 Schematic of the ER.mSREBP-1a and -2 fusion constructs

Schematics showing:
A) The full-length SREBP protein with the major domains highlighted. Amino acid numbers correspond to those in the human SREBP-1a protein.
B) The fusion protein constructs; the N-terminus of SREBP-1a or -2 (mature SREBP) is fused via a 20bp linker to a modified hormone-binding domain of the murine oestrogen receptor (ER). The modified ER domain has a point mutation (G>R at amino acid 525) that renders it unable to bind its native ligand, oestrogen, but still able to bind and be conformationally altered by 4-hydroxytamoxifen (Tmx) (Littlewood et al 1995). Mature SREBPs (mSREBPs) are active, nuclear localised transcription factors. The fusion proteins (ER.mSREBP-1a or -2) therefore enable Tmx dependent activation of mSREBP dependent transcription.
C) Activation of the ER.mSREBP proteins: The ER.mSREBPs are constitutively expressed. In the absence of tamoxifen the ER domain complexes with heatshock protein 90 (HSP90) molecules rendering the ER.mSREBP inactive. Binding of tamoxifen to the ER domain induces a conformational change that leads to dissociation of the HSP90 molecules and activation of the ER.mSREBP (i.e. activation of the mSREBP transcription factor function).

Western blot analyses were performed against the modified oestrogen receptor (anti-ERα) to confirm expression of the ER.mSREBP fusion proteins (Figure 5.12). The ER.mSREBP construct is ~80kDa, therefore in the NR ER.mSREBP cell lines the upper band represents the SREBP construct and the lower band represents the ~60kDa RafER construct (Figure 5.12 C & D). Tmx stabilises the RafER fusion protein and, because the ER.mSREBP band was so much stronger than the RafER band, the RafER ERα band was essentially only visible after Tmx treatment. Interestingly, simultaneous activation of the SREBPs and Raf kinase (i.e. +Tmx in the NR ER.mSREBP cells) also increased expression of the SREBP construct over time (Figure 5.12 C & D). Unlike the RafER, it is unlikely Tmx induced stabilisation of the protein, as activation of ER.mSREBP1a and 2 in the absence of Raf kinase activation (i.e. +Tmx to the NS ER.mSREBP cells) decreased the expression of the SREBP fusion protein (Figure 5.12 A & B). The SREBPs undergo activity dependent degradation, which may explain the latter observation (Hirano et al., 2001, Punga et al., 2006, Sundqvist et al., 2005, Sundqvist and Ericsson, 2003). These results suggest Raf/ ERK signalling specifically stabilises the construct; perhaps via activation of the transcriptional co-activator p300, which is an ERK target and is known to acetylate and stabilise the SREBPs (Giandomenico et al., 2003, Meissner et al., 2011, Wang et al., 2006). It may also reflect increased activity of the retroviral promoter. Reassuringly, strong induction of pERK was seen upon Tmx treatment of the NR cells expressing either construct (Figure 5.12 C & D), further demonstrating that cells continued to express the Tmx inducible Raf kinase construct.

There was a progressive band shift of the ER.mSREBP1a protein over time in the presence of simultaneous Raf kinase activation, which may suggest post-translational modification of the protein (Figure 5.12 C). Both SREBP-1a and -2 can be targets for ERK dependent phosphorylation, which enhances their transcriptional activity and this may be responsible for the observed mobility shift of the ER.mSREBP1a protein (Kotzka et al., 2004, Kotzka et al., 2000, Roth et al., 2000). Consistent with this hypothesis, no band shift was observed upon activation of the construct in the absence of a sustained Raf kinase signal (i.e. in the NS ER.mSREBP1a cells) (Figure 5.12 A). A similar band shift was not observed for ER.mSREBP2 upon simultaneous Raf kinase activation, however (Figure 5.12 D).

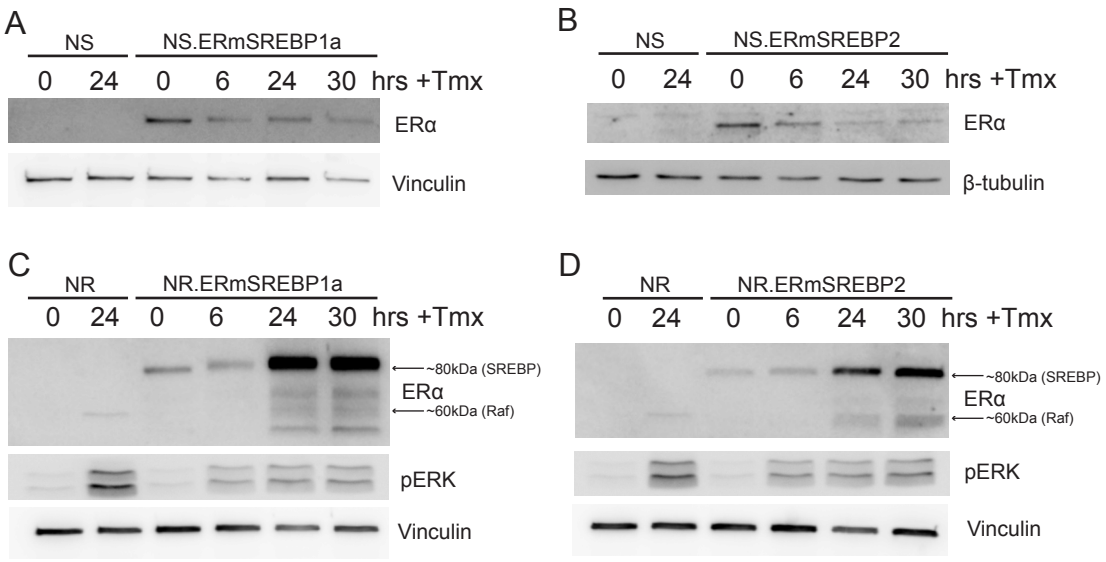

Figure 5.12 Expression of ER.mSREBP -1a and ER.mSREBP-2 in Normal Schwann (NS) and NSΔRafER (NR) cells

Cells were retrovirally transduced with ER.mSREBP -1a or ER.mSREBP-2 constructs. The ER.mSREBP expressing cell lines and the non-expressing controls were aphidicolin arrested before being treated with Tmx for times as indicated and cell lysates collected. Western blot analysis was performed against the ER domain of the constructs, using an anti-ERα antibody. Continued activity of the RafER construct in the NR cells was confirmed by western blot analysis against pERK1/2 (Thr202/Thr183).
A) NS.ERmSREBP1a cells and NS cell controls.
B) NS.ERmSREBP2 cells and NS cell controls.
C) NR.ERmSREBP1a cells and NR cell controls.
D) NR.ERmSREBP2 cells and NR cell controls.

The Western blot analyses demonstrated that at least some cells in the population express the SREBP fusion constructs. However, for an SREBP dependent change in cell volume to be observed by Coulter Counter analyses, a large proportion of the population must express the protein and therefore be subject to the induced change in cell volume. To determine the proportion of cells that expressed the SREBP fusion construct anti-ERα immunofluorescence analyses were performed, cells cultured in normal Schwann cell medium (3% FCS) were treated with Tmx or the control solvent ethanol (EtOH) and fixed and immunostained after 24 hours.

ERα labelling was visible in cells expressing the constructs as intense nuclear staining after Tmx treatment (Figure 5.13 A i & B i). Although in the NR cells both the RafER and ER.mSREBP fusion proteins would have been detected by the antibody, intense nuclear staining after Tmx treatment was seen only in NR ER.mSREBP cells (Figure 5.13 B i). The proportion of ERα positive nuclei after Tmx treatment was quantified and taken to represent the proportion of ER.mSREBP expressing cells in each cell line. These analyses showed that ~60% of the NS ER.mSREBP-1a and NS ER.mSREBP-2 populations (Figure 5.13 A ii), >85% of the NR ER.mSREBP1a and >60% of the NR ER.mSREBP2 populations (Figure 5.13 B ii) were positive for nuclear ERα.

To confirm the ERα staining in the NR ER.mSREBP cells, where there was the potential confounding effect of the simultaneous RafER expression, anti-SREBP-1 and anti-SREBP-2 immunofluorescence analyses were also performed. Strong nuclear staining was observed in both NR ER.mSREBP cell lines after Tmx treatment and labelling with the corresponding SREBP antibody, but not in NR cells lacking the construct (Figure 5.14). As for the anti-ERα immunofluorescence, over 50% of the NR ER.mSREBP-1a and -2 populations showed positive nuclear staining with their corresponding antibody (Figure 5.14 A ii & B ii, respectively). These values should be sufficient for any SREBP dependent change in cell volume to be detected in Coulter Counter analyses of these populations.

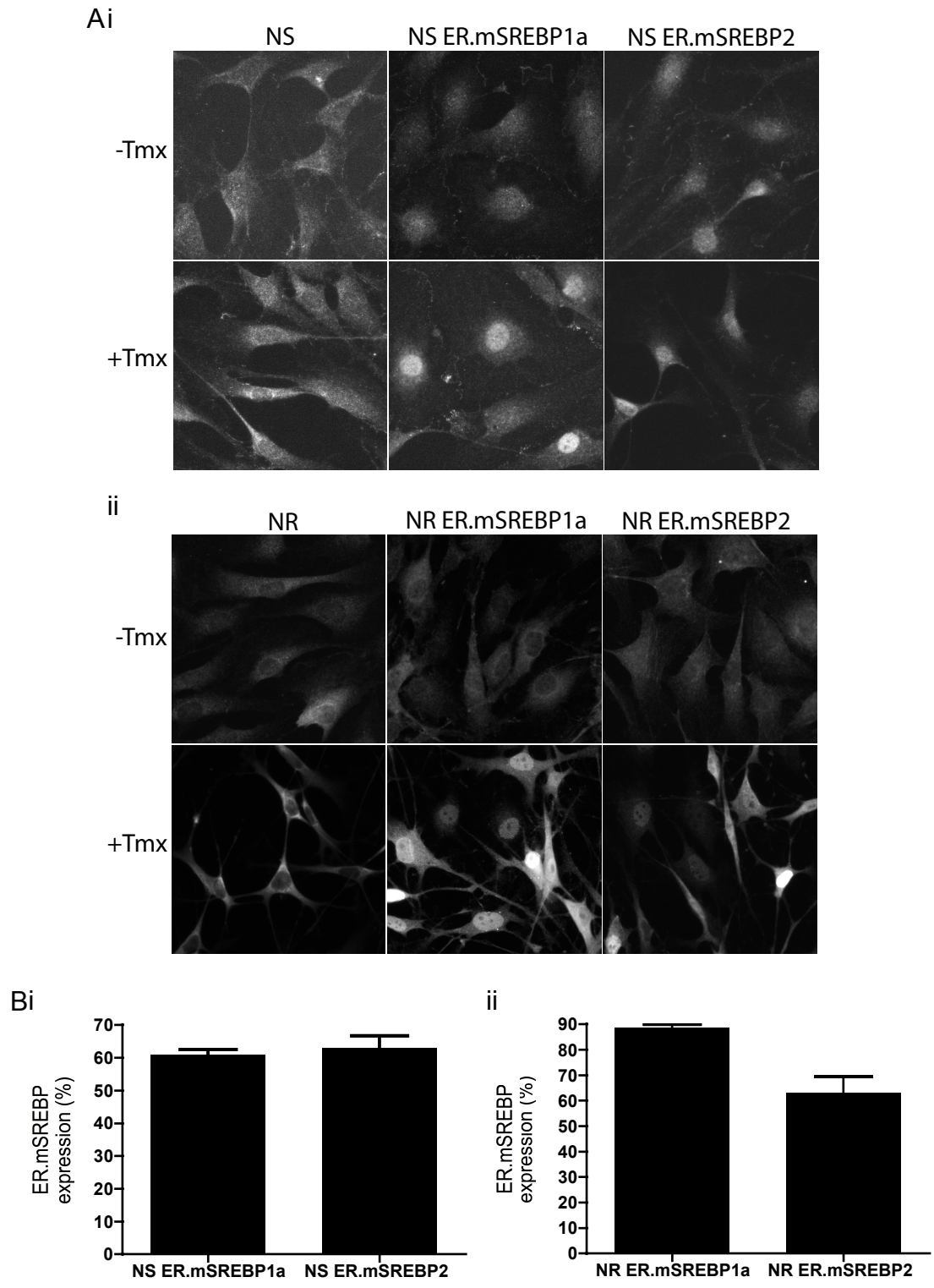

Figure 5.13 Anti-ERα immunofluorescence demonstrates the proportion of cells expressing the ER.mSREBP-1a or -2 construct

NSΔRafER (NR) or normal Schwann (NS) cells that had been transduced with retroviral ER.mSREBP -1a or -2 constructs, as indicated, were treated +/-Tmx in 3%FCS for 24hrs before being processed for anti-ERα immunofluorescence to label the expressed ER.mSREBP constructs.

A) Representative widefield microscopy images of labelled cells +/- Tmx i) Normal Schwann (NS) cells and ii) NSΔRafER (NR) cells.

B) Quantification of the proportion of cells positive for nuclear anti-ERα labelling, i) Normal Schwann (NS) cells and ii) NSΔRafER (NR) cells. Bar charts show mean +SEM of 3 experiments.

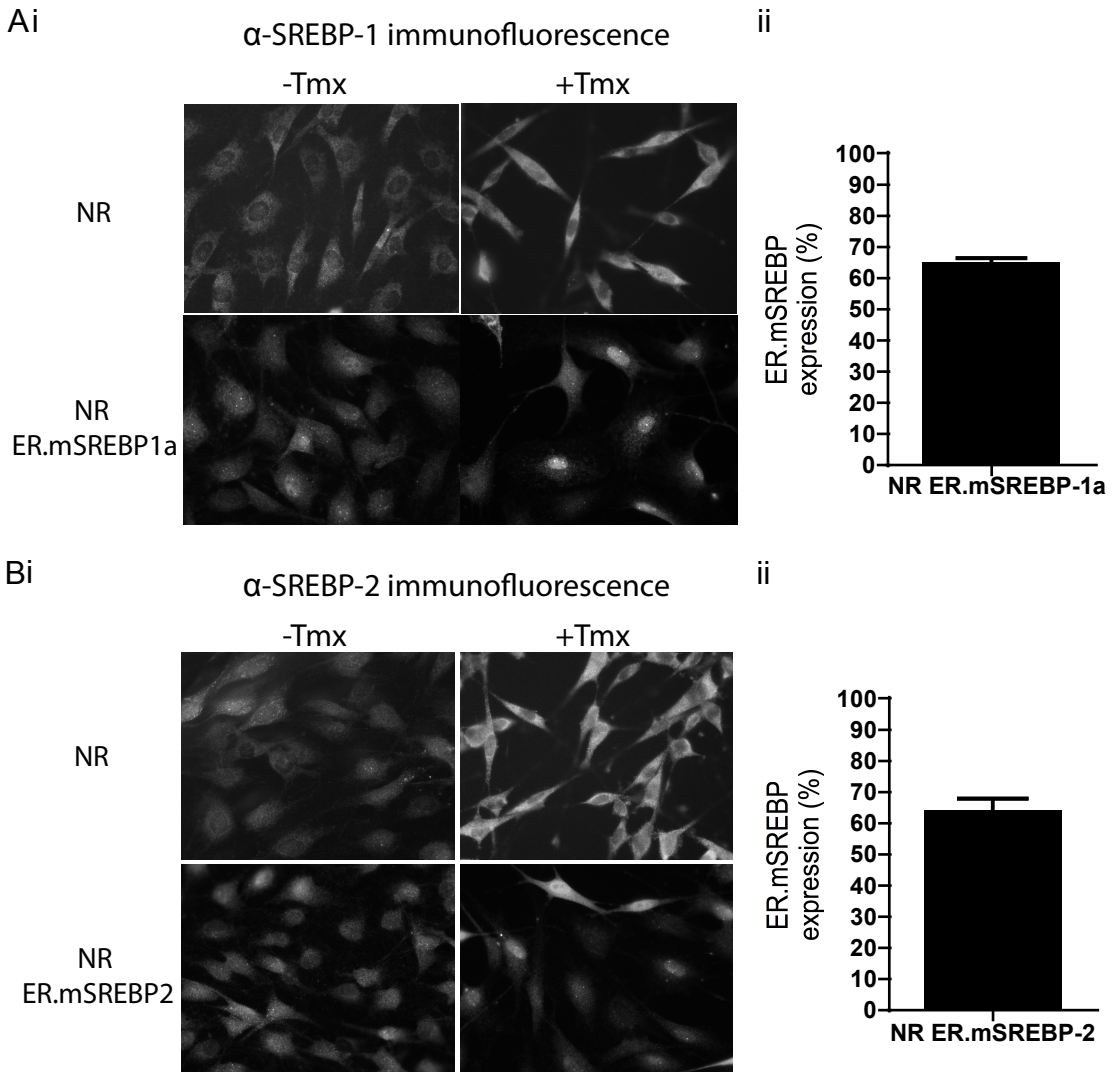

Figure 5.14 Anti-SREBP immunofluorescence demonstrates the proportion of cells expressing the ER.mSREBP-1a or -2 construct

NSΔRafER (NR) cells that had/ not been transduced with retroviral ER.mSREBP -1a or -2 constructs, as indicated, were treated +/-Tmx in 3%FCS for 24hrs before being processed for immunofluorescence to label the expressed ER.mSREBP constructs, as indicated.
A) Anti-SREBP-1 immunofluorescence i) Representative widefield microscopy images of labelled cells and ii) Quantification of the proportion of NR ER.mSREBP1a cells positive for nuclear anti-SREBP1 labelling. Bar chart shows mean +SEM of 3 experiments.
B) Anti-SREBP-2 immunofluorescence i) Representative widefield microscopy images of labelled cells and ii) Quantification of the proportion of NR ER.mSREBP-2 cells positive for nuclear anti-SREBP1 labelling. Bar chart shows mean +SEM of 3 experiments.

To confirm the constructs are active, the mRNA levels of the SREBP target genes FASN and HMGCoR were analysed by RT-qPCR after addition of Tmx to activate the constructs (Figure 5.15 & 5.16). These experiments reverted back to the standard cell culture protocol: cells were seeded and then cell-cycle arrested using aphidicolin in normal Schwann cell medium for 24 hours before being transferred into Minimal Medium plus aphidicolin for 24 hours. Cells were then treated with factors (IGF-1 and/ or Tmx) for 6 hours before total RNA was collected for analysis by RT-qPCR. Tmx treatment induced FASN mRNA expression in all 4 cell lines, indicating that the constructs are active (Figure 5.15 Tmx+/IGF-1- & EtOH+/IGF-1+). This induction was ~ equivalent to IGF-1 treatment. In 3 of the 4 cell lines SREBP activation also induced HMGCoR mRNA expression to a level ~equivalent to IGF-1 treatment (Figure 5.16). The reason HMGCoR mRNA expression was not increased compared to control in Tmx treated NS ER.mSREBP-1a cells is not clear- it may suggest that (in the absence of simultaneous Raf kinase activation) SREBP-1a does not act strongly on the HMGCoR promoter in Schwann cells (Figure 5.16 A i). Interestingly, there seemed to be an additive effect of combined IGF-1 treatment and SREBP activation on FASN and HMGCoR expression, in both the presence and absence of simultaneous Raf kinase activation (Figure 5.15 & 5.16, Tmx+/ IGF-1+). Quantifying the mRNA expression of FASN in normal Schwann cells +/- Tmx treatment and/ or IGF-1 stimulation confirmed the increase in mRNA levels of SREBP target genes was not an artefact of Tmx treatment (Figure 5.17).

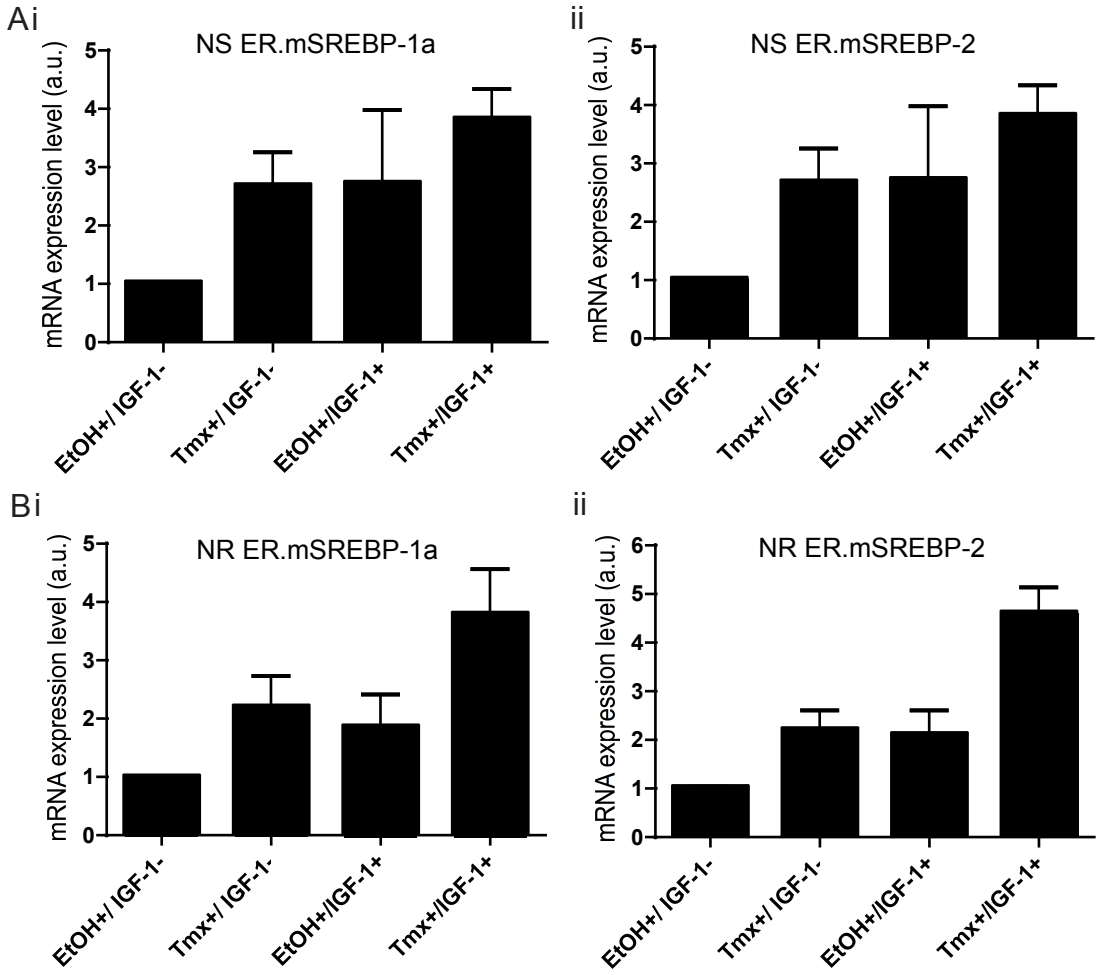

Figure 5.15 Activation of ER.mSREBP-1a or -2 induces the mRNA expression of FASN, a key SREBP target gene

Aphidicolin arrested NS ER.mSREBP cells were treated as indicated for 6hrs before total RNA was extracted. mRNA levels were analysed by RT-qPCR and normalised to B2M as a loading control; FASN mRNA levels are expressed relative to EtOH+/IGF-1-.
A) NS i) ER.mSREBP-1a cells and ii) ER.mSREBP-2 cells.
B) NR i) ER.mSREBP-1a cells and ii) ER.mSREBP-2 cells.
Bar charts show mean +SEM of 3 experiments.

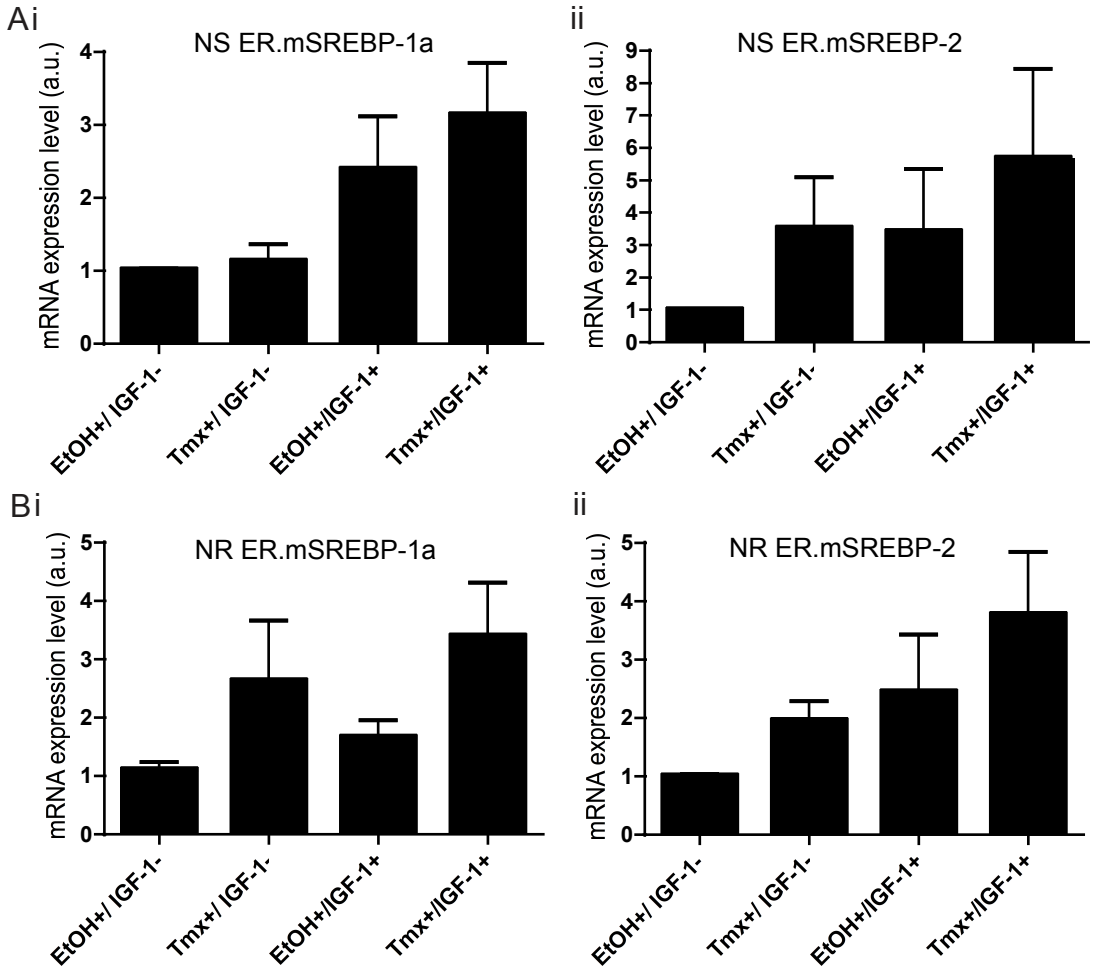

Figure 5.16 Activation of ER.mSREBP-1a or -2 can induce the mRNA expression of HMGCoR, a key SREBP target gene

Aphidicolin arrested NS & NR ER.mSREBP cells were treated as indicated for 6hrs before total RNA was extracted. mRNA levels were analysed by RT-qPCR and normalised to B2M as a loading control; HMGCoR mRNA levels are expressed relative to EtOH+/IGF-1-.
A) NS i) ER.mSREBP-1a cells and ii) ER.mSREBP-2 cells.
B) NR i) ER.mSREBP-1a cells and ii) ER.mSREBP-2 cells.
Bar charts show mean +SEM of 3 experiments.

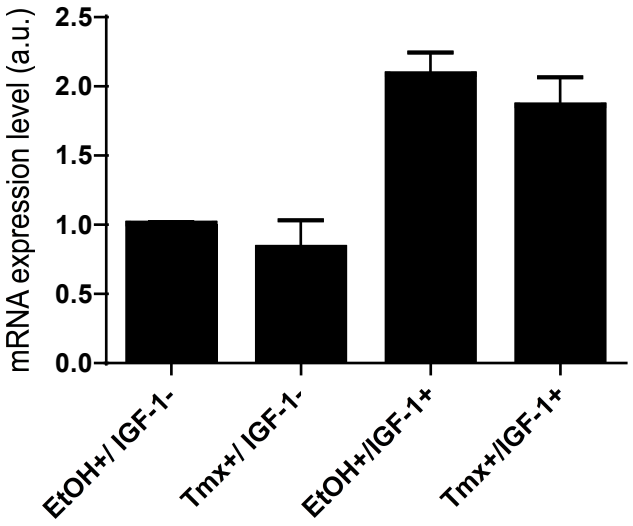

Figure 5.17 Tmx does not induce the mRNA expression of FASN, a key SREBP target gene

Aphidicolin arrested NS cells were treated as indicated for 6hrs before total RNA was extracted. FASN mRNA levels were analysed by RT-qPCR and normalised to B2M as a loading control; mRNA levels are normalised to EtOH+/IGF-1-. Bar charts show mean +SEM of 3 experiments.

Having demonstrated that the SREBP fusion proteins are expressed and can activate target gene expression, the effect of inducing SREBP activation on cell volume addition was assayed. NS ER.mSREBP and NR ER.mSREBP were treated according to the standard protocol, i.e. factors (Tmx and/ or IGF-1) were added to cells that were cell cycle arrested and in defined conditions (Minimal Medium). Cell volume was quantified by Coulter Counter analysis after 24 hours. Activation of SREBP-1a (Figure 5.18 A) or SREBP-2 (Figure 5.18 B) alone was not sufficient to drive addition of cell volume (Tmx+/IGF-1-) and did not synergise with IGF-1 to drive further addition of cell volume than the addition of IGF-1 alone (Tmx+/IGF-1+). Similarly, combined activation of Raf kinase and SREBP-1a (Figure 5.19 A) or SREBP-2 (Figure 5.19 B) was not sufficient to drive addition of cell volume (Tmx+/IGF-1-) and also did not synergise with IGF-1 to drive further addition of cell volume than the addition of IGF-1 alone (Tmx+/IGF-1+).

In conclusion, although IGF-1 dependent addition of cell volume and the maintenance of cell volume in the presence or absence of Raf kinase activation is dependent on SREBP-2 and HMGCoR (Section 5.2), activation of SREBP-1a or SREBP-2 does not seem to be sufficient to drive addition of cell volume- alone or in combination with Raf kinase activation- and does not synergise with IGF-1 to enhance IGF-1 dependent addition of cell volume. This suggests other factors also limit cell volume addition.

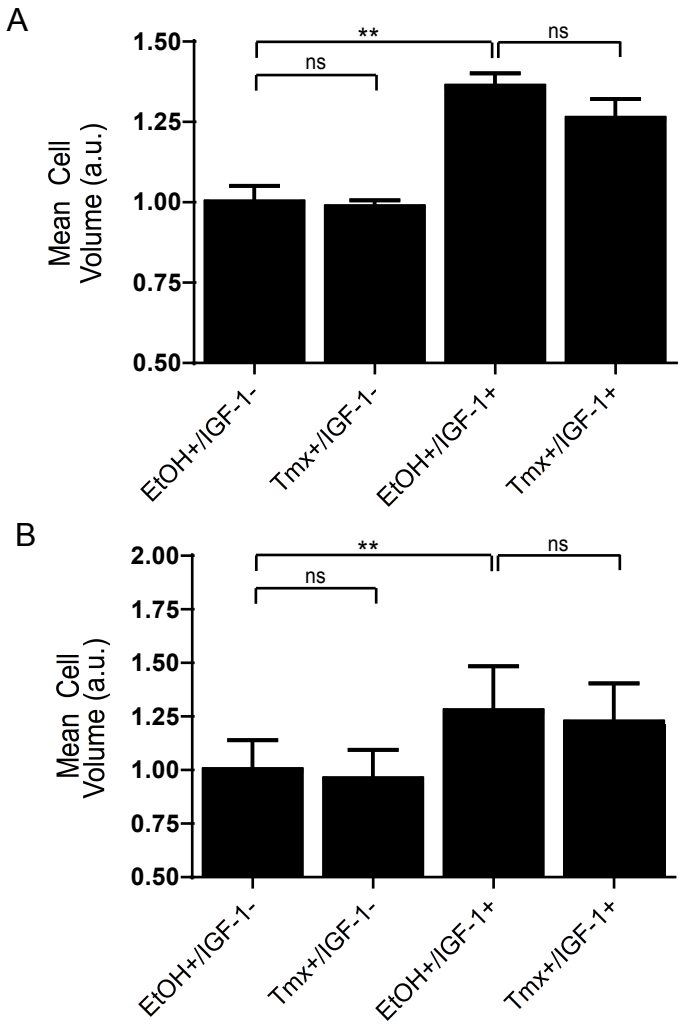

Figure 5.18 Activation of SREBP-1a or -2 has no effect on Schwann cell volume

Aphidicolin arrested NS ER.mSREBP -1a or -2 cells were treated as indicated before cell volume was quantified using a Coulter Counter. Bar charts show mean cell volume +SEM.
A) NS ER.mSREBP1a cells.
B) NS ER.mSREBP2 cells.
Bar charts show mean +SEM of 3 experiments. Repeated Measures One-Way ANOVA A) and B) $p<0.001$. Select post hoc Tukey's as indicated on the graphs.

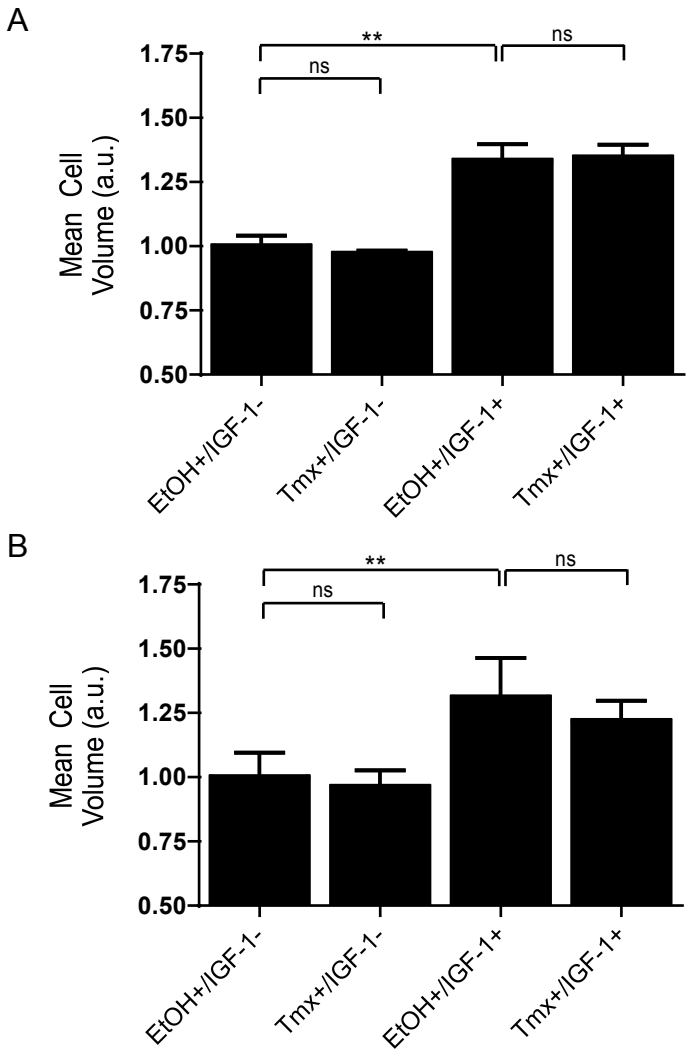

Figure 5.19 Activation of Raf kinase and SREBP-1a or -2 has no effect on Schwann cell volume

Aphidicolin arrested NR ER.mSREBP -1a or -2 cells were treated as indicated before cell volume was quantified using a Coulter Counter. Bar charts show mean cell volume +SEM.
A) NR ER.mSREBP1a cells.
B) NR ER.mSREBP2 cells.
Bar charts show mean +SEM of 3 experiments. Repeated Measures One-Way ANOVA A) and B) $p<0.001$. Select post hoc Tukey's as indicated on the graphs.

5.4 Addition of Fatty Acids and Cholesterol to the Cell Culture Medium (in a Chemically Defined Supplement) Does not Drive Cell Volume Addition

In the presence of growth factors, cells in vivo and *in vitro* will preferentially take up extracellular lipids to provide the substrates for new lipid synthesis, rather than undergo de novo lipogenesis (Goldstein and Brown, 1977, Bailey et al., 1972). De novo lipogenesis is metabolically expensive and preferential use of extracellular lipids is likely to preserve cell resources. Although there are essentially no exogenous lipids in the defined cell culture medium used in these studies, trace fatty acids will be bound to the bovine serum albumin (BSA) used to make the Minimal Medium supplement. This is because albumin is a fatty acid carrier protein in vivo and therefore, unless it has been delipidated, fatty acids can remain bound to albumin purified from animal sera. To determine whether these trace fatty acids have a significant effect on Schwann cell volume, the volume of cells cultured in Minimal Medium made with delipidated or standard BSA were compared by Coulter Counter analysis. As shown in Figure 5.20, the volume of control or IGF-1 treated Schwann cells was equivalent in Minimal Medium made using either type of BSA, demonstrating that BSA-bound fatty acids have no significant effect on Schwann cell volume in these conditions.

Although the results in the preceding section demonstrate that activating SREBP-1a or SREBP-2 (which would be predicted to induce de novo lipogenesis) is not sufficient to drive addition of cell volume, it was interesting to determine whether providing cells with exogenous lipid is sufficient to increase Schwann cell volume- in the presence or absence of Raf kinase activation or IGF-1 stimulation. Exogenous lipids were added in the form of a commercially available chemically defined lipid concentrate (Gibco) consisting of fatty acids and cholesterol in an aqueous mix with surfactants to solubilise the lipids and facilitate their uptake by the cell. A chemically defined lipid mixture was used because lipids purified from biological sources, such as serum, are potentially likely to contain traces of extracellular factors that could independently regulate cell volume. The final concentration of fatty acids in the cell culture medium after the supplement was added was ~equivalent to medium containing around 0.7% foetal calf serum (FCS) and the concentration of cholesterol was ~equivalent to that in 1.4% FCS, although it is not clear whether such a

comparison of concentrations is biologically relevant, because lipids in serum are found in different forms (bound to albumin for the fatty acids, or in lipoproteins for the cholesterol) to the way they are in this supplement (free) (Spector et al., 1980). The lipid concentrate was added in the defined (Minimal) medium 30 minutes prior to the addition of IGF-1 or Tmx and cell volume was quantified using the Coulter Counter after 24 hours. As can be seen in Figure 5.21 A, addition of the lipid supplement did not drive addition of cell volume in the control (EtOH+/IGF-1-) or Raf kinase activated (Tmx+/IGF-1-) conditions and had no effect on cell volume addition downstream of IGF-1.

Although the lipid supplement contains surfactants to optimise lipid entry into the cell, it may be that the supplement had no effect on cell volume because the cells could not take up and utilise the added lipids. As uptake of extracellular lipids represses de novo lipogenesis, the mRNA levels of FASN and HMGCoR were quantified by RT-qPCR 6 hours +/- the supplement, to indicate whether the cells were utilising the supplement's lipids. The presence of exogenous lipids significantly reduced the mRNA expression of both FASN and HMGCoR downstream of IGF-1, suggesting the lipids were utilised by IGF-1 treated cells (Figure 5.21 B). These results, together with the fact overexpression of the SREBPs did not affect Schwann cell volume (Section 5.3), indicate that factors other than lipid availability also limit IGF-1 volume addition.

FASN and HMGCoR expression was not reduced in control (EtOH+/IGF-1-) or Raf kinase activated (Tmx+/IGF-1-) cells, which may suggest the supplement was not utilised by these cells. However, it could also be that, in the absence of a direct block to their transcription, FASN and HMGCoR expression is already at basal levels in these cells and therefore will not be reduced even if extracellular lipids are taken up and utilised.

In conclusion, the addition of exogenous lipids in a chemically defined lipid concentrate (containing free fatty acids and cholesterol) is not sufficient to drive addition of Schwann cell volume in the presence or absence of Raf kinase activation or IGF-1 treatment, although the supplement does appear to be utilised in IGF-1 treated cells at least. It cannot be excluded that alternative lipids, higher concentrations of lipid and/ or lipids delivered in a more physiological manner, would increase cell volume.

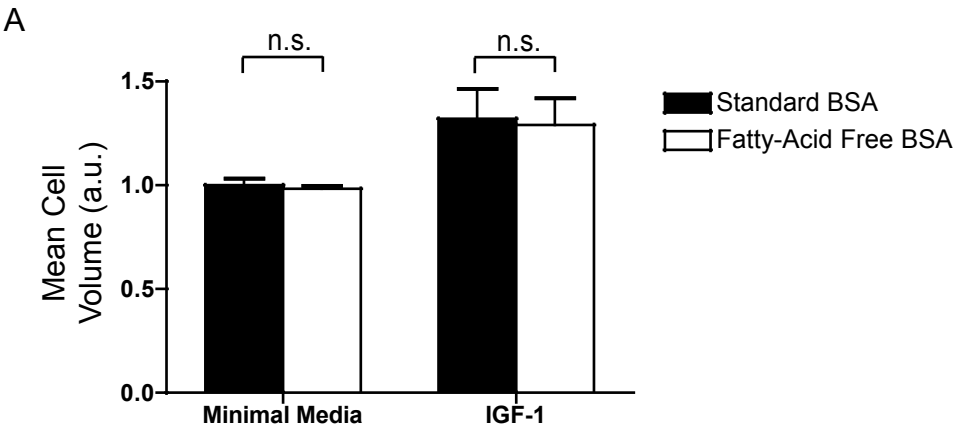

Figure 5.20 IGF-1 drives an increase in cell volume independent of residual fatty acids on the bovine serum albumin (BSA) used in the cell culture medium

Aphidicolin arrested NSΔRafER cells were treated as indicated for 24hrs before cell volume was quantified using a Coulter Counter.
A) Representative frequency distribution of cell volumes in the measured populations (μm^3).
B) Quantification of mean cell volume (μm^3). Bar chart shows mean + standard error of the mean (SEM) of 3 experiments, performed in duplicate per condition per experiment. Repeated Measures Two-Way ANOVA, Minimal Medium vs IGF-1 $p<0.05$.

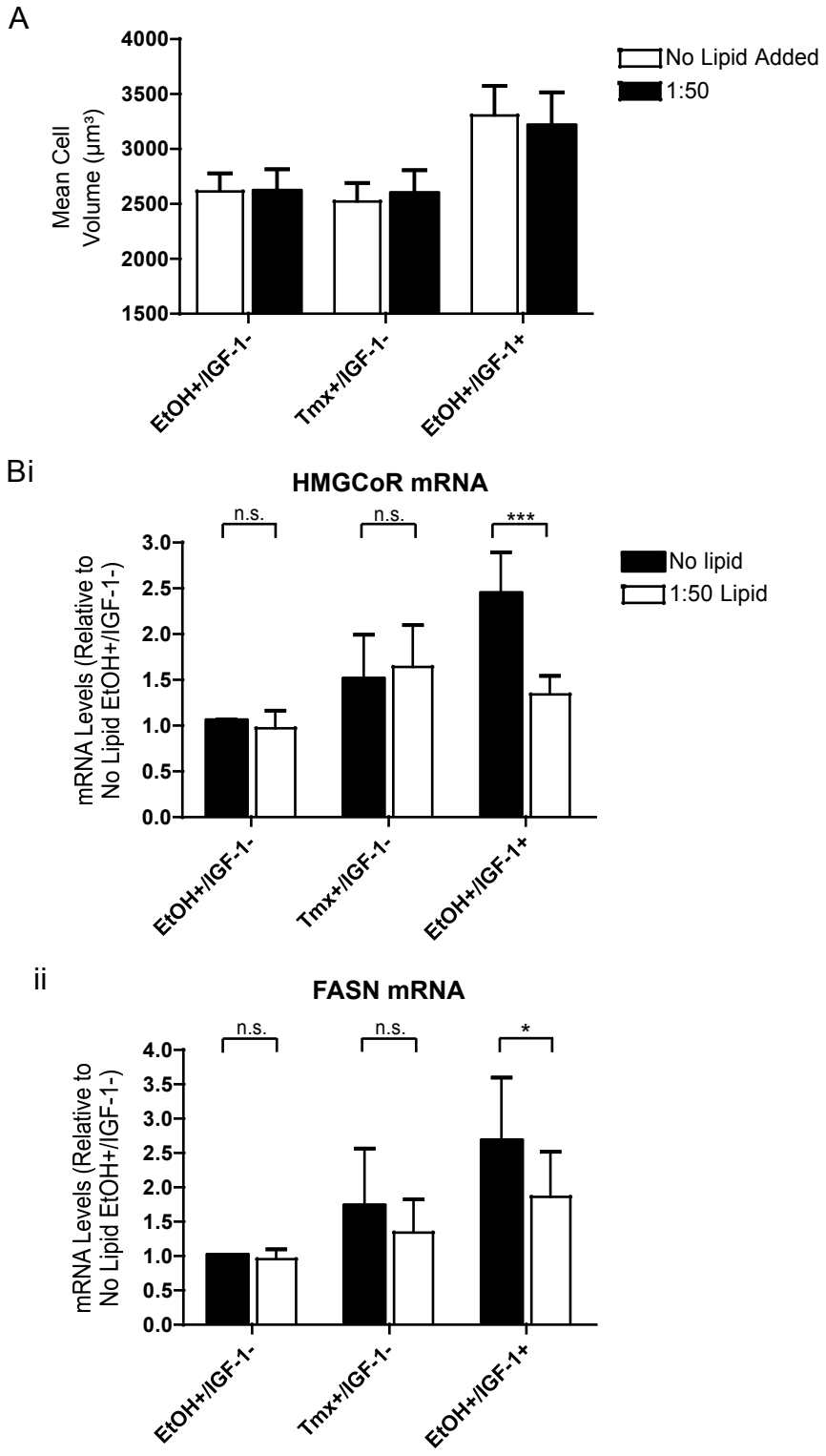

Figure 5.21 Supplementing the cell culture medium with a chemically defined mixture of fatty acids and cholesterol does not drive cell volume addition, although IGF-1 induced FASN and HMGCoR mRNA expression is inhibited

Aphidicolin arrested NSΔRafER cells were treated as indicated for:
A) 24hrs before cell volume was quantified using a Coulter Counter. Bar chart shows quantification of mean cell volume (µm³).
B) 8hrs before RNA was extracted and mRNA expression of SREBP target genes i) HMGCoR and ii) FASN was analysed by RT-qPCR. mRNA levels of target genes were normalised to B2M as a loading control.
Bar charts show mean +SEM of A) 3 experiments performed in duplicate and B)i) 4 and ii) 5 experiments. Repeated Measures Two-Way ANOVA A) Growth Factor $p<0.001$ B) i) Lipid $p<0.01$, Interaction $p<0.05$ and ii) Lipid $p<0.05$. Post hoc Bonferroni as indicated on the graphs.

5.5 Addition of Fatty Acids and Cholesterol to the Cell Culture Medium Does not Rescue Cell Volume Addition After SREBP-2 siRNA Knockdown or Chemical Inhibition of Sterol Synthesis

Although the lipid supplement had no effect on Schwann cell volume in the experiments described above, because the FASN and HMGCoR mRNA expression data suggested the lipids were utilised in the IGF-1 treated cells at least, this suggested the lipid supplement might rescue the inhibition of cell volume if de novo lipogenesis is inhibited, i.e. as is predicted to occur after SREBP-2 silencing, or chemical inhibition of HMGCoR (Section 5.2, Figure 5.4 & 5.8). Extracellular lipid supplementation can partially rescue the loss of myelination, i.e. the synthesis of extensive lipid membranes, caused by inhibiting SREBP dependent lipogenesis *in vitro* (Verheijen et al., 2009). To test this hypothesis, as in the previous assays, the lipid supplement was added 30 minutes before the factors (IGF-1 or Tmx) to cells treated either with simvastastin (to inhibit sterol synthesis) or after siRNA knockdown of SREBP-2 (all as described in Section 5.2 and Materials & Methods 2.1). As previously, cell volume was quantified using the Coulter Counter 24 hours after factor addition. The additional two inhibitors used to block de novo lipogenesis in Section 5.2 (cerulenin and C75) were not assayed because of the concern that the drugs may be having non-specific toxic effects (as described in Section 5.2).

The addition of the lipid supplement did not rescue the inhibition of cell volume downstream of SREBP-2 silencing (Figure 5.22) or simvastatin treatment (Figure 5.23). As described in the preceding section, it was not clear whether the control and Raf kinase activated cells utilised the lipid supplement and this may be the reason for the lack of volume rescue in these experiments. Alternatively, the blocks to de novo lipogenesis (SREBP-2 silencing or simvastatin treatment) may reduce the cell's lipid supply to a greater degree than can be rescued by the lipid supplement and this may be why cell volume was not rescued. It is also possible that there must be a basal flux through the SREBP/ de novo lipogenic pathway to sustain cell volume and/ or the lipid supplement does not contain the composition of lipids necessary to sustain cell volume.

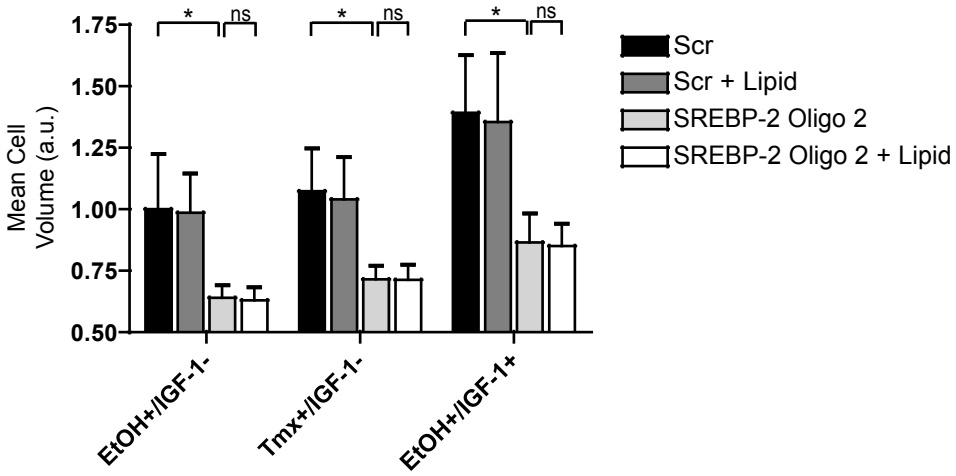

Figure 5.22 Supplementing the cell culture medium with a chemically defined mixture of fatty acids and cholesterol does not rescue the cell volume inhibition downstream of SREBP-2 knockdown (siRNA).

NSΔRafER cells were transfected with siRNAs as indicated in normal (3% FCS) Schwann cell medium for 18hrs then transferred into defined (no factor) conditions plus aphidicolin for 24hrs before lipid supplement and/ or factors (Tmx or IGF-1) were added as indicated for a further 24hrs. Final cell volume was quantified using a Coulter Counter. Bar chart shows mean cell volume +SEM of 3 experiments. Repeated Measures Two-Way ANOVA, siRNA/Lipid effect $p<0.001$. Select post hoc Bonferroni as indicated on the graph.

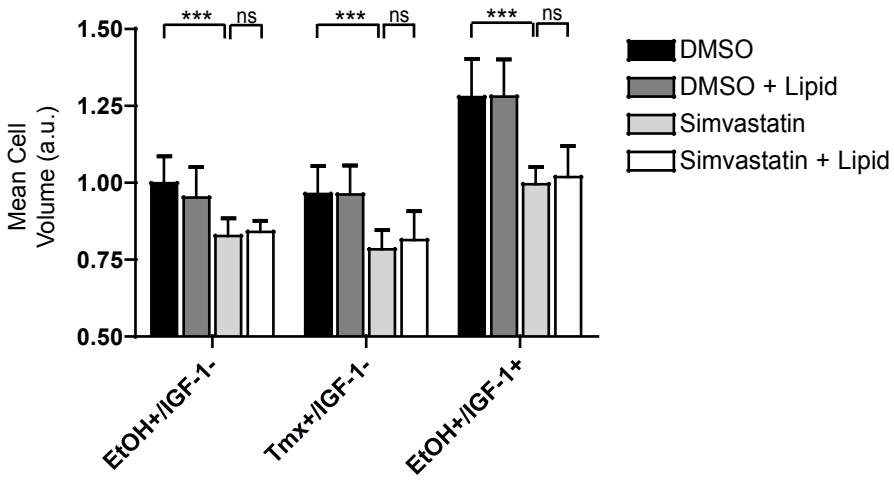

Figure 5.23 Supplementing the cell culture medium with a chemically defined mixture of fatty acids and cholesterol does not rescue the cell volume inhibition downstream of simvastatin.

Aphidicolin arrested NSΔRafER cells were treated +/- Simvastatin (5μM) and +/- lipid supplement, as indicated, for 24hrs before cell volume was quantified using a Coulter Counter. Bar chart shows mean +SEM of 3 experiments. Repeated Measures Two-Way ANOVA, Inhibitor/ Lipid effect $p<0.001$. Select post hoc Bonferroni as indicated on the graph.

In conclusion, although the addition of chemically defined lipids (free fatty acids and cholesterol) suppressed mRNA expression of genes required for de novo lipogenesis in IGF-1 treated cells, it was not sufficient to rescue cell volume inhibition downstream of a likely block to de novo lipogenesis resulting from siRNA silencing of SREBP-2, or chemical inhibition of HMGCoR.

5.6 Chapter 5: Summary

The findings described in this chapter can be summarised as follows:

- IGF-1, but not Raf kinase activation, activates the master transcription factor regulators of de novo lipogenesis, SREBP-1 and -2, to drive SREBP dependent transcription and de novo lipogenesis. This phenotype correlates with the IGF-1 specific increase in cell volume.
- SREBP-2 and de novo sterol/ isoprenoid synthesis appear to be necessary for the addition and maintenance of cell volume. The role of SREBP-1 and de novo fatty acid synthesis requires further investigation.
- However, expression of constitutively active SREBP-1a or SREBP-2 is not sufficient to drive addition of cell volume and does not cooperate with IGF-1 to increase IGF-1 driven addition of cell volume.
- Similarly, addition of exogenous fatty acids and cholesterol in a chemically defined lipid supplement (Gibco) is not sufficient to drive addition of cell volume and does not cooperate with IGF-1 to increase IGF-1 driven addition of cell volume.
- The addition of this lipid supplement is also not sufficient to rescue the inhibition of cell volume induced by silencing SREBP-2 or chemical inhibitors of fatty acid and sterol synthesis.

5.7 Chapter 5: Discussion

5.7.1 SREBP-2 and De Novo Lipogenesis are Required for the Addition and Maintenance of Schwann Cell Volume

The work in this study shows that not only the addition, but also the maintenance of Schwann cell volume requires SREBP-2 and de novo lipogenesis, demonstrating that lipogenesis is critical to the regulation of cell volume. As the SREBP pathway is activated downstream of IGF-1 in the Schwann cell and is required for the IGF-1 dependent addition of cell volume, this suggests it has an active role in the addition of cell volume. However, although necessary, the findings of this study suggest that SREBP activation is not the only factor downstream of IGF-1 required for the addition of cell volume, because activating SREBP in the absence of IGF-1 is not sufficient to drive an increase in cell volume.

A role for the SREBPs and de novo lipogenesis in the regulation of cell volume is consistent with the findings of other studies *in vitro*. Combined silencing of SREBP-1 and -2 inhibited Akt driven cell volume addition in conditions with limited exogenous lipid *in vitro* (1% lipoprotein-deprived serum (LPDS)) (Porstmann et al., 2008). Moreover, at the highest siRNA concentrations where SREBP knockdown was most efficient, Porstmann et al found that the volume of control cells also seemed to be reduced, consistent with our findings. Silencing SREBP-1 also reduced the volume of senescent cells, where senescence was induced by stress (immortalised human hepatocytes) or replicative senescence (human diploid fibroblasts), *in vitro* (Kim et al., 2010). Moreover, lipogenesis is required for the rapid growth of a number of tumour cell models (Bauer et al., 2005, Brusselmans et al., 2005, Hatzivassiliou et al., 2005, Kim et al., 2010, Kuhajda et al., 2000, Menendez and Lupu, 2007, Porstmann et al., 2005, Porstmann et al., 2008).

The role of the SREBPs in the regulation of cell volume and cell growth *in vivo* is not as clear. SREBPs appear to be expressed, at least at a low level, across a number of tissues *in vivo* (Shimomura et al., 1997b, de Preux et al., 2007). However, it is not yet clear whether all tissues require a certain level of de novo lipogenesis, regulated by SREBP activity, or whether the SREBPs are expressed only to be retained inactive in the ER in case a shortage occurs in

the supply of exogenous lipid. *In vivo*, mice lacking SREBP-2, or all three isoforms, are embryonic lethal, precluding studies of the role of SREBPs in cell and tissue growth during later development (Horton et al., 2002, Mitchell et al., 2001, Shimano et al., 1997b). At the time of lethality, however, the embryos appeared phenotypically normal suggesting that the SREBPs are not required for gross embryonic growth to this point, although the findings do not preclude changes in intracellular structure and composition. Between 15-45% of mice lacking SREBP-1 (SREBP-1a and -1c) survive and develop apparently normally, without reduced body size (Shimano et al., 1997b). However, SREBP-2 is upregulated and this appears to compensate for the loss of SREBP-1. Therefore it cannot be excluded that SREBP-1 normally functions in cell growth during development. The proper development of particular tissues has been shown to require the SREBPs and de novo lipogenesis. SREBP and target gene expression peaks during Schwann cell myelination, which is when these cells are synthesising massive amounts of lipid membrane to produce the extensive myelin sheath and, perhaps unsurprisingly, formation of the myelin sheath has been shown to require SREBPs and de novo cholesterol biosynthesis (Chrast et al., 2011, de Preux et al., 2007, Leblanc et al., 2005, Verheijen et al., 2009). Loss of the SREBP escort protein, SCAP (the SREBP escort protein required for SREBP processing) in myelinating Schwann cells blocked SREBP and target gene expression and mice exhibited severe hypomyelination- the myelin that did form required extracellular lipids (Verheijen et al., 2009). Similarly, loss of squalene synthase, an enzyme required for cholesterol synthesis also resulted in hypomyelination (Chrast et al., 2011). Myelinating Schwann cells are a highly specialised cell type, with a dramatically exaggerated requirement for membrane, however consistent with a role for the SREBPs in cell growth during development, Porstmann et al showed that loss of dSREBP during development reduces cell and organ size in *Drosophila* (Porstmann et al., 2008). These examples demonstrate that the SREBPs and de novo lipogenesis have a physiologically role in the growth of at least certain cell types.

It seems inevitable that the addition of cell volume during cell growth will require lipogenesis for the biogenesis of membranous organelles and the plasma membrane. It may initially seem less obvious why the maintenance of cell volume would also require lipogensis. However, even cells that are

maintaining a constant cell size must continually turnover of macromolecules and organelles in order to replace those that are worn out and damaged and this includes replacing damaged and degraded lipids and membranes. If the replacement of these lipids is blocked, for example because lipid synthesis is blocked, then damaged organelle membranes and the plasma membrane cannot be replaced and it does not seem unreasonable to assume they will shrink/ be lost and the cell will shrink and lose volume. So, it can be seen how SREBP and the de novo lipogenic pathway could be required for both the addition and maintenance of cell volume.

In addition to the structural role outlined above, the product of HMGCoR activity (inhibited by the use of simvastatin, which reduced cell volume)- mevalonate- is also used for the synthesis of isoprenoids that post-translationally modify proteins in a process called prenylation (Goldstein and Brown, 1990). Prenylation affects the localisation (membrane targeting) and function of a number of proteins, including signalling and structural proteins such as Ras and nuclear lamins, respectively (Schafer and Rine, 1992). It is possible that loss of prenylation upon loss of SREBP-2/ inhibition of HMGCoR may also contribute to the block to cell volume by causing the mislocalisation of signalling proteins required to regulate cellular processes required for cell volume regulation and/ or structural proteins required for cell volume addition.

Further work is required to clarify the role of the SREBPs and de novo lipogenesis in the Schwann cell system used in this study. It is important to determine whether SREBP-1 is dispensable for the regulation of Schwann cell volume, perhaps because SREBP-2 is able to compensate, as can occur *in vivo*. If siRNA knockdown is not effectively silencing SREBP-1 then alternative strategies should be tested- perhaps stable inducible shRNAs, or dominant negative SREBP proteins. It will also be important to clarify the role of de novo fatty acid and sterol synthesis, which could be investigated using siRNAs targeting enzymes in each of these pathways, including FASN and HMGCoR. Finally, it is necessary to establish whether SREBP-2 silencing is blocking either fatty acid and/ or sterol synthesis; in other words, to determine whether de novo lipogenesis is the pathway downstream of SREBP-2 that is critical for the regulation of cell volume. In addition to de novo lipogenesis, the SREBPs also regulate other metabolic pathways- including the One Carbon Cycle (1CC) and

the Pentose Phosphate Pathway (PPP) (Duvel et al., 2010, Liang et al., 2002, Shimano et al., 1999, Walker et al., 2011). These pathways are linked to de novo lipogenesis- flux through the PPP produces NADPH that can be used for de novo lipogenesis, for example. However, they also participate in wider cell metabolism and it would be interesting to determine whether these pathways have a role in the regulation of Schwann cell volume downstream of SREBP signalling.

The IGF-1 dependent addition of protein mass did not require the addition of cell volume, demonstrated by the finding that simvastatin inhibited IGF-1 driven addition of cell volume, but not protein mass. Thus, not only can IGF-1 drive an increase in volume in the absence of an increase in protein mass (as demonstrated in Chapter 3, using the MEK inhibitor), but can also drive an increase in protein mass in the absence of an increase in volume. This finding further emphasising that cell protein mass and volume can be separately and independently regulated. This suggests that, at least at the gross level, the coupled addition of protein and lipid is not required.

As an aside: considering membrane biogenesis, it is noteworthy that Raf kinase activation did not significantly increase SREBP target gene mRNA expression or the incorporation of extracellular radiolabelled pyruvate into lipid. However, Raf kinase appears to drive a significant increase in the amount of two highly membranous organelles- the mitochondria and the endoplasmic reticulum (Chapter 3). It might have been predicted this would require an increase in the rate of de novo lipogenesis. The rate of de novo lipogenesis from lipogenic precursors other than extracellular pyruvate (e.g. glucose or glutamine) may be increased downstream of Raf kinase, which was not assayed in this study. If so, this may have been driven by altered post-translational modification of lipogenic enzymes such as FASN and HMGCoR, rather than an increase in their transcription (Jin et al., 2010, Parker et al., 1986). Alternatively, lipolysis may be reduced and/ or intracellular lipid stores (i.e. in lipid droplets) may be sufficient to fuel any membrane biogenesis. It is also possible that the amount of de novo lipogenesis required for the synthesis of these membranes represents a minor fraction of total de novo lipogenesis and so was not detected in this study.

5.7.2 Inducing SREBP Activity is not Sufficient to Drive Cell Volume Addition

Although the results of this study indicate that SREBP-2 is required for the addition and maintenance of Schwann cell volume, activation of either SREBP-1a or SREBP-2 was not sufficient to drive addition of cell volume in the presence or absence of Raf kinase activation and did not enhance cell volume addition downstream of IGF-1. This suggests that activation of the de novo lipogenic pathway does not appear to be sufficient to drive the addition of cell volume and therefore other factors also limit cell volume addition. In other systems *in vitro* and *in vivo*, the response to overexpressing active SREBPs is variable and depends on cell type and SREBP isoform (the latter highlighting that the different SREBP isoforms regulate different although overlapping subsets of genes) (Amemiya-Kudo et al., 2002, Horton et al., 2002, Horton et al., 2003a, Shimano et al., 1997a). This highlights that the cellular response depends on both the specific activity of the cell type in question, as well as the specific activity of the SREBP isoform introduced.

For example, liver and adipose tissue- tissues that store and mobilise lipids in response to whole body nutrition- might be predicted to have hypertrophic responses to activation of the lipogenic pathway. However, even in these tissues the response to overexpressing mature SREBP depends of the SREBP isoform. Expression of mature SREBP-1a induces adipocyte hypertrophy, whereas expression of mature SREBP-1c inhibits adipocyte differentiation and fails to induce lipogenic gene expression (Horton et al., 2003a, Sekiya et al., 2007, Shimomura et al., 1998). In the liver, overexpressing mature SERBP-1a or -1c induces hypertrophy, associated with excessive accumulation of triglycerides, whereas mature SREBP-2 does not, although hepatic cholesterol and triglyceride levels increase (Horton et al., 1998, Kotzka et al., 2012, Shimano et al., 1996, Shimano et al., 1997a). Interestingly, although the livers of the SREBP-1a transgenic mice are hypertrophic, they fail to regenerate after hepatectomy and this is associated with a cell cycle arrest, highlighting how blocking proliferation can limit tissue growth (Nakakuki et al., 2007). It is worthwhile to note that, in each of the above examples, SREBP expression was altered constitutively and throughout development. Therefore the phenotypes may reflect longer term, compensatory and/ or indirect effects

of altering the de novo lipogenic pathway, rather than immediate effects, as would have been observed with the inducible system used in this study.

Interestingly, activating drosophila SREBP (mdSREBP) in the *Drosophila* wing disc during development inhibits wing growth (Porstmann et al., 2008). In mammalian cells, high levels of SREBP-1a can induce G1 cell-cycle arrest in some conditions and Porstmann *et al* hypothesise this is the cause of the growth arrest in the *Drosophila* wing (Inoue et al., 2005, Nakakuki et al., 2007, Porstmann et al., 2008). Although cell-cycle arrest does not necessarily inhibit cell growth, it will limit tissue growth and patterning. This is because there will be an upper limit to the size an individual cell can grow to. Therefore, where cell-cycle arrest limits the number of cells in a tissue, so this limits the maximum size to which the tissue can grow. This finding highlights that, *in vivo*, tissue growth is more complex than simple cell growth and suggests that there may be pleiotropic effects of changes in gene expression and activity, i.e. in this case, SREBP activity.

From a mechanistic perspective and in the context of this Schwann cell study: it is possible that SREBP activation and the resulting increase in lipogenic target gene expression did not drive cell volume addition because de novo lipogenesis was not induced (which was not investigated, although the mRNA expression of genes rate limiting for de novo fatty acid and sterol synthesis, FASN and HMGCoR respectively, increased). This could occur if, for example, negative regulators of the process were also activated- for example the protein kinase AMPK, which is activated in conditions of low cell energy (energetic stress). Active AMPK supresses most anabolic processes within the cell, in order to conserve energy (Hardie, 2011). This includes de novo fatty acid and sterol synthesis- AMPK phosphorylates and inhibits HMGCoR, ACC (Acetyl-CoA carboxylase) and SREBP-1 (Carling et al., 1987, Li et al., 2011, Sato et al., 1993). As demonstrated in Chapter 4, cells in the absence of growth factors/ growth factor activated signalling (IGF-1/ Raf kinase activation) are autophagic and slowly lose volume- likely because they cannot utilise sufficient extracellular nutrients. Therefore it is tempting to speculate whether, in this condition at least, activating the SREBPs and, initially, de novo lipogenesis induces energetic stress, AMPK activation and inhibition of further de novo lipogenesis. An important next step in these studies will be to determine if there

is sustained de novo lipogenesis after activation of the SREBP constructs, by assaying the incorporation of radiolabelled precursors into lipid.

Alternatively, if sustained de novo lipogenesis is induced after SREBP activation, this demonstrates that simply driving lipogenesis is insufficient to drive cell volume addition. This could be consistent with the finding that the addition of a chemically defined exogenous lipid supplement had no effect of Schwann cell volume. Why might driving lipogenesis be insufficient to induce volume addition? One possibility is that the ability to utilise the synthesised lipids may be limiting. In other words, additional pathways are needed to direct the use of the synthesised lipids into structures/ functions that increase cell volume. Organelle biogenesis is metabolically expensive, requiring the coordinated synthesis of many protein and lipid species, and is therefore carefully regulated according to need. Therefore it would perhaps not be surprising that, in the absence of appropriate biogenic stimuli, such as specific growth factors, cells do not self-assemble the lipid into functional membranous organelles that might be required for volume addition. Linked to this, it would be interesting to quantify lipid droplet and peroxisome number following SREBP activation, as both have roles in cell lipid metabolism and correlate with the induction of the SREBP pathway and cell volume downstream of IGF-1 (Chapter 3). In addition to the ability to utilise lipids, other factors/ signals may also be required to add cell volume. For example, as cells add volume during cell growth the cell cortex (actin cytoskeleton) must expand. The actin cytoskeleton is carefully controlled to control cell shape and size and therefore it seems likely that signals to add volume might specifically regulate the remodelling of this structure. Other functions of cytoskeletal structures may also be required for cell volume addition. For example, trafficking along microtubules may be required to transport vesicles containing plasma membrane to the cell surface for plasma membrane expansion, or to transport substrates between organelles for their growth and functioning.

It was striking to note that even in IGF-1 treated cells that are already adding volume, inducing exogenous SREBP activation did not augment volume addition. Although the IGF-1 concentration used is saturating for growth downstream of this factor, IGF-1 treated cells are not at the physiological limit of Schwann cell volume as more potent growth factors (including serum) can

induce larger increases in cell volume. Therefore even in this condition, other factors must limit cell volume addition. In this regard, it is interesting that IGF-1 treatment causes an increase in the number and total volume of lipid droplets per cell, compared to control and Raf kinase activated cells. A major role of this organelle is as a storage site for excess lipids, which might suggest IGF-1 alone drives lipogenesis in excess of any required for IGF-1 dependent volume addition.

5.7.3 Other Factors can Limit Cell Volume

The results presented in this Chapter, indicate that factors other than the SREBPs and, potentially, lipogenesis are required to add cell volume. As discussed, this may include the ability to utilise synthesised lipids, or the size of the actin cytoskeleton. Another factor that has the potential to limit increases in cell volume is the addition of cell water. Approximately 70% of the weight of the cell is water and water can move rapidly into and out of the cell. Given that this movement is carefully regulated to prevent inappropriate changes in cell volume, this may be one additional factor that limits cell volume addition. It seems inevitable that increases during cell growth must be accompanied by, and at least partially the result of, water uptake. However, whilst much attention has been paid to how water movement is regulated to maintain a constant cell volume, there has been a distinct lack of attention to the role of water uptake during mammalian cell growth.

Water uptake during cell growth may occur simply as an indirect passive ‘by-product’ of other aspects of cell growth. It has been proposed that cells regulate water movement to maintain a constant cell volume by sensing deviations in plasma membrane tension from a set point (Lang, 2007, Lang et al., 1998). Changes in cell volume, result in changes in tension on the plasma membrane. The tension-mediated hypothesis states that changes in plasma membrane tension are sensed by the cell, which then induces the appropriate change in the direction of net water transport into/ out of the cell to reverse the change in cell volume. If the plasma membrane expands during cell growth, this could reduce plasma membrane tension and induce water uptake to restore membrane tension- resulting in an increase in cell volume. As an aside: as discussed at the end of Chapter 4, it has also been proposed that plasma membrane size is controlled by plasma membrane tension. If membrane

tension drives plasma membrane expansion during cell growth then cell volume must increase before the plasma membrane expands. Therefore, clearly, the tension hypothesis is mutually exclusive for water uptake and plasma membrane expansion. It remains to be determined which process, if either, tension regulates.

An alternative mechanism is that growth factors might actively regulate cell surface water channels (Aquaporins) and actively increase intracellular osmolarity to drive water uptake (Burg, 2000, Burg and Ferraris, 2008, King et al., 2004, Lang, 2007, Lang et al., 1998, Verkman, 2011). Intracellular osmolarity is controlled by regulating the uptake and secretion of inorganic ions and organic osmolytes (e.g. myo-inositol, sorbitol, amino acids and betaine), as well as the synthesis and degradation of the latter (Burg and Ferraris, 2008, Lang et al., 1998). High intracellular ion concentrations are toxic because they can disrupt the structure and function of molecules including proteins and DNA, therefore if growth stimuli drive an increase in intracellular osmolarity to drive water uptake it might be most likely that this is through driving the accumulation of organic osmolytes (Lang et al., 1998). In this regard, it would be very interesting to investigate whether growth factor signalling activates the transcription factor NFAT5 (Also known as TonEBP/ OREBP) during cell growth. NFAT5 drives expression of Aquaporin2 and organic osmolyte transporters and synthetic enzymes and PI3K has been shown to activate NFAT5 in response to hypoxia, high intracellular sodium chloride levels and DNA damage (Burg and Ferraris, 2008, Hasler et al., 2006, Irarrazabal et al., 2006, Villanueva et al., 2012).

Intriguingly, mice deficient in the adipose specific Aquaporin- 7 (AQP7) develop adipocyte hypertrophy and obesity (Hara-Chikuma et al., 2005, Hibuse et al., 2005). However AQP7 is an aquaglyceroporin that also transports small, uncharged solutes such as glycerol and it transpires that inhibiting glycerol export out of adipocytes is sufficient to drive hypertrophy and therefore explain the phenotype. It must be noted, however, that a role for water transport was not investigated in the study.

5.7.4 Conclusion

This study demonstrates that SREBP-2 and the de novo lipogenic pathway is required not only for the IGF-1 dependent addition of Schwann cell volume, but also to maintain the volume of control and Raf kinase activated cells. Lipids are critical structural components of cell membranes, therefore it seems inevitable that the requirement for cellular lipids is, at least in part, because they are required both to maintain and to drive the expansion of organelle membranes and the plasma membrane. However, given that inducing SREBP activity is not sufficient to increase cell volume, this highlights that additional factors must also be required. These may include the ability to utilise synthesised lipids, e.g. assemble them into functional organelle membranes, or it may be a factor largely independent of cellular lipids, such as the regulation of cell water uptake. In order to fully understand how cell volume is regulated during cell growth, it is absolutely necessary to understand the additional mechanisms that can limit cell volume.

Chapter 6: Final Discussion

The findings presented in this thesis both demonstrate the complexity of cell growth and cell size regulation and highlight that our understanding of how these processes are regulated remains, for the most part, poor. This study has shown that cell mass and volume can be separately and independently regulated. Although the ability to uncouple mass and volume- and, linked to this, differentially regulate organelle content downstream of distinct biogenic stimuli- can help generate the diversity in cell size, morphology and organelle content observed in vivo, it presents a complex regulatory challenge. Multiple layers of cell regulatory control will be necessary so that cell protein, lipid and organelle biogenesis can be separately and independently regulated and these control mechanisms remain poorly understood. The complexity of regulating cell biogenesis is further highlighted by the finding in this study that the plasma membrane, despite maintaining a constant barrier between the cytosol and extracellular environment, is incredibly dynamic and is internalised between 2-4 times per hour. This finding was particularly remarkable because the rapid rate of turnover is maintained in starved cells. These cells are maintaining a constant plasma membrane size, which means these cells must be able to control the rapid processes of plasma membrane removal and delivery with enough precision to maintain a constant membrane area. This demonstrates that all cells, whether they are growing or not, maintain active and tight control of the rapid turnover of cell material.

Technological advances have made high throughput confocal microscopy image based screens feasible and this is an attractive approach to begin to address these questions, as such screens have the potential to yield a wealth of unbiased and informative data. Using a primary growth factor receptive cell such as the Schwann cell it should be possible to perform siRNA screens to identify genes that regulate the addition of cell mass and/ or volume downstream of growth factors such as serum and IGF-1. Protein mass could be quantified from the fluorescence intensity per cell after Succinimidyl Ester labelling, as used in these studies, and cell volume from image stacks through the depth of labelled cells. If organelles were also labelled, e.g. by immunofluorescence, organelle size could be correlated with effects on cell mass/ volume, which could then be followed up with functional investigations.

As this type of screen, although powerful, provides only snapshots of the outputs of biogenesis, alternative techniques must be used in parallel to understand the dynamic regulation of cell macromolecules and organelles by biogenic stimuli- i.e. the control of their synthesis and degradation. It is only by understanding both the biosynthetic processes driving cell growth and the resulting outputs of biogenesis, i.e. the 'snapshot', that we will have a complete understanding of the mechanisms that control cell growth.

The proper control of cell growth is absolutely necessary for the correct development and maintenance of all organisms. Understanding how organelle biogenesis links to driving mass and/ or volume addition will both advance our understanding of how cell growth is normally regulated, as well as the ways in which it can become deregulated leading to disease. This will be critical to understanding how deregulated cell growth could be targeted therapeutically in a range of diseases, such as cancer, cardiac hypertrophy and autistic spectrum disorders, in which it plays a fundamental role.

References

ABE, N., BORSON, S. H., GAMBELLO, M. J., WANG, F. & CAVALLI, V. 2010. Mammalian target of rapamycin (mTOR) activation increases axonal growth capacity of injured peripheral nerves. *The Journal of biological chemistry,* 285**,** 28034-43.

ADAMS, G. R. & MCCUE, S. A. 1998. Localized infusion of IGF-I results in skeletal muscle hypertrophy in rats. *Journal of applied physiology,* 84**,** 1716-22.

ALBERTS, B., JOHNSON, A., LEWIS, J., RAFF, M., ROBERTS, K. AND WALTER, P. 2002. *Molecular Biology of the Cell, 4th edition,* New York, Garland Science.

ALESSI, D. R., DEAK, M., CASAMAYOR, A., CAUDWELL, F. B., MORRICE, N., NORMAN, D. G., GAFFNEY, P., REESE, C. B., MACDOUGALL, C. N., HARBISON, D., ASHWORTH, A. & BOWNES, M. 1997. 3-Phosphoinositide-dependent protein kinase-1 (PDK1): structural and functional homology with the Drosophila DSTPK61 kinase. *Curr Biol,* 7**,** 776-89.

ALTMAN, B. J., WOFFORD, J. A., ZHAO, Y., COLOFF, J. L., FERGUSON, E. C., WIEMAN, H. L., DAY, A. E., ILKAYEVA, O. & RATHMELL, J. C. 2009. Autophagy provides nutrients but can lead to Chop-dependent induction of Bim to sensitize growth factor-deprived cells to apoptosis. *Mol Biol Cell,* 20**,** 1180-91.

AMEMIYA-KUDO, M., SHIMANO, H., HASTY, A. H., YAHAGI, N., YOSHIKAWA, T., MATSUZAKA, T., OKAZAKI, H., TAMURA, Y., IIZUKA, Y., OHASHI, K., OSUGA, J., HARADA, K., GOTODA, T., SATO, R., KIMURA, S., ISHIBASHI, S. & YAMADA, N. 2002. Transcriptional activities of nuclear SREBP-1a, -1c, and -2 to different target promoters of lipogenic and cholesterogenic genes. *J Lipid Res,* 43**,** 1220-35.

ANDERSON, E. C., BELL, G. I., PETERSEN, D. F. & TOBEY, R. A. 1969. Cell growth and division. IV. Determination of volume growth rate and division probability. *Biophys J,* 9**,** 246-63.

ARITO, M., HORIBA, T., HACHIMURA, S., INOUE, J. & SATO, R. 2008. Growth factor-induced phosphorylation of sterol regulatory element-binding proteins inhibits sumoylation, thereby stimulating the expression of their target genes, low density lipoprotein uptake, and lipid synthesis. *J Biol Chem,* 283**,** 15224-31.

ATANASOSKI, S., SCHERER, S. S., SIRKOWSKI, E., LEONE, D., GARRATT, A. N., BIRCHMEIER, C. & SUTER, U. 2006. ErbB2 signaling in Schwann cells is mostly dispensable for maintenance of myelinated peripheral nerves and proliferation of adult Schwann cells after injury. *J Neurosci,* 26**,** 2124-31.

BAAR, K. & ESSER, K. 1999. Phosphorylation of p70(S6k) correlates with increased skeletal muscle mass following resistance exercise. *Am J Physiol,* 276**,** C120-7.

BABURINA, I. & JACKOWSKI, S. 1999. Cellular responses to excess phospholipid. *J Biol Chem,* 274**,** 9400-8.

BAILEY, J. M., HOWARD, B. V., DUNBAR, L. M. & TILLMAN, S. F. 1972. Control of lipid metabolism in cultured cells. *Lipids,* 7**,** 125-34.

BARATA, J. T., SILVA, A., BRANDAO, J. G., NADLER, L. M., CARDOSO, A. A. & BOUSSIOTIS, V. A. 2004. Activation of PI3K is indispensable for interleukin 7-mediated viability, proliferation, glucose use, and growth of T cell acute lymphoblastic leukemia cells. *J Exp Med,* 200**,** 659-69.

BARTON-DAVIS, E. R., SHOTURMA, D. I., MUSARO, A., ROSENTHAL, N. & SWEENEY, H. L. 1998. Viral mediated expression of insulin-like growth factor I blocks the aging-related loss of skeletal muscle function. *Proceedings of the National Academy of Sciences of the United States of America,* 95**,** 15603-7.

BAUER, D. E., HATZIVASSILIOU, G., ZHAO, F., ANDREADIS, C. & THOMPSON, C. B. 2005. ATP citrate lyase is an important component of cell growth and transformation. *Oncogene,* 24**,** 6314-22.

BENGOECHEA-ALONSO, M. T. & ERICSSON, J. 2007. SREBP in signal transduction: cholesterol metabolism and beyond. *Curr Opin Cell Biol,* 19**,** 215-22.

BERG, J., TYMOCZKO, JL, STRYER, L 2002. *Biochemistry,* New York, W H Freeman.

BERTRAND, C. A., LABOISSE, C., HOPFER, U., BRIDGES, R. J. & FRIZZELL, R. A. 2006. Methods for detecting internalized, FM 1-43 stained particles in epithelial cells and monolayers. *Biophys J,* 91**,** 3872-83.

BERWICK, D. C., HERS, I., HEESOM, K. J., MOULE, S. K. & TAVARE, J. M. 2002. The identification of ATP-citrate lyase as a protein kinase B (Akt) substrate in primary adipocytes. *J Biol Chem,* 277**,** 33895-900.

BETSCHINGER, J., MECHTLER, K. & KNOBLICH, J. A. 2006. Asymmetric segregation of the tumor suppressor brat regulates self-renewal in Drosophila neural stem cells. *Cell,* 124**,** 1241-53.

BETZ, W. J., MAO, F. & SMITH, C. B. 1996. Imaging exocytosis and endocytosis. *Curr Opin Neurobiol,* 6**,** 365-71.

BIOLO, G., MAGGI, S. P., WILLIAMS, B. D., TIPTON, K. D. & WOLFE, R. R. 1995. Increased rates of muscle protein turnover and amino acid transport after resistance exercise in humans. *Am J Physiol,* 268**,** E514-20.

BODINE, S. C., LATRES, E., BAUMHUETER, S., LAI, V. K., NUNEZ, L., CLARKE, B. A., POUEYMIROU, W. T., PANARO, F. J., NA, E., DHARMARAJAN, K., PAN, Z. Q., VALENZUELA, D. M., DECHIARA, T. M., STITT, T. N., YANCOPOULOS, G. D. & GLASS, D. J. 2001a. Identification of ubiquitin ligases required for skeletal muscle atrophy. *Science,* 294**,** 1704-8.

BODINE, S. C., STITT, T. N., GONZALEZ, M., KLINE, W. O., STOVER, G. L., BAUERLEIN, R., ZLOTCHENKO, E., SCRIMGEOUR, A., LAWRENCE, J. C., GLASS, D. J. & YANCOPOULOS, G. D. 2001b. Akt/mTOR pathway is a crucial regulator of skeletal muscle hypertrophy and can prevent muscle atrophy in vivo. *Nature cell biology,* 3**,** 1014-9.

BOEHLKE, C., KOTSIS, F., PATEL, V., BRAEG, S., VOELKER, H., BREDT, S., BEYER, T., JANUSCH, H., HAMANN, C., GODEL, M., MULLER, K., HERBST, M., HORNUNG, M., DOERKEN, M., KOTTGEN, M., NITSCHKE, R., IGARASHI, P., WALZ, G. & KUEHN, E. W. 2010. Primary cilia regulate mTORC1 activity and cell size through Lkb1. *Nat Cell Biol,* 12**,** 1115-22.

BOHNI, R., RIESGO-ESCOVAR, J., OLDHAM, S., BROGIOLO, W., STOCKER, H., ANDRUSS, B. F., BECKINGHAM, K. & HAFEN, E. 1999. Autonomous control of cell and organ size by CHICO, a Drosophila homolog of vertebrate IRS1-4. *Cell,* 97**,** 865-75.

BONEN, A., HAN, X. X., HABETS, D. D., FEBBRAIO, M., GLATZ, J. F. & LUIKEN, J. J. 2007. A null mutation in skeletal muscle FAT/CD36 reveals its essential role in insulin- and AICAR-stimulated fatty acid metabolism. *Am J Physiol Endocrinol Metab,* 292**,** E1740-9.

BONNEAU, D. & LONGY, M. 2000. Mutations of the human PTEN gene. *Hum Mutat,* 16**,** 109-22.

BOUCROT, E. & KIRCHHAUSEN, T. 2007. Endosomal recycling controls plasma membrane area during mitosis. *Proc Natl Acad Sci U S A,* 104**,** 7939-44.

BOUCROT, E., SAFFARIAN, S., ZHANG, R. & KIRCHHAUSEN, T. 2010. Roles of AP-2 in clathrin-mediated endocytosis. *PLoS One,* 5**,** e10597.

BOURAJJAJ, M., ARMAND, A. S., DA COSTA MARTINS, P. A., WEIJTS, B., VAN DER NAGEL, R., HEENEMAN, S., WEHRENS, X. H. & DE WINDT, L. J. 2008. NFATc2 is a necessary mediator of calcineurin-dependent cardiac hypertrophy and heart failure. *J Biol Chem,* 283**,** 22295-303.

BRUSSELMANS, K., DE SCHRIJVER, E., VERHOEVEN, G. & SWINNEN, J. V. 2005. RNA interference-mediated silencing of the acetyl-CoA-carboxylase-alpha gene induces growth inhibition and apoptosis of prostate cancer cells. *Cancer Res,* 65**,** 6719-25.

BRYAN, A. K., GORANOV, A., AMON, A. & MANALIS, S. R. 2010. Measurement of mass, density, and volume during the cell cycle of yeast. *Proc Natl Acad Sci U S A,* 107**,** 999-1004.

BUCHBERGER, A., BUKAU, B. & SOMMER, T. 2010. Protein quality control in the cytosol and the endoplasmic reticulum: brothers in arms. *Mol Cell,* 40**,** 238-52.

BUENO, O. F., DE WINDT, L. J., TYMITZ, K. M., WITT, S. A., KIMBALL, T. R., KLEVITSKY, R., HEWETT, T. E., JONES, S. P., LEFER, D. J., PENG, C. F., KITSIS, R. N. & MOLKENTIN, J. D. 2000. The MEK1-ERK1/2 signaling pathway promotes compensated cardiac hypertrophy in transgenic mice. *EMBO J,* 19**,** 6341-50.

BUENO, O. F., WILKINS, B. J., TYMITZ, K. M., GLASCOCK, B. J., KIMBALL, T. F., LORENZ, J. N. & MOLKENTIN, J. D. 2002. Impaired cardiac hypertrophic response in Calcineurin Abeta -deficient mice. *Proc Natl Acad Sci U S A,* 99**,** 4586-91.

BURG, M. B. 2000. Macromolecular crowding as a cell volume sensor. *Cell Physiol Biochem,* 10**,** 251-6.

BURG, M. B. & FERRARIS, J. D. 2008. Intracellular organic osmolytes: function and regulation. *J Biol Chem,* 283**,** 7309-13.

BURGERT, H. G. & THILO, L. 1983. Internalization and recycling of plasma membrane glycoconjugates during pinocytosis in the macrophage cell line, P388D1. Kinetic evidence for compartmentation of internalized membranes. *Exp Cell Res,* 144**,** 127-42.

BUTLER, M. G., DASOUKI, M. J., ZHOU, X. P., TALEBIZADEH, Z., BROWN, M., TAKAHASHI, T. N., MILES, J. H., WANG, C. H., STRATTON, R., PILARSKI, R. & ENG, C. 2005. Subset of individuals with autism spectrum disorders and extreme macrocephaly associated with germline PTEN tumour suppressor gene mutations. *J Med Genet,* 42**,** 318-21.

CARLING, D., ZAMMIT, V. A. & HARDIE, D. G. 1987. A common bicyclic protein kinase cascade inactivates the regulatory enzymes of fatty acid and cholesterol biosynthesis. *FEBS Lett,* 223**,** 217-22.

CARRIERE, A., CARGNELLO, M., JULIEN, L. A., GAO, H., BONNEIL, E., THIBAULT, P. & ROUX, P. P. 2008. Oncogenic MAPK signaling stimulates mTORC1 activity by promoting RSK-mediated raptor phosphorylation. *Curr Biol,* 18**,** 1269-77.

CARRIERE, A., ROMEO, Y., ACOSTA-JAQUEZ, H. A., MOREAU, J., BONNEIL, E., THIBAULT, P., FINGAR, D. C. & ROUX, P. P. 2011. ERK1/2 phosphorylate Raptor to promote Ras-dependent activation of mTOR complex 1 (mTORC1). *J Biol Chem,* 286**,** 567-77.

CASLEY, C. S., LAND, J. M., SHARPE, M. A., CLARK, J. B., DUCHEN, M. R. & CANEVARI, L. 2002. Beta-amyloid fragment 25-35 causes mitochondrial dysfunction in primary cortical neurons. *Neurobiol Dis,* 10**,** 258-67.

CASTORENO, A. B., WANG, Y., STOCKINGER, W., JARZYLO, L. A., DU, H., PAGNON, J. C., SHIEH, E. C. & NOHTURFFT, A. 2005. Transcriptional regulation of phagocytosis-induced membrane biogenesis by sterol regulatory element binding proteins. *Proc Natl Acad Sci U S A,* 102**,** 13129-34.

CHAN, J. C., HANNAN, K. M., RIDDELL, K., NG, P. Y., PECK, A., LEE, R. S., HUNG, S., ASTLE, M. V., BYWATER, M., WALL, M., POORTINGA, G., JASTRZEBSKI, K., SHEPPARD, K. E., HEMMINGS, B. A., HALL, M. N., JOHNSTONE, R. W., MCARTHUR, G. A., HANNAN, R. D. & PEARSON, R. B. 2011. AKT promotes rRNA synthesis and cooperates with c-MYC to stimulate ribosome biogenesis in cancer. *Sci Signal,* 4**,** ra56.

CHARVET, C., HOUBRON, C., PARLAKIAN, A., GIORDANI, J., LAHOUTE, C., BERTRAND, A., SOTIROPOULOS, A., RENOU, L., SCHMITT, A., MELKI, J., LI, Z., DAEGELEN, D. & TUIL, D. 2006. New role for serum response factor in postnatal skeletal muscle growth and regeneration via the interleukin 4 and insulin-like growth factor 1 pathways. *Mol Cell Biol,* 26**,** 6664-74.

CHEN, C., JACK, J. & GAROFALO, R. S. 1996. The Drosophila insulin receptor is required for normal growth. *Endocrinology,* 137**,** 846-56.

CHEN, H., PAN, Y. X., DUDENHAUSEN, E. E. & KILBERG, M. S. 2004. Amino acid deprivation induces the transcription rate of the human asparagine synthetase gene through a timed program of expression and promoter binding of nutrient-responsive basic region/leucine zipper transcription factors as well as localized histone acetylation. *J Biol Chem,* 279**,** 50829-39.

CHEN, S., MURPHY, J., TOTH, R., CAMPBELL, D. G., MORRICE, N. A. & MACKINTOSH, C. 2008. Complementary regulation of TBC1D1 and AS160 by growth factors, insulin and AMPK activators. *Biochem J,* 409**,** 449-59.

CHENG, L., ESCH, F. S., MARCHIONNI, M. A. & MUDGE, A. W. 1998. Control of Schwann cell survival and proliferation: autocrine factors and neuregulins. *Mol Cell Neurosci,* 12**,** 141-56.

CHENG, L., KHAN, M. & MUDGE, A. W. 1995. Calcitonin gene-related peptide promotes Schwann cell proliferation. *J Cell Biol,* 129**,** 789-96.

CHENG, L. Y., BAILEY, A. P., LEEVERS, S. J., RAGAN, T. J., DRISCOLL, P. C. & GOULD, A. P. 2011. Anaplastic Lymphoma Kinase Spares Organ Growth during Nutrient Restriction in Drosophila. *Cell,* 146**,** 435-47.

CHIEREGATTI, E. & MELDOLESI, J. 2005. Regulated exocytosis: new organelles for non-secretory purposes. *Nat Rev Mol Cell Biol,* 6**,** 181-7.

CHRAST, R., SAHER, G., NAVE, K. A. & VERHEIJEN, M. H. 2011. Lipid metabolism in myelinating glial cells: lessons from human inherited disorders and mouse models. *J Lipid Res,* 52**,** 419-34.

CLAYPOOL, J. A., FRENCH, S. L., JOHZUKA, K., ELIASON, K., VU, L., DODD, J. A., BEYER, A. L. & NOMURA, M. 2004. Tor pathway regulates Rrn3p-dependent recruitment of yeast RNA polymerase I to the promoter but does not participate in alteration of the number of active genes. *Mol Biol Cell,* 15**,** 946-56.

COLLEY, K. J. 1997. Golgi localization of glycosyltransferases: more questions than answers. *Glycobiology,* 7**,** 1-13.

COLLINS, M. J., NAPOLI, I., RIBEIRO, S., ROBERTS, S. & LLOYD, A. C. 2012. Loss of Rb co-operates with Ras to drive oncogenic growth in mammalian cells. *Current biology : CB,* In Press.

CONLON, I. & RAFF, M. 1999. Size control in animal development. *Cell,* 96**,** 235-44.

CONLON, I. & RAFF, M. 2003. Differences in the way a mammalian cell and yeast cells coordinate cell growth and cell-cycle progression. *Journal of biology,* 2**,** 7.

CONLON, I. J., DUNN, G. A., MUDGE, A. W. & RAFF, M. C. 2001. Extracellular control of cell size. *Nature cell biology,* 3**,** 918-21.

CONNER, S. D. & SCHMID, S. L. 2003. Regulated portals of entry into the cell. *Nature,* 422**,** 37-44.

COSTA, J. J., KEFFER, J. M., GOFF, J. P. & METCALFE, D. D. 1992. Aphidicolin-induced proliferative arrest of murine mast cells: morphological and biochemical changes are not accompanied by alterations in cytokine gene induction. *Immunology,* 76**,** 413-21.

COTTER, L., OZCELIK, M., JACOB, C., PEREIRA, J. A., LOCHER, V., BAUMANN, R., RELVAS, J. B., SUTER, U. & TRICAUD, N. 2010. Dlg1-PTEN interaction regulates myelin thickness to prevent damaging peripheral nerve overmyelination. *Science,* 328**,** 1415-8.

COURCHESNE, E., PIERCE, K., SCHUMANN, C. M., REDCAY, E., BUCKWALTER, J. A., KENNEDY, D. P. & MORGAN, J. 2007. Mapping early brain development in autism. *Neuron,* 56**,** 399-413.

CROSS, F. R. 1990. Cell cycle arrest caused by CLN gene deficiency in Saccharomyces cerevisiae resembles START-I arrest and is independent of the mating-pheromone signalling pathway. *Mol Cell Biol,* 10**,** 6482-90.

CUNNINGHAM, J. T., RODGERS, J. T., ARLOW, D. H., VAZQUEZ, F., MOOTHA, V. K. & PUIGSERVER, P. 2007. mTOR controls mitochondrial oxidative function through a YY1-PGC-1alpha transcriptional complex. *Nature,* 450**,** 736-40.

CUPERS, P., VEITHEN, A., KISS, A., BAUDHUIN, P. & COURTOY, P. J. 1994. Clathrin polymerization is not required for bulk-phase endocytosis in rat fetal fibroblasts. *J Cell Biol,* 127**,** 725-35.

DAVIS, T. A. & FIOROTTO, M. L. 2009. Regulation of muscle growth in neonates. *Curr Opin Clin Nutr Metab Care,* 12**,** 78-85.

DE PREUX, A. S., GOOSEN, K., ZHANG, W., SIMA, A. A., SHIMANO, H., OUWENS, D. M., DIAMANT, M., HILLEBRANDS, J. L., ROZING, J., LEMKE, G., BECKMANN, J. S., SMIT, A. B., VERHEIJEN, M. H. & CHRAST, R. 2007. SREBP-1c expression in Schwann cells is affected by diabetes and nutritional status. *Mol Cell Neurosci,* 35**,** 525-34.

DEBERARDINIS, R. J., LUM, J. J., HATZIVASSILIOU, G. & THOMPSON, C. B. 2008a. The biology of cancer: metabolic reprogramming fuels cell growth and proliferation. *Cell metabolism,* 7**,** 11-20.

DEBERARDINIS, R. J., MANCUSO, A., DAIKHIN, E., NISSIM, I., YUDKOFF, M., WEHRLI, S. & THOMPSON, C. B. 2007. Beyond aerobic glycolysis: transformed cells can engage in glutamine metabolism that exceeds the requirement for protein and nucleotide synthesis. *Proceedings of the National Academy of Sciences of the United States of America,* 104**,** 19345-50.

DEBERARDINIS, R. J., SAYED, N., DITSWORTH, D. & THOMPSON, C. B. 2008b. Brick by brick: metabolism and tumor cell growth. *Current opinion in genetics & development,* 18**,** 54-61.

DEBOSCH, B., TRESKOV, I., LUPU, T. S., WEINHEIMER, C., KOVACS, A., COURTOIS, M. & MUSLIN, A. J. 2006. Akt1 is required for physiological cardiac growth. *Circulation,* 113**,** 2097-104.

DEBOSCH, B. J. & MUSLIN, A. J. 2008. Insulin signaling pathways and cardiac growth. *Journal of molecular and cellular cardiology,* 44**,** 855-64.

DEBOSE-BOYD, R. A., BROWN, M. S., LI, W. P., NOHTURFFT, A., GOLDSTEIN, J. L. & ESPENSHADE, P. J. 1999. Transport-dependent proteolysis of SREBP: relocation of site-1 protease from Golgi to ER obviates the need for SREBP transport to Golgi. *Cell,* 99**,** 703-12.

DEMONTIS, F. & PERRIMON, N. 2009. Integration of Insulin receptor/Foxo signaling and dMyc activity during muscle growth regulates body size in Drosophila. *Development,* 136**,** 983-93.

DEMOULIN, J. B., ERICSSON, J., KALLIN, A., RORSMAN, C., RONNSTRAND, L. & HELDIN, C. H. 2004. Platelet-derived growth factor stimulates membrane lipid synthesis through activation of phosphatidylinositol 3-kinase and sterol regulatory element-binding proteins. *J Biol Chem,* 279**,** 35392-402.

DI TALIA, S., SKOTHEIM, J. M., BEAN, J. M., SIGGIA, E. D. & CROSS, F. R. 2007. The effects of molecular noise and size control on variability in the budding yeast cell cycle. *Nature,* 448**,** 947-51.

DIBBLE, C. C., ASARA, J. M. & MANNING, B. D. 2009. Characterization of Rictor phosphorylation sites reveals direct regulation of mTOR complex 2 by S6K1. *Mol Cell Biol,* 29**,** 5657-70.

DICE, J. F. 1990. Peptide sequences that target cytosolic proteins for lysosomal proteolysis. *Trends Biochem Sci,* 15**,** 305-9.

DOLZNIG, H., GREBIEN, F., SAUER, T., BEUG, H. & MULLNER, E. W. 2004. Evidence for a size-sensing mechanism in animal cells. *Nature cell biology,* 6**,** 899-905.

DONG, J., QIU, H., GARCIA-BARRIO, M., ANDERSON, J. & HINNEBUSCH, A. G. 2000. Uncharged tRNA activates GCN2 by displacing the protein kinase moiety from a bipartite tRNA-binding domain. *Mol Cell,* 6**,** 269-79.

DORN, G. W., 2ND & FORCE, T. 2005. Protein kinase cascades in the regulation of cardiac hypertrophy. *J Clin Invest,* 115**,** 527-37.

DREYER, H. C., FUJITA, S., CADENAS, J. G., CHINKES, D. L., VOLPI, E. & RASMUSSEN, B. B. 2006. Resistance exercise increases AMPK activity and reduces 4E-BP1 phosphorylation and protein synthesis in human skeletal muscle. *J Physiol,* 576**,** 613-24.

DU, X., KRISTIANA, I., WONG, J. & BROWN, A. J. 2006. Involvement of Akt in ER-to-Golgi transport of SCAP/SREBP: a link between a key cell proliferative pathway and membrane synthesis. *Mol Biol Cell,* 17**,** 2735-45.

DUNCAN, E. A., BROWN, M. S., GOLDSTEIN, J. L. & SAKAI, J. 1997. Cleavage site for sterol-regulated protease localized to a leu-Ser bond in the lumenal loop of sterol regulatory element-binding protein-2. *J Biol Chem,* 272**,** 12778-85.

DUNCAN, E. A., DAVE, U. P., SAKAI, J., GOLDSTEIN, J. L. & BROWN, M. S. 1998. Second-site cleavage in sterol regulatory element-binding protein occurs at transmembrane junction as determined by cysteine panning. *J Biol Chem,* 273**,** 17801-9.

DUVEL, K., YECIES, J. L., MENON, S., RAMAN, P., LIPOVSKY, A. I., SOUZA, A. L., TRIANTAFELLOW, E., MA, Q., GORSKI, R., CLEAVER, S., VANDER HEIDEN, M. G., MACKEIGAN, J. P., FINAN, P. M., CLISH, C. B., MURPHY, L. O. & MANNING, B. D. 2010. Activation of a metabolic gene regulatory network downstream of mTOR complex 1. *Mol Cell,* 39**,** 171-83.

DYER, N., REBOLLO, E., DOMINGUEZ, P., ELKHATIB, N., CHAVRIER, P., DAVIET, L., GONZALEZ, C. & GONZALEZ-GAITAN, M. 2007. Spermatocyte cytokinesis requires rapid membrane addition mediated by ARF6 on central spindle recycling endosomes. *Development,* 134**,** 4437-47.

EBERLE, D., HEGARTY, B., BOSSARD, P., FERRE, P. & FOUFELLE, F. 2004. SREBP transcription factors: master regulators of lipid homeostasis. *Biochimie,* 86**,** 839-48.

ECHAVE, P., CONLON, I. J. & LLOYD, A. C. 2007. Cell size regulation in mammalian cells. *Cell cycle,* 6**,** 218-24.

ECHAVE, P., MACHADO-DA-SILVA, G., ARKELL, R. S., DUCHEN, M. R., JACOBSON, J., MITTER, R. & LLOYD, A. C. 2009. Extracellular growth factors and mitogens cooperate to drive mitochondrial biogenesis. *Journal of cell science,* 122**,** 4516-25.

EDGAR, B. A. 1999. From small flies come big discoveries about size control. *Nat Cell Biol,* 1**,** E191-3.

EDGAR, B. A. 2006. How flies get their size: genetics meets physiology. *Nature reviews. Genetics,* 7**,** 907-16.

EDINGER, A. L. 2007. Controlling cell growth and survival through regulated nutrient transporter expression. *Biochem J,* 406**,** 1-12.

EDINGER, A. L. & THOMPSON, C. B. 2002. Akt maintains cell size and survival by increasing mTOR-dependent nutrient uptake. *Molecular biology of the cell,* 13**,** 2276-88.

EGAN, D. F., SHACKELFORD, D. B., MIHAYLOVA, M. M., GELINO, S., KOHNZ, R. A., MAIR, W., VASQUEZ, D. S., JOSHI, A., GWINN, D. M., TAYLOR, R., ASARA, J. M., FITZPATRICK, J., DILLIN, A., VIOLLET, B., KUNDU, M., HANSEN, M. & SHAW, R. J. 2011. Phosphorylation of ULK1 (hATG1) by AMP-activated protein kinase connects energy sensing to mitophagy. *Science,* 331**,** 456-61.

ELLIOTT, S. G. & MCLAUGHLIN, C. S. 1978. Rate of macromolecular synthesis through the cell cycle of the yeast Saccharomyces cerevisiae. *Proc Natl Acad Sci U S A,* 75**,** 4384-8.

ELSTROM, R. L., BAUER, D. E., BUZZAI, M., KARNAUSKAS, R., HARRIS, M. H., PLAS, D. R., ZHUANG, H., CINALLI, R. M., ALAVI, A., RUDIN, C. M. & THOMPSON, C. B. 2004. Akt stimulates aerobic glycolysis in cancer cells. *Cancer Res,* 64**,** 3892-9.

EMOTO, K., PARRISH, J. Z., JAN, L. Y. & JAN, Y. N. 2006. The tumour suppressor Hippo acts with the NDR kinases in dendritic tiling and maintenance. *Nature,* 443**,** 210-3.

ENGELMAN, J. A., LUO, J. & CANTLEY, L. C. 2006. The evolution of phosphatidylinositol 3-kinases as regulators of growth and metabolism. *Nat Rev Genet,* 7**,** 606-19.

ESPENSHADE, P. J., LI, W. P. & YABE, D. 2002. Sterols block binding of COPII proteins to SCAP, thereby controlling SCAP sorting in ER. *Proc Natl Acad Sci U S A,* 99**,** 11694-9.

FAN, Y., DICKMAN, K. G. & ZONG, W. X. 2010. Akt and c-Myc differentially activate cellular metabolic programs and prime cells to bioenergetic inhibition. *J Biol Chem,* 285**,** 7324-33.

FANKHAUSER, G. 1945. Maintenance of normal structure in heteroploid salamander larvae, through compensation of changes in cell size by adjustment of cell number and cell shape. *The Journal of experimental zoology,* 100**,** 445-55.

FANTES, P. & NURSE, P. 1977. Control of cell size at division in fission yeast by a growth-modulated size control over nuclear division. *Exp Cell Res,* 107**,** 377-86.

FEDEROVITCH, C. M., RON, D. & HAMPTON, R. Y. 2005. The dynamic ER: experimental approaches and current questions. *Current opinion in cell biology,* 17**,** 409-14.

FERO, M. L., RIVKIN, M., TASCH, M., PORTER, P., CAROW, C. E., FIRPO, E., POLYAK, K., TSAI, L. H., BROUDY, V., PERLMUTTER, R. M., KAUSHANSKY, K. & ROBERTS, J. M. 1996. A syndrome of multiorgan hyperplasia with features of gigantism, tumorigenesis, and female sterility in p27(Kip1)-deficient mice. *Cell,* 85**,** 733-44.

FINGAR, D. C., SALAMA, S., TSOU, C., HARLOW, E. & BLENIS, J. 2002. Mammalian cell size is controlled by mTOR and its downstream targets S6K1 and 4EBP1/eIF4E. *Genes Dev,* 16**,** 1472-87.

FLEMMING, A. J., SHEN, Z. Z., CUNHA, A., EMMONS, S. W. & LEROI, A. M. 2000. Somatic polyploidization and cellular proliferation drive body size evolution in nematodes. *Proceedings of the National Academy of Sciences of the United States of America,* 97**,** 5285-90.

FLORES, A. I., NARAYANAN, S. P., MORSE, E. N., SHICK, H. E., YIN, X., KIDD, G., AVILA, R. L., KIRSCHNER, D. A. & MACKLIN, W. B. 2008. Constitutively active Akt induces enhanced myelination in the CNS. *J Neurosci,* 28**,** 7174-83.

FOSTER, D. A. 2009. Phosphatidic acid signaling to mTOR: signals for the survival of human cancer cells. *Biochim Biophys Acta,* 1791**,** 949-55.

FRANK, D. J., EDGAR, B. A. & ROTH, M. B. 2002. The Drosophila melanogaster gene brain tumor negatively regulates cell growth and ribosomal RNA synthesis. *Development,* 129**,** 399-407.

FRANKLIN, J. L. & JOHNSON, E. M. 1998. Control of neuronal size homeostasis by trophic factor-mediated coupling of protein degradation to protein synthesis. *The Journal of cell biology,* 142**,** 1313-24.

FRICKER, F. R. & BENNETT, D. L. 2011. The role of neuregulin-1 in the response to nerve injury. *Future Neurol,* 6**,** 809-822.

FRICKER, F. R., LAGO, N., BALARAJAH, S., TSANTOULAS, C., TANNA, S., ZHU, N., FAGEIRY, S. K., JENKINS, M., GARRATT, A. N., BIRCHMEIER, C. & BENNETT, D. L. 2011. Axonally derived neuregulin-1 is required for remyelination and regeneration after nerve injury in adulthood. *J Neurosci,* 31**,** 3225-33.

GAFFIELD, M. A. & BETZ, W. J. 2006. Imaging synaptic vesicle exocytosis and endocytosis with FM dyes. *Nat Protoc,* 1**,** 2916-21.

GALVEZ, T., TERUEL, M. N., HEO, W. D., JONES, J. T., KIM, M. L., LIOU, J., MYERS, J. W. & MEYER, T. 2007. siRNA screen of the human signaling proteome identifies the PtdIns(3,4,5)P3-mTOR signaling pathway as a primary regulator of transferrin uptake. *Genome Biol,* 8**,** R142.

GAO, P., TCHERNYSHYOV, I., CHANG, T. C., LEE, Y. S., KITA, K., OCHI, T., ZELLER, K. I., DE MARZO, A. M., VAN EYK, J. E., MENDELL, J. T. & DANG, C. V. 2009. c-Myc suppression of miR-23a/b enhances mitochondrial glutaminase expression and glutamine metabolism. *Nature,* 458**,** 762-5.

GAO, X. & PAN, D. 2001. TSC1 and TSC2 tumor suppressors antagonize insulin signaling in cell growth. *Genes & development,* 15**,** 1383-92.

GARRATT, A. N., BRITSCH, S. & BIRCHMEIER, C. 2000a. Neuregulin, a factor with many functions in the life of a schwann cell. *Bioessays,* 22**,** 987-96.

GARRATT, A. N., VOICULESCU, O., TOPILKO, P., CHARNAY, P. & BIRCHMEIER, C. 2000b. A dual role of erbB2 in myelination and in expansion of the schwann cell precursor pool. *J Cell Biol,* 148**,** 1035-46.

GEBERT, N., RYAN, M. T., PFANNER, N., WIEDEMANN, N. & STOJANOVSKI, D. 2011. Mitochondrial protein import machineries and lipids: a functional connection. *Biochim Biophys Acta,* 1808**,** 1002-11.

GIACINTI, C. & GIORDANO, A. 2006. RB and cell cycle progression. *Oncogene,* 25**,** 5220-7.

GIANDOMENICO, V., SIMONSSON, M., GRONROOS, E. & ERICSSON, J. 2003. Coactivator-dependent acetylation stabilizes members of the SREBP family of transcription factors. *Mol Cell Biol,* 23**,** 2587-99.

GLASS, D. J. 2003. Signalling pathways that mediate skeletal muscle hypertrophy and atrophy. *Nat Cell Biol,* 5**,** 87-90.

GLEBOVA, N. O. & GINTY, D. D. 2004. Heterogeneous requirement of NGF for sympathetic target innervation in vivo. *J Neurosci,* 24**,** 743-51.

GODIN, M., DELGADO, F. F., SON, S., GROVER, W. H., BRYAN, A. K., TZUR, A., JORGENSEN, P., PAYER, K., GROSSMAN, A. D., KIRSCHNER, M. W. & MANALIS, S. R. 2010. Using buoyant mass to measure the growth of single cells. *Nature methods,* 7**,** 387-90.

GOEBBELS, S., OLTROGGE, J. H., KEMPER, R., HEILMANN, I., BORMUTH, I., WOLFER, S., WICHERT, S. P., MOBIUS, W., LIU, X., LAPPE-SIEFKE, C., ROSSNER, M. J., GROSZER, M., SUTER, U., FRAHM, J., BORETIUS, S. & NAVE, K. A. 2010. Elevated phosphatidylinositol 3,4,5-trisphosphate in glia triggers cell-autonomous membrane wrapping and myelination. *J Neurosci,* 30**,** 8953-64.

GOHIL, V. M. & GREENBERG, M. L. 2009. Mitochondrial membrane biogenesis: phospholipids and proteins go hand in hand. *J Cell Biol,* 184**,** 469-72.

GOLDBERG, I. J., ECKEL, R. H. & ABUMRAD, N. A. 2009. Regulation of fatty acid uptake into tissues: lipoprotein lipase- and CD36-mediated pathways. *J Lipid Res,* 50 Suppl**,** S86-90.

GOLDSTEIN, J. L. & BROWN, M. S. 1977. The low-density lipoprotein pathway and its relation to atherosclerosis. *Annu Rev Biochem,* 46**,** 897-930.

GOLDSTEIN, J. L. & BROWN, M. S. 1990. Regulation of the mevalonate pathway. *Nature,* 343**,** 425-30.

GOLDSTEIN, J. L., DEBOSE-BOYD, R. A. & BROWN, M. S. 2006. Protein sensors for membrane sterols. *Cell,* 124**,** 35-46.

GOMES, L. C., DI BENEDETTO, G. & SCORRANO, L. 2011a. During autophagy mitochondria elongate, are spared from degradation and sustain cell viability. *Nat Cell Biol,* 13**,** 589-98.

GOMES, L. C., DI BENEDETTO, G. & SCORRANO, L. 2011b. Essential amino acids and glutamine regulate induction of mitochondrial elongation during autophagy. *Cell Cycle,* 10**,** 2635-9.

GOMES, L. C. & SCORRANO, L. 2011. Mitochondrial elongation during autophagy: a stereotypical response to survive in difficult times. *Autophagy,* 7**,** 1251-3.

GONG, Y., LEE, J. N., LEE, P. C., GOLDSTEIN, J. L., BROWN, M. S. & YE, J. 2006. Sterol-regulated ubiquitination and degradation of Insig-1 creates a convergent mechanism for feedback control of cholesterol synthesis and uptake. *Cell Metab,* 3**,** 15-24.

GORANOV, A. I. & AMON, A. 2010. Growth and division--not a one-way road. *Curr Opin Cell Biol,* 22**,** 795-800.

GRAEF, I. A., WANG, F., CHARRON, F., CHEN, L., NEILSON, J., TESSIER-LAVIGNE, M. & CRABTREE, G. R. 2003. Neurotrophins and netrins require calcineurin/NFAT signaling to stimulate outgrowth of embryonic axons. *Cell,* 113**,** 657-70.

GRANT, B. D. & DONALDSON, J. G. 2009. Pathways and mechanisms of endocytic recycling. *Nat Rev Mol Cell Biol,* 10**,** 597-608.
GRAVES, J. A., WANG, Y., SIMS-LUCAS, S., CHEROK, E., ROTHERMUND, K., BRANCA, M. F., ELSTER, J., BEER-STOLZ, D., VAN HOUTEN, B., VOCKLEY, J. & PROCHOWNIK, E. V. 2012. Mitochondrial Structure, Function and Dynamics Are Temporally Controlled by c-Myc. *PLoS One,* 7**,** e37699.
GREWAL, S. S. & EDGAR, B. A. 2003. Controlling cell division in yeast and animals: does size matter? *J Biol,* 2**,** 5.
GREWAL, S. S., EVANS, J. R. & EDGAR, B. A. 2007. Drosophila TIF-IA is required for ribosome synthesis and cell growth and is regulated by the TOR pathway. *J Cell Biol,* 179**,** 1105-13.
GREWAL, S. S., LI, L., ORIAN, A., EISENMAN, R. N. & EDGAR, B. A. 2005. Myc-dependent regulation of ribosomal RNA synthesis during Drosophila development. *Nat Cell Biol,* 7**,** 295-302.
GRIFFITHS, G., BACK, R. & MARSH, M. 1989. A quantitative analysis of the endocytic pathway in baby hamster kidney cells. *J Cell Biol,* 109**,** 2703-20.
GUERCI, A., LAHOUTE, C., HEBRARD, S., COLLARD, L., GRAINDORGE, D., FAVIER, M., CAGNARD, N., BATONNET-PICHON, S., PRECIGOUT, G., GARCIA, L., TUIL, D., DAEGELEN, D. & SOTIROPOULOS, A. 2012. Srf-dependent paracrine signals produced by myofibers control satellite cell-mediated skeletal muscle hypertrophy. *Cell Metab,* 15**,** 25-37.
GUERTIN, D. A., GUNTUR, K. V., BELL, G. W., THOREEN, C. C. & SABATINI, D. M. 2006. Functional genomics identifies TOR-regulated genes that control growth and division. *Curr Biol,* 16**,** 958-70.
GULVE, E. A. & DICE, J. F. 1989. Regulation of protein synthesis and degradation in L8 myotubes. Effects of serum, insulin and insulin-like growth factors. *Biochem J,* 260**,** 377-87.
GUO, F. & CAVENER, D. R. 2007. The GCN2 eIF2alpha kinase regulates fatty-acid homeostasis in the liver during deprivation of an essential amino acid. *Cell Metab,* 5**,** 103-14.
GUTHRIE, H. A. & BROWN, M. L. 1968. Effect of severe undernutrition in early life on growth, brain size and composition in adult rats. *The Journal of nutrition,* 94**,** 419-26.
GWINN, D. M., SHACKELFORD, D. B., EGAN, D. F., MIHAYLOVA, M. M., MERY, A., VASQUEZ, D. S., TURK, B. E. & SHAW, R. J. 2008. AMPK phosphorylation of raptor mediates a metabolic checkpoint. *Mol Cell,* 30**,** 214-26.
HADWIGER, J. A., WITTENBERG, C., RICHARDSON, H. E., DE BARROS LOPES, M. & REED, S. I. 1989. A family of cyclin homologs that control the G1 phase in yeast. *Proc Natl Acad Sci U S A,* 86**,** 6255-9.
HAGIWARA, A., CORNU, M., CYBULSKI, N., POLAK, P., BETZ, C., TRAPANI, F., TERRACCIANO, L., HEIM, M. H., RUEGG, M. A. & HALL, M. N. 2012. Hepatic mTORC2 activates glycolysis and lipogenesis through Akt, glucokinase, and SREBP1c. *Cell Metab,* 15**,** 725-38.
HAHN, W. C. & WEINBERG, R. A. 2002. Modelling the molecular circuitry of cancer. *Nat Rev Cancer,* 2**,** 331-41.
HANNAH, V. C., OU, J., LUONG, A., GOLDSTEIN, J. L. & BROWN, M. S. 2001. Unsaturated fatty acids down-regulate srebp isoforms 1a and 1c by two mechanisms in HEK-293 cells. *J Biol Chem,* 276**,** 4365-72.
HANNAN, K. M., BRANDENBURGER, Y., JENKINS, A., SHARKEY, K., CAVANAUGH, A., ROTHBLUM, L., MOSS, T., POORTINGA, G., MCARTHUR, G. A., PEARSON, R. B. & HANNAN, R. D. 2003. mTOR-dependent regulation of ribosomal gene

transcription requires S6K1 and is mediated by phosphorylation of the carboxy-terminal activation domain of the nucleolar transcription factor UBF. *Mol Cell Biol,* 23**,** 8862-77.

HAO, M., LIN, S. X., KARYLOWSKI, O. J., WUSTNER, D., MCGRAW, T. E. & MAXFIELD, F. R. 2002. Vesicular and non-vesicular sterol transport in living cells. The endocytic recycling compartment is a major sterol storage organelle. *J Biol Chem,* 277**,** 609-17.

HAO, M. & MAXFIELD, F. R. 2000. Characterization of rapid membrane internalization and recycling. *J Biol Chem,* 275**,** 15279-86.

HARA-CHIKUMA, M., SOHARA, E., RAI, T., IKAWA, M., OKABE, M., SASAKI, S., UCHIDA, S. & VERKMAN, A. S. 2005. Progressive adipocyte hypertrophy in aquaporin-7-deficient mice: adipocyte glycerol permeability as a novel regulator of fat accumulation. *J Biol Chem,* 280**,** 15493-6.

HARDIE, D. G. 2011. AMP-activated protein kinase: an energy sensor that regulates all aspects of cell function. *Genes Dev,* 25**,** 1895-908.

HARDING, H. P., NOVOA, I., ZHANG, Y., ZENG, H., WEK, R., SCHAPIRA, M. & RON, D. 2000. Regulated translation initiation controls stress-induced gene expression in mammalian cells. *Mol Cell,* 6**,** 1099-108.

HARDING, H. P., ZHANG, Y., ZENG, H., NOVOA, I., LU, P. D., CALFON, M., SADRI, N., YUN, C., POPKO, B., PAULES, R., STOJDL, D. F., BELL, J. C., HETTMANN, T., LEIDEN, J. M. & RON, D. 2003. An integrated stress response regulates amino acid metabolism and resistance to oxidative stress. *Mol Cell,* 11**,** 619-33.

HARRISINGH, M. C., PEREZ-NADALES, E., PARKINSON, D. B., MALCOLM, D. S., MUDGE, A. W. & LLOYD, A. C. 2004. The Ras/Raf/ERK signalling pathway drives Schwann cell dedifferentiation. *EMBO J,* 23**,** 3061-71.

HASLER, U., JEON, U. S., KIM, J. A., MORDASINI, D., KWON, H. M., FERAILLE, E. & MARTIN, P. Y. 2006. Tonicity-responsive enhancer binding protein is an essential regulator of aquaporin-2 expression in renal collecting duct principal cells. *J Am Soc Nephrol,* 17**,** 1521-31.

HATZIVASSILIOU, G., ZHAO, F., BAUER, D. E., ANDREADIS, C., SHAW, A. N., DHANAK, D., HINGORANI, S. R., TUVESON, D. A. & THOMPSON, C. B. 2005. ATP citrate lyase inhibition can suppress tumor cell growth. *Cancer Cell,* 8**,** 311-21.

HEALLEN, T., ZHANG, M., WANG, J., BONILLA-CLAUDIO, M., KLYSIK, E., JOHNSON, R. L. & MARTIN, J. F. 2011. Hippo pathway inhibits Wnt signaling to restrain cardiomyocyte proliferation and heart size. *Science,* 332**,** 458-61.

HEGARTY, B. D., BOBARD, A., HAINAULT, I., FERRE, P., BOSSARD, P. & FOUFELLE, F. 2005. Distinct roles of insulin and liver X receptor in the induction and cleavage of sterol regulatory element-binding protein-1c. *Proc Natl Acad Sci U S A,* 102**,** 791-6.

HENERY, C. C., BARD, J. B. & KAUFMAN, M. H. 1992. Tetraploidy in mice, embryonic cell number, and the grain of the developmental map. *Developmental biology,* 152**,** 233-41.

HENNIG, K. M., COLOMBANI, J. & NEUFELD, T. P. 2006. TOR coordinates bulk and targeted endocytosis in the Drosophila melanogaster fat body to regulate cell growth. *J Cell Biol,* 173**,** 963-74.

HERBERT, T. P., KILHAMS, G. R., BATTY, I. H. & PROUD, C. G. 2000. Distinct signalling pathways mediate insulin and phorbol ester-stimulated eukaryotic initiation factor 4F assembly and protein synthesis in HEK 293 cells. *J Biol Chem,* 275**,** 11249-56.

HERRANZ, H., HONG, X., PEREZ, L., FERREIRA, A., OLIVIERI, D., COHEN, S. M. & MILAN, M. 2010. The miRNA machinery targets Mei-P26 and regulates Myc protein levels in the Drosophila wing. *The EMBO journal,* 29**,** 1688-98.

HIBUSE, T., MAEDA, N., FUNAHASHI, T., YAMAMOTO, K., NAGASAWA, A., MIZUNOYA, W., KISHIDA, K., INOUE, K., KURIYAMA, H., NAKAMURA, T., FUSHIKI, T., KIHARA, S. & SHIMOMURA, I. 2005. Aquaporin 7 deficiency is associated with development of obesity through activation of adipose glycerol kinase. *Proc Natl Acad Sci U S A,* 102**,** 10993-8.

HIRANO, Y., MURATA, S., TANAKA, K., SHIMIZU, M. & SATO, R. 2003. Sterol regulatory element-binding proteins are negatively regulated through SUMO-1 modification independent of the ubiquitin/26 S proteasome pathway. *J Biol Chem,* 278**,** 16809-19.

HIRANO, Y., YOSHIDA, M., SHIMIZU, M. & SATO, R. 2001. Direct demonstration of rapid degradation of nuclear sterol regulatory element-binding proteins by the ubiquitin-proteasome pathway. *J Biol Chem,* 276**,** 36431-7.

HOCK, M. B. & KRALLI, A. 2009. Transcriptional control of mitochondrial biogenesis and function. *Annu Rev Physiol,* 71**,** 177-203.

HOGAN, P. G., CHEN, L., NARDONE, J. & RAO, A. 2003. Transcriptional regulation by calcium, calcineurin, and NFAT. *Genes Dev,* 17**,** 2205-32.

HORTON, J. D., GOLDSTEIN, J. L. & BROWN, M. S. 2002. SREBPs: activators of the complete program of cholesterol and fatty acid synthesis in the liver. *J Clin Invest,* 109**,** 1125-31.

HORTON, J. D., SHAH, N. A., WARRINGTON, J. A., ANDERSON, N. N., PARK, S. W., BROWN, M. S. & GOLDSTEIN, J. L. 2003a. Combined analysis of oligonucleotide microarray data from transgenic and knockout mice identifies direct SREBP target genes. *Proc Natl Acad Sci U S A,* 100**,** 12027-32.

HORTON, J. D., SHIMOMURA, I., BROWN, M. S., HAMMER, R. E., GOLDSTEIN, J. L. & SHIMANO, H. 1998. Activation of cholesterol synthesis in preference to fatty acid synthesis in liver and adipose tissue of transgenic mice overproducing sterol regulatory element-binding protein-2. *J Clin Invest,* 101**,** 2331-9.

HORTON, J. D., SHIMOMURA, I., IKEMOTO, S., BASHMAKOV, Y. & HAMMER, R. E. 2003b. Overexpression of sterol regulatory element-binding protein-1a in mouse adipose tissue produces adipocyte hypertrophy, increased fatty acid secretion, and fatty liver. *J Biol Chem,* 278**,** 36652-60.

HSIEH, A. C., LIU, Y., EDLIND, M. P., INGOLIA, N. T., JANES, M. R., SHER, A., SHI, E. Y., STUMPF, C. R., CHRISTENSEN, C., BONHAM, M. J., WANG, S., REN, P., MARTIN, M., JESSEN, K., FELDMAN, M. E., WEISSMAN, J. S., SHOKAT, K. M., ROMMEL, C. & RUGGERO, D. 2012. The translational landscape of mTOR signalling steers cancer initiation and metastasis. *Nature,* 485**,** 55-61.

HU, X., HE, W., DIACONU, C., TANG, X., KIDD, G. J., MACKLIN, W. B., TRAPP, B. D. & YAN, R. 2008. Genetic deletion of BACE1 in mice affects remyelination of sciatic nerves. *FASEB J,* 22**,** 2970-80.

HU, X., HICKS, C. W., HE, W., WONG, P., MACKLIN, W. B., TRAPP, B. D. & YAN, R. 2006. Bace1 modulates myelination in the central and peripheral nervous system. *Nat Neurosci,* 9**,** 1520-5.

HUA, X., NOHTURFFT, A., GOLDSTEIN, J. L. & BROWN, M. S. 1996. Sterol resistance in CHO cells traced to point mutation in SREBP cleavage-activating protein. *Cell,* 87**,** 415-26.

HUANG, J. & MANNING, B. D. 2008. The TSC1-TSC2 complex: a molecular switchboard controlling cell growth. *Biochem J,* 412**,** 179-90.

IKEGAMI, S., TAGUCHI, T., OHASHI, M., OGURO, M., NAGANO, H. & MANO, Y. 1978. Aphidicolin prevents mitotic cell division by interfering with the activity of DNA polymerase-alpha. *Nature,* 275**,** 458-60.

INOKI, K., CORRADETTI, M. N. & GUAN, K. L. 2005. Dysregulation of the TSC-mTOR pathway in human disease. *Nat Genet,* 37**,** 19-24.

INOKI, K., LI, Y., XU, T. & GUAN, K. L. 2003a. Rheb GTPase is a direct target of TSC2 GAP activity and regulates mTOR signaling. *Genes & development,* 17**,** 1829-34.

INOKI, K., LI, Y., ZHU, T., WU, J. & GUAN, K. L. 2002. TSC2 is phosphorylated and inhibited by Akt and suppresses mTOR signalling. *Nat Cell Biol,* 4**,** 648-57.

INOKI, K., ZHU, T. & GUAN, K. L. 2003b. TSC2 mediates cellular energy response to control cell growth and survival. *Cell,* 115**,** 577-90.

INOUE, M., ZHAI, H., SAKAZAKI, H., FURUYAMA, H., FUKUYAMA, Y. & HIRAMA, M. 2004. TMC-95A, a reversible proteasome inhibitor, induces neurite outgrowth in PC12 cells. *Bioorg Med Chem Lett,* 14**,** 663-5.

INOUE, N., SHIMANO, H., NAKAKUKI, M., MATSUZAKA, T., NAKAGAWA, Y., YAMAMOTO, T., SATO, R., TAKAHASHI, A., SONE, H., YAHAGI, N., SUZUKI, H., TOYOSHIMA, H. & YAMADA, N. 2005. Lipid synthetic transcription factor SREBP-1a activates p21WAF1/CIP1, a universal cyclin-dependent kinase inhibitor. *Mol Cell Biol,* 25**,** 8938-47.

IRARRAZABAL, C. E., BURG, M. B., WARD, S. G. & FERRARIS, J. D. 2006. Phosphatidylinositol 3-kinase mediates activation of ATM by high NaCl and by ionizing radiation: Role in osmoprotective transcriptional regulation. *Proc Natl Acad Sci U S A,* 103**,** 8882-7.

IRITANI, B. M. & EISENMAN, R. N. 1999. c-Myc enhances protein synthesis and cell size during B lymphocyte development. *Proc Natl Acad Sci U S A,* 96**,** 13180-5.

JACKSON, R. J., HELLEN, C. U. & PESTOVA, T. V. 2010. The mechanism of eukaryotic translation initiation and principles of its regulation. *Nat Rev Mol Cell Biol,* 11**,** 113-27.

JAGOE, R. T. & GOLDBERG, A. L. 2001. What do we really know about the ubiquitin-proteasome pathway in muscle atrophy? *Curr Opin Clin Nutr Metab Care,* 4**,** 183-90.

JAMES, M. J. & ZOMERDIJK, J. C. 2004. Phosphatidylinositol 3-kinase and mTOR signaling pathways regulate RNA polymerase I transcription in response to IGF-1 and nutrients. *J Biol Chem,* 279**,** 8911-8.

JECKEL, D., KARRENBAUER, A., BIRK, R., SCHMIDT, R. R. & WIELAND, F. 1990. Sphingomyelin is synthesized in the cis Golgi. *FEBS Lett,* 261**,** 155-7.

JEFFERIES, H. B., FUMAGALLI, S., DENNIS, P. B., REINHARD, C., PEARSON, R. B. & THOMAS, G. 1997. Rapamycin suppresses 5'TOP mRNA translation through inhibition of p70s6k. *EMBO J,* 16**,** 3693-704.

JEON, H. & BLACKLOW, S. C. 2005. Structure and physiologic function of the low-density lipoprotein receptor. *Annu Rev Biochem,* 74**,** 535-62.

JIN, Q., YUAN, L. X., BOULBES, D., BAEK, J. M., WANG, Y. N., GOMEZ-CABELLO, D., HAWKE, D. H., YEUNG, S. C., LEE, M. H., HORTOBAGYI, G. N., HUNG, M. C. & ESTEVA, F. J. 2010. Fatty acid synthase phosphorylation: a novel therapeutic target in HER2-overexpressing breast cancer cells. *Breast Cancer Res,* 12**,** R96.

JOHNSTON, G. C., PRINGLE, J. R. & HARTWELL, L. H. 1977. Coordination of growth with cell division in the yeast Saccharomyces cerevisiae. *Experimental cell research,* 105**,** 79-98.

JOHNSTON, L. A., PROBER, D. A., EDGAR, B. A., EISENMAN, R. N. & GALLANT, P. 1999. Drosophila myc regulates cellular growth during development. *Cell,* 98**,** 779-90.

JORGENSEN, P., EDGINGTON, N. P., SCHNEIDER, B. L., RUPES, I., TYERS, M. & FUTCHER, B. 2007. The size of the nucleus increases as yeast cells grow. *Mol Biol Cell,* 18**,** 3523-32.

JORGENSEN, P., NISHIKAWA, J. L., BREITKREUTZ, B. J. & TYERS, M. 2002. Systematic identification of pathways that couple cell growth and division in yeast. *Science,* 297**,** 395-400.

JORGENSEN, P., RUPES, I., SHAROM, J. R., SCHNEPER, L., BROACH, J. R. & TYERS, M. 2004. A dynamic transcriptional network communicates growth potential to ribosome synthesis and critical cell size. *Genes Dev,* 18**,** 2491-505.

JORGENSEN, P. & TYERS, M. 2004. How cells coordinate growth and division. *Curr Biol,* 14**,** R1014-27.

JULIEN, L. A., CARRIERE, A., MOREAU, J. & ROUX, P. P. 2010. mTORC1-activated S6K1 phosphorylates Rictor on threonine 1135 and regulates mTORC2 signaling. *Mol Cell Biol,* 30**,** 908-21.

JUNG, C. H., RO, S. H., CAO, J., OTTO, N. M. & KIM, D. H. 2010. mTOR regulation of autophagy. *FEBS Lett,* 584**,** 1287-95.

KAO, S. C., WU, H., XIE, J., CHANG, C. P., RANISH, J. A., GRAEF, I. A. & CRABTREE, G. R. 2009. Calcineurin/NFAT signaling is required for neuregulin-regulated Schwann cell differentiation. *Science,* 323**,** 651-4.

KAPLAN, M. R. & SIMONI, R. D. 1985. Intracellular transport of phosphatidylcholine to the plasma membrane. *J Cell Biol,* 101**,** 441-5.

KAST, H. R., NGUYEN, C. M., ANISFELD, A. M., ERICSSON, J. & EDWARDS, P. A. 2001. CTP:phosphocholine cytidylyltransferase, a new sterol- and SREBP-responsive gene. *J Lipid Res,* 42**,** 1266-72.

KAVAKEBI, P., HAUSOTT, B., TOMASINO, A., INGOROKVA, S. & KLIMASCHEWSKI, L. 2005. The N-end rule ubiquitin-conjugating enzyme, HR6B, is up-regulated by nerve growth factor and required for neurite outgrowth. *Mol Cell Neurosci,* 29**,** 559-68.

KEHAT, I. & MOLKENTIN, J. D. 2010. Molecular pathways underlying cardiac remodeling during pathophysiological stimulation. *Circulation,* 122**,** 2727-35.

KELLNER-WEIBEL, G., JEROME, W. G., SMALL, D. M., WARNER, G. J., STOLTENBORG, J. K., KEARNEY, M. A., CORJAY, M. H., PHILLIPS, M. C. & ROTHBLAT, G. H. 1998. Effects of intracellular free cholesterol accumulation on macrophage viability: a model for foam cell death. *Arterioscler Thromb Vasc Biol,* 18**,** 423-31.

KILLANDE.D & ZETTERBE.A 1965a. A Quantitative Cytochemical Investigation of Relationship between Cell Mass and Initiation of DNA Synthesis in Mouse Fibroblasts in Vitro. *Experimental cell research,* 40**,** 12-&.

KILLANDE.D & ZETTERBE.A 1965b. Quantitative Cytochemical Studies on Interphase Growth .I. Determination of DNA Rna and Mass Content of Age Determined Mouse Fibroblasts in Vitro and of Intercellular Variation in Generation Time. *Experimental cell research,* 38**,** 272-&.

KIM, D. H., SARBASSOV, D. D., ALI, S. M., KING, J. E., LATEK, R. R., ERDJUMENT-BROMAGE, H., TEMPST, P. & SABATINI, D. M. 2002. mTOR interacts with raptor to form a nutrient-sensitive complex that signals to the cell growth machinery. *Cell,* 110**,** 163-75.

KIM, E., GORAKSHA-HICKS, P., LI, L., NEUFELD, T. P. & GUAN, K. L. 2008a. Regulation of TORC1 by Rag GTPases in nutrient response. *Nature cell biology,* 10**,** 935-45.

KIM, J., KUNDU, M., VIOLLET, B. & GUAN, K. L. 2011. AMPK and mTOR regulate autophagy through direct phosphorylation of Ulk1. *Nat Cell Biol,* 13**,** 132-41.

KIM, J., LEE, J. H. & IYER, V. R. 2008b. Global identification of Myc target genes reveals its direct role in mitochondrial biogenesis and its E-box usage in vivo. *PLoS One,* 3**,** e1798.

KIM, J., WENDE, A. R., SENA, S., THEOBALD, H. A., SOTO, J., SLOAN, C., WAYMENT, B. E., LITWIN, S. E., HOLZENBERGER, M., LEROITH, D. & ABEL, E. D. 2008c. Insulin-like growth factor I receptor signaling is required for exercise-induced cardiac hypertrophy. *Molecular endocrinology,* 22**,** 2531-43.

KIM, S., LI, Q., DANG, C. V. & LEE, L. A. 2000. Induction of ribosomal genes and hepatocyte hypertrophy by adenovirus-mediated expression of c-Myc in vivo. *Proc Natl Acad Sci U S A,* 97**,** 11198-202.

KIM, Y. M., SHIN, H. T., SEO, Y. H., BYUN, H. O., YOON, S. H., LEE, I. K., HYUN, D. H., CHUNG, H. Y. & YOON, G. 2010. Sterol regulatory element-binding protein (SREBP)-1-mediated lipogenesis is involved in cell senescence. *J Biol Chem,* 285**,** 29069-77.

KIM, Y. M., STONE, M., HWANG, T. H., KIM, Y. G., DUNLEVY, J. R., GRIFFIN, T. J. & KIM, D. H. 2012. SH3BP4 Is a Negative Regulator of Amino Acid-Rag GTPase-mTORC1 Signaling. *Mol Cell*.

KIMBALL, S. R. 2002. Regulation of global and specific mRNA translation by amino acids. *J Nutr,* 132**,** 883-6.

KING, L. S., KOZONO, D. & AGRE, P. 2004. From structure to disease: the evolving tale of aquaporin biology. *Nat Rev Mol Cell Biol,* 5**,** 687-98.

KIRK, S. J., CLIFF, J. M., THOMAS, J. A. & WARD, T. H. 2010. Biogenesis of secretory organelles during B cell differentiation. *Journal of leukocyte biology,* 87**,** 245-55.

KIRKLAND, R. A. & FRANKLIN, J. L. 2007. Rate of neurite outgrowth in sympathetic neurons is highly resistant to suppression of protein synthesis: role of protein degradation/synthesis coupling. *Neuroscience letters,* 411**,** 52-5.

KIYOKAWA, H., KINEMAN, R. D., MANOVA-TODOROVA, K. O., SOARES, V. C., HOFFMAN, E. S., ONO, M., KHANAM, D., HAYDAY, A. C., FROHMAN, L. A. & KOFF, A. 1996. Enhanced growth of mice lacking the cyclin-dependent kinase inhibitor function of p27(Kip1). *Cell,* 85**,** 721-32.

KOCKEL, L., KERR, K. S., MELNICK, M., BRUCKNER, K., HEBROK, M. & PERRIMON, N. 2010. Dynamic switch of negative feedback regulation in Drosophila Akt-TOR signaling. *PLoS Genet,* 6**,** e1000990.

KOGA, D. & USHIKI, T. 2006. Three-dimensional ultrastructure of the Golgi apparatus in different cells: high-resolution scanning electron microscopy of osmium-macerated tissues. *Arch Histol Cytol,* 69**,** 357-74.

KONG, D. & YAMORI, T. 2007. ZSTK474 is an ATP-competitive inhibitor of class I phosphatidylinositol 3 kinase isoforms. *Cancer Sci,* 98**,** 1638-42.

KOTZKA, J., KNEBEL, B., HAAS, J., KREMER, L., JACOB, S., HARTWIG, S., NITZGEN, U. & MULLER-WIELAND, D. 2012. Preventing phosphorylation of sterol regulatory element-binding protein 1a by MAP-kinases protects mice from fatty liver and visceral obesity. *PLoS One,* 7**,** e32609.

KOTZKA, J., LEHR, S., ROTH, G., AVCI, H., KNEBEL, B. & MULLER-WIELAND, D. 2004. Insulin-activated Erk-mitogen-activated protein kinases phosphorylate

sterol regulatory element-binding Protein-2 at serine residues 432 and 455 in vivo. *J Biol Chem,* 279**,** 22404-11.

KOTZKA, J., MULLER-WIELAND, D., ROTH, G., KREMER, L., MUNCK, M., SCHURMANN, S., KNEBEL, B. & KRONE, W. 2000. Sterol regulatory element binding proteins (SREBP)-1a and SREBP-2 are linked to the MAP-kinase cascade. *J Lipid Res,* 41**,** 99-108.

KOVAL, M. & PAGANO, R. E. 1990. Sorting of an internalized plasma membrane lipid between recycling and degradative pathways in normal and Niemann-Pick, type A fibroblasts. *J Cell Biol,* 111**,** 429-42.

KUHAJDA, F. P., PIZER, E. S., LI, J. N., MANI, N. S., FREHYWOT, G. L. & TOWNSEND, C. A. 2000. Synthesis and antitumor activity of an inhibitor of fatty acid synthase. *Proc Natl Acad Sci U S A,* 97**,** 3450-4.

KURTH-KRACZEK, E. J., HIRSHMAN, M. F., GOODYEAR, L. J. & WINDER, W. W. 1999. 5' AMP-activated protein kinase activation causes GLUT4 translocation in skeletal muscle. *Diabetes,* 48**,** 1667-71.

KWON, C. H., LUIKART, B. W., POWELL, C. M., ZHOU, J., MATHENY, S. A., ZHANG, W., LI, Y., BAKER, S. J. & PARADA, L. F. 2006. Pten regulates neuronal arborization and social interaction in mice. *Neuron,* 50**,** 377-88.

KWON, C. H., ZHU, X., ZHANG, J., KNOOP, L. L., THARP, R., SMEYNE, R. J., EBERHART, C. G., BURGER, P. C. & BAKER, S. J. 2001. Pten regulates neuronal soma size: a mouse model of Lhermitte-Duclos disease. *Nature genetics,* 29**,** 404-11.

LA MARCA, R., CERRI, F., HORIUCHI, K., BACHI, A., FELTRI, M. L., WRABETZ, L., BLOBEL, C. P., QUATTRINI, A., SALZER, J. L. & TAVEGGIA, C. 2011. TACE (ADAM17) inhibits Schwann cell myelination. *Nat Neurosci,* 14**,** 857-65.

LAI, K. M., GONZALEZ, M., POUEYMIROU, W. T., KLINE, W. O., NA, E., ZLOTCHENKO, E., STITT, T. N., ECONOMIDES, A. N., YANCOPOULOS, G. D. & GLASS, D. J. 2004. Conditional activation of akt in adult skeletal muscle induces rapid hypertrophy. *Mol Cell Biol,* 24**,** 9295-304.

LANG, F. 2007. Mechanisms and significance of cell volume regulation. *J Am Coll Nutr,* 26**,** 613S-623S.

LANG, F., BUSCH, G. L., RITTER, M., VOLKL, H., WALDEGGER, S., GULBINS, E. & HAUSSINGER, D. 1998. Functional significance of cell volume regulatory mechanisms. *Physiol Rev,* 78**,** 247-306.

LAPLANTE, M. & SABATINI, D. M. 2010. mTORC1 activates SREBP-1c and uncouples lipogenesis from gluconeogenesis. *Proc Natl Acad Sci U S A,* 107**,** 3281-2.

LAPLANTE, M. & SABATINI, D. M. 2012. mTOR Signaling. *Cold Spring Harb Perspect Biol,* 4.

LARON, Z. 2004. Laron syndrome (primary growth hormone resistance or insensitivity): the personal experience 1958-2003. *J Clin Endocrinol Metab,* 89**,** 1031-44.

LASER, H., MACK, T. G., WAGNER, D. & COLEMAN, M. P. 2003. Proteasome inhibition arrests neurite outgrowth and causes "dying-back" degeneration in primary culture. *J Neurosci Res,* 74**,** 906-16.

LAZAROW, P. B. 2003. Peroxisome biogenesis: advances and conundrums. *Curr Opin Cell Biol,* 15**,** 489-97.

LEBLANC, S. E., SRINIVASAN, R., FERRI, C., MAGER, G. M., GILLIAN-DANIEL, A. L., WRABETZ, L. & SVAREN, J. 2005. Regulation of cholesterol/lipid biosynthetic genes by Egr2/Krox20 during peripheral nerve myelination. *J Neurochem,* 93**,** 737-48.

LECKER, S. H., SOLOMON, V., PRICE, S. R., KWON, Y. T., MITCH, W. E. & GOLDBERG, A. L. 1999. Ubiquitin conjugation by the N-end rule pathway and mRNAs for its components increase in muscles of diabetic rats. *The Journal of clinical investigation,* 104**,** 1411-20.

LECUIT, T. & WIESCHAUS, E. 2000. Polarized insertion of new membrane from a cytoplasmic reservoir during cleavage of the Drosophila embryo. *J Cell Biol,* 150**,** 849-60.

LEE, J. N., ZHANG, X., FERAMISCO, J. D., GONG, Y. & YE, J. 2008. Unsaturated fatty acids inhibit proteasomal degradation of Insig-1 at a postubiquitination step. *J Biol Chem,* 283**,** 33772-83.

LEE, K. P., LEE, J. H., KIM, T. S., KIM, T. H., PARK, H. D., BYUN, J. S., KIM, M. C., JEONG, W. I., CALVISI, D. F., KIM, J. M. & LIM, D. S. 2010. The Hippo-Salvador pathway restrains hepatic oval cell proliferation, liver size, and liver tumorigenesis. *Proc Natl Acad Sci U S A,* 107**,** 8248-53.

LEEVERS, S. J., WEINKOVE, D., MACDOUGALL, L. K., HAFEN, E. & WATERFIELD, M. D. 1996. The Drosophila phosphoinositide 3-kinase Dp110 promotes cell growth. *The EMBO journal,* 15**,** 6584-94.

LEMMON, M. A. & SCHLESSINGER, J. 2010. Cell signaling by receptor tyrosine kinases. *Cell,* 141**,** 1117-34.

LEMONS, J. M., FENG, X. J., BENNETT, B. D., LEGESSE-MILLER, A., JOHNSON, E. L., RAITMAN, I., POLLINA, E. A., RABITZ, H. A., RABINOWITZ, J. D. & COLLER, H. A. 2010. Quiescent fibroblasts exhibit high metabolic activity. *PLoS biology,* 8**,** e1000514.

LETO, D. & SALTIEL, A. R. 2012. Regulation of glucose transport by insulin: traffic control of GLUT4. *Nat Rev Mol Cell Biol,* 13**,** 383-96.

LI, F., WANG, Y., ZELLER, K. I., POTTER, J. J., WONSEY, D. R., O'DONNELL, K. A., KIM, J. W., YUSTEIN, J. T., LEE, L. A. & DANG, C. V. 2005. Myc stimulates nuclearly encoded mitochondrial genes and mitochondrial biogenesis. *Mol Cell Biol,* 25**,** 6225-34.

LI, S., BROWN, M. S. & GOLDSTEIN, J. L. 2010. Bifurcation of insulin signaling pathway in rat liver: mTORC1 required for stimulation of lipogenesis, but not inhibition of gluconeogenesis. *Proc Natl Acad Sci U S A,* 107**,** 3441-6.

LI, Y., XU, S., MIHAYLOVA, M. M., ZHENG, B., HOU, X., JIANG, B., PARK, O., LUO, Z., LEFAI, E., SHYY, J. Y., GAO, B., WIERZBICKI, M., VERBEUREN, T. J., SHAW, R. J., COHEN, R. A. & ZANG, M. 2011. AMPK phosphorylates and inhibits SREBP activity to attenuate hepatic steatosis and atherosclerosis in diet-induced insulin-resistant mice. *Cell Metab,* 13**,** 376-88.

LIANG, G., CLINE, G. W. & MACICA, C. M. 2007. IGF-1 stimulates de novo fatty acid biosynthesis by Schwann cells during myelination. *Glia,* 55**,** 632-41.

LIANG, G., YANG, J., HORTON, J. D., HAMMER, R. E., GOLDSTEIN, J. L. & BROWN, M. S. 2002. Diminished hepatic response to fasting/refeeding and liver X receptor agonists in mice with selective deficiency of sterol regulatory element-binding protein-1c. *J Biol Chem,* 277**,** 9520-8.

LITTLEWOOD, T. D., HANCOCK, D. C., DANIELIAN, P. S., PARKER, M. G. & EVAN, G. I. 1995. A modified oestrogen receptor ligand-binding domain as an improved switch for the regulation of heterologous proteins. *Nucleic Acids Res,* 23**,** 1686-90.

LIU, K., LU, Y., LEE, J. K., SAMARA, R., WILLENBERG, R., SEARS-KRAXBERGER, I., TEDESCHI, A., PARK, K. K., JIN, D., CAI, B., XU, B., CONNOLLY, L., STEWARD, O., ZHENG, B. & HE, Z. 2010. PTEN deletion enhances the regenerative ability of adult corticospinal neurons. *Nat Neurosci,* 13**,** 1075-81.

LIU, X., MA, C. & SUBRAMANI, S. 2012. Recent advances in peroxisomal matrix protein import. *Curr Opin Cell Biol,* 24**,** 484-9.
LLOYD, A. C. 2006. Distinct functions for ERKs? *J Biol,* 5**,** 13.
LLOYD, A. C., OBERMULLER, F., STADDON, S., BARTH, C. F., MCMAHON, M. & LAND, H. 1997. Cooperating oncogenes converge to regulate cyclin/cdk complexes. *Genes Dev,* 11**,** 663-77.
LUBY-PHELPS, K. 2000. Cytoarchitecture and physical properties of cytoplasm: volume, viscosity, diffusion, intracellular surface area. *Int Rev Cytol,* 192**,** 189-221.
LUM, J. J., BAUER, D. E., KONG, M., HARRIS, M. H., LI, C., LINDSTEN, T. & THOMPSON, C. B. 2005a. Growth factor regulation of autophagy and cell survival in the absence of apoptosis. *Cell,* 120**,** 237-48.
LUM, J. J., DEBERARDINIS, R. J. & THOMPSON, C. B. 2005b. Autophagy in metazoans: cell survival in the land of plenty. *Nature reviews. Molecular cell biology,* 6**,** 439-48.
LUNT, S. Y. & VANDER HEIDEN, M. G. 2011. Aerobic glycolysis: meeting the metabolic requirements of cell proliferation. *Annu Rev Cell Dev Biol,* 27**,** 441-64.
LUPU, F., TERWILLIGER, J. D., LEE, K., SEGRE, G. V. & EFSTRATIADIS, A. 2001. Roles of growth hormone and insulin-like growth factor 1 in mouse postnatal growth. *Dev Biol,* 229**,** 141-62.
LUU, W., SHARPE, L. J., STEVENSON, J. & BROWN, A. J. 2012. Akt acutely activates the cholesterogenic transcription factor SREBP-2. *Biochim Biophys Acta,* 1823**,** 458-64.
LYNEN, F. 1966. [The biochemical basis of the biosynthesis of cholesterol and fatty acids]. *Wien Klin Wochenschr,* 78**,** 489-97.
MA, L., CHEN, Z., ERDJUMENT-BROMAGE, H., TEMPST, P. & PANDOLFI, P. P. 2005. Phosphorylation and functional inactivation of TSC2 by Erk implications for tuberous sclerosis and cancer pathogenesis. *Cell,* 121**,** 179-93.
MACKLIN, W. B. 2010. The myelin brake: when enough is enough. *Sci Signal,* 3**,** pe32.
MANNING, B. D. & CANTLEY, L. C. 2007. AKT/PKB signaling: navigating downstream. *Cell,* 129**,** 1261-74.
MARKUS, A., ZHONG, J. & SNIDER, W. D. 2002. Raf and akt mediate distinct aspects of sensory axon growth. *Neuron,* 35**,** 65-76.
MARSHALL, C. J. 1995. Specificity of receptor tyrosine kinase signaling: transient versus sustained extracellular signal-regulated kinase activation. *Cell,* 80**,** 179-85.
MARTIN, S. & PARTON, R. G. 2006. Lipid droplets: a unified view of a dynamic organelle. *Nat Rev Mol Cell Biol,* 7**,** 373-8.
MARTIN, S. G. 2009. Geometric control of the cell cycle. *Cell Cycle,* 8**,** 3643-7.
MARTIN, S. G. & BERTHELOT-GROSJEAN, M. 2009. Polar gradients of the DYRK-family kinase Pom1 couple cell length with the cell cycle. *Nature,* 459**,** 852-6.
MASIERO, E. & SANDRI, M. 2010. Autophagy inhibition induces atrophy and myopathy in adult skeletal muscles. *Autophagy,* 6**,** 307-9.
MATHON, N. F., MALCOLM, D. S., HARRISINGH, M. C., CHENG, L. & LLOYD, A. C. 2001. Lack of replicative senescence in normal rodent glia. *Science,* 291**,** 872-5.
MATSUDA, M., KORN, B. S., HAMMER, R. E., MOON, Y. A., KOMURO, R., HORTON, J. D., GOLDSTEIN, J. L., BROWN, M. S. & SHIMOMURA, I. 2001. SREBP cleavage-

activating protein (SCAP) is required for increased lipid synthesis in liver induced by cholesterol deprivation and insulin elevation. *Genes Dev,* 15**,** 1206-16.

MAUREL, P. & SALZER, J. L. 2000. Axonal regulation of Schwann cell proliferation and survival and the initial events of myelination requires PI 3-kinase activity. *J Neurosci,* 20**,** 4635-45.

MAXFIELD, F. R. & MCGRAW, T. E. 2004. Endocytic recycling. *Nat Rev Mol Cell Biol,* 5**,** 121-32.

MAYER, C. & GRUMMT, I. 2006. Ribosome biogenesis and cell growth: mTOR coordinates transcription by all three classes of nuclear RNA polymerases. *Oncogene,* 25**,** 6384-91.

MAYER, C., ZHAO, J., YUAN, X. & GRUMMT, I. 2004. mTOR-dependent activation of the transcription factor TIF-IA links rRNA synthesis to nutrient availability. *Genes Dev,* 18**,** 423-34.

MAYOR, S., PRESLEY, J. F. & MAXFIELD, F. R. 1993. Sorting of membrane components from endosomes and subsequent recycling to the cell surface occurs by a bulk flow process. *J Cell Biol,* 121**,** 1257-69.

MCMULLEN, J. R., SHIOI, T., ZHANG, L., TARNAVSKI, O., SHERWOOD, M. C., KANG, P. M. & IZUMO, S. 2003. Phosphoinositide 3-kinase(p110alpha) plays a critical role for the induction of physiological, but not pathological, cardiac hypertrophy. *Proceedings of the National Academy of Sciences of the United States of America,* 100**,** 12355-60.

MEDINA, R., WING, S. S. & GOLDBERG, A. L. 1995. Increase in levels of polyubiquitin and proteasome mRNA in skeletal muscle during starvation and denervation atrophy. *Biochem J,* 307 (Pt 3)**,** 631-7.

MEIKLE, L., POLLIZZI, K., EGNOR, A., KRAMVIS, I., LANE, H., SAHIN, M. & KWIATKOWSKI, D. J. 2008. Response of a neuronal model of tuberous sclerosis to mammalian target of rapamycin (mTOR) inhibitors: effects on mTORC1 and Akt signaling lead to improved survival and function. *The Journal of neuroscience : the official journal of the Society for Neuroscience,* 28**,** 5422-32.

MEIKLE, L., TALOS, D. M., ONDA, H., POLLIZZI, K., ROTENBERG, A., SAHIN, M., JENSEN, F. E. & KWIATKOWSKI, D. J. 2007. A mouse model of tuberous sclerosis: neuronal loss of Tsc1 causes dysplastic and ectopic neurons, reduced myelination, seizure activity, and limited survival. *The Journal of neuroscience : the official journal of the Society for Neuroscience,* 27**,** 5546-58.

MEISSNER, J. D., FREUND, R., KRONE, D., UMEDA, P. K., CHANG, K. C., GROS, G. & SCHEIBE, R. J. 2011. Extracellular signal-regulated kinase 1/2-mediated phosphorylation of p300 enhances myosin heavy chain I/beta gene expression via acetylation of nuclear factor of activated T cells c1. *Nucleic Acids Res,* 39**,** 5907-25.

MENDOZA, M. C., ER, E. E. & BLENIS, J. 2011. The Ras-ERK and PI3K-mTOR pathways: cross-talk and compensation. *Trends Biochem Sci,* 36**,** 320-8.

MENENDEZ, J. A. & LUPU, R. 2007. Fatty acid synthase and the lipogenic phenotype in cancer pathogenesis. *Nat Rev Cancer,* 7**,** 763-77.

METALLO, C. M. & VANDER HEIDEN, M. G. 2010. Metabolism strikes back: metabolic flux regulates cell signaling. *Genes Dev,* 24**,** 2717-22.

METCALF, D. 1963. The Autonomous Behaviour of Normal Thymus Grafts. *Aust J Exp Biol Med Sci,* 41**,** SUPPL437-47.

METCALF, D. 1964. Restricted Growth Capacity of Multiple Spleen Grafts. *Transplantation,* 2**,** 387-92.
MEYER, N. & PENN, L. Z. 2008. Reflecting on 25 years with MYC. *Nat Rev Cancer,* 8**,** 976-90.
MICHAILOV, G. V., SEREDA, M. W., BRINKMANN, B. G., FISCHER, T. M., HAUG, B., BIRCHMEIER, C., ROLE, L., LAI, C., SCHWAB, M. H. & NAVE, K. A. 2004. Axonal neuregulin-1 regulates myelin sheath thickness. *Science,* 304**,** 700-3.
MIHAYLOVA, M. M. & SHAW, R. J. 2011. The AMPK signalling pathway coordinates cell growth, autophagy and metabolism. *Nat Cell Biol,* 13**,** 1016-23.
MIRON, M., VERDU, J., LACHANCE, P. E., BIRNBAUM, M. J., LASKO, P. F. & SONENBERG, N. 2001. The translational inhibitor 4E-BP is an effector of PI(3)K/Akt signalling and cell growth in Drosophila. *Nat Cell Biol,* 3**,** 596-601.
MITCHELL, K. J., PINSON, K. I., KELLY, O. G., BRENNAN, J., ZUPICICH, J., SCHERZ, P., LEIGHTON, P. A., GOODRICH, L. V., LU, X., AVERY, B. J., TATE, P., DILL, K., PANGILINAN, E., WAKENIGHT, P., TESSIER-LAVIGNE, M. & SKARNES, W. C. 2001. Functional analysis of secreted and transmembrane proteins critical to mouse development. *Nat Genet,* 28**,** 241-9.
MIZUSHIMA, N. 2007. Autophagy: process and function. *Genes Dev,* 21**,** 2861-73.
MOLKENTIN, J. D., LU, J. R., ANTOS, C. L., MARKHAM, B., RICHARDSON, J., ROBBINS, J., GRANT, S. R. & OLSON, E. N. 1998. A calcineurin-dependent transcriptional pathway for cardiac hypertrophy. *Cell,* 93**,** 215-28.
MONTAGNE, J., STEWART, M. J., STOCKER, H., HAFEN, E., KOZMA, S. C. & THOMAS, G. 1999. Drosophila S6 kinase: a regulator of cell size. *Science,* 285**,** 2126-9.
MOORE, S. A. 1988. Kinetic evidence for a critical rate of protein synthesis in the Saccharomyces cerevisiae yeast cell cycle. *J Biol Chem,* 263**,** 9674-81.
MORRIS, C. E. & HOMANN, U. 2001. Cell surface area regulation and membrane tension. *J Membr Biol,* 179**,** 79-102.
MORRISH, F., NERETTI, N., SEDIVY, J. M. & HOCKENBERY, D. M. 2008. The oncogene c-Myc coordinates regulation of metabolic networks to enable rapid cell cycle entry. *Cell Cycle,* 7**,** 1054-66.
MOSELEY, J. B., MAYEUX, A., PAOLETTI, A. & NURSE, P. 2009. A spatial gradient coordinates cell size and mitotic entry in fission yeast. *Nature,* 459**,** 857-60.
MOTAMED, M., ZHANG, Y., WANG, M. L., SEEMANN, J., KWON, H. J., GOLDSTEIN, J. L. & BROWN, M. S. 2011. Identification of luminal Loop 1 of Scap protein as the sterol sensor that maintains cholesterol homeostasis. *J Biol Chem,* 286**,** 18002-12.
MUSARO, A., MCCULLAGH, K., PAUL, A., HOUGHTON, L., DOBROWOLNY, G., MOLINARO, M., BARTON, E. R., SWEENEY, H. L. & ROSENTHAL, N. 2001. Localized Igf-1 transgene expression sustains hypertrophy and regeneration in senescent skeletal muscle. *Nat Genet,* 27**,** 195-200.
MUSARO, A., MCCULLAGH, K. J., NAYA, F. J., OLSON, E. N. & ROSENTHAL, N. 1999. IGF-1 induces skeletal myocyte hypertrophy through calcineurin in association with GATA-2 and NF-ATc1. *Nature,* 400**,** 581-5.
NAKAKUKI, M., SHIMANO, H., INOUE, N., TAMURA, M., MATSUZAKA, T., NAKAGAWA, Y., YAHAGI, N., TOYOSHIMA, H., SATO, R. & YAMADA, N. 2007. A transcription factor of lipid synthesis, sterol regulatory element-binding protein (SREBP)-1a causes G(1) cell-cycle arrest after accumulation of cyclin-dependent kinase (cdk) inhibitors. *FEBS J,* 274**,** 4440-52.
NAKAYAMA, K., ISHIDA, N., SHIRANE, M., INOMATA, A., INOUE, T., SHISHIDO, N., HORII, I., LOH, D. Y. & NAKAYAMA, K. 1996. Mice lacking p27(Kip1) display

increased body size, multiple organ hyperplasia, retinal dysplasia, and pituitary tumors. *Cell,* 85**,** 707-20.

NAPOLI, I., NOON, L. A., RIBEIRO, S., KERAI, A. P., PARRINELLO, S., ROSENBERG, L. H., COLLINS, M. J., HARRISINGH, M. C., WHITE, I. J., WOODHOO, A. & LLOYD, A. C. 2012. A central role for the ERK-signaling pathway in controlling Schwann cell plasticity and peripheral nerve regeneration in vivo. *Neuron,* 73**,** 729-42.

NARAYANAN, S. P., FLORES, A. I., WANG, F. & MACKLIN, W. B. 2009. Akt signals through the mammalian target of rapamycin pathway to regulate CNS myelination. *J Neurosci,* 29**,** 6860-70.

NASH, R., TOKIWA, G., ANAND, S., ERICKSON, K. & FUTCHER, A. B. 1988. The WHI1+ gene of Saccharomyces cerevisiae tethers cell division to cell size and is a cyclin homolog. *EMBO J,* 7**,** 4335-46.

NEUFELD, T. P., DE LA CRUZ, A. F., JOHNSTON, L. A. & EDGAR, B. A. 1998. Coordination of growth and cell division in the Drosophila wing. *Cell,* 93**,** 1183-93.

NEUMULLER, R. A., BETSCHINGER, J., FISCHER, A., BUSHATI, N., POERNBACHER, I., MECHTLER, K., COHEN, S. M. & KNOBLICH, J. A. 2008. Mei-P26 regulates microRNAs and cell growth in the Drosophila ovarian stem cell lineage. *Nature,* 454**,** 241-5.

NEWBERN, J. M., LI, X., SHOEMAKER, S. E., ZHOU, J., ZHONG, J., WU, Y., BONDER, D., HOLLENBACK, S., COPPOLA, G., GESCHWIND, D. H., LANDRETH, G. E. & SNIDER, W. D. 2011. Specific functions for ERK/MAPK signaling during PNS development. *Neuron,* 69**,** 91-105.

NICKLIN, P., BERGMAN, P., ZHANG, B., TRIANTAFELLOW, E., WANG, H., NYFELER, B., YANG, H., HILD, M., KUNG, C., WILSON, C., MYER, V. E., MACKEIGAN, J. P., PORTER, J. A., WANG, Y. K., CANTLEY, L. C., FINAN, P. M. & MURPHY, L. O. 2009. Bidirectional transport of amino acids regulates mTOR and autophagy. *Cell,* 136**,** 521-34.

NINOV, N., MANJON, C. & MARTIN-BLANCO, E. 2009. Dynamic control of cell cycle and growth coupling by ecdysone, EGFR, and PI3K signaling in Drosophila histoblasts. *PLoS biology,* 7**,** e1000079.

NURSE, P. 1985. *The genetic control of cell volume*, John Wiley and Sons.

NURSE, P. 1991. The Florey Lecture, 1990. How is the cell division cycle regulated? *Philos Trans R Soc Lond B Biol Sci,* 332**,** 271-6.

OJAMAA, K. 2010. Signaling mechanisms in thyroid hormone-induced cardiac hypertrophy. *Vascular pharmacology,* 52**,** 113-9.

OLIVER, E. R., SAUNDERS, T. L., TARLE, S. A. & GLASER, T. 2004. Ribosomal protein L24 defect in belly spot and tail (Bst), a mouse Minute. *Development,* 131**,** 3907-20.

OSHIRO, N., TAKAHASHI, R., YOSHINO, K., TANIMURA, K., NAKASHIMA, A., EGUCHI, S., MIYAMOTO, T., HARA, K., TAKEHANA, K., AVRUCH, J., KIKKAWA, U. & YONEZAWA, K. 2007. The proline-rich Akt substrate of 40 kDa (PRAS40) is a physiological substrate of mammalian target of rapamycin complex 1. *J Biol Chem,* 282**,** 20329-39.

OSTHUS, R. C., SHIM, H., KIM, S., LI, Q., REDDY, R., MUKHERJEE, M., XU, Y., WONSEY, D., LEE, L. A. & DANG, C. V. 2000. Deregulation of glucose transporter 1 and glycolytic gene expression by c-Myc. *J Biol Chem,* 275**,** 21797-800.

PALACIN, M., ESTEVEZ, R., BERTRAN, J. & ZORZANO, A. 1998. Molecular biology of mammalian plasma membrane amino acid transporters. *Physiol Rev,* 78**,** 969-1054.

PAN, D. 2007. Hippo signaling in organ size control. *Genes Dev,* 21**,** 886-97.
PAN, D. 2010. The hippo signaling pathway in development and cancer. *Dev Cell,* 19**,** 491-505.
PAN, K. Z. & CHANG, F. 2009. Cell-cycle control: don't supersize me. *Curr Biol,* 19**,** R517-9.
PARK, K. K., LIU, K., HU, Y., SMITH, P. D., WANG, C., CAI, B., XU, B., CONNOLLY, L., KRAMVIS, I., SAHIN, M. & HE, Z. 2008. Promoting axon regeneration in the adult CNS by modulation of the PTEN/mTOR pathway. *Science,* 322**,** 963-6.
PARKER, R. A., MILLER, S. J. & GIBSON, D. M. 1986. Phosphorylation state of HMG CoA reductase affects its catalytic activity and degradation. *Adv Enzyme Regul,* 25**,** 329-43.
PARRINELLO, S., NOON, L. A., HARRISINGH, M. C., DIGBY, P. W., ROSENBERG, L. H., CREMONA, C. A., ECHAVE, P., FLANAGAN, A. M., PARADA, L. F. & LLOYD, A. C. 2008. NF1 loss disrupts Schwann cell-axonal interactions: a novel role for semaphorin 4F. *Genes Dev,* 22**,** 3335-48.
PARRISH, J. Z., EMOTO, K., JAN, L. Y. & JAN, Y. N. 2007. Polycomb genes interact with the tumor suppressor genes hippo and warts in the maintenance of Drosophila sensory neuron dendrites. *Genes Dev,* 21**,** 956-72.
PEARSE, B. M. & ROBINSON, M. S. 1990. Clathrin, adaptors, and sorting. *Annu Rev Cell Biol,* 6**,** 151-71.
PELISSIER, A., CHAUVIN, J. P. & LECUIT, T. 2003. Trafficking through Rab11 endosomes is required for cellularization during Drosophila embryogenesis. *Curr Biol,* 13**,** 1848-57.
PELKMANS, L., FAVA, E., GRABNER, H., HANNUS, M., HABERMANN, B., KRAUSZ, E. & ZERIAL, M. 2005. Genome-wide analysis of human kinases in clathrin- and caveolae/raft-mediated endocytosis. *Nature,* 436**,** 78-86.
PENDE, M., UM, S. H., MIEULET, V., STICKER, M., GOSS, V. L., MESTAN, J., MUELLER, M., FUMAGALLI, S., KOZMA, S. C. & THOMAS, G. 2004. S6K1(-/-)/S6K2(-/-) mice exhibit perinatal lethality and rapamycin-sensitive 5'-terminal oligopyrimidine mRNA translation and reveal a mitogen-activated protein kinase-dependent S6 kinase pathway. *Mol Cell Biol,* 24**,** 3112-24.
PENG, X. D., XU, P. Z., CHEN, M. L., HAHN-WINDGASSEN, A., SKEEN, J., JACOBS, J., SUNDARARAJAN, D., CHEN, W. S., CRAWFORD, S. E., COLEMAN, K. G. & HAY, N. 2003. Dwarfism, impaired skin development, skeletal muscle atrophy, delayed bone development, and impeded adipogenesis in mice lacking Akt1 and Akt2. *Genes Dev,* 17**,** 1352-65.
PETERSON, T. R., LAPLANTE, M., THOREEN, C. C., SANCAK, Y., KANG, S. A., KUEHL, W. M., GRAY, N. S. & SABATINI, D. M. 2009. DEPTOR is an mTOR inhibitor frequently overexpressed in multiple myeloma cells and required for their survival. *Cell,* 137**,** 873-86.
PETERSON, T. R., SENGUPTA, S. S., HARRIS, T. E., CARMACK, A. E., KANG, S. A., BALDERAS, E., GUERTIN, D. A., MADDEN, K. L., CARPENTER, A. E., FINCK, B. N. & SABATINI, D. M. 2011. mTOR Complex 1 Regulates Lipin 1 Localization to Control the SREBP Pathway. *Cell,* 146**,** 408-20.
PFENNINGER, K. H. 2009. Plasma membrane expansion: a neuron's Herculean task. *Nat Rev Neurosci,* 10**,** 251-61.
PICONE, R., REN, X., IVANOVITCH, K. D., CLARKE, J. D., MCKENDRY, R. A. & BAUM, B. 2010. A polarised population of dynamic microtubules mediates homeostatic length control in animal cells. *PLoS Biol,* 8**,** e1000542.

PIERCE, S. B., YOST, C., BRITTON, J. S., LOO, L. W., FLYNN, E. M., EDGAR, B. A. & EISENMAN, R. N. 2004. dMyc is required for larval growth and endoreplication in Drosophila. *Development,* 131**,** 2317-27.

PLAS, D. R., TALAPATRA, S., EDINGER, A. L., RATHMELL, J. C. & THOMPSON, C. B. 2001. Akt and Bcl-xL promote growth factor-independent survival through distinct effects on mitochondrial physiology. *J Biol Chem,* 276**,** 12041-8.

POPESCU, G., IKEDA, T., DASARIO, R. R. & Feld, M. S. 2006. Diffraction phase microscopy for quantifying cell structure and dynamics. *Opt. Lett.*, 31, 775-77.

POPOLO, L., VANONI, M. & ALBERGHINA, L. 1982. Control of the yeast cell cycle by protein synthesis. *Exp Cell Res,* 142**,** 69-78.

PORSTMANN, T., GRIFFITHS, B., CHUNG, Y. L., DELPUECH, O., GRIFFITHS, J. R., DOWNWARD, J. & SCHULZE, A. 2005. PKB/Akt induces transcription of enzymes involved in cholesterol and fatty acid biosynthesis via activation of SREBP. *Oncogene,* 24**,** 6465-81.

PORSTMANN, T., SANTOS, C. R., GRIFFITHS, B., CULLY, M., WU, M., LEEVERS, S., GRIFFITHS, J. R., CHUNG, Y. L. & SCHULZE, A. 2008. SREBP activity is regulated by mTORC1 and contributes to Akt-dependent cell growth. *Cell metabolism,* 8**,** 224-36.

PORSTMANN, T., SANTOS, C. R., LEWIS, C., GRIFFITHS, B. & SCHULZE, A. 2009. A new player in the orchestra of cell growth: SREBP activity is regulated by mTORC1 and contributes to the regulation of cell and organ size. *Biochem Soc Trans,* 37**,** 278-83.

POTTER, C. J., PEDRAZA, L. G. & XU, T. 2002. Akt regulates growth by directly phosphorylating Tsc2. *Nat Cell Biol,* 4**,** 658-65.

POTTER, C. J. & XU, T. 2001. Mechanisms of size control. *Curr Opin Genet Dev,* 11**,** 279-86.

PRAGER-KHOUTORSKY, M. & SPIRA, M. E. 2009. Neurite retraction and regrowth regulated by membrane retrieval, membrane supply, and actin dynamics. *Brain Res,* 1251**,** 65-79.

PRINZ, W. A. 2010. Lipid trafficking sans vesicles: where, why, how? *Cell,* 143**,** 870-4.

PUNGA, T., BENGOECHEA-ALONSO, M. T. & ERICSSON, J. 2006. Phosphorylation and ubiquitination of the transcription factor sterol regulatory element-binding protein-1 in response to DNA binding. *J Biol Chem,* 281**,** 25278-86.

PURVES, D., SNIDER, W. D. & VOYVODIC, J. T. 1988. Trophic regulation of nerve cell morphology and innervation in the autonomic nervous system. *Nature,* 336**,** 123-8.

RADHAKRISHNAN, A., IKEDA, Y., KWON, H. J., BROWN, M. S. & GOLDSTEIN, J. L. 2007. Sterol-regulated transport of SREBPs from endoplasmic reticulum to Golgi: oxysterols block transport by binding to Insig. *Proc Natl Acad Sci U S A,* 104**,** 6511-8.

RADHAKRISHNAN, A., SUN, L. P., KWON, H. J., BROWN, M. S. & GOLDSTEIN, J. L. 2004. Direct binding of cholesterol to the purified membrane region of SCAP: mechanism for a sterol-sensing domain. *Mol Cell,* 15**,** 259-68.

RATHMELL, J. C., VANDER HEIDEN, M. G., HARRIS, M. H., FRAUWIRTH, K. A. & THOMPSON, C. B. 2000. In the absence of extrinsic signals, nutrient utilization by lymphocytes is insufficient to maintain either cell size or viability. *Molecular cell,* 6**,** 683-92.

RICHARDSON, H. E., WITTENBERG, C., CROSS, F. & REED, S. I. 1989. An essential G1 function for cyclin-like proteins in yeast. *Cell,* 59**,** 1127-33.

RIDGWAY, N. D. & LAGACE, T. A. 2003. Regulation of the CDP-choline pathway by sterol regulatory element binding proteins involves transcriptional and post-transcriptional mechanisms. *Biochem J,* 372**,** 811-9.

ROLFE, M., MCLEOD, L. E., PRATT, P. F. & PROUD, C. G. 2005. Activation of protein synthesis in cardiomyocytes by the hypertrophic agent phenylephrine requires the activation of ERK and involves phosphorylation of tuberous sclerosis complex 2 (TSC2). *Biochem J,* 388**,** 973-84.

ROMMEL, C., BODINE, S. C., CLARKE, B. A., ROSSMAN, R., NUNEZ, L., STITT, T. N., YANCOPOULOS, G. D. & GLASS, D. J. 2001. Mediation of IGF-1-induced skeletal myotube hypertrophy by PI(3)K/Akt/mTOR and PI(3)K/Akt/GSK3 pathways. *Nat Cell Biol,* 3**,** 1009-13.

ROTH, G., KOTZKA, J., KREMER, L., LEHR, S., LOHAUS, C., MEYER, H. E., KRONE, W. & MULLER-WIELAND, D. 2000. MAP kinases Erk1/2 phosphorylate sterol regulatory element-binding protein (SREBP)-1a at serine 117 in vitro. *J Biol Chem,* 275**,** 33302-7.

ROUX, P. P., SHAHBAZIAN, D., VU, H., HOLZ, M. K., COHEN, M. S., TAUNTON, J., SONENBERG, N. & BLENIS, J. 2007. RAS/ERK signaling promotes site-specific ribosomal protein S6 phosphorylation via RSK and stimulates cap-dependent translation. *J Biol Chem,* 282**,** 14056-64.

RUDNEY, H. & SEXTON, R. C. 1986. Regulation of cholesterol biosynthesis. *Annu Rev Nutr,* 6**,** 245-72.

RUDRA, D. & WARNER, J. R. 2004. What better measure than ribosome synthesis? *Genes Dev,* 18**,** 2431-6.

RUSH, J. S., SWEITZER, T., KENT, C., DECKER, G. L. & WAECHTER, C. J. 1991. Biogenesis of the endoplasmic reticulum in activated B lymphocytes: temporal relationships between the induction of protein N-glycosylation activity and the biosynthesis of membrane protein and phospholipid. *Archives of biochemistry and biophysics,* 284**,** 63-70.

RUVINSKY, I., SHARON, N., LERER, T., COHEN, H., STOLOVICH-RAIN, M., NIR, T., DOR, Y., ZISMAN, P. & MEYUHAS, O. 2005. Ribosomal protein S6 phosphorylation is a determinant of cell size and glucose homeostasis. *Genes & development,* 19**,** 2199-211.

SACHECK, J. M., OHTSUKA, A., MCLARY, S. C. & GOLDBERG, A. L. 2004. IGF-I stimulates muscle growth by suppressing protein breakdown and expression of atrophy-related ubiquitin ligases, atrogin-1 and MuRF1. *American journal of physiology. Endocrinology and metabolism,* 287**,** E591-601.

SAKAI, J., NOHTURFFT, A., CHENG, D., HO, Y. K., BROWN, M. S. & GOLDSTEIN, J. L. 1997. Identification of complexes between the COOH-terminal domains of sterol regulatory element-binding proteins (SREBPs) and SREBP cleavage-activating protein. *J Biol Chem,* 272**,** 20213-21.

SAKAI, J., NOHTURFFT, A., GOLDSTEIN, J. L. & BROWN, M. S. 1998. Cleavage of sterol regulatory element-binding proteins (SREBPs) at site-1 requires interaction with SREBP cleavage-activating protein. Evidence from in vivo competition studies. *J Biol Chem,* 273**,** 5785-93.

SALBREUX, G., CHARRAS, G. & PALUCH, E. 2012. Actin cortex mechanics and cellular morphogenesis. *Trends Cell Biol*.

SAMPSON, J. R. 2003. TSC1 and TSC2: genes that are mutated in the human genetic disorder tuberous sclerosis. *Biochem Soc Trans,* 31**,** 592-6.

SAMUELS, M. L., WEBER, M. J., BISHOP, J. M. & MCMAHON, M. 1993. Conditional transformation of cells and rapid activation of the mitogen-activated

protein kinase cascade by an estradiol-dependent human raf-1 protein kinase. *Mol Cell Biol,* 13**,** 6241-52.

SANCAK, Y., BAR-PELED, L., ZONCU, R., MARKHARD, A. L., NADA, S. & SABATINI, D. M. 2010. Ragulator-Rag complex targets mTORC1 to the lysosomal surface and is necessary for its activation by amino acids. *Cell,* 141**,** 290-303.

SANCAK, Y., PETERSON, T. R., SHAUL, Y. D., LINDQUIST, R. A., THOREEN, C. C., BAR-PELED, L. & SABATINI, D. M. 2008. The Rag GTPases bind raptor and mediate amino acid signaling to mTORC1. *Science,* 320**,** 1496-501.

SANCAK, Y., THOREEN, C. C., PETERSON, T. R., LINDQUIST, R. A., KANG, S. A., SPOONER, E., CARR, S. A. & SABATINI, D. M. 2007. PRAS40 is an insulin-regulated inhibitor of the mTORC1 protein kinase. *Mol Cell,* 25**,** 903-15.

SANDRI, M., SANDRI, C., GILBERT, A., SKURK, C., CALABRIA, E., PICARD, A., WALSH, K., SCHIAFFINO, S., LECKER, S. H. & GOLDBERG, A. L. 2004. Foxo transcription factors induce the atrophy-related ubiquitin ligase atrogin-1 and cause skeletal muscle atrophy. *Cell,* 117**,** 399-412.

SARBASSOV, D. D., ALI, S. M. & SABATINI, D. M. 2005a. Growing roles for the mTOR pathway. *Curr Opin Cell Biol,* 17**,** 596-603.

SARBASSOV, D. D., GUERTIN, D. A., ALI, S. M. & SABATINI, D. M. 2005b. Phosphorylation and regulation of Akt/PKB by the rictor-mTOR complex. *Science,* 307**,** 1098-101.

SATO, R., GOLDSTEIN, J. L. & BROWN, M. S. 1993. Replacement of serine-871 of hamster 3-hydroxy-3-methylglutaryl-CoA reductase prevents phosphorylation by AMP-activated kinase and blocks inhibition of sterol synthesis induced by ATP depletion. *Proc Natl Acad Sci U S A,* 90**,** 9261-5.

SATO, R., YANG, J., WANG, X., EVANS, M. J., HO, Y. K., GOLDSTEIN, J. L. & BROWN, M. S. 1994. Assignment of the membrane attachment, DNA binding, and transcriptional activation domains of sterol regulatory element-binding protein-1 (SREBP-1). *J Biol Chem,* 269**,** 17267-73.

SAUCEDO, L. J. & EDGAR, B. A. 2002. Why size matters: altering cell size. *Current opinion in genetics & development,* 12**,** 565-71.

SCHAFER, W. R. & RINE, J. 1992. Protein prenylation: genes, enzymes, targets, and functions. *Annu Rev Genet,* 26**,** 209-37.

SCHARSCHMIDT, B. F., LAKE, J. R., RENNER, E. L., LICKO, V. & VAN DYKE, R. W. 1986. Fluid phase endocytosis by cultured rat hepatocytes and perfused rat liver: implications for plasma membrane turnover and vesicular trafficking of fluid phase markers. *Proc Natl Acad Sci U S A,* 83**,** 9488-92.

SCHAUB, M. C., HEFTI, M. A., HARDER, B. A. & EPPENBERGER, H. M. 1997. Various hypertrophic stimuli induce distinct phenotypes in cardiomyocytes. *J Mol Med (Berl),* 75**,** 901-20.

SCHIAFFINO, M. V. 2010. Signaling pathways in melanosome biogenesis and pathology. *Int J Biochem Cell Biol,* 42**,** 1094-104.

SCHIEKE, S. M., PHILLIPS, D., MCCOY, J. P., JR., APONTE, A. M., SHEN, R. F., BALABAN, R. S. & FINKEL, T. 2006. The mammalian target of rapamycin (mTOR) pathway regulates mitochondrial oxygen consumption and oxidative capacity. *J Biol Chem,* 281**,** 27643-52.

SCHREIBER-AGUS, N., STEIN, D., CHEN, K., GOLTZ, J. S., STEVENS, L. & DEPINHO, R. A. 1997. Drosophila Myc is oncogenic in mammalian cells and plays a role in the diminutive phenotype. *Proc Natl Acad Sci U S A,* 94**,** 1235-40.

SCHUCK, S., PRINZ, W. A., THORN, K. S., VOSS, C. & WALTER, P. 2009. Membrane expansion alleviates endoplasmic reticulum stress independently of the unfolded protein response. *J Cell Biol,* 187**,** 525-36.

SCHUHMACHER, M., STAEGE, M. S., PAJIC, A., POLACK, A., WEIDLE, U. H., BORNKAMM, G. W., EICK, D. & KOHLHUBER, F. 1999. Control of cell growth by c-Myc in the absence of cell division. *Curr Biol,* 9**,** 1255-8.

SEARS, R., NUCKOLLS, F., HAURA, E., TAYA, Y., TAMAI, K. & NEVINS, J. R. 2000. Multiple Ras-dependent phosphorylation pathways regulate Myc protein stability. *Genes Dev,* 14**,** 2501-14.

SEARS, R. C. 2004. The life cycle of C-myc: from synthesis to degradation. *Cell Cycle,* 3**,** 1133-7.

SEKIYA, M., YAHAGI, N., MATSUZAKA, T., TAKEUCHI, Y., NAKAGAWA, Y., TAKAHASHI, H., OKAZAKI, H., IIZUKA, Y., OHASHI, K., GOTODA, T., ISHIBASHI, S., NAGAI, R., YAMAZAKI, T., KADOWAKI, T., YAMADA, N., OSUGA, J. & SHIMANO, H. 2007. SREBP-1-independent regulation of lipogenic gene expression in adipocytes. *J Lipid Res,* 48**,** 1581-91.

SENGUPTA, S., PETERSON, T. R. & SABATINI, D. M. 2010. Regulation of the mTOR complex 1 pathway by nutrients, growth factors, and stress. *Mol Cell,* 40**,** 310-22.

SHAW, R. J. & CANTLEY, L. C. 2006. Ras, PI(3)K and mTOR signalling controls tumour cell growth. *Nature,* 441**,** 424-30.

SHEN, B. W., SCANU, A. M. & KEZDY, F. J. 1977. Structure of human serum lipoproteins inferred from compositional analysis. *Proc Natl Acad Sci U S A,* 74**,** 837-41.

SHENG, Z., OTANI, H., BROWN, M. S. & GOLDSTEIN, J. L. 1995. Independent regulation of sterol regulatory element-binding proteins 1 and 2 in hamster liver. *Proc Natl Acad Sci U S A,* 92**,** 935-8.

SHERMAN, D. L., KROLS, M., WU, L. M., GROVE, M., NAVE, K. A., GANGLOFF, Y. G. & BROPHY, P. J. 2012. Arrest of myelination and reduced axon growth when Schwann cells lack mTOR. *J Neurosci,* 32**,** 1817-25.

SHIMA, H., PENDE, M., CHEN, Y., FUMAGALLI, S., THOMAS, G. & KOZMA, S. C. 1998. Disruption of the p70(s6k)/p85(s6k) gene reveals a small mouse phenotype and a new functional S6 kinase. *The EMBO journal,* 17**,** 6649-59.

SHIMANO, H. 2001. Sterol regulatory element-binding proteins (SREBPs): transcriptional regulators of lipid synthetic genes. *Prog Lipid Res,* 40**,** 439-52.

SHIMANO, H., HORTON, J. D., HAMMER, R. E., SHIMOMURA, I., BROWN, M. S. & GOLDSTEIN, J. L. 1996. Overproduction of cholesterol and fatty acids causes massive liver enlargement in transgenic mice expressing truncated SREBP-1a. *J Clin Invest,* 98**,** 1575-84.

SHIMANO, H., HORTON, J. D., SHIMOMURA, I., HAMMER, R. E., BROWN, M. S. & GOLDSTEIN, J. L. 1997a. Isoform 1c of sterol regulatory element binding protein is less active than isoform 1a in livers of transgenic mice and in cultured cells. *J Clin Invest,* 99**,** 846-54.

SHIMANO, H., SHIMOMURA, I., HAMMER, R. E., HERZ, J., GOLDSTEIN, J. L., BROWN, M. S. & HORTON, J. D. 1997b. Elevated levels of SREBP-2 and cholesterol synthesis in livers of mice homozygous for a targeted disruption of the SREBP-1 gene. *J Clin Invest,* 100**,** 2115-24.

SHIMANO, H., YAHAGI, N., AMEMIYA-KUDO, M., HASTY, A. H., OSUGA, J., TAMURA, Y., SHIONOIRI, F., IIZUKA, Y., OHASHI, K., HARADA, K., GOTODA, T., ISHIBASHI, S. & YAMADA, N. 1999. Sterol regulatory element-binding protein-1 as a key transcription factor for nutritional induction of lipogenic enzyme genes. *J Biol Chem,* 274**,** 35832-9.

SHIMOMURA, I., BASHMAKOV, Y., SHIMANO, H., HORTON, J. D., GOLDSTEIN, J. L. & BROWN, M. S. 1997a. Cholesterol feeding reduces nuclear forms of sterol regulatory element binding proteins in hamster liver. *Proc Natl Acad Sci U S A,* 94**,** 12354-9.

SHIMOMURA, I., HAMMER, R. E., RICHARDSON, J. A., IKEMOTO, S., BASHMAKOV, Y., GOLDSTEIN, J. L. & BROWN, M. S. 1998. Insulin resistance and diabetes mellitus in transgenic mice expressing nuclear SREBP-1c in adipose tissue: model for congenital generalized lipodystrophy. *Genes Dev,* 12**,** 3182-94.

SHIMOMURA, I., SHIMANO, H., HORTON, J. D., GOLDSTEIN, J. L. & BROWN, M. S. 1997b. Differential expression of exons 1a and 1c in mRNAs for sterol regulatory element binding protein-1 in human and mouse organs and cultured cells. *J Clin Invest,* 99**,** 838-45.

SHIOI, T., KANG, P. M., DOUGLAS, P. S., HAMPE, J., YBALLE, C. M., LAWITTS, J., CANTLEY, L. C. & IZUMO, S. 2000. The conserved phosphoinositide 3-kinase pathway determines heart size in mice. *The EMBO journal,* 19**,** 2537-48.

SHIRATORI, Y., OKWU, A. K. & TABAS, I. 1994. Free cholesterol loading of macrophages stimulates phosphatidylcholine biosynthesis and up-regulation of CTP: phosphocholine cytidylyltransferase. *J Biol Chem,* 269**,** 11337-48.

SHOHAT, M., JANOSSY, G. & DOURMASHKIN, R. R. 1973. Development of rough endoplasmic reticulum in mouse splenic lymphocytes stimulated by mitogens. *European journal of immunology,* 3**,** 680-7.

SLEIGHT, R. G. 1987. Intracellular lipid transport in eukaryotes. *Annu Rev Physiol,* 49**,** 193-208.

SLEIGHT, R. G. & PAGANO, R. E. 1983. Rapid appearance of newly synthesized phosphatidylethanolamine at the plasma membrane. *J Biol Chem,* 258**,** 9050-8.

SMITH, T. M., GILLILAND, K., CLAWSON, G. A. & THIBOUTOT, D. 2008. IGF-1 induces SREBP-1 expression and lipogenesis in SEB-1 sebocytes via activation of the phosphoinositide 3-kinase/Akt pathway. *J Invest Dermatol,* 128**,** 1286-93.

SNIDER, W. D. 1988. Nerve growth factor enhances dendritic arborization of sympathetic ganglion cells in developing mammals. *J Neurosci,* 8**,** 2628-34.

SOMSEL RODMAN, J. & WANDINGER-NESS, A. 2000. Rab GTPases coordinate endocytosis. *J Cell Sci,* 113 Pt 2**,** 183-92.

SON, S., TZUR, A., WENG, Y., JORGENSEN, P., KIM, J., KIRSCHNER, M. W. & MANALIS, S. R. 2012. Direct observation of mammalian cell growth and size regulation. *Nat Methods*.

SONENBERG, N. & HINNEBUSCH, A. G. 2009. Regulation of translation initiation in eukaryotes: mechanisms and biological targets. *Cell,* 136**,** 731-45.

SONG, E. J., HONG, H. M. & YOO, Y. S. 2009. Proteasome inhibition induces neurite outgrowth through posttranslational modification of TrkA receptor. *Int J Biochem Cell Biol,* 41**,** 539-45.

SONG, H., MAK, K. K., TOPOL, L., YUN, K., HU, J., GARRETT, L., CHEN, Y., PARK, O., CHANG, J., SIMPSON, R. M., WANG, C. Y., GAO, B., JIANG, J. & YANG, Y. 2010. Mammalian Mst1 and Mst2 kinases play essential roles in organ size control and tumor suppression. *Proc Natl Acad Sci U S A,* 107**,** 1431-6.

SONG, M. S., SALMENA, L. & PANDOLFI, P. P. 2012. The functions and regulation of the PTEN tumour suppressor. *Nat Rev Mol Cell Biol,* 13**,** 283-96.

SOOD, R., PORTER, A. C., OLSEN, D. A., CAVENER, D. R. & WEK, R. C. 2000. A mammalian homologue of GCN2 protein kinase important for translational

control by phosphorylation of eukaryotic initiation factor-2alpha. *Genetics,* 154**,** 787-801.

SOUSA-NUNES, R., YEE, L. L. & GOULD, A. P. 2011. Fat cells reactivate quiescent neuroblasts via TOR and glial insulin relays in Drosophila. *Nature,* 471**,** 508-12.

SPECTOR, A. A., MATHUR, S. N., KADUCE, T. L. & HYMAN, B. T. 1980. Lipid nutrition and metabolism of cultured mammalian cells. *Prog Lipid Res,* 19**,** 155-86.

SPECTOR, A. A. & YOREK, M. A. 1985. Membrane lipid composition and cellular function. *J Lipid Res,* 26**,** 1015-35.

STEINMAN, R. M., BRODIE, S. E. & COHN, Z. A. 1976. Membrane flow during pinocytosis. A stereologic analysis. *J Cell Biol,* 68**,** 665-87.

STITT, T. N., DRUJAN, D., CLARKE, B. A., PANARO, F., TIMOFEYVA, Y., KLINE, W. O., GONZALEZ, M., YANCOPOULOS, G. D. & GLASS, D. J. 2004. The IGF-1/PI3K/Akt pathway prevents expression of muscle atrophy-induced ubiquitin ligases by inhibiting FOXO transcription factors. *Molecular cell,* 14**,** 395-403.

SUDBERY, P. E., GOODEY, A. R. & CARTER, B. L. 1980. Genes which control cell proliferation in the yeast Saccharomyces cerevisiae. *Nature,* 288**,** 401-4.

SUN, L. P., LI, L., GOLDSTEIN, J. L. & BROWN, M. S. 2005. Insig required for sterol-mediated inhibition of Scap/SREBP binding to COPII proteins in vitro. *J Biol Chem,* 280**,** 26483-90.

SUN, L. P., SEEMANN, J., GOLDSTEIN, J. L. & BROWN, M. S. 2007. Sterol-regulated transport of SREBPs from endoplasmic reticulum to Golgi: Insig renders sorting signal in Scap inaccessible to COPII proteins. *Proc Natl Acad Sci U S A,* 104**,** 6519-26.

SUNDQVIST, A., BENGOECHEA-ALONSO, M. T., YE, X., LUKIYANCHUK, V., JIN, J., HARPER, J. W. & ERICSSON, J. 2005. Control of lipid metabolism by phosphorylation-dependent degradation of the SREBP family of transcription factors by SCF(Fbw7). *Cell Metab,* 1**,** 379-91.

SUNDQVIST, A. & ERICSSON, J. 2003. Transcription-dependent degradation controls the stability of the SREBP family of transcription factors. *Proc Natl Acad Sci U S A,* 100**,** 13833-8.

TAKEUCHI, Y., YAHAGI, N., IZUMIDA, Y., NISHI, M., KUBOTA, M., TERAOKA, Y., YAMAMOTO, T., MATSUZAKA, T., NAKAGAWA, Y., SEKIYA, M., IIZUKA, Y., OHASHI, K., OSUGA, J., GOTODA, T., ISHIBASHI, S., ITAKA, K., KATAOKA, K., NAGAI, R., YAMADA, N., KADOWAKI, T. & SHIMANO, H. 2010. Polyunsaturated fatty acids selectively suppress sterol regulatory element-binding protein-1 through proteolytic processing and autoloop regulatory circuit. *J Biol Chem,* 285**,** 11681-91.

TANG, D. G., TOKUMOTO, Y. M., APPERLY, J. A., LLOYD, A. C. & RAFF, M. C. 2001. Lack of replicative senescence in cultured rat oligodendrocyte precursor cells. *Science,* 291**,** 868-71.

TAVEGGIA, C., ZANAZZI, G., PETRYLAK, A., YANO, H., ROSENBLUTH, J., EINHEBER, S., XU, X., ESPER, R. M., LOEB, J. A., SHRAGER, P., CHAO, M. V., FALLS, D. L., ROLE, L. & SALZER, J. L. 2005. Neuregulin-1 type III determines the ensheathment fate of axons. *Neuron,* 47**,** 681-94.

THILO, L. & VOGEL, G. 1980. Kinetics of membrane internalization and recycling during pinocytosis in Dictyostelium discoideum. *Proc Natl Acad Sci U S A,* 77**,** 1015-9.

THOREEN, C. C., CHANTRANUPONG, L., KEYS, H. R., WANG, T., GRAY, N. S. & SABATINI, D. M. 2012. A unifying model for mTORC1-mediated regulation of mRNA translation. *Nature,* 485**,** 109-13.

THOREEN, C. C., KANG, S. A., CHANG, J. W., LIU, Q., ZHANG, J., GAO, Y., REICHLING, L. J., SIM, T., SABATINI, D. M. & GRAY, N. S. 2009. An ATP-competitive mammalian target of rapamycin inhibitor reveals rapamycin-resistant functions of mTORC1. *J Biol Chem,* 284**,** 8023-32.

TOGNON, C. E. & SORENSEN, P. H. 2012. Targeting the insulin-like growth factor 1 receptor (IGF1R) signaling pathway for cancer therapy. *Expert Opin Ther Targets,* 16**,** 33-48.

TSAI, P. T., HULL, C., CHU, Y., GREENE-COLOZZI, E., SADOWSKI, A. R., LEECH, J. M., STEINBERG, J., CRAWLEY, J. N., REGEHR, W. G. & SAHIN, M. 2012. Autistic-like behaviour and cerebellar dysfunction in Purkinje cell Tsc1 mutant mice. *Nature*.

TZUR, A., KAFRI, R., LEBLEU, V. S., LAHAV, G. & KIRSCHNER, M. W. 2009. Cell growth and size homeostasis in proliferating animal cells. *Science,* 325**,** 167-71.

UEYAMA, T., KAWASHIMA, S., SAKODA, T., RIKITAKE, Y., ISHIDA, T., KAWAI, M., YAMASHITA, T., ISHIDO, S., HOTTA, H. & YOKOYAMA, M. 2000. Requirement of activation of the extracellular signal-regulated kinase cascade in myocardial cell hypertrophy. *J Mol Cell Cardiol,* 32**,** 947-60.

UMEN, J. G. 2005. The elusive sizer. *Current opinion in cell biology,* 17**,** 435-41.

VAN RIGGELEN, J., YETIL, A. & FELSHER, D. W. 2010. MYC as a regulator of ribosome biogenesis and protein synthesis. *Nat Rev Cancer,* 10**,** 301-9.

VANDER HAAR, E., LEE, S. I., BANDHAKAVI, S., GRIFFIN, T. J. & KIM, D. H. 2007. Insulin signalling to mTOR mediated by the Akt/PKB substrate PRAS40. *Nat Cell Biol,* 9**,** 316-23.

VANDER HEIDEN, M. G., CANTLEY, L. C. & THOMPSON, C. B. 2009. Understanding the Warburg effect: the metabolic requirements of cell proliferation. *Science,* 324**,** 1029-33.

VANDER HEIDEN, M. G., PLAS, D. R., RATHMELL, J. C., FOX, C. J., HARRIS, M. H. & THOMPSON, C. B. 2001. Growth factors can influence cell growth and survival through effects on glucose metabolism. *Molecular and cellular biology,* 21**,** 5899-912.

VENTURA-CLAPIER, R., GARNIER, A. & VEKSLER, V. 2008. Transcriptional control of mitochondrial biogenesis: the central role of PGC-1alpha. *Cardiovasc Res,* 79**,** 208-17.

VERDU, J., BURATOVICH, M. A., WILDER, E. L. & BIRNBAUM, M. J. 1999. Cell-autonomous regulation of cell and organ growth in Drosophila by Akt/PKB. *Nat Cell Biol,* 1**,** 500-6.

VERHEIJEN, M. H., CAMARGO, N., VERDIER, V., NADRA, K., DE PREUX CHARLES, A. S., MEDARD, J. J., LUOMA, A., CROWTHER, M., INOUYE, H., SHIMANO, H., CHEN, S., BROUWERS, J. F., HELMS, J. B., FELTRI, M. L., WRABETZ, L., KIRSCHNER, D., CHRAST, R. & SMIT, A. B. 2009. SCAP is required for timely and proper myelin membrane synthesis. *Proc Natl Acad Sci U S A,* 106**,** 21383-8.

VERKMAN, A. S. 2011. Aquaporins at a glance. *J Cell Sci,* 124**,** 2107-12.

VERMA, P., CHIERZI, S., CODD, A. M., CAMPBELL, D. S., MEYER, R. L., HOLT, C. E. & FAWCETT, J. W. 2005. Axonal protein synthesis and degradation are necessary for efficient growth cone regeneration. *J Neurosci,* 25**,** 331-42.

VILLANUEVA, S., SUAZO, C., SANTAPAU, D., PEREZ, F., QUIROZ, M., CARRENO, J. E., ILLANES, S., LAVANDERO, S., MICHEA, L. & IRARRAZABAL, C. E. 2012. NFAT5 is activated by hypoxia: role in ischemia and reperfusion in the rat kidney. *PLoS One,* 7**,** e39665.

VILLEMURE, I. & STOKES, I. A. 2009. Growth plate mechanics and mechanobiology. A survey of present understanding. *J Biomech,* 42**,** 1793-803.

VIVANCO, I. & SAWYERS, C. L. 2002. The phosphatidylinositol 3-Kinase AKT pathway in human cancer. *Nat Rev Cancer,* 2**,** 489-501.

VOYVODIC, J. T. 1989. Peripheral target regulation of dendritic geometry in the rat superior cervical ganglion. *J Neurosci,* 9**,** 1997-2010.

WAKIL, S. J., STOOPS, J. K. & JOSHI, V. C. 1983. Fatty acid synthesis and its regulation. *Annu Rev Biochem,* 52**,** 537-79.

WALENKAMP, M. J. & WIT, J. M. 2007. Genetic disorders in the GH IGF-I axis in mouse and man. *Eur J Endocrinol,* 157 Suppl 1**,** S15-26.

WALKER, A. K., JACOBS, R. L., WATTS, J. L., ROTTIERS, V., JIANG, K., FINNEGAN, D. M., SHIODA, T., HANSEN, M., YANG, F., NIEBERGALL, L. J., VANCE, D. E., TZONEVA, M., HART, A. C. & NAAR, A. M. 2011. A conserved SREBP-1/phosphatidylcholine feedback circuit regulates lipogenesis in metazoans. *Cell,* 147**,** 840-52.

WALKEY, C. J., KALMAR, G. B. & CORNELL, R. B. 1994. Overexpression of rat liver CTP:phosphocholine cytidylyltransferase accelerates phosphatidylcholine synthesis and degradation. *J Biol Chem,* 269**,** 5742-9.

WALTHER, T. C. & FARESE, R. V., JR. 2009. The life of lipid droplets. *Biochim Biophys Acta,* 1791**,** 459-66.

WAN, M., LEAVENS, K. F., SALEH, D., EASTON, R. M., GUERTIN, D. A., PETERSON, T. R., KAESTNER, K. H., SABATINI, D. M. & BIRNBAUM, M. J. 2011. Postprandial hepatic lipid metabolism requires signaling through Akt2 independent of the transcription factors FoxA2, FoxO1, and SREBP1c. *Cell Metab,* 14**,** 516-27.

WANDERS, R. J., FERDINANDUSSE, S., BRITES, P. & KEMP, S. 2010. Peroxisomes, lipid metabolism and lipotoxicity. *Biochim Biophys Acta,* 1801**,** 272-80.

WANG, L., WANG, X. & PROUD, C. G. 2000. Activation of mRNA translation in rat cardiac myocytes by insulin involves multiple rapamycin-sensitive steps. *Am J Physiol Heart Circ Physiol,* 278**,** H1056-68.

WANG, X., SATO, R., BROWN, M. S., HUA, X. & GOLDSTEIN, J. L. 1994. SREBP-1, a membrane-bound transcription factor released by sterol-regulated proteolysis. *Cell,* 77**,** 53-62.

WANG, Y. N., CHEN, Y. J. & CHANG, W. C. 2006. Activation of extracellular signal-regulated kinase signaling by epidermal growth factor mediates c-Jun activation and p300 recruitment in keratin 16 gene expression. *Mol Pharmacol,* 69**,** 85-98.

WARBURG, O. 1956. On the origin of cancer cells. *Science,* 123**,** 309-14.

WARNER, J. R. 1999. The economics of ribosome biosynthesis in yeast. *Trends Biochem Sci,* 24**,** 437-40.

WATT, M. J. & STEINBERG, G. R. 2008. Regulation and function of triacylglycerol lipases in cellular metabolism. *Biochem J,* 414**,** 313-25.

WEBSTER, H. D. 1971. The geometry of peripheral myelin sheaths during their formation and growth in rat sciatic nerves. *J Cell Biol,* 48**,** 348-67.

WEIBEL, E. R. 1962. [Morphometric analysis of the number, volume and surface of the alveoli and capillaries of the human lung]. *Z Zellforsch Mikrosk Anat,* 57**,** 648-66.

WELLEN, K. E., LU, C., MANCUSO, A., LEMONS, J. M., RYCZKO, M., DENNIS, J. W., RABINOWITZ, J. D., COLLER, H. A. & THOMPSON, C. B. 2010. The hexosamine biosynthetic pathway couples growth factor-induced glutamine uptake to glucose metabolism. *Genes Dev,* 24**,** 2784-99.

WELLEN, K. E. & THOMPSON, C. B. 2012. A two-way street: reciprocal regulation of metabolism and signalling. *Nat Rev Mol Cell Biol,* 13**,** 270-6.

WICKRAMASINGHE, S. R., ALVANIA, R. S., RAMANAN, N., WOOD, J. N., MANDAI, K. & GINTY, D. D. 2008. Serum response factor mediates NGF-dependent target innervation by embryonic DRG sensory neurons. *Neuron,* 58**,** 532-45.

WIEMAN, H. L., HORN, S. R., JACOBS, S. R., ALTMAN, B. J., KORNBLUTH, S. & RATHMELL, J. C. 2009. An essential role for the Glut1 PDZ-binding motif in growth factor regulation of Glut1 degradation and trafficking. *Biochem J,* 418**,** 345-67.

WIEMAN, H. L., WOFFORD, J. A. & RATHMELL, J. C. 2007. Cytokine stimulation promotes glucose uptake via phosphatidylinositol-3 kinase/Akt regulation of Glut1 activity and trafficking. *Mol Biol Cell,* 18**,** 1437-46.

WILKINS, B. J., DAI, Y. S., BUENO, O. F., PARSONS, S. A., XU, J., PLANK, D. M., JONES, F., KIMBALL, T. R. & MOLKENTIN, J. D. 2004. Calcineurin/NFAT coupling participates in pathological, but not physiological, cardiac hypertrophy. *Circulation research,* 94**,** 110-8.

WILLIAMSON, D. L., KUBICA, N., KIMBALL, S. R. & JEFFERSON, L. S. 2006. Exercise-induced alterations in extracellular signal-regulated kinase 1/2 and mammalian target of rapamycin (mTOR) signalling to regulatory mechanisms of mRNA translation in mouse muscle. *J Physiol,* 573**,** 497-510.

WINICK, M. & NOBLE, A. 1966. Cellular response in rats during malnutrition at various ages. *The Journal of nutrition,* 89**,** 300-6.

WINTER, J. N., JEFFERSON, L. S. & KIMBALL, S. R. 2011. ERK and Akt signaling pathways function through parallel mechanisms to promote mTORC1 signaling. *Am J Physiol Cell Physiol,* 300**,** C1172-80.

WISE, D. R., DEBERARDINIS, R. J., MANCUSO, A., SAYED, N., ZHANG, X. Y., PFEIFFER, H. K., NISSIM, I., DAIKHIN, E., YUDKOFF, M., MCMAHON, S. B. & THOMPSON, C. B. 2008. Myc regulates a transcriptional program that stimulates mitochondrial glutaminolysis and leads to glutamine addiction. *Proceedings of the National Academy of Sciences of the United States of America,* 105**,** 18782-7.

WIZNITZER, M. 2004. Autism and tuberous sclerosis. *J Child Neurol,* 19**,** 675-9.

WOLPERT, L. 2010. Arms and the man: the problem of symmetric growth. *PLoS Biol,* 8.

WU, D. C. & JOHNSTON, L. A. 2010. Control of wing size and proportions by Drosophila myc. *Genetics,* 184**,** 199-211.

WULLSCHLEGER, S., LOEWITH, R. & HALL, M. N. 2006. TOR signaling in growth and metabolism. *Cell,* 124**,** 471-84.

YABE, D., BROWN, M. S. & GOLDSTEIN, J. L. 2002. Insig-2, a second endoplasmic reticulum protein that binds SCAP and blocks export of sterol regulatory element-binding proteins. *Proc Natl Acad Sci U S A,* 99**,** 12753-8.

YANG, T., ESPENSHADE, P. J., WRIGHT, M. E., YABE, D., GONG, Y., AEBERSOLD, R., GOLDSTEIN, J. L. & BROWN, M. S. 2002. Crucial step in cholesterol homeostasis: sterols promote binding of SCAP to INSIG-1, a membrane protein that facilitates retention of SREBPs in ER. *Cell,* 110**,** 489-500.

YE, B., ZHANG, Y., SONG, W., YOUNGER, S. H., JAN, L. Y. & JAN, Y. N. 2007. Growing dendrites and axons differ in their reliance on the secretory pathway. *Cell,* 130**,** 717-29.

YECIES, J. L., ZHANG, H. H., MENON, S., LIU, S., YECIES, D., LIPOVSKY, A. I., GORGUN, C., KWIATKOWSKI, D. J., HOTAMISLIGIL, G. S., LEE, C. H. & MANNING, B. D. 2011. Akt stimulates hepatic SREBP1c and lipogenesis through parallel mTORC1-dependent and independent pathways. *Cell Metab,* 14**,** 21-32.

YELLATURU, C. R., DENG, X., CAGEN, L. M., WILCOX, H. G., MANSBACH, C. M., 2ND, SIDDIQI, S. A., PARK, E. A., RAGHOW, R. & ELAM, M. B. 2009a. Insulin enhances post-translational processing of nascent SREBP-1c by promoting its phosphorylation and association with COPII vesicles. *J Biol Chem,* 284**,** 7518-32.

YELLATURU, C. R., DENG, X., PARK, E. A., RAGHOW, R. & ELAM, M. B. 2009b. Insulin enhances the biogenesis of nuclear sterol regulatory element-binding protein (SREBP)-1c by posttranscriptional down-regulation of Insig-2A and its dissociation from SREBP cleavage-activating protein (SCAP).SREBP-1c complex. *J Biol Chem,* 284**,** 31726-34.

YOKOYAMA, C., WANG, X., BRIGGS, M. R., ADMON, A., WU, J., HUA, X., GOLDSTEIN, J. L. & BROWN, M. S. 1993. SREBP-1, a basic-helix-loop-helix-leucine zipper protein that controls transcription of the low density lipoprotein receptor gene. *Cell,* 75**,** 187-97.

YOON, S. & SEGER, R. 2006. The extracellular signal-regulated kinase: multiple substrates regulate diverse cellular functions. *Growth Factors,* 24**,** 21-44.

YU, L., MCPHEE, C. K., ZHENG, L., MARDONES, G. A., RONG, Y., PENG, J., MI, N., ZHAO, Y., LIU, Z., WAN, F., HAILEY, D. W., OORSCHOT, V., KLUMPERMAN, J., BAEHRECKE, E. H. & LENARDO, M. J. 2010. Termination of autophagy and reformation of lysosomes regulated by mTOR. *Nature,* 465**,** 942-6.

ZDANOWICZ, M. M., MOYSE, J., WINGERTZAHN, M. A., O'CONNOR, M., TEICHBERG, S. & SLONIM, A. E. 1995. Effect of insulin-like growth factor I in murine muscular dystrophy. *Endocrinology,* 136**,** 4880-6.

ZETTERBERG, A., ENGSTROM, W. & DAFGARD, E. 1984. The relative effects of different types of growth factors on DNA replication, mitosis, and cellular enlargement. *Cytometry,* 5**,** 368-75.

ZETTERBERG, A. & KILLANDER, D. 1965a. Quantitative cytochemical studies on interphase growth. II. Derivation of synthesis curves from the distribution of DNA, RNA and mass values of individual mouse fibroblasts in vitro. *Exp Cell Res,* 39**,** 22-32.

ZETTERBERG, A. & KILLANDER, D. 1965b. Quantitative cytophotometric and autoradiographic studies on the rate of protein synthesis during interphase in mouse fibroblasts in vitro. *Exp Cell Res,* 40**,** 1-11.

ZHANG, X., AZHAR, G., CHAI, J., SHERIDAN, P., NAGANO, K., BROWN, T., YANG, J., KHRAPKO, K., BORRAS, A. M., LAWITTS, J., MISRA, R. P. & WEI, J. Y. 2001a. Cardiomyopathy in transgenic mice with cardiac-specific overexpression of serum response factor. *Am J Physiol Heart Circ Physiol,* 280**,** H1782-92.

ZHANG, X., CHAI, J., AZHAR, G., SHERIDAN, P., BORRAS, A. M., FURR, M. C., KHRAPKO, K., LAWITTS, J., MISRA, R. P. & WEI, J. Y. 2001b. Early postnatal cardiac changes and premature death in transgenic mice overexpressing a mutant form of serum response factor. *J Biol Chem,* 276**,** 40033-40.

ZHAO, S., XU, W., JIANG, W., YU, W., LIN, Y., ZHANG, T., YAO, J., ZHOU, L., ZENG, Y., LI, H., LI, Y., SHI, J., AN, W., HANCOCK, S. M., HE, F., QIN, L., CHIN, J., YANG, P.,

CHEN, X., LEI, Q., XIONG, Y. & GUAN, K. L. 2010. Regulation of cellular metabolism by protein lysine acetylation. *Science,* 327**,** 1000-4.

ZHOU, H. & HUANG, S. 2010. The complexes of mammalian target of rapamycin. *Curr Protein Pept Sci,* 11**,** 409-24.

ZHOU, J., BLUNDELL, J., OGAWA, S., KWON, C. H., ZHANG, W., SINTON, C., POWELL, C. M. & PARADA, L. F. 2009. Pharmacological inhibition of mTORC1 suppresses anatomical, cellular, and behavioral abnormalities in neural-specific Pten knock-out mice. *J Neurosci,* 29**,** 1773-83.

ZHOU, R. H., YAO, M., LEE, T. S., ZHU, Y., MARTINS-GREEN, M. & SHYY, J. Y. 2004. Vascular endothelial growth factor activation of sterol regulatory element binding protein: a potential role in angiogenesis. *Circ Res,* 95**,** 471-8.

ZONCU, R., BAR-PELED, L., EFEYAN, A., WANG, S., SANCAK, Y. & SABATINI, D. M. 2011. mTORC1 senses lysosomal amino acids through an inside-out mechanism that requires the vacuolar H(+)-ATPase. *Science,* 334**,** 678-83.

ZONG, H., REN, J. M., YOUNG, L. H., PYPAERT, M., MU, J., BIRNBAUM, M. J. & SHULMAN, G. I. 2002. AMP kinase is required for mitochondrial biogenesis in skeletal muscle in response to chronic energy deprivation. *Proc Natl Acad Sci U S A,* 99**,** 15983-7.

ZWEYTICK, D., ATHENSTAEDT, K. & DAUM, G. 2000. Intracellular lipid particles of eukaryotic cells. *Biochim Biophys Acta,* 1469**,** 101-20.